LIÈGE université
Sciences Appliquées

Resonant phase lags of nonlinear mechanical systems

A thesis submitted in partial fulfillment of the requirements
for the degree of Doctor of Philosophy (PhD) in Engineering Science

by

Martin Volvert

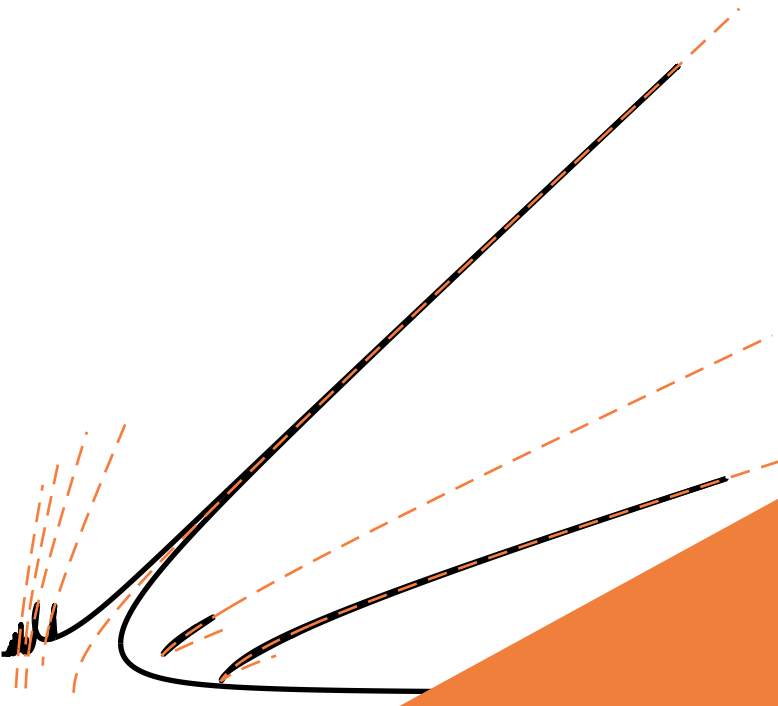

Supervisor: Gaëtan Kerschen

Doctoral college in Aerospace and Mechanics

January 2024

Members of the examination committee

President
Prof. Jean-Philippe Ponthot
University of Liège

Supervisor
Prof. Gaëtan Kerschen
University of Liège

Members
Prof. Olivier Brüls
University of Liège

Prof. Loïc Salles
University of Liège

Prof. Olivier Thomas
Arts et Métiers

Prof. Cyril Touzé
ENSTA Paris

Prof. Alexander Vakakis
University of Illinois Urbana-Champaign

Resonant phase lags of nonlinear mechanical systems

Martin Volvert

Abstract

The concept of a resonance is central in structural dynamics, because the maximum amplitude at which a system vibrates occurs near resonance frequencies. Unlike linear systems, nonlinear systems can exhibit different types of resonances including primary and secondary (superharmonic, subharmonic, ultra-subharmonic) resonances. An effective theoretical framework to characterize nonlinear resonances is nonlinear modal analysis, which has been developed since more than half a century. In this context, primary resonances received the most attention whereas very little effort was devoted to the characterization of secondary resonances.

This thesis is an attempt to answer two key questions: (*i*) How to define the primary and secondary resonances of a nonlinear system? and (*ii*) How to characterize these resonances analytically, numerically and experimentally ? To answer the former question, the concept of a resonant phase lag associated with the amplitude resonance of the l-th harmonic of the l:ν resonance is proposed. For the latter question, a new definition of a nonlinear normal mode termed phase resonance nonlinear mode which corresponds to the structural deformation at the resonant phase lag is introduced. These novel concepts are introduced based on analytical investigations, validated numerically on single- and multiple-degree-of-freedom nonlinear systems and demonstrated experimentally on two beam structures thanks to phase-locked loop testing.

Acknowledgements

Nous y sommes, c'est la fin d'une grande aventure...

Je tiens tout d'abord à remercier Gaëtan Kerschen, mon promoteur. Merci pour ton suivi, tes conseils, ta disponibilité, ta motivation et ton enthousiasme. Je n'aurais pas su y arriver sans tout ça. On y rajoute les quelques restaurants, les barbecues et les conférences, et on peut dire que c'était une thèse très agréable!

Merci à mon comité de thèse, O. Brüls et J.-P. Ponthot, pour leur suivi et leurs encouragements pendant toutes ces années. Merci aussi au jury qui a accepté de relire ce travail.

Pendant 6 ans, j'ai aussi été assistant au sein du département A&M. Je remercie toutes les personnes qui font tourner ce département: les secrétaires, le personnel d'entretien, les différents présidents qui se sont succédé et toutes les autres personnes qui travaillent pour ce département. Merci aussi à M. Bruyneel et J.-P. Ponthot pour qui j'ai donné les séances d'exercices et de projets, la tâche d'assistant aurait pu être beaucoup plus compliquée sans votre disponibilité et bienveillance.

Pendant 6 ans, j'ai fait partie d'un labo, le *S3L*, au sein duquel j'ai rencontré pas mal de belles personnes. Gaëtan, Jenni, Jean-Philippe, Geoffrey, Xavier, Tong, Giancarlo, Sam, Nicolas, Thibaut et Ghislain. Merci d'avoir fait de ce labo un endroit facile à vivre et bon vivant! Plus particulièrement, j'aimerais remercier 3 membres de ce labo. Tout d'abord Ghislain, ma constante. Merci d'avoir été à mes côtés durant ces 6 années, du début à la fin tu étais là et ça me fait bizarre de ne plus être ton collègue! Tu as toujours été disponible, bienveillant et d'une aide précieuse. Ensuite, Thibaut. Tu as été la première personne à m'accueillir dans le labo, à m'y faire me sentir bien et à m'aider à prendre mes marques en début de thèse. Je n'oublierai jamais les *relief songs*. Enfin, Nicolas, merci d'avoir été là ces dernières années, pour les discussions, les (nombreuses) pauses, les desserts que tu ramenais et tous ces temps de midi à aller courir.

Merci à Olaf d'être le chien que j'ai toujours rêvé d'avoir, merci pour toutes ces balades.

Enfin, merci à Camille de m'avoir supporté durant ces années de thèse, dans les bons et mauvais moments. Merci pour tous ces moments passés ensemble, à la maison, en balade, etc. Merci pour l'organisation de nos citytrips et grands voyages. Ces moments m'ont fait énormément de bien.

Nomenclature

Latin letters

$\mathbb{I}_r$	Null matrix of size $n \times n$ except for the r-th diagonal term which is equal to 1
$\mathbf{C}$	Damping matrix
$\mathbf{f}_r$	Vector with only one non-zero entry of strictly positive amplitude f at the r-th degree of freedom
$\mathbf{f}_{ext}$	Vector of external forcing
$\mathbf{f}_{nc}$	Vector of nonconservative forces
$\mathbf{F}_{nl}$	Vector of the Fourier coefficients of the nonlinear forces
$\mathbf{f}_{nl}$	Vector of nonlinear forces
$\mathbf{I}_n$	Identity matrix of size $n \times n$
$\mathbf{J}$	Jacobian matrix
$\mathbf{K}$	Stiffness matrix
$\mathbf{M}$	Mass matrix
$\mathbf{m}$	Multi-index of nonnegative integers
$\mathbf{Q}$	Harmonic basis
$\mathbf{Q}$	Vector
$\mathbf{R}_\alpha$	Rotation matrix
$\mathbf{S}$	Vector of the Fourier coefficients of the perturbation
$\mathbf{s}_l^f, \mathbf{c}_l^f$	Sine and cosine vectors of the l-th harmonic of the nonlinear forces
$\mathbf{s}_l^x, \mathbf{c}_l^x$	Sine and cosine vectors of the l-th harmonic of the displacements
$\mathbf{T}_f$	Filtering matrix
$\mathbf{T}_T$	T-periodic rendering matrix
$\mathbf{U}, \mathbf{V}$	Vector of constraint equations
$\mathbf{w}$	Weight vector of the least mean squares algorithm
$\mathbf{X}$	Vector of the Fourier coefficients of the displacements
$\mathbf{x}$	Vector of displacements
$\mathbf{x}^*$	Periodic solution of displacements
$\mathbf{z}$	Vector of displacements and velocities
$\mathbf{z}_i$	Eigenvector of the i-th mode
$\mathcal{B}$	Complex matrix
$\mathcal{L}$	Eigenvector of the monodromy matrix
$\mathcal{M}$	Monodromy matrix
$\mathcal{P}$	Constant or T-periodic matrix
i	Imaginary unit

A	Amplitude
A_l	Amplitude of the l-th harmonic
$A_{l,\bar{\alpha}}, \phi_{l,\bar{\alpha}}$	Polar coordinates of the stiffness term of the l-th harmonic of the Van der Pol transformation
$A_{l,\Omega}, \phi_{l,\Omega}$	Polar coordinates of the frequency detuning term of the l-th harmonic of the Van der Pol transformation
$A_{l,\bar{\zeta}}, \phi_{l,\bar{\zeta}}$	Polar coordinates of the damping term of the l-th harmonic of the Van der Pol transformation
A_{max}	Maximum of amplitude
a_{p_1}, a_{p_2}	Clearances
c	Damping coefficient
C_d	Coefficient related to the stiffness of order d
c_i	Modal damping of the i-th mode
d	Stiffness order
D_n	Partial derivative with respect to T_n
e	Error of the least mean squares algorithm
E_{in}	Energy injected
E_{out}	Energy dissipated
f	Forcing amplitude
f_{ext}	External forcing
f_{nl}	Nonlinear force
f'_{nl}	Derivative of the nonlinear force with respect to the displacement
g_p, g_p, g_i	Gains of the PID controller
h_{ij}	Hermite polynomials
i, j	Integer indexes
K	Complete elliptic integral
k	Stiffness coefficient
$k'_{i,k}$	Restoring force derivative
k_d	Stiffness coefficient of the d-th order stiffness term
k_i	Modal stiffness of the i-th mode
l	Harmonic index
l_2	Harmonic index
m	Mass coefficient
m_i	Modal mass of the i-th mode
n	Number of degrees-of-freedom
N_H	Number of harmonics
p, q	Integer indexes
$p_{1,\pm}, p_{2,\pm}$	Regularization functions
r	index of the forced degree of freedom
r_{ss}	Step size scalar of the least mean squares algorithm
s	Perturbation
s_l, c_l	Sine and cosine amplitudes of the l-th harmonic
S_l^f, C_l^f	Sine and cosine amplitudes of the l-th harmonic of the nonlinear forces
s_l^f, c_l^f	Sine and cosine amplitudes of the l-th harmonic of the nonlinear forces

$S_{l_2}^{f'_l}, C_{l_2}^{f'_l}$	Sine and cosine amplitudes of the l_2-th harmonic of the l-th component of f'_{nl}
$s_{l_2}^{f'}, c_{l_2}^{f'}$	Sine and cosine amplitudes of the l_2-th harmonic of f'_{nl}
T	Period
t	Time
T^*	Least common multiple period
T_i	Period of the i-th harmonic
T_n	Time scale of order n
t_p	Local scaled abscissa
u, v	Cartesian coordinates of the Van der Pol transformation
u_l, v_l	Cartesian coordinates of the l-th harmonic of the Van der Pol transformation
u_Ω, v_Ω	Cartesian coordinates of the frequency detuning term of the Van der Pol transformation
U_i, V_i	Constraint equations
u_i, v_i	Variables related to the state-space variables
u_s, v_s	Pair of state-space variables
$u_{\bar{\alpha}}, v_{\bar{\alpha}}$	Cartesian coordinates of the stiffness term of the Van der Pol transformation
$u_{\bar{\gamma}}, v_\gamma$	Cartesian coordinates of the forcing term of the Van der Pol transformation
$u_{\bar{\zeta}}, v_{\bar{\zeta}}$	Cartesian coordinates of the damping term of the Van der Pol transformation
w_i	Modal amplitude of the i-th mode
x	Displacement
$x_0, \dot{x}_0$	Initial displacement and velocity
x_i	Displacement of the i-th DOF
x_r	Displacement of the forced DOF
x_{nnm}	Nonlinear normal mode motion
y_i	i-th term of the asymptotic expansion

Greek letters

α	Delay
α_d	Mass-normalized stiffness coefficient of the d-th order stiffness term
$\bar{\sigma}$	Hill's coefficient
χ	Normalized amplitude
δ	Gain for the EPMC
$\Delta\bullet$	Difference between two values of the quantity $\bullet$
Δ_a	Clearance size
Δ_{PL}	Coefficient related to the resonant phase lag approach
Δ_{VF}	Coefficient related to the velocity feedback approach
Γ	*Gamma* function
γ	Mass-normalized forcing amplitude
γ_{ext}	Mass-normalized external forcing
κ	Normalized forcing
Λ	Amplitude of the undamped, forced linear oscillator away from the resonance
λ_i	Floquet multiplier
μ	Gain for the PRNM
ν	Integer that accounts for the subharmonic terms
Ω	Detuning parameter of the primary resonance

ω	Frequency
ω_0	Natural frequency of the linear oscillator
Ω_l	Detuning parameter of the l:ν resonance
ω_l	Frequency of the l-th harmonic
ω_d	Damped natural frequency
ω_J	Frequency of the Jacobi elliptic functions
ϕ	Phase lag
ϕ'_l	Phase lag combination of the l:1 resonance
ϕ_l	Phase lag of the l-th harmonic
$\bar{\boldsymbol{\sigma}}$	Diagonal matrix of the Hill's coefficients
$\boldsymbol{\lambda}$	Matrix of the Floquet multipliers
$\boldsymbol{\nabla}(\omega)$	Differential operator
$\boldsymbol{\nabla}_l$	Diagonal element of the differential operator $\boldsymbol{\nabla}(\omega)$
$\boldsymbol{\sigma}$	Diagonal matrix of the Floquet exponents
Ψ	Fundamental matrix of a first-order differential equation
ψ	Angle
ψ_i	Column-vector solution of a first-order differential equation
ρ	Elliptic modulus
σ_i	Floquet exponent
ν	Subharmonic index
τ	Adimensional time
θ	Angle corresponding to the frequency ω
θ_l	Angle corresponding to the frequency ω_l
υ_i	Complex frequency of the i-th mode
ε	Scaling parameter
φ_l	Resonant phase lag of the l:ν resonance
ζ	Modal damping ratio

Subscripts

$\bullet_a$	Quantity $\bullet$ at amplitude resonance
$\bullet_p$	Quantity $\bullet$ at phase resonance
$\bullet_{PL}$	Quantity $\bullet$ related to the resonant phase lag approach
$\bullet_{VF}$	Quantity $\bullet$ related to the velocity feedback approach

Superscripts

$\bar{\bullet}$	Scaled quantity $\bullet$
$\bullet^\dagger$	Pseudo-inverse of the quantity $\bullet$
$\bullet^\ddagger$	Complex conjugate of the quantity $\bullet$
$\bullet^T$	Transpose of the quantity $\bullet$
$\ddot{\bullet}$	Second-order time derivative of the quantity $\bullet$
$\dot{\bullet}$	First-order time derivative of the quantity $\bullet$
$\tilde{\ddot{\bullet}}$	Second-order adimensional time derivative of the quantity $\bullet$
$\tilde{\dot{\bullet}}$	First-order adimensional time derivative of the quantity $\bullet$

Acronyms

AM	Averaging method
DMC	Damped motion concept

DOF	Degree of freedom
EB	Energy balance
EPMC	Extended periodic motion concept
HBM	Harmonic balance method
IM	Invariant manifold
MDOF	Multiple-degree-of-freedom
MMS	Method of multiple scales
NFRC	Nonlinear frequency response curve
NNM	Nonlinear normal mode
PID	Proportional, integral and Differential
PLL	Phase-locked loop
PLOPT	Phase lag oriented perturbation technique
PRNM	Phase resonance nonlinear mode
SDOF	Single-degree-of-freedom

Contents

Chapter 1

Introduction

1.1 Context

The world surrounding us is intrinsically nonlinear. Yet, real-life problems are often linearized to obtain an easier solution that approximates sufficiently well the studied phenomenon. This also holds in aerospace and mechanical engineering in which the vibrating response is often predicted numerically using a linear (or linearized) model.

The theory behind linear modal analysis is well-established and possesses sound theoretical, numerical and experimental backgrounds [1, 2]. For linear models, it is easy to compute the resonance frequencies, normal modes and damping ratios as well as the response under an external excitation. Specifically, if a structure is excited with harmonic forcing of frequency ω, the steady-state response has the same frequency ω. If the frequency is close to one of the resonance frequencies, the response amplitude can be high with the risk of damaging the structure. Away from the resonance frequencies, the response amplitude is, however, much lower. Finally, the principle of superposition applies for linear structures, namely, if an input f_a (resp. f_b) gives an output x_a (resp. x_b), then, $f_a + f_b$ gives $x_a + x_b$.

Driven by the climate crisis, there is a need to reduce fuel consumption, noise and gas emissions. This implies the reduction of the total mass, through the design of thinner structures, which can eventually lead to large deformations. Novel materials featuring nonlinear constitutive laws such as elastomers and composite materials are also more commonly employed. In addition, contact and friction can occur in real-life structures, which linear models cannot model.

One of the key features of nonlinear vibration is the dependence of resonance frequencies on the input level [3]. The resulting hardening or softening behavior can generate multi-stable solutions [4] implying the failure of the superposition principle. Another important dynamical feature is that nonlinear systems may no longer respond at a single frequency in the case of harmonic forcing. Specifically, new harmonics appear in the response and can, in turn, lead to new resonances; the so-called secondary resonances appear at fractions or multiples of the primary resonance frequencies. Their amplitude may sometimes be sufficiently high so as to damage the structure [5].

Nonlinear modal analysis theories have thus been developed to extend the concept

of a normal mode to nonlinear structures [3, 6–10]. These developments concentrate mainly on primary resonances. Low-order secondary resonances were studied using first-order perturbation techniques [4, 11, 12] in order to characterize the relation between the response amplitude and the resonance frequency. To study more complex secondary resonances, Yagasaki developed a *Mathematica* package that solves higher-order averaging problems [13–15]. The focus in his studies was not on the dynamical characterization of these resonances, but rather on the study of the fixed points as well as on time series computation. Recently, experimental techniques based on phase-locked loops (PLLs) for identifying nonlinear frequency response curves (NFRCs) and nonlinear modes have emerged, see, e.g., [16–20]. A PLL enables the experimenter to impose a specific phase lag between the response and the excitation by the means of a PID controller. For instance, the backbone curves of primary resonances can be identified by setting $\frac{\pi}{2}$ as the phase lag target.

However, the existing body of literature rarely discusses the relation between the response amplitude and the phase lag for secondary resonances. This represents the main thrust of this thesis.

1.2 Contributions of the thesis

This thesis attempts to answer two key questions:

i. *How to define the l:ν resonance of a nonlinear system where l and ν are arbitrary integers?*

ii. *How to characterize these resonances analytically, numerically and experimentally?*

To this end, the present thesis centers on the link that exists between the so-called *amplitude and phase resonances* of nonlinear systems. With this objective in mind, first- and higher-order perturbation techniques [14, 15] are employed to derive the equations governing the dynamics around the l:ν resonance. Then, its amplitude-phase lag relation is derived giving rise to the concept of a *resonant phase lag*. These developments form the basis of a new definition of a nonlinear normal mode (NNM) termed *phase resonance nonlinear mode* (PRNM). Eventually, PRNMs can be exploited to fully characterize the behavior of primary and secondary resonances numerically using continuation techniques and experimentally using PLLs.

The thesis is organized as follows. Chapter 2 evidences the main differences that exist between the resonant behavior of linear and nonlinear oscillators. First, a harmonically-forced linear oscillator is studied around its amplitude and phase resonances. Second, a Duffing oscillator [12] is taken as a motivating example. The exact solution of the undamped, unforced system obtained using elliptic functions is compared to the solutions derived using perturbation techniques. Then, the resonant behavior of the harmonically-forced, damped system is studied numerically for different forcing levels. It is shown that this seemingly simple nonlinear oscillator can exhibit a wide variety of secondary resonances.

The distinction between the amplitude and phase resonances of nonlinear oscillators is rarely discussed in the literature. To this end, first-order averaging is used in Chapter 3 to characterize the primary resonance of a single-degree-of-freedom (SDOF) oscillator with nonlinear polynomial stiffness. Under the assumption of light to moderate damping, it is established that the resonant phase lag is $\pi/2$ meaning that phase resonance happens in the immediate neighbourhood of amplitude resonance.

Chapter 4 studies the dynamical behavior around secondary resonances of SDOF nonlinear oscillators. The resonant phase lags of the $d:1$ and $1:d$ resonances of an oscillator with polynomial stiffness or order d are first derived using first-order averaging. The analytical developments are illustrated using a Duffing oscillator, a Hemlholtz oscillator and an oscillator with a quintic stiffness. Higher-order averaging is then exploited to compute the governing equations of more complex secondary resonances of the Duffing oscillator and to derive the corresponding resonant phase lags.

Chapter 5 builds upon the outcomes of Chapters 3 and 4 to define the concept of a PRNM. The PRNM of the $l{:}\nu$ resonance corresponds to the structural deformation at the corresponding resonant phase lag. Two numerical methods for computing PRNMs are developed based on velocity feedback and resonant phase lag approaches. The latter approach is the method of choice and is then demonstrated numerically using several nonlinear oscillators.

Chapter 6 shows that exploiting the resonant phase lags derived for SDOF systems in the case of multi-degree-of-freedom (MDOF) systems should be achieved with great care. In SDOF systems, the different resonances are well-separated. In MDOF systems, primary and secondary resonances of different modes can interact, which, in turn, influences the evolution of the phase lag. Thus, a perturbation technique is used to study the phase lag of different higher-order harmonics across lower-order resonances. The results obtained evidence that an *augmented* resonant phase lag combining carefully selected phase lags of different harmonics should be considered to track the secondary resonances of MDOF systems. The developments are demonstrated experimentally using two beam structures, namely a nonlinear cantilever beam and a nonlinear clamped-clamped beam.

Finally, conclusions and perspectives are drawn in Chapter 7.

Chapter 2

Resonances of linear and nonlinear oscillators

2.1 Introduction

The study of the dynamical behavior of linear systems possesses solid theoretical and experimental backgrounds [1, 21]. Discrepancies between numerical predictions and experimental results may happen if the nonlinearities can no longer be ignored. Differences between linear and nonlinear systems can take multiple forms. Under a linear assumption, the system responds mono-harmonically to a mono-harmonic input, and resonances occur at frequencies which do not change with the forcing level. In nonlinear oscillators, however, the response to mono-harmonic excitation is generally multi-harmonic, and resonance frequencies can shift according to the forcing amplitude [3], which can lead to jump phenomena and multi-stable solutions [11]. Furthermore, the multi-harmonic response can generate new resonances, located at fractions or multiples of the amplitude-dependent resonance frequency of the system [22].

This chapter illustrates these differences. First, the well-defined amplitude and phase resonances are recalled for the linear oscillator. Second, the exact solution of the undamped, unforced Duffing oscillator is compared to approximate solutions derived using perturbation techniques. Third, the harmonically-forced, damped Duffing oscillator is studied numerically to highlight the multi-harmonic behavior of the system as well as the numerous secondary resonances that exist. Finally, a preliminary answer to the two central questions of this thesis is provided, namely (*i*) How to define the l:ν resonance of a nonlinear system where l and ν are arbitrary integers? and (*ii*) How to characterize primary and secondary resonances analytically, numerically and experimentally?

2.2 Linear oscillators

2.2.1 The harmonic oscillator

The equation of the harmonic oscillator is

$$m\ddot{x}(t) + kx(t) = 0 \tag{2.1}$$

where $x(t)$ is the displacement, m is the mass and k is the linear stiffness. Time derivatives are represented using overdots. Through mass normalization, Equation (2.1) can be recast into

$$\ddot{x}(t) + \omega_0^2 x(t) = 0 \tag{2.2}$$

where $\omega_0 = \sqrt{\frac{k}{m}}$ represents the natural frequency of the system. The solution of Equation (2.2), which is a second-order differential equation with constant coefficients, is harmonic

$$x(t) = A\sin(\omega_0 t - \phi) \tag{2.3}$$

where A is the amplitude of the free vibration, and ϕ is the phase lag. A and ϕ depend on the initial displacement x_0 and velocity $\dot{x}_0$ of the system

$$A = \sqrt{x_0^2 + \left(\frac{\dot{x}_0}{\omega_0}\right)^2} \quad \text{and} \quad \tan\phi = -\frac{\omega_0 x_0}{\dot{x}_0}. \tag{2.4}$$

2.2.2 The damped harmonic oscillator

Dissipation can be introduced in Equation (2.1) through viscous damping $c\dot{x}$, where c is the viscous damping coefficient,

$$m\ddot{x}(t) + c\dot{x}(t) + kx(t) = 0 \tag{2.5}$$

Through mass normalization, the equation of motion reads

$$\ddot{x}(t) + 2\zeta\omega_0\dot{x}(t) + \omega_0^2 x(t) = 0 \tag{2.6}$$

where $\zeta = \frac{c}{2\sqrt{km}}$ is the damping ratio. Assuming a solution of the form $x(t) = e^{vt}$, the characteristic equation admits two roots

$$v_{1,2} = \omega_0\left(-\zeta \pm \mathrm{i}\sqrt{1-\zeta^2}\right) \tag{2.7}$$

and the solution depends on the sign of $1-\zeta^2$. Because the damping ratios of mechanical and aerospace structures are generally around 1%, only the case $\zeta < 1$ is considered herein. The resulting solution is harmonic with a decaying exponential envelope

$$x(t) = e^{-\zeta\omega_0 t}\left(C_1\cos\omega_d t + C_2\sin\omega_d t\right) \tag{2.8}$$

where $\omega_d = \sqrt{1-\zeta^2}\omega_0$ is the damped natural frequency. The constants C_1 and C_2 depend on the initial conditions

$$C_1 = x_0 \quad \text{and} \quad C_2 = \frac{1}{\omega_d}\left(\dot{x}_0 + \zeta\omega_0 x_0\right). \tag{2.9}$$

2.2.3 The damped, forced harmonic oscillator

Considering now the damped, forced harmonic oscillator, we have

$$m\ddot{x}(t) + c\dot{x}(t) + kx(t) = f\sin\omega t \tag{2.10}$$

where f and ω are the forcing amplitude and frequency, respectively. Equation (2.10) is recast into

$$\ddot{x}(t) + 2\zeta\omega_0\dot{x}(t) + \omega_0^2 x(t) = \gamma\sin\omega t \tag{2.11}$$

where $\gamma = f/m$. The solution of this equation is the superposition of the homogeneous solution, obtained by solving Equation (2.6), and the particular solution of the form

$$x(t) = A\sin(\omega t - \phi) \tag{2.12}$$

Injecting (2.12) into (2.11) and projecting onto $\sin\omega t$ and $\cos\omega t$ yields

$$\begin{cases} 2\zeta\omega_0\omega A = \gamma\sin\phi \\ (\omega_0^2 - \omega^2)A = \gamma\cos\phi. \end{cases} \tag{2.13}$$

This system is easily solved for A and ϕ

$$\begin{cases} A = \frac{\gamma}{\sqrt{4\zeta^2\omega_0^2\omega^2 + \left(\omega_0^2 - \omega^2\right)^2}} \\ \tan\phi = \frac{2\zeta\omega_0\omega}{\omega_0^2 - \omega^2}. \end{cases} \tag{2.14}$$

The particular solution is the steady-state response of the system from which resonances can be studied.

2.2.3.1 Amplitude resonance

Amplitude resonance corresponds to a local maximum of the response. It occurs when both $\frac{\partial A}{\partial\omega}$ and $\frac{\partial A}{\partial\phi}$ are equal to 0. From Equation (2.13), we obtain

$$\begin{cases} \frac{\partial A}{\partial\phi} = \frac{\gamma}{2\zeta\omega_0\omega}\left(\cos\phi - \frac{\sin\phi}{\omega}\frac{\partial\omega}{\partial\phi}\right) = 0 \\ \frac{\partial A}{\partial\omega} = \frac{\gamma}{2\zeta\omega_0\omega}\left(\cos\phi\frac{\partial\phi}{\partial\omega} - \frac{\sin\phi}{\omega}\right) = 0. \end{cases} \tag{2.15}$$

Both relations are equivalent. The second relation of Equation (2.13) provides an expression for ω

$$\omega = \sqrt{\omega_0^2 - \frac{\gamma}{A}\cos\phi} \tag{2.16}$$

from which $\frac{\partial\omega}{\partial\phi}$ can be deduced

$$\frac{\partial\omega}{\partial\phi} = \frac{1}{2\sqrt{\omega_0^2 - \frac{\gamma}{A}\cos\phi}}\left(\frac{\gamma}{A}\sin\phi + \frac{\gamma}{A^2}\cos\phi\frac{\partial A}{\partial\phi}\right). \tag{2.17}$$

This quantity can be inserted in the first relation of (2.15):

$$\frac{\partial A}{\partial \phi} = \frac{\gamma \sin\phi}{2\zeta\omega_0\omega} \frac{(\omega - \zeta\omega_0 \tan\phi)}{(\omega \tan\phi + \zeta\omega_0)} = 0. \tag{2.18}$$

This relationship is satisfied when the phase lag takes the form

$$\tan\phi_a = \frac{\omega_a}{\zeta\omega_0} = \frac{\sqrt{1-2\zeta^2}}{\zeta} \tag{2.19}$$

where $\bullet_a$ denotes a quantity at amplitude resonance. The corresponding frequency and amplitude are

$$\omega_a = \omega_0\sqrt{1-2\zeta^2}, \quad A_a = \frac{\gamma}{2\zeta\omega_0^2\sqrt{1-\zeta^2}} \tag{2.20}$$

in accordance with [21].

2.2.3.2 Phase resonance

Phase resonance takes place at phase quadrature $\phi_p = \frac{\pi}{2}$ where $\bullet_p$ denotes a quantity at phase resonance. It occurs when the excitation frequency corresponds to the natural frequency of the undamped system, i.e., when $\omega = \omega_p = \omega_0$ in Equation (2.13). In this case, injecting the solution $x(t) = -A\cos\omega_0 t$ into Equation (2.11) gives

$$A\omega_0^2\cos\omega_0 t + 2\zeta\omega_0 A\omega_0 \sin\omega_0 t - \omega_0^2 A\cos\omega_0 t = \gamma\sin\omega_0 t. \tag{2.21}$$

Equating the coefficients of $\cos\omega_0 t$ and $\sin\omega_0 t$ evidences that the inertia and stiffness terms compensate each other and that the damping term counterbalances the forcing term, respectively. The amplitude at phase resonance is

$$A_p = \frac{\gamma}{2\zeta\omega_0^2}. \tag{2.22}$$

2.2.3.3 Results and discussion

For small damping, i.e., for $\zeta \ll 1$, a reasonable assumption for mechanical and aerospace structures, there is no need to distinguish between amplitude and phase resonances. In fact, if we define the difference between amplitude and phase resonances for the amplitude, frequency and phase lag as

$$\begin{aligned}
\Delta A &= A_a - A_p = \frac{\gamma}{2\zeta\omega_0^2\sqrt{1-\zeta^2}} - \frac{\gamma}{2\zeta\omega_0^2} \\
\Delta\omega &= \omega_a - \omega_p = \omega_0\sqrt{1-2\zeta^2} - \omega_0 \\
\Delta\phi &= \phi_a - \phi_p = \operatorname{atan}\frac{\sqrt{1-2\zeta^2}}{\zeta} - \frac{\pi}{2}
\end{aligned} \tag{2.23}$$

and perform a Taylor series expansion around $\zeta = 0$ for ΔA, $\Delta\omega$ and $\Delta\phi$, we obtain

$$\begin{aligned}
\Delta A &= \mathcal{O}\left(\zeta^2\right) \\
\Delta\omega &= \mathcal{O}\left(\zeta^2\right) \\
\Delta\phi &= \mathcal{O}\left(\zeta\right).
\end{aligned} \tag{2.24}$$

For illustration, the frequency response in Figure 2.1 calculated for $\zeta = 0.5\%$ and $\omega_0 = 1$ rad/s shows that the difference between the two resonance frequencies is indeed very small, i.e., 2.5×10^{-3} %.

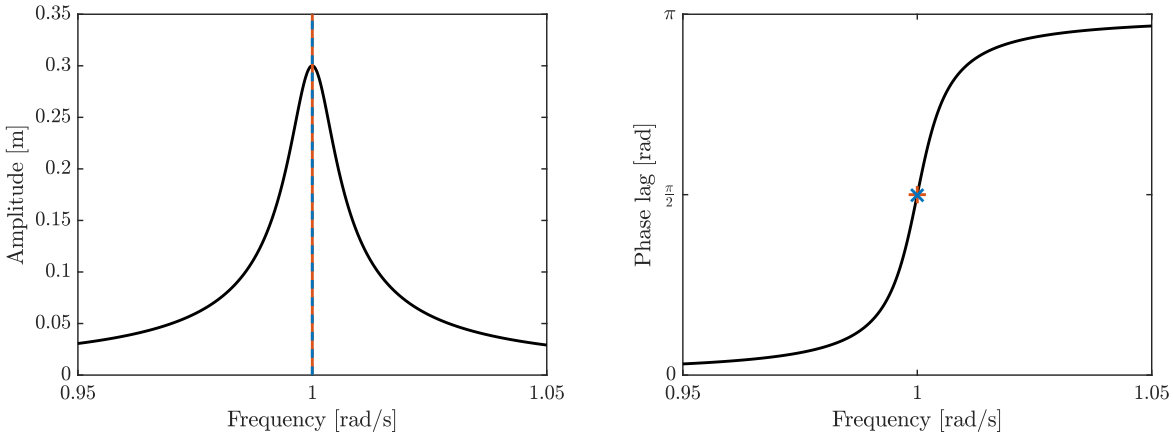

(a) **(b)**

Figure 2.1: Frequency response (black) of a linear oscillator for a forcing amplitude of 0.003 N/kg. (a) Amplitude and (b) phase lag. Amplitude (blue) and phase (orange) resonances.

2.3 Nonlinear oscillators

Calculating the response of a nonlinear oscillator of the form

$$m\ddot{x}(t) + kx(t) = f_{nl}\left(x(t), \dot{x}(t)\right) \tag{2.25}$$

with $f_{nl}\left(x(t), \dot{x}(t)\right)$ a nonlinear function, is much more complicated than in the linear case. Dedicated analytical (e.g., perturbations methods [11, 23]) and numerical (e.g., shooting [24–27] and HBM [4, 28, 29]) techniques are required. Some of them are reviewed in what follows and applied to the free vibration of the Duffing oscillator.

2.3.1 The undamped, unforced Duffing oscillator

We consider the free vibration of the undamped Duffing oscillator:

$$m\ddot{x}(t) + kx(t) + k_3x^3(t) = 0 \tag{2.26}$$

where k_3 is the cubic stiffness coefficient. Through mass normalization, we have

$$\ddot{x}(t) + \omega_0^2x(t) + \alpha_3x^3(t) = 0 \tag{2.27}$$

where $\alpha_3 = k_3/m$. In this study, the initial conditions are

$$x(0) = x_0, \quad \dot{x}(0) = 0. \tag{2.28}$$

2.3.1.1 The exact solution

There exists an exact analytical solution to Equation (2.27) based on Jacobi elliptic functions [12, 30, 31]

$$x(t) = A\,\mathrm{cn}\left(\omega_J t - \phi, \rho\right) \tag{2.29}$$

where cn is the *cosine elliptic* function with ω_J and ρ the frequency and the modulus of the Jacobi elliptic functions, respectively, such that

$$\omega_J = \sqrt{\omega_0^2 + \alpha_3 A^2} \tag{2.30}$$

$$\rho = \frac{\alpha_3 A^2}{2\left(\omega_0^2 + \alpha_3 A^2\right)}. \tag{2.31}$$

Plugging (2.29) into (2.27) leads to

$$A = \sqrt{-\frac{\omega_0^2}{\alpha_3} + \frac{\omega_0^2 + \alpha_3 x_0^2}{\alpha_3}\sqrt{1 + \frac{2\dot{x}_0^2\alpha_3}{\omega_0^2}}} \tag{2.32}$$

$$\frac{\mathrm{sn}(\phi,\rho)}{\mathrm{cn}(\phi,\rho)}\mathrm{dn}(\phi,\rho) = -\frac{\dot{x}_0}{x_0\omega_J} \tag{2.33}$$

for general initial displacement x_0 and velocity $\dot{x}_0$. With the initial conditions from (2.28), *i.e.*, when $\dot{x}_0 = 0$, we have $A = x_0$ and $\phi = 0$, leading to

$$x(t) = x_0\,\mathrm{cn}\left(\omega_J t, \rho\right). \tag{2.34}$$

The associated period T of the solution is

$$T = \frac{4K(\rho)}{\omega_J} \tag{2.35}$$

where $K(\rho)$ is the complete elliptic integral of first kind [30]. The corresponding frequency is

$$\omega = \frac{2\pi}{T} = \frac{\pi\omega_J}{2K(\rho)}. \tag{2.36}$$

For small-amplitude motion, ω can be simplified into

$$\omega = \omega_0\sqrt{1 + \frac{3\alpha_3}{4\omega_0^2}x_0^2}. \tag{2.37}$$

From (2.37), we see that if $\alpha_3 > 0$ ($\alpha_3 < 0$), then the frequency increases (decreases) with x_0 and the system is said to be hardening (softening).

There exist very few nonlinear systems that admit an exact analytical solution. For instance, the damped, forced Duffing oscillator does not admit such a solution. This is why we must rely on other techniques to find solutions that approximate, with a sufficient accuracy, the exact solution.

2.3.1.2 The averaging method

The averaging method (AM) is based on the Krylov and Bogoliubov technique [11, 32, 33]. It is applied to the general weakly nonlinear oscillator

$$\ddot{x}(t) + \omega_0^2 x(t) = \varepsilon \bar{f}_{nl}(x(t), \dot{x}(t)) \tag{2.38}$$

where $f_{nl}\left(x(t), \dot{x}(t)\right) = \varepsilon \bar{f}_{nl}\left(x(t), \dot{x}(t)\right)$, where $0 < \varepsilon \ll 1$ is a small parameter. When $\varepsilon = 0$, the system is *unperturbed*, and the periodic solution of (2.38) is written as

$$x(t) = A \sin\left(\omega_0 t - \phi\right) \tag{2.39}$$

where A and ϕ are constants. When $\varepsilon \neq 0$, the system is *perturbed*. It is assumed that the solution can still be expressed as in Equation (2.39) but with time-dependent, slowly-varying A and ϕ

$$x(t) = A(t) \sin\left(\omega_0 t - \phi(t)\right) \tag{2.40}$$

such that the velocity can be expressed with the same form as when $\varepsilon = 0$, *i.e.*,

$$\dot{x}(t) = A(t)\omega_0 \cos\left(\omega_0 t - \phi(t)\right). \tag{2.41}$$

Equation (2.41) holds only if

$$\dot{A}(t) \cos\left(\omega_0 t - \phi(t)\right) - A\dot{\phi}(t) \cos\left(\omega_0 t - \phi(t)\right) = 0. \tag{2.42}$$

Differentiating Equation (2.41) and replacing $\ddot{x}(t)$ and $x(t)$ in Equation (2.38) yields

$$\begin{aligned} \dot{A}(t)\omega_0 \cos\left(\omega_0 t - \phi(t)\right) + A(t)\dot{\phi}(t)\omega_0 \cos\left(\omega_0 t - \phi(t)\right) = \\ \varepsilon f\left[A(t) \sin\left(\omega_0 t - \phi(t)\right), A(t)\omega_0 \cos\left(\omega_0 t - \phi(t)\right)\right]. \end{aligned} \tag{2.43}$$

Finally, taking into account Equations (2.42) and (2.43) and solving for $\dot{A}$ and $\dot{\phi}$, a system of first-order equations is obtained

$$\begin{aligned} \dot{A} &= \frac{\varepsilon}{\omega_0} \bar{f}_{nl}\left[A(t) \sin\left(\omega_0 t - \phi(t)\right), A(t)\omega_0 \cos\left(\omega_0 t - \phi(t)\right)\right] \cos\left(\omega_0 t - \phi(t)\right) \\ \dot{\phi} &= \frac{\varepsilon}{A(t)\omega_0} \bar{f}_{nl}\left[A(t) \sin\left(\omega_0 t - \phi(t)\right), A(t)\omega_0 \cos\left(\omega_0 t - \phi(t)\right)\right] \sin\left(\omega_0 t - \phi(t)\right) \end{aligned} \tag{2.44}$$

where $\dot{A}$ and $\dot{\phi}$ are slowly varying since they are of order $\mathcal{O}(\varepsilon)$. This system has a suitable form for first-order averaging. These equations are thus integrated over the period of motion T during which A and ϕ are considered to be constant

$$\begin{aligned} \dot{A} &= \frac{\varepsilon}{\omega_0} \frac{1}{T} \int_0^T \bar{f}_{nl}\left[\sin\left(\omega_0 t - \phi\right), A\omega_0 \cos\left(\omega_0 t - \phi\right)\right] \cos\left(\omega_0 t - \phi\right) \mathrm{d}t \\ \dot{\phi} &= \frac{\varepsilon}{A\omega_0} \frac{1}{T} \int_0^T \bar{f}_{nl}\left[A \sin\left(\omega_0 t - \phi\right), A\omega_0 \cos\left(\omega_0 t - \phi\right)\right] \sin\left(\omega_0 t - \phi\right) \mathrm{d}t \end{aligned} \tag{2.45}$$

Applying the AM to Equation (2.27) where $\alpha_3 = \varepsilon\bar{\alpha}_3$ yields

$$\dot{A} = 0 \ , \quad \dot{\phi} = -\frac{3\alpha_3}{8\omega_0}A^2. \tag{2.46}$$

A is thus a constant C_1 and $\phi = -\frac{3\alpha_3}{8\omega_0}A_0^2 t + C_2$, where $C_1 = x_0$ and $C_2 = \frac{\pi}{2}$ based on the initial conditions (2.28). Eventually,

$$x(t) = x_0 \cos\left(\omega_0\left[1 + \frac{3\alpha_3}{8\omega_0^2}x_0^2\right]t\right) + \mathcal{O}(\varepsilon) \tag{2.47}$$

where the frequency of the free vibration increases ($\alpha_3 > 0$) or decreases ($\alpha_3 < 0$) with the initial displacement x_0

$$\omega = \omega_0 + \frac{3\alpha_3}{8\omega_0}x_0^2 \tag{2.48}$$

2.3.1.3 The method of multiple scales

The method of multiple scales (MMS) [23] also solves weakly nonlinear oscillators as expressed in Equation (2.38). If $\varepsilon = 0$, the solution $x(t)$ can be expressed as in Equation (2.3). When $0 < \varepsilon \ll 1$, the solution $x(t)$ is seen as an asymptotic expansion of the form

$$x(t) = y_0(t) + \varepsilon y_1(t) + \varepsilon^2 y_2(t) + \varepsilon^3 y_3(t) + \dots \tag{2.49}$$

where each term y_i in the expansion adds a smaller and smaller correction to the solution. In general, only a few terms are retained in the approximate solution.

The MMS assumes that the expansion is a function of multiple independent time scales rather than only t. To do so, N new time scales T_0, T_1,..., T_N are introduced

$$T_n = \varepsilon^n t \tag{2.50}$$

where n is an integer such that T_n is slower than T_{n-1}. $x(t)$ thus takes the form

$$\begin{aligned} x(t,\varepsilon) &= y_0(T_0, T_1, T_2, \dots) + \varepsilon y_1(T_0, T_1, T_2, \dots) + \varepsilon^2 y_2(T_0, T_1, T_2, \dots) + \dots \\ &= \sum_{i=0}^{N-1} y_n(T_0, T_1, T_2, \dots, T_N) + \mathcal{O}\left(\varepsilon T_N\right) \end{aligned} \tag{2.51}$$

The error being of the order of $\mathcal{O}\left(\varepsilon T_N\right)$, this expansion is valid for times up to $\mathcal{O}\left(\varepsilon^{-N}\right)$. Time derivatives are calculated using the chain rule

$$\begin{aligned} \frac{d}{dt} &= D_0 + \varepsilon D_1 + \varepsilon^2 D_2 + \dots \\ \frac{d^2}{dt^2} &= D_0^2 + 2\varepsilon D_1 D_0 + \varepsilon^2(D_1 + 2D_2 D_0) + \dots \end{aligned} \tag{2.52}$$

where $D_n = \frac{\partial}{\partial T_n}$. Substituting Equations (2.51) and (2.52) into Equation (2.38) and equating the coefficients of like powers of ε, a set of N partial differential equations is to

be solved sequentially. For a first-order approximation, *i.e.*, writing $x(t,\varepsilon) = y_0(T_0,T_1) + \varepsilon y_1(T_0,T_1) + \dots$ and subsituting in Equation (2.38) gives

$$D_0^2 y_0 + \omega_0^2 y_0 = 0 \tag{2.53}$$
$$D_0^2 y_1 + \omega_0^2 y_1 = \bar{f}_{nl}(u_0, D_0 u_0) - 2D_1 D_0 u_0 \tag{2.54}$$

The general solution of Equation (2.53) is

$$y_0 = A\sin(\omega_0 T_0 - \phi) \tag{2.55}$$

which can be injected into Equation (2.54) to yield

$$\begin{aligned} D_0^2 y_1 + \omega_0^2 y_1 =& \bar{f}_{nl}(A\sin(\omega_0 T_0 - \phi), A\omega_0\cos(\omega_0 T_0 - \phi)) \\ &- 2A'\omega_0\cos(\omega_0 T_0 - \phi) - 2A\phi'\omega_0\sin(\omega_0 T_0 - \phi) \end{aligned} \tag{2.56}$$

The symbol $'$ represents the partial derivative with respect to T_1. In order to keep εu_1 small compared to u_0, the secular terms are eliminated in Equation (2.56), *i.e.*, the coefficients of $\sin(\omega_0 T_0 - \phi)$ and $\cos(\omega_0 T_0 - \phi)$ are set to 0. The two new equations govern the evolution of A and ϕ.

Applying the MMS to Equation (2.27) where α_3 is scaled such that $\alpha_3 = \varepsilon\bar{\alpha}_3$ yields

$$A' = 0\ , \quad \phi' = -\frac{3\bar{\alpha}_3}{8\omega_0}A^2. \tag{2.57}$$

A is thus a constant C_1 and $\phi = -\frac{3\alpha}{8\omega_0}A_0^2 T_1 + C_2$ where $C_1 = x_0$ and $C_2 = \frac{\pi}{2}$ based on the initial conditions of the system. Finally, replacing T_0 and T_1 by t and εt, respectively, the MMS gives at first approximation the same solution as with the AM both for the displacement

$$x(t) = x_0\cos\left(\omega_0\left[1 + \frac{3\alpha_3}{8\omega_0^2}x_0^2\right]t\right) + \mathcal{O}(\varepsilon) \tag{2.58}$$

and the frequency

$$\omega = \omega_0 + \frac{3\alpha_3}{8\omega_0}x_0^2. \tag{2.59}$$

2.3.1.4 The harmonic balance method

The harmonic balance method (HBM) has been used extensively in the literature to compute the periodic responses of large-scale nonlinear mechanical systems [29, 34–38]. The periodic solutions are represented as truncated Fourier series up to the order N_H

$$x(t) = c_0 + \sum_{l=1}^{N_H}(s_l\sin\omega_l t + c_l\cos\omega_l t) = \sum_{l=0}^{N_H} A_l\sin(\omega_l t - \phi_l) \tag{2.60}$$

where $A_l = \sqrt{s_l^2 + c_l^2}$, $\phi_l = \mathrm{atan2}(-c_l, s_l)$ and $\omega_l = \frac{l\omega}{\nu}$, where ν is an integer. The ν-th harmonic of the series $l = \nu$ is defined as the fundamental harmonic whereas the other harmonics are defined as secondary harmonics.

Substituting Equation (2.60) in Equation (2.27), equating the coefficient of each harmonic $\sin \omega_l t$ and $\cos \omega_l t$ to 0 and neglecting the higher-order harmonic terms produced by the nonlinearities results in a set of $2N_H + 1$ nonlinear algebraic equations to solve for $2N_H + 2$ unknowns, namely ω and the $2N_H + 1$ Fourier coefficients. An additional equation, the phase condition [25], is needed to close the system. In general, this phase condition sets the phase lag of the first harmonic ϕ_1 to 0 or, equivalently, c_1 to 0. The system can then be solved using, for example, a Newton-Raphson procedure. Limiting our developments to the first harmonic provides an analytical approximation of the frequency of the free response

$$\omega = \omega_0 \sqrt{1 + \frac{3\alpha_3}{4\omega_0^2} A_1^2}. \tag{2.61}$$

The displacement is expressed as

$$x(t) = A_1 \sin\left(\left[\omega_0 \sqrt{1 + \frac{3\alpha_3}{4\omega_0^2} A_1^2}\right] t - \phi_1\right). \tag{2.62}$$

Using the initial conditions (2.28), we find that $A_1 = x_0$ and $\phi_1 = \frac{\pi}{2}$, yielding

$$\omega = \omega_0 \sqrt{1 + \frac{3\alpha_3}{4\omega_0^2} x_0^2} \tag{2.63}$$

and

$$x(t) = x_0 \cos\left(\left[\omega_0 \sqrt{1 + \frac{3\alpha_3}{4\omega_0^2} x_0^2}\right] t\right). \tag{2.64}$$

The frequency corresponds to that of the exact solution in Equation (2.37) when small amplitudes are considered. Furthermore, if x_0 is small, we perform a Taylor expansion of Equation (2.61) up to the second order such that

$$\omega = \omega_0 \left(1 + \frac{3\alpha_3}{8\omega_0^2} x_0^2\right) + \mathcal{O}(x_0^3). \tag{2.65}$$

Equation (2.64) is rewritten as

$$x(t) = x_0 \cos\left(\omega_0 \left[1 + \frac{3\alpha_3}{8\omega_0^2} x_0^2\right] t\right) \tag{2.66}$$

and we retrieve the solution obtained using the AM and MMS in Equations (2.47) and (2.58), respectively.

A more accurate response can be found by adding more harmonics in the approximate solution. In practice, however, only the first few harmonics which have a non-negligible amplitude are retained. This is especially the case for large-scale nonlinear systems where a trade-off between accuracy and computational cost is usually sought.

2.3.1.5 Comparison of the analytical solutions

The different methods highlight that, as the motion amplitude increases, the frequency increases or decreases when α_3 is positive or negative, respectively. This evolution is depicted in Figure 2.2a with $\omega_0 = 1$ rad/s and $\alpha_3 = 0.1$ N/(kg.m^3). At small amplitudes, all methods agree well. When the amplitude increases, the discrepancy between the frequency of the exact solution and of the approximation methods increases; the HBM with one harmonic corresponds to the most accurate approximation. For an initial displacement of 3m, the frequency error with HBM is around 0.3% whereas it is around 3.7% for the AM and MMS. This is because the latter methods assume a small scaling parameter ε.

The displacement in Figure 2.2b confirms the superior accuracy of the HBM. However, the corresponding velocity and acceleration signals in Figure 2.3 evidence that the higher-order harmonics are missed by the HBM with one harmonic. The addition of a third harmonic greatly improves the agreement with the exact solution.

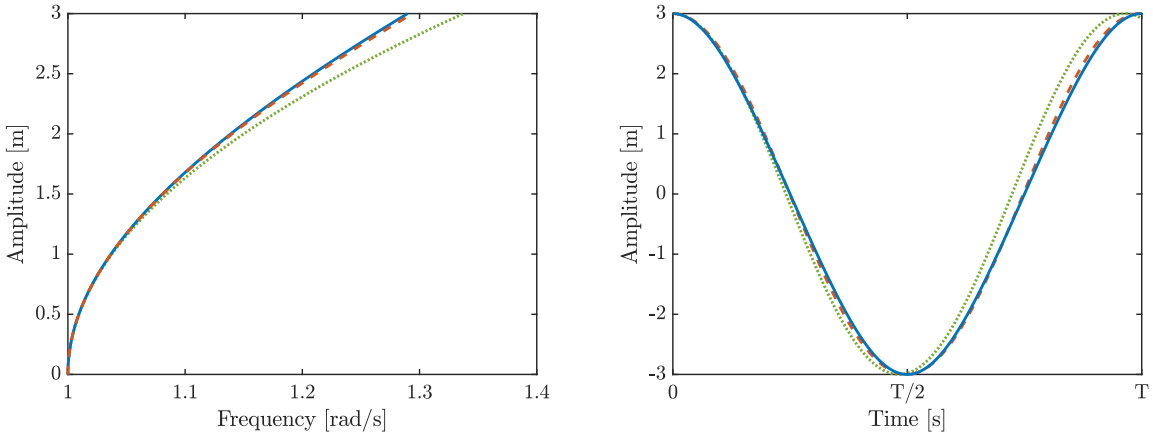

(a) **(b)**

Figure 2.2: (a) Frequency as a function of the amplitude of the Duffing oscillator with $\alpha_3 = 0.1$ and $\omega_0 = 1$, and (b) displacement. Blue: exact solution; orange: HBM with one harmonic, and green: AM and MMS.

2.3.2 The harmonically-forced, damped Duffing oscillator

The resonances of a harmonically-forced, damped Duffing oscillator

$$m\ddot{x}(t) + c\dot{x}(t) + kx(t) + k_3x^3(t) = f\sin\omega t \tag{2.67}$$

are studied in detail in this section. The Duffing oscillator is said to be hardening when $k_3 > 0$, and softening when $k_3 < 0$ as evidenced in Section 2.3.1.1. Through mass normalization, Equation (2.67) is recast into

$$\ddot{x}(t) + 2\zeta\omega_0\dot{x}(t) + \omega_0^2x(t) + \alpha_3x^3(t) = \gamma\sin\omega t. \tag{2.68}$$

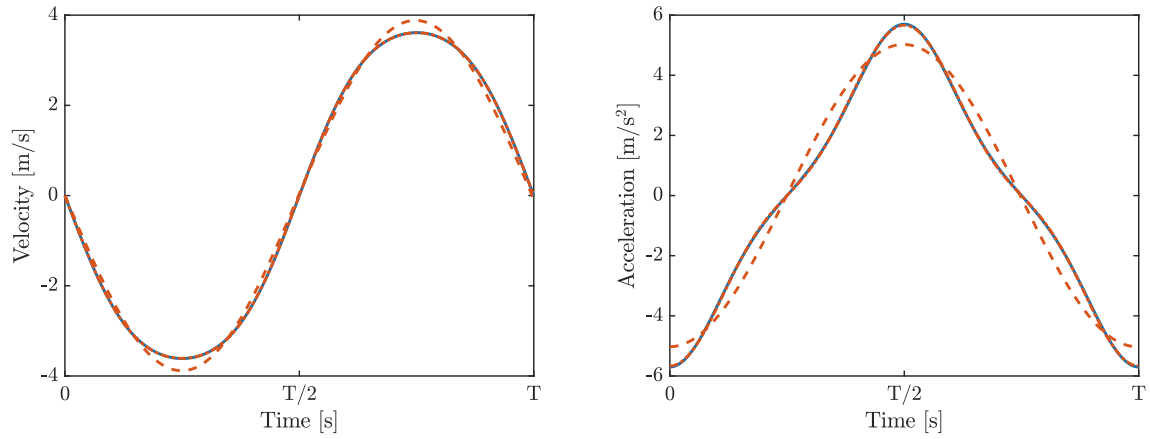

(a) **(b)**

Figure 2.3: Time series of the Duffing oscillator: (a) Velocity and (b) acceleration. Blue: exact solution; orange: HBM with 1 (dashed) and 3 (dotted) harmonics.

It should be noted that Equation (2.68) can be further normalized by scaling the time and amplitude variables as $\tau = \omega_0 t$ and $\chi = \frac{\sqrt{\alpha}}{\omega_0} x$ such that:

$$\tilde{\tilde{\chi}} + 2\zeta\tilde{\chi} + \chi + \chi^3 = \kappa \sin \frac{\omega}{\omega_0}\tau \tag{2.69}$$

with $\tilde{\chi} = \frac{d\chi}{d\tau}$. In this case, only two parameters remain free, namely the damping ratio ζ and the forcing $\kappa = \frac{\sqrt{\alpha_3}\gamma}{\omega_0^3}$ [19]. However, this formulation is not retained here. Equation (2.68) can be solved analytically using, for instance, the MMS for the primary resonance but also for the 3:1 and 1:3 resonances [4, 11, 23]. Since the MMS is restricted to weak nonlinearities, Equation (2.68) is solved numerically using HBM. This allows to study a wider range of forcing amplitudes. Each harmonic l of the Fourier series of the response may trigger a resonance if $\omega_l = l\omega/\nu$ corresponds to the (amplitude-dependent) frequency of the primary resonance of the system. According to Stoker [39], the resonances can be divided into four categories, namely

- $1:1$ primary/fundamental resonance ($l = \nu = 1$);
- $l:1$ superharmonic or ultraharmonic resonances;
- $1:\nu$ subharmonic resonances;
- $l:\nu$ ultra-subharmonic resonances.

The resonances are calculated using $15 \times \nu$ harmonics where the value of ν depends on the type of resonance studied. The system parameters are $\zeta = 0.5\%$, $\omega_0 = 1$ rad/s and $\alpha_3 = 1$ N/(kg.m^3). Stability analysis is also performed using Hill's method in the HBM formalism [36, 40].

2.3.2.1 Primary resonance

The primary resonance is excited by setting the forcing frequency ω in the vicinity of ω_0. Figure 2.4 illustrates the NFRCs for the hardening ($\alpha_3 = 1$ N/(kg.m^3)) and softening ($\alpha_3 = -1$ N/(kg.m^3)) cases for a forcing of $\gamma = 0.003$ N/kg. In both cases, the frequency shift leads to multi-stable solutions delimited by the fold bifurcations, *i.e.*, when $\frac{\partial \omega}{\partial A} = 0$, which can lead to a jump phenomenon [11, 39]. The solutions between the two bifurcations are unstable. Furthermore, it is observed that for the same forcing, the softening (resp. hardening) oscillator leads to the greatest (resp. lowest) maximum amplitude.

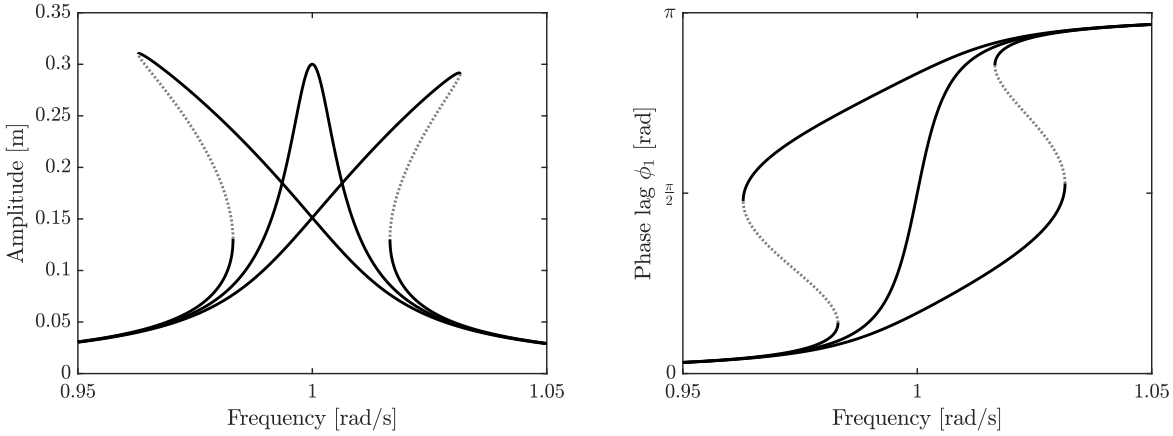

(a) **(b)**

Figure 2.4: NFRCs around the primary resonance of the hardening and softening Duffing oscillators and the linear oscillator ($\gamma = 0.003$ N/kg): (a) amplitude and (b) phase lag. Black: stable; grey: unstable.

2.3.2.2 Secondary resonances

$\gamma = 0.25$ N/kg

At this forcing level, two secondary resonances can be observed in Figure 2.5, namely a small peak around $\omega_0/3$ and an isolated branch after $3\omega_0$.

Figure 2.6a represents the 3:1 superharmonic resonance around $\omega_0/3$ whereas Figure 2.6b displays the harmonic ratio for the first and third harmonics. This latter figure evidences the underlying mechanism, i.e., since $3\omega \simeq \omega_0$, the third harmonic enters into resonance and dictates the dynamics of the response.

The $1:3$ subharmonic resonance in Figure 2.7 appears as an isolated response, *i.e.*, it is detached from the main branch. In this case, the first harmonic in the vicinity of the primary resonance is dominant throughout the resonance; the third harmonic is almost absent. Both resonances, as for primary resonances, can have unstable and multi-stable solutions that seem to appear between the fold bifurcations.

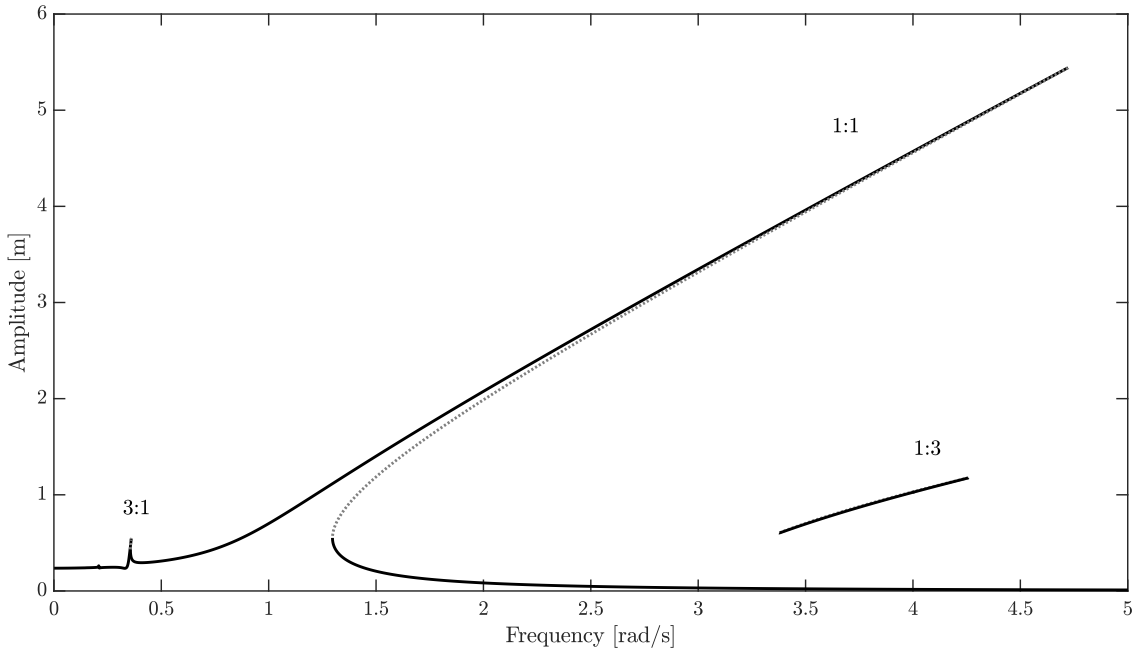

Figure 2.5: NFRC of the Duffing oscillator ($\gamma = 0.25$ N/kg). Black: stable; grey: unstable.

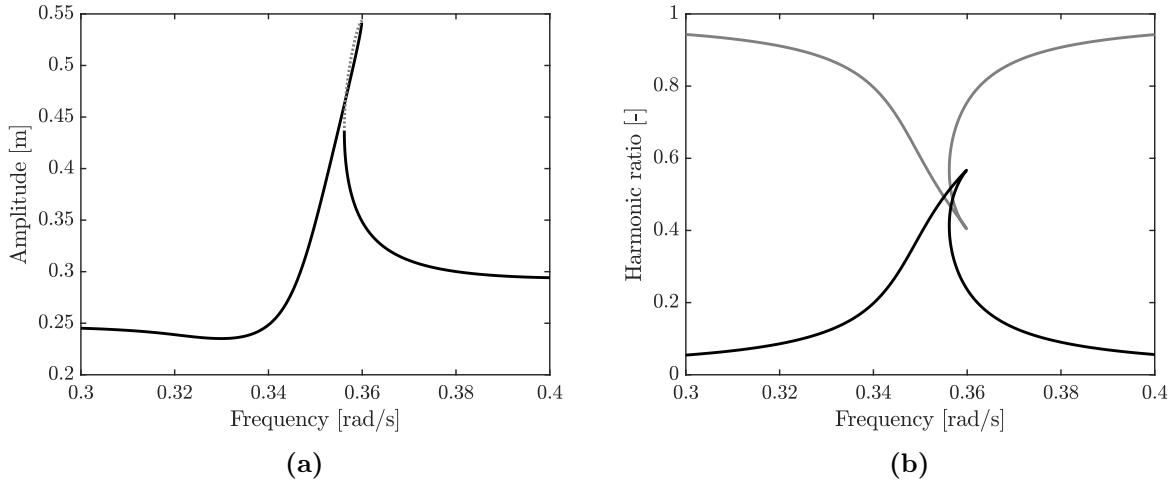

Figure 2.6: NFRC around the 3:1 resonance ($\gamma = 0.25$ N/kg): (a) amplitude (black: stable; grey: unstable) and (b) harmonic ratio (black: $l = 3$; grey: $l = 1$).

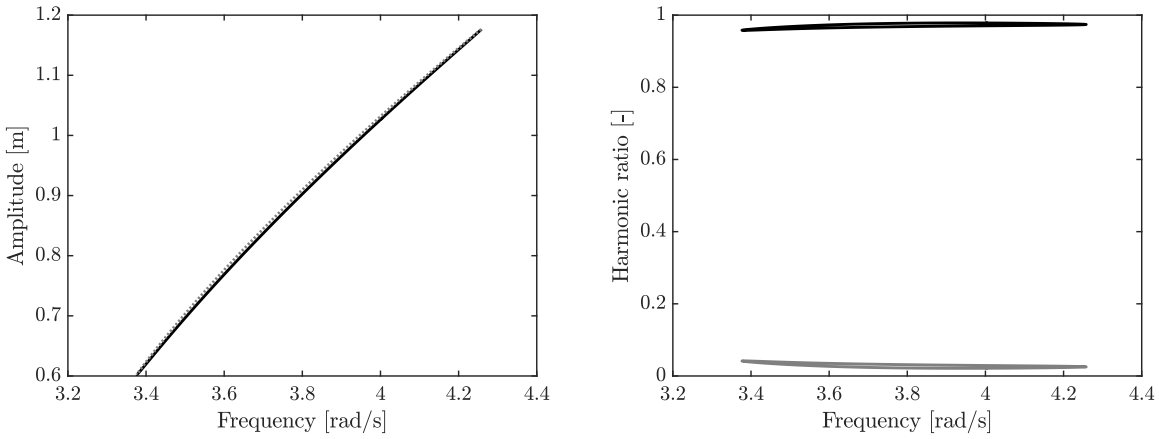

(a) **(b)**

Figure 2.7: NFRC around the 1:3 resonance ($\gamma = 0.25$ N/kg): (a) amplitude (black: stable; grey: unstable) and (b) harmonic ratio (black: $l = 1$; grey: $l = 3$).

$\gamma = 1$ N/kg

In addition to the 3:1 and 1:3 resonances, new secondary resonances appear in Figure 2.8, both below and above the primary resonance.

Figure 2.9a reveals that a series of superharmonic resonances for which l is odd and $\nu = 1$ appear in the direct continuation of the main branch. We thus observe the 3:1, 5:1, 7:1... resonances. For each of these resonances, the corresponding harmonic l becomes more and more dominant in the response as the forcing increases. Besides, around $\omega = 0.72$ rad/s, a loss of stability occurs on the main branch, and another resonance bifurcates out of it. The same scenario appears between the 5:1 and 3:1 resonances. These resonances correspond to even superharmonic resonances, namely the 2:1 and 4:1 resonances, respectively. Figure 2.9b highlights that the 2:1 resonance follows a mechanism similar to the odd resonances. The newly-created 1:2 subharmonic resonance is plotted in Figure 2.10.

$\gamma = 3$ N/kg

Many new $l : \nu$ resonances (with both l and ν different from 1) appear as isolated branches in the superharmonic and subharmonic regimes in Figure 2.11.

Close-ups of the superharmonic and subharmonic resonances are available in Figures 2.12a and 2.12b, respectively. In the superharmonic case, apart from the odd and even $k : 1$ resonances, we can observe from left to right the 7:2, 7:3, 5:3, 3:2, 7,5 and 4:3 ultra-subharmonic resonances. In the subharmonic regime, from left to right, we observe the 1:4, 5:7, 2:3 and 3:5 ultra-subharmonic resonances, as well as the 1:2 and 1:3 resonances. For each $l : \nu$ resonance, as the forcing increases, the l-th harmonic is more and more dominant compared to the other harmonics of the response. Finally, we note that each resonance for which $\nu > 1$ appears as an isolated branch.

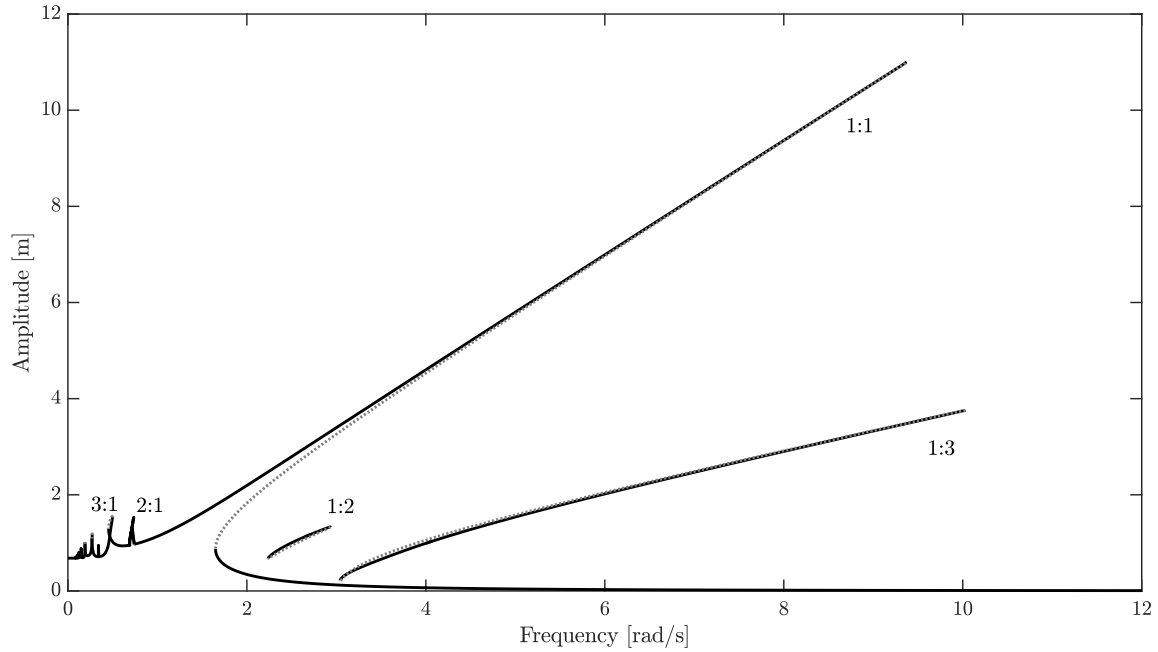

Figure 2.8: NFRC of the Duffing oscillator ($\gamma = 1$ N/kg). Black: stable; grey: unstable.

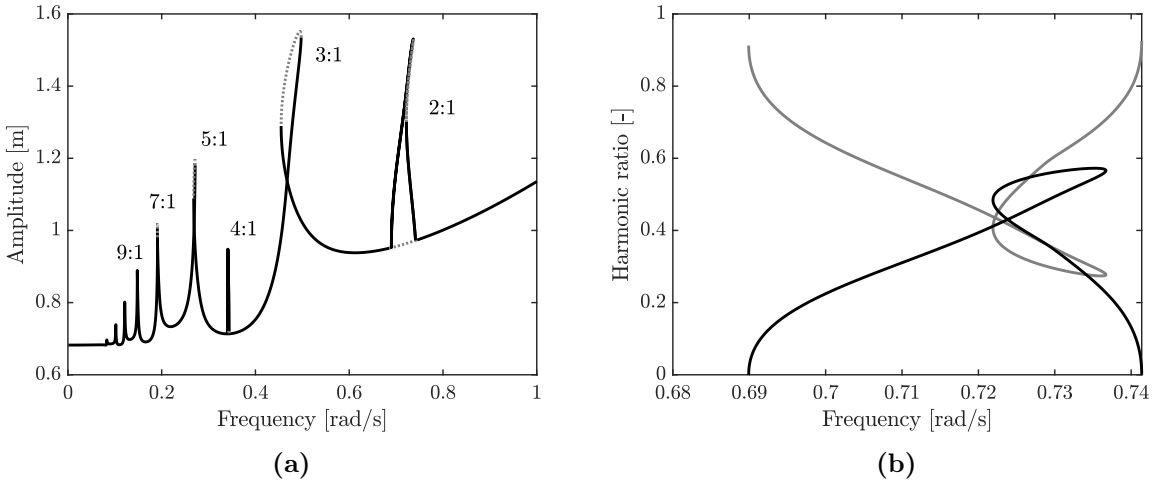

Figure 2.9: NFRC in the superharmonic regime ($\gamma = 1$ N/kg): (a) amplitude (black: stable; grey: unstable) and (b) harmonic ratio ($l = 2$: black, $l = 1$: grey).

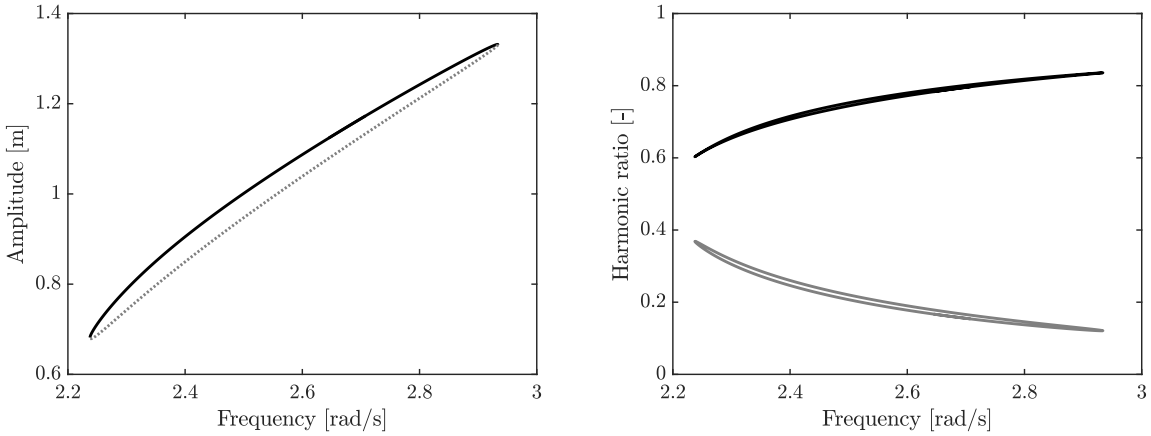

Figure 2.10: NFRC around the 1:2 resonance ($\gamma = 1$ N/kg): (a) amplitude (black: stable; grey: unstable) and (b) harmonic ratio ($l = 1$: black, $l = 2$: grey).

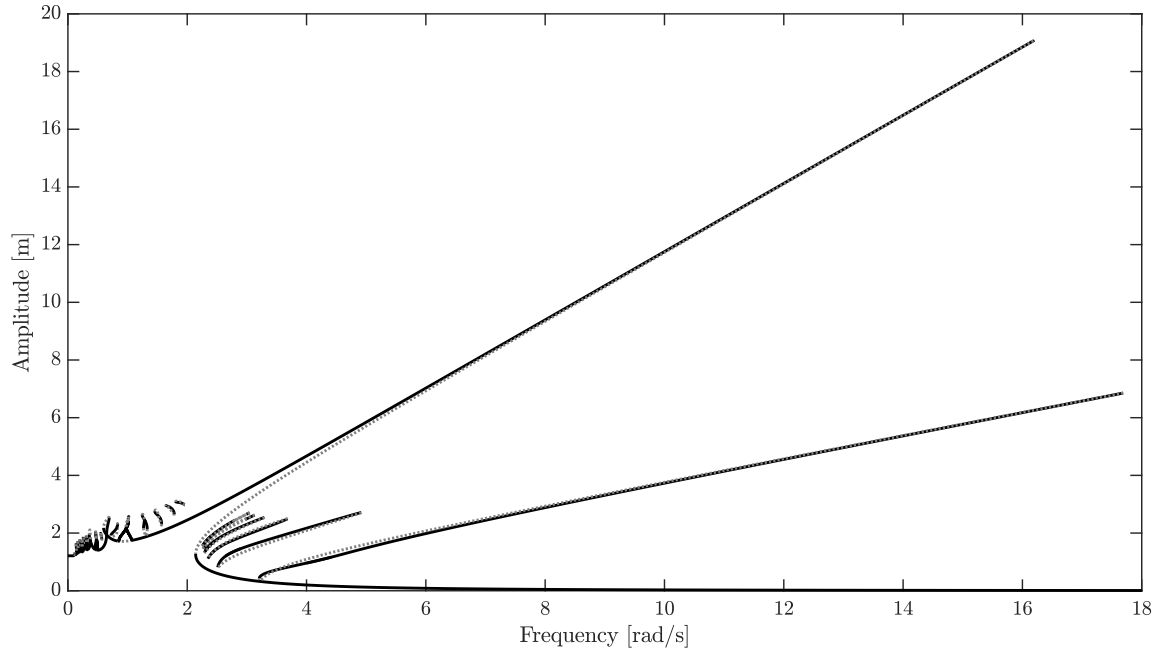

Figure 2.11: NFRC of the Duffing oscillator ($\gamma = 3$ N/kg). Black: stable; grey: unstable.

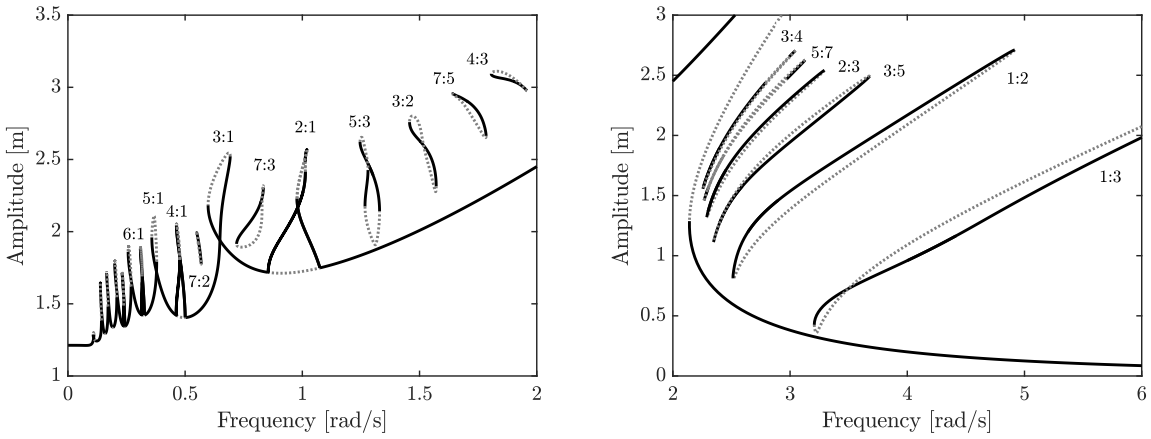

(a) **(b)**

Figure 2.12: NFRC of the Duffing oscillator ($\gamma = 3$ N/kg): (a) superharmonic regime and (b) subharmonic regime. Black: stable; grey: unstable.

2.4 Conclusions and discussion

In this chapter, the resonances of linear and Duffing oscillators were studied both analytically and numerically to highlight the main differences that exist between linear and nonlinear systems.

As exemplified in Figures 2.4, 2.5, 2.8 and 2.11, the resonant behavior of nonlinear systems is much more complex than that of linear systems. First, the primary resonance undergoes a hardening effect that shifts the resonance peak toward greater frequencies. This is accompanied by the appearance of two fold bifurcations giving rise to the coexistence of stable and unstable solutions. The presence of multiple solutions can lead to a jump phenomenon, *i.e.*, the system can switch from one stable solution to another, with potential damage to the system [5, 11]. Another major difference with linear systems is the multi-harmonic nature of the system response, which can, in turn, generate secondary resonances. As seen in Figure 2.11, before and after the primary resonance, many resonance peaks coexist. The l:1 superharmonic resonances with l odd, associated with the resonance of the l-th harmonic of the Fourier series, appear in the continuation of the main branch; they can thus be easily calculated using numerical continuation [41, 42]. Conversely, the l:1 superharmonic resonances with l even bifurcate out of the main branch, meaning that they should be calculated using advanced bifurcation analysis techniques [29, 43, 44]. The remaining resonances appear as isolated branches of solutions, require a minimum forcing amplitude to exist and can be revealed through the calculation of basins of attraction.

All in all, characterizing the resonant behavior of a nonlinear system remains a great challenge both numerically and experimentally; it represents the main thrust of this thesis.

Definition of the resonances of linear systems

The most natural definition of a resonance is the amplitude resonance. Expressing the system's response as $x(t) = A\sin(\omega t - \phi)$, amplitude resonance corresponds to a local maximum in the frequency response function, i.e., $\frac{\mathrm{d}A}{\mathrm{d}\omega} = 0$.

A much less obvious definition is the phase resonance introduced by Fraiejs de Veubeke [45]. It occurs when the motion is in quadrature with the excitation, i.e., $\phi_p = \frac{\pi}{2}$. The underlying motivation for phase resonance testing [46] is that the structural response corresponds to the undamped normal mode and that the excitation frequency is the natural frequency of the undamped system; this greatly facilitates the correlation between numerical and experimental results. Moreover, since the phase is very sensitive to frequency alterations in the neighborhood of resonance, the phase measurement is an ideal way to ascertain resonance conditions. The consideration of phase resonance is particularly suitable in the case of light damping, because it occurs in the immediate neighborhood of amplitude resonance. Historically, phase resonance laid down the foundations of the first experimental modal analysis methods.

Definition of the resonances of nonlinear systems

For nonlinear oscillators, the response $x(t)$ is written as a Fourier series

$$x(t) = \sum_{l=0}^{\infty} A_l \sin(\omega_l t - \phi_l) \tag{2.70}$$

and any harmonic l can trigger a resonance $l:\nu$, as discussed in Section 2.3.2. The response has a period $T_\nu = \frac{2\nu\pi}{\omega}$ which corresponds to the period of its first harmonic term. The maximum of amplitude over one period T_ν is labelled $A_{\max}$.

Amplitude resonance

The amplitude resonance of a nonlinear system occurs when $\frac{\mathrm{d}A_{max}}{\mathrm{d}\omega} = 0$. Despite its apparent simplicity, this definition is not straightforward to implement numerically and experimentally. Indeed, it is only very recently that a multi-harmonic numerical continuation method that can track the locus of the points of maximum amplitude has been devised [47]. Experimentally, no such method exists yet.

Because the l-th harmonic plays a key role in the dynamics of the $l{:}\nu$ resonance, a simpler alternative is to consider the amplitude resonance of this harmonic, i.e., $\frac{\mathrm{d}A_l}{\mathrm{d}\omega} = 0$. Since a single harmonic comes into play, this definition facilitates analytical and numerical investigations. For instance, Petrov [48] was the first to develop a numerical method to track the amplitude resonance of a single harmonic, both for primary and odd superharmonic resonances. Interestingly, Renault et al [49] proposed a similar method to track the antiresonances of nonlinear frequency responses. However, an experimental version of those algorithms is yet to be developed.

Phase resonance

Similarly to linear systems, the phase resonance of a nonlinear system amounts to excite the undamped nonlinear normal mode (NNM) at the undamped nonlinear natural frequency. To do so, a multi-harmonic forcing must counterbalance the damping forces with the result that each harmonic of the displacement is in phase quadrature with the corresponding harmonic of the forcing [50]. If the numerical computation of nonlinear modes has now reached maturity [26, 27, 51, 52], there is still no constructive experimental method to identify the NNMs *exactly* as this requires an unpractical multi-point, multi-harmonic forcing. We note that a relatively accurate identification of an isolated NNM can be obtained using phase quadrature testing and mono-point, mono-harmonic forcing [26, 50, 53, 54], but secondary resonances and modal interactions cannot be tackled using this testing strategy.

Goal of the thesis

It turns out that none of the previous definitions of a nonlinear resonance can be applied numerically and experimentally to primary and secondary resonances. To address this problem, we make the choice to restrict ourselves in this thesis to nonlinear systems excited by a mono-point, mono-harmonic forcing. This choice is also motivated by the fact that this is a commonly-used excitation signal in academia and industry.

Inspired by the work of Leung and Fung in [55] and the recent progress of phase-locked-loop testing [16–20], we concentrate our attention on the evolution of the phase lag between the l-th harmonic of the displacement and the harmonic forcing around the $l{:}\nu$ resonance. Specifically, nonlinear resonance is said to occur at the phase lag which corresponds to the amplitude resonance of the l-th harmonic. This strategy is termed *phase resonance of the l-th harmonic*, and the corresponding phase lag is termed *resonant phase lag*. For primary resonances, the resonant phase lag is $\pi/2$ [50, 56]. Interestingly, Haller demonstrated using Melnikov analysis that the resonant phase lag is close to $\pi/2$ for $1:\nu$ subharmonic resonances with ν odd, but the proof was for the ν-th harmonic and not the l-th harmonic. Consequently, one key objective of this thesis is to determine the resonant phase lags for the different families of secondary resonances. This will be (i) achieved through analytical developments in Chapters 3 and 4, (ii) validated numerically for SDOF and MDOF systems in Chapters 5 and 6, and (iii) demonstrated experimentally in Chapter 6.

If successful, this strategy would be particularly suitable for numerical and experimental investigations. Indeed, it is relatively easy to follow a specific phase lag numerically using numerical continuation but also experimentally using phase-locked loops. An important remark is that, because mono-harmonic forcing is considered, the structural deformation at the phase resonance of the l-th harmonic will deviate away from a NNM and will be termed *phase resonance nonlinear mode* (PRNM) in this manuscript.

Chapter 3

Primary resonance of nonlinear oscillators

3.1 Introduction

Exact analytical solutions of nonlinear mechanical systems do not always exist even for very simple problems. For instance, the undamped, unforced Duffing oscillator admits an exact analytical solution, but the damped, forced one does not. Therefore, perturbation techniques are often used to derive approximate analytical solutions provided that the problem at hand is weakly nonlinear. Several perturbation techniques exist in the literature. Among them, the AM and the MMS were already discussed in Chapter 2 for the undamped, unforced Duffing oscillator. Other techniques exist such as the Melnikov analysis [32, 57] and normal forms theory [58–62].

In the first part of this chapter, a near-resonance AM is applied to a damped, forced oscillator with polynomial stiffness to derive analytical solutions around the primary resonance. A peculiar attention is devoted to the amplitude and phase resonances as well as their stability. In the second part of the chapter, the analytical solutions for different systems, including the Duffing oscillator [4, 15, 22, 63–68], the Helmholtz oscillator [69] and an oscillator with quintic and sceptic stiffness, are compared to the numerical solution computed with the HBM.

3.2 Oscillator with polynomial stiffness

The equation of motion of a harmonically-forced, damped oscillator with polynomial stiffness is

$$m\ddot{x}(t) + c\dot{x}(t) + kx(t) + \sum_{d=2}^{n} k_d x^d(t) = f \sin \omega t \tag{3.1}$$

where k_d represents the nonlinear stiffness coefficient of order d. The natural frequency of the undamped, linearized system is $\omega_0 = \sqrt{\frac{k}{m}}$. Through mass normalization, Equation

(3.1) can be recast into

$$\ddot{x}(t) + 2\zeta\omega_0\dot{x}(t) + \omega_0^2 x(t) + \sum_{d=2}^{\infty} \alpha_d x^d(t) = \gamma \sin \omega t \tag{3.2}$$

where $\alpha_d = k_d/m$. Equation (3.2) is scaled such that $\zeta = \varepsilon\bar{\zeta}$, $\alpha_d = \varepsilon\bar{\alpha}_d$ and $\gamma = \varepsilon\bar{\gamma}$, with $\bar{\zeta}$, $\bar{\alpha}_d$, $\bar{\gamma} = \mathcal{O}(1)$ and $0 < \varepsilon \ll 1$ a small parameter, to obtain a weakly nonlinear oscillator

$$\ddot{x}(t) + \omega_0^2 x(t) = \varepsilon \left(\bar{\gamma} \sin \omega t - 2\bar{\zeta}\omega_0\dot{x}(t) - \sum_{d=2}^{\infty} \bar{\alpha}_d x^d(t) \right). \tag{3.3}$$

Since this oscillator is forced harmonically with a frequency ω, we seek a near-resonance solution of frequency ω close to ω_0 [70].

3.2.1 The near-resonance averaging method

The response of system (3.3) is expressed using a Van der Pol transformation with a frequency ω such that $\omega^2 - \omega_0^2 = \varepsilon\Omega$

$$x(t) = u(t) \cos \omega t - v(t) \sin \omega t. \tag{3.4}$$

The rest of the procedure is similar to that in Section 2.3.1.2. First, we impose the condition that the velocity should be

$$\dot{x}(t) = -u(t)\omega \sin \omega t - v(t)\omega \cos \omega t \tag{3.5}$$

which only holds if

$$\dot{u}(t) \cos \omega t - \dot{v}(t) \sin \omega t = 0. \tag{3.6}$$

Second, we differentiate Equation (3.5) and replace $\ddot{x}(t)$ and $x(t)$ in Equation (2.38). It yields

$$\dot{u}(t)\omega \sin \omega t + \dot{v}(t)\omega \cos \omega t = -\varepsilon \left(\bar{f}_{nl}(x(t), \dot{x}(t)) + \Omega x(t) \right). \tag{3.7}$$

The frequency detuning parameter Ω now appears in the weakly nonlinear term. Finally, taking into account Equations (3.6) and (3.7) and solving for $\dot{u}$ and $\dot{v}$, a system of first-order equations is obtained

$$\begin{cases} \dot{u}(t) = -\frac{\varepsilon}{\omega} \left(\bar{f}_{nl}(x(t), \dot{x}(t)) + \Omega x(t) \right) \sin \omega t \\ \dot{v}(t) = -\frac{\varepsilon}{\omega} \left(\bar{f}_{nl}(x(t), \dot{x}(t)) + \Omega x(t) \right) \cos \omega t \end{cases} \tag{3.8}$$

which has a suitable form to apply first-order AM

$$\begin{cases} \dot{u}(t) = -\frac{\varepsilon}{\omega} \frac{1}{T} \int_0^T \left(\bar{f}_{nl}(x(t), \dot{x}(t)) + \Omega x(t) \right) \sin \omega t \, \mathrm{d}t \\ \dot{v}(t) = -\frac{\varepsilon}{\omega} \frac{1}{T} \int_0^T \left(\bar{f}_{nl}(x(t), \dot{x}(t)) + \Omega x(t) \right) \cos \omega t \, \mathrm{d}t. \end{cases} \tag{3.9}$$

With the change of variable $\omega t = \theta$, Equation (3.9) is rewritten as

$$\begin{cases} \dot{u}(t) = -\frac{\varepsilon}{\omega}\frac{1}{2\pi}\int_0^{2\pi} \left(f(x(\theta),\dot{x}(\theta)) + \Omega x(\theta)\right)\sin\theta\,\mathrm{d}\theta \\ \dot{v}(t) = -\frac{\varepsilon}{\omega}\frac{1}{2\pi}\int_0^{2\pi} \left(f(x(\theta),\dot{x}(\theta)) + \Omega x(\theta)\right)\cos\theta\,\mathrm{d}\theta. \end{cases} \tag{3.10}$$

The solution $x(t)$ is often represented in polar coordinates $x(t) = A(t)\sin\left(\omega t - \phi(t)\right)$ with

$$\begin{cases} A(t) = \sqrt{u^2(t) + v^2(t)} \\ \phi(t) = \mathrm{atan2}(-u(t), -v(t)). \end{cases} \tag{3.11}$$

Conversely, $u(t) = -A(t)\sin\phi(t)$ and $v(t) = -A(t)\cos\phi(t)$. Furthermore, we can express the time derivatives of A and ϕ as

$$\begin{cases} \dot{A} = \frac{\partial A}{\partial u}\dot{u} + \frac{\partial A}{\partial v}\dot{v} = \frac{1}{A}\left(u\dot{u} + v\dot{v}\right) \\ \dot{\phi} = \frac{\partial \phi}{\partial u}\dot{u} + \frac{\partial \phi}{\partial v}\dot{v} = \frac{1}{A^2}\left(v\dot{u} - u\dot{v}\right) \end{cases} \tag{3.12}$$

where, for conciseness, the time dependence for u, v, A and ϕ is dropped.

3.2.2 Averaging around the primary resonance

Applying the AM to the oscillator (3.1) consists in solving

$$\begin{cases} \dot{u} = -\frac{\varepsilon}{\omega}\frac{1}{2\pi}\int_0^{2\pi} \left(\bar{\gamma}\sin\theta - 2\bar{\zeta}\omega_0\dot{x}(\theta) - \sum_{d=2}^{\infty}\bar{\alpha}_d x^d(\theta) + \Omega x(\theta)\right)\sin\theta\,\mathrm{d}\theta \\ \dot{v} = -\frac{\varepsilon}{\omega}\frac{1}{2\pi}\int_0^{2\pi} \left(\bar{\gamma}\sin\theta - 2\bar{\zeta}\omega_0\dot{x}(\theta) - \sum_{d=2}^{\infty}\bar{\alpha}_d x^d(\theta) + \Omega x(\theta)\right)\cos\theta\,\mathrm{d}\theta. \end{cases} \tag{3.13}$$

Equation (3.13) is solved by averaging the different physical terms, namely the forcing, damping, frequency detuning and polynomial stiffness terms separately. For clarity, Equation (3.13) is rewritten as

$$\begin{cases} \dot{u} = -\frac{\varepsilon}{\omega}\left(\dot{u}_{\bar{\gamma}} + \dot{u}_{\bar{\zeta}} + \dot{u}_{\bar{\alpha}_d} + \dot{u}_{\Omega}\right) \\ \dot{v} = -\frac{\varepsilon}{\omega}\left(\dot{v}_{\bar{\gamma}} + \dot{v}_{\bar{\zeta}} + \dot{v}_{\bar{\alpha}_d} + \dot{v}_{\Omega}\right) \end{cases} \tag{3.14}$$

where the pairs $(\dot{u}_{\bar{\gamma}}, \dot{v}_{\bar{\gamma}})$, $\left(\dot{u}_{\bar{\zeta}}, \dot{v}_{\bar{\zeta}}\right)$, $(\dot{u}_{\bar{\alpha}_d}, \dot{v}_{\bar{\alpha}_d})$ and $(\dot{u}_{\Omega}, \dot{v}_{\Omega})$ correspond to the $\dot{u}$ and $\dot{v}$ coordinates of the forcing, damping, polynomial stiffness and frequency detuning, respectively. To solve these integrals, the following trigonometric integral over a full circle (see Appendix B) is used

$$\frac{1}{2\pi}\int_0^{2\pi}\cos^a\theta\sin^b\theta\,\mathrm{d}\theta = \frac{1}{4\pi}\left[(-1)^a + 1\right]\left[(-1)^b + 1\right]\frac{\Gamma\left(\frac{a}{2}+\frac{1}{2}\right)\Gamma\left(\frac{b}{2}+\frac{1}{2}\right)}{\Gamma\left(\frac{a}{2}+\frac{b}{2}+1\right)} \tag{3.15}$$

where Γ is the *Gamma* function. Equation (3.15) is always equal to 0 if either a or b is odd. Replacing $a \to 2a$ and $b \to 2b$ yields

$$\frac{1}{2\pi}\int_0^{2\pi}\cos^{2a}\theta\sin^{2b}\theta\,\mathrm{d}\theta = \frac{1}{\pi}\frac{\Gamma\left(a+\frac{1}{2}\right)\Gamma\left(b+\frac{1}{2}\right)}{\Gamma\left(a+b+1\right)}. \tag{3.16}$$

3.2.2.1 Averaging of the forcing term

For $\dot{u}$ and $\dot{v}$, we have respectively

$$\dot{u}_{\bar{\gamma}} = \frac{1}{2\pi}\int_0^{2\pi} \bar{\gamma}\sin^2\theta\,\mathrm{d}\theta = \frac{\bar{\gamma}}{2} \tag{3.17}$$

and

$$\dot{v}_{\bar{\gamma}} = \frac{1}{2\pi}\int_0^{2\pi} \bar{\gamma}\cos\theta\sin\theta\,\mathrm{d}\theta = 0. \tag{3.18}$$

3.2.2.2 Averaging of the damping term

For $\dot{u}$ and $\dot{v}$, we have respectively

$$\dot{u}_{\bar{\zeta}} = -\frac{1}{2\pi}\int_0^{2\pi} 2\bar{\zeta}\omega_0\left(-u\omega\sin^2\theta - v\omega\cos\theta\sin\theta\right)\,\mathrm{d}\theta = \bar{\zeta}\omega_0\omega u \tag{3.19}$$

and

$$\dot{v}_{\bar{\zeta}} = -\frac{1}{2\pi}\int_0^{2\pi} 2\bar{\zeta}\omega_0\left(-u\omega\cos\theta\sin\theta - v\omega\cos^2\theta\right)\,\mathrm{d}\theta = \bar{\zeta}\omega_0\omega v. \tag{3.20}$$

3.2.2.3 Averaging of the frequency detuning term

For $\dot{u}$ and $\dot{v}$, we have respectively

$$\dot{u}_{\Omega} = \frac{1}{2\pi}\int_0^{2\pi} \Omega\left(u\cos\theta\sin\theta - v\sin^2\theta\right)\,\mathrm{d}\theta = -\frac{\Omega v}{2} \tag{3.21}$$

and

$$\dot{v}_{\Omega} = \frac{1}{2\pi}\int_0^{2\pi} \Omega\left(u\cos^2\theta - v\cos\theta\sin\theta\right)\,\mathrm{d}\theta = \frac{\Omega u}{2}. \tag{3.22}$$

3.2.2.4 Averaging of the polynomial stiffness term

For $\dot{u}$ and $\dot{v}$, we need to solve respectively

$$\dot{u}_{\bar{\alpha}_d} = -\sum_{d=2}^{\infty}\frac{1}{2\pi}\int_0^{2\pi} \bar{\alpha}_d\left(u\cos\theta - v\sin\theta\right)^d\sin\theta\,\mathrm{d}\theta \tag{3.23}$$

and

$$\dot{v}_{\bar{\alpha}_d} = -\sum_{d=2}^{\infty}\frac{1}{2\pi}\int_0^{2\pi} \bar{\alpha}_d\left(u\cos\theta - v\sin\theta\right)^d\cos\theta\,\mathrm{d}\theta. \tag{3.24}$$

To do so, the binomial expansion is applied to the polynomial term

$$(u\cos\theta - v\sin\theta)^d = \sum_{p=0}^{d}\binom{d}{p}(u\cos\phi)^{d-p}(-v\sin\theta)^p. \tag{3.25}$$

It yields

$$\dot{u}_{\bar{\alpha}_d} = -\sum_{d=2}^{\infty} \alpha_d \sum_{p=0}^{d} \binom{d}{p} u^{d-p}(-v)^p \frac{1}{2\pi} \int_0^{2\pi} \cos^{d-p}\theta \sin^{p+1}\theta \,\mathrm{d}\theta \tag{3.26}$$

and

$$\dot{v}_{\bar{\alpha}_d} = -\sum_{d=2}^{\infty} \bar{\alpha}_d \sum_{p=0}^{d} \binom{d}{p} u^{d-p}(-v)^p \frac{1}{2\pi} \int_0^{2\pi} \cos^{d-p+1}\theta \sin^{p}\theta \,\mathrm{d}\theta. \tag{3.27}$$

The result of the integrals depends on the parity of the exponents of the sine and cosine terms, *i.e.*, the parity of d and p. Therefore, $\dot{u}_{\bar{\alpha}_d}$ and $\dot{v}_{\bar{\alpha}_d}$ are split into

$$\begin{cases} \dot{u}_{\bar{\alpha}_d} = \dot{u}_{\bar{\alpha}_{2i+1,2j+1}} + \dot{u}_{\bar{\alpha}_{2i+1,2j}} + \dot{u}_{\bar{\alpha}_{2i,2j}} + \dot{u}_{\bar{\alpha}_{2i,2j+1}} \\ \dot{v}_{\bar{\alpha}_d} = \dot{v}_{\bar{\alpha}_{2i+1,2j+1}} + \dot{v}_{\bar{\alpha}_{2i+1,2j}} + \dot{v}_{\bar{\alpha}_{2i,2j}} + \dot{v}_{\bar{\alpha}_{2i,2j+1}} \end{cases} \tag{3.28}$$

where the different terms $\dot{u}_{\bar{\alpha}_{\bullet,\bullet}}$ and $\dot{v}_{\bar{\alpha}_{\bullet,\bullet}}$ account for the parity of d and p. The different combinations are studied hereafter.

Case 1: d and p are odd. We set $d = 2i+1$ and $p = 2j+1$. We have

$$\dot{u}_{\bar{\alpha}_{2i+1,2j+1}} = \sum_{i=1}^{\infty} \bar{\alpha}_{2i+1} \sum_{j=0}^{i} \binom{2i+1}{2j+1} u^{2(i-j)} v^{2j+1} \frac{1}{2\pi} \int_0^{2\pi} \cos^{2(i-j)}\theta \sin^{2(j+1)}\theta \,\mathrm{d}\theta \neq 0 \tag{3.29}$$

and

$$\dot{v}_{\bar{\alpha}_{2i+1,2j+1}} = \sum_{i=1}^{\infty} \bar{\alpha}_{2i+1} \sum_{j=0}^{i} \binom{2i+1}{2j+1} u^{2(i-j)} v^{2j+1} \frac{1}{2\pi} \int_0^{2\pi} \cos^{2(i-j)+1}\theta \sin^{2j+1}\theta \,\mathrm{d}\theta = 0 \tag{3.30}$$

since both exponents are odd.

Case 2: d is odd and p is even. We set $d = 2i+1$ and $p = 2j$

$$\dot{u}_{\bar{\alpha}_{2i+1,2j}} = -\sum_{i=1}^{\infty} \bar{\alpha}_{2i+1} \sum_{j=0}^{i} \binom{2i+1}{2j} u^{2(i-j)} v^{2j} \frac{1}{2\pi} \int_0^{2\pi} \cos^{2(i-j)+1}\theta \sin^{2j+1}\theta \,\mathrm{d}\theta = 0 \tag{3.31}$$

and

$$\dot{v}_{\bar{\alpha}_{2i+1,2j}} = -\sum_{i=1}^{\infty} \bar{\alpha}_{2i+1} \sum_{j=0}^{i} \binom{2i+1}{2j} u^{2(i-j)+1} v^{2j} \frac{1}{2\pi} \int_0^{2\pi} \cos^{2(i-j+1)}\theta \sin^{2j}\theta \,\mathrm{d}\theta \neq 0 \tag{3.32}$$

Case 3: d and p are even. We set $d = 2i$ and $p = 2j$

$$\dot{u}_{\bar{\alpha}_{2i,2j}} = -\sum_{i=0}^{\infty} \bar{\alpha}_{2i} \sum_{j=0}^{i} \binom{2i}{2j} u^{2(i-j)} v^{2j} \frac{1}{2\pi} \int_0^{2\pi} \cos^{2(i-j)}\theta \sin^{2j+1}\theta \,\mathrm{d}\theta = 0 \tag{3.33}$$

and

$$\dot{u}_{\bar{\alpha}_{2i,2j}} = -\sum_{i=0}^{\infty} \bar{\alpha}_{2i} \sum_{j=0}^{i} \binom{2i}{2j+1} u^{2(i-j)} v^{2j} \frac{1}{2\pi} \int_0^{2\pi} \cos^{2(i-j)+1}\theta \sin^{2j}\theta \,\mathrm{d}\theta = 0 \tag{3.34}$$

Case 4: d is even and p is odd. We set $d = 2i$ and $p = 2j + 1$

$$\dot{u}_{\bar{\alpha}_{2i+1,2j}} = \sum_{i=0}^{\infty} \bar{\alpha}_{2i} \sum_{j=0}^{i} \binom{2i}{2j+1} u^{2(i-j)-1} v^{2j+1} \frac{1}{2\pi} \int_0^{2\pi} \cos^{2(i-j)-1}\theta \sin^{2(j+1)}\theta \, \mathrm{d}\theta = 0 \tag{3.35}$$

and

$$\dot{u}_{\bar{\alpha}_{2i+1,2j}} = \sum_{i=0}^{\infty} \bar{\alpha}_{2i} \sum_{j=0}^{i} \binom{2i}{2j+1} u^{2(i-j)-1} v^{2j+1} \frac{1}{2\pi} \int_0^{2\pi} \cos^{2(i-j)}\theta \sin^{2j+1}\theta \, \mathrm{d}\theta = 0 \tag{3.36}$$

Summary: It follows that only $\dot{u}_{\bar{\alpha}_{2i+1,2j+1}}$ and $\dot{v}_{\bar{\alpha}_{2i+1,2j}}$ are non null and therefore

$$\begin{cases} \dot{u}_{\bar{\alpha}_d} = \dot{u}_{\bar{\alpha}_{2i+1,2j+1}} \\ \dot{v}_{\bar{\alpha}_d} = \dot{v}_{\bar{\alpha}_{2i+1,2j}}. \end{cases} \tag{3.37}$$

We note that the stiffness terms of even order do not participate in the motion around the primary resonance at first order.

3.2.2.5 Averaged solution of the oscillator with polynomial stiffness

Finally, the averaged equations for $\dot{u}$ and for $\dot{v}$ are

$$\begin{cases} \dot{u} = -\frac{\varepsilon}{\omega} \left(\frac{\bar{\gamma}}{2} + \bar{\zeta}\omega_0\omega u - \frac{\Omega v}{2} + \sum_{i=1}^{\infty} \bar{\alpha}_{2i+1} \sum_{j=0}^{i} \binom{2i+1}{2j+1} \frac{u^{2(i-j)} v^{2j+1}}{2\pi} \int_0^{2\pi} \cos^{2(i-j)}\theta \sin^{2(j+1)}\theta \, \mathrm{d}\theta \right) \\ \dot{v} = -\frac{\varepsilon}{\omega} \left(\bar{\zeta}\omega_0\omega v + \frac{\Omega u}{2} - \sum_{i=1}^{\infty} \bar{\alpha}_{2i+1} \sum_{j=0}^{i} \binom{2i+1}{2j} \frac{u^{2(i-j)+1} v^{2j}}{2\pi} \int_0^{2\pi} \cos^{2(i-j+1)}\theta \sin^{2j}\theta \, \mathrm{d}\theta \right). \end{cases} \tag{3.38}$$

Using the same notation as in Equation (3.14), the solution in polar coordinates reads

$$\begin{cases} \dot{A} = -\frac{\varepsilon}{\omega} \left(\dot{A}_{\bar{\gamma}} + \dot{A}_{\bar{\zeta}} + \dot{A}_{\bar{\alpha}_3} + \dot{A}_{\Omega} \right) \\ \dot{\phi} = -\frac{\varepsilon}{\omega} \left(\dot{\phi}_{\bar{\gamma}} + \dot{\phi}_{\bar{\zeta}} + \dot{\phi}_{\bar{\alpha}_3} + \dot{\phi}_{\Omega} \right) \end{cases} \tag{3.39}$$

where the $A_\bullet$ and $\phi_\bullet$ terms are computed thanks to Equation (3.12). We have

$$\begin{cases} \dot{A}_{\bar{\gamma}} = -\frac{\bar{\gamma}}{2} \sin\phi \\ \dot{A}_{\bar{\zeta}} = -\bar{\zeta}\omega_0\omega A \\ \dot{A}_{\Omega} = 0 \\ \dot{A}_{\bar{\alpha}} = \frac{1}{A} \left(u\dot{u}_{\bar{\alpha}_{2i+1,2j+1}} + v\dot{v}_{\bar{\alpha}_{2i+1,2j}} \right) \end{cases} \tag{3.40}$$

and

$$\begin{cases} \dot{\phi}_{\bar{\gamma}} = -\frac{\bar{\gamma}}{2A} \cos\phi \\ \dot{\phi}_{\bar{\zeta}} = 0 \\ \dot{\phi}_{\Omega} = -\frac{\Omega}{2} \\ \dot{\phi}_{\bar{\alpha}} = \frac{1}{A^2} \left(v\dot{u}_{\bar{\alpha}_{2i+1,2j+1}} - u\dot{v}_{\bar{\alpha}_{2i+1,2j}} \right). \end{cases} \tag{3.41}$$

However, the simplification of the expression of the polynomial stiffness terms $\dot{A}_{\bar{\alpha}_d}$ and $\dot{\phi}_{\bar{\alpha}_d}$ is not straightforward. Some developments are necessary and are detailed hereafter.

3.2.2.6 Polynomial stiffness solution for $\dot{A}_{\bar{\alpha}_d}$

From (3.12), we have

$$\begin{aligned}\dot{A}_{\bar{\alpha}_d} =& \frac{1}{2\pi A}\sum_{i=1}^{\infty}\bar{\alpha}_{2i+1}\Bigg(\sum_{j=0}^{i}\binom{2i+1}{2j+1}u^{2(i-j)+1}v^{2j+1}\int_0^{2\pi}\cos^{2(i-j)}\theta\sin^{2(j+1)}\theta\,\mathrm{d}\theta \\ &-\sum_{j=0}^{i}\binom{2i+1}{2j}u^{2(i-j)+1}v^{2j+1}\int_0^{2\pi}\cos^{2(i-j+1)}\theta\sin^{2j}\theta\,\mathrm{d}\theta\Bigg).\end{aligned} \tag{3.42}$$

The goal of this section is to prove that this relation is equal to 0. Equivalently, we want to prove that

$$\binom{2i+1}{2j+1}\int_0^{2\pi}\cos\theta^{2(i-j)}\sin^{2(j+1)}\theta\,\mathrm{d}\theta-\binom{2i+1}{2j}\int_0^{2\pi}\cos\theta^{2(i-j+1)}\sin^{2j}\theta\,\mathrm{d}\theta=0. \tag{3.43}$$

First, we use Equation (3.16) to rewrite the left hand side of Equation (3.43) as

$$\begin{aligned}\frac{2}{\Gamma(i+2)}\Bigg(&\binom{2i+1}{2j+1}\Gamma\left(i-j+\frac{1}{2}\right)\Gamma\left(j+1+\frac{1}{2}\right) \\ &-\binom{2i+1}{2j}\Gamma\left(i+1-j+\frac{1}{2}\right)\Gamma\left(j+\frac{1}{2}\right)\Bigg).\end{aligned} \tag{3.44}$$

Second, we can make use of the following property of the *Gamma* function

$$\Gamma\left(n+\frac{1}{2}\right)=\binom{n-\frac{1}{2}}{n}n!\sqrt{\pi} \tag{3.45}$$

for non-negative integer values of n and the following binomial coefficient recurrence property

$$\binom{n}{i}=\frac{n-i+1}{i}\binom{n}{i-1} \tag{3.46}$$

to rewrite Equation (3.44) as

$$\frac{2\pi}{\Gamma(i+2)}(i-j)!j!\binom{i-j-\frac{1}{2}}{i-j}\binom{j-\frac{1}{2}}{j}\binom{2i+1}{2j}\left(\frac{2i-2j+1}{2j+1}\left(j+\frac{1}{2}\right)-\left(i-j+\frac{1}{2}\right)\right) \tag{3.47}$$

which is equal to 0. This proves the relation from Equation (3.42) and

$$\dot{A}_{\bar{\alpha}_d}=0. \tag{3.48}$$

3.2.2.7 Polynomial stiffness solution for $\dot{\phi}_{\bar{\alpha}_d}$

From (3.12), we have

$$\begin{aligned}\dot{\phi}_{\bar{\alpha}_d} =& \frac{1}{A^2}\sum_{i=1}^{\infty}\bar{\alpha}_{2i+1}\Bigg(\sum_{j=0}^{i}\binom{2i+1}{2j+1}u^{2(i-j)}v^{2(j+1)}\frac{1}{2\pi}\int_0^{2\pi}\cos^{2(i-j)}\theta\sin^{2(j+1)}\theta\,\mathrm{d}\theta \\ &+\sum_{j=0}^{i}\binom{2i+1}{2j}u^{2(i-j+1)}v^{2j+1}\frac{1}{2\pi}\int_0^{2\pi}\cos^{2(i-j+1)}\theta\sin^{2j}\theta\,\mathrm{d}\theta\Bigg).\end{aligned} \tag{3.49}$$

The goal of this section is to show that

$$\begin{aligned}&\sum_{j=0}^{i}\binom{2i+1}{2j+1}u^{2(i-j)}v^{2(j+1)}\frac{1}{2\pi}\int_0^{2\pi}\cos^{2(i-j)}\theta\sin^{2(j+1)}\theta\,\mathrm{d}\theta\\&+\sum_{j=0}^{i}\binom{2i+1}{2j}u^{2(i-j+1)}v^{2j}\frac{1}{2\pi}\int_0^{2\pi}\cos^{2(i-j+1)}\theta\sin^{2j}\theta\,\mathrm{d}\theta=C_{2i+1}A^{2(i+1)}\end{aligned}\tag{3.50}$$

with C_{2i+1} a constant to be determined, such that

$$\dot{\phi}_{\bar{\alpha}_d}=\frac{1}{A^2}\sum_{i=1}^{\infty}\bar{\alpha}_{2i+1}C_{2i+1}A^{2(i+1)}.\tag{3.51}$$

First, from the left hand side of Equation (3.50), we take out the $j=i$ and $j=0$ terms of the first and second summation terms, respectively, leaving

$$\begin{aligned}&\binom{2i+1}{0}u^{2(i+1)}\frac{1}{2\pi}\int_0^{2\pi}\cos^{2(i+1)}\theta\,\mathrm{d}\theta\\&+\sum_{j=1}^{i}\binom{2i+1}{2j}u^{2(i-j+1)}v^{2j}\int_0^{2\pi}\cos^{2(i-j+1)}\theta\sin^{2j}\theta\,\mathrm{d}\theta\\&+\sum_{j=0}^{i-1}\binom{2i+1}{2j+1}u^{2(i-j)}v^{2(j+1)}\frac{1}{2\pi}\int_0^{2\pi}\cos^{2(i-j)}\theta\sin^{2(j+1)}\theta\,\mathrm{d}\theta\\&\binom{2i+1}{2i+1}v^{2(i+1)}\frac{1}{2\pi}\int_0^{2\pi}\sin^{2(i+1)}\theta\,\mathrm{d}\theta.\end{aligned}\tag{3.52}$$

Second, on the third term of (3.52), we make the change of variable $j\to j-1$ such that it is rewritten

$$\sum_{j=1}^{i}\binom{2i+1}{2j-1}u^{2(i-j+1)}v^{2j}\frac{1}{2\pi}\int_0^{2\pi}\cos^{2(i-j+1)}\theta\sin^{2j}\theta\,\mathrm{d}\theta.\tag{3.53}$$

Equation (3.52) becomes

$$\begin{aligned}&\binom{2i+1}{0}u^{2(i+1)}\frac{1}{2\pi}\int_0^{2\pi}\cos^{2(i+1)}\theta\,\mathrm{d}\theta\\&+\sum_{j=1}^{i}\left(\binom{2i+1}{2j-1}+\binom{2i+1}{2j}\right)u^{2(i+1-j)}v^{2j}\frac{1}{2\pi}\int_0^{2\pi}\cos^{2(i+1-j)}\theta\sin^{2j}\theta\,\mathrm{d}\theta\\&\binom{2i+1}{2i+1}v^{2(i+1)}\frac{1}{2\pi}\int_0^{2\pi}\sin^{2(i+1)}\theta\,\mathrm{d}\theta.\end{aligned}\tag{3.54}$$

Third, using the recurrence relation of the binomial coefficients, we have

$$\binom{2i+1}{2j-1}+\binom{2i+1}{2j}=\binom{2(i+1)}{2j}.\tag{3.55}$$

Fourth, the following relations are always verified

$$\begin{aligned}\binom{2i+1}{0} &= 1 = \binom{2(i+1)}{0} \\ \binom{2i+1}{2i+1} &= 1 = \binom{2(i+1)}{2(i+1)}.\end{aligned} \tag{3.56}$$

Equation (3.54) becomes

$$\sum_{j=0}^{i+1} \binom{2(i+1)}{2j} u^{2(i+1-j)} v^{2j} \frac{1}{2\pi} \int_0^{2\pi} \cos^{2(i+1-j)}\theta \sin^{2j}\theta \,\mathrm{d}\theta. \tag{3.57}$$

Furthermore, it can be proven (see Appendix B) that

$$\binom{2(i+1)}{2j} = \binom{i+1}{j} \frac{\Gamma(i+1+\frac{1}{2})}{\Gamma(j+\frac{1}{2})\Gamma(i+1-j+\frac{1}{2})}. \tag{3.58}$$

From (3.16), it yields

$$\binom{2(i+1)}{2j} \frac{1}{2\pi} \int_0^{2\pi} \cos^{2(i+1-j)}\theta \sin^{2j}\theta \,\mathrm{d}\theta = C_{2i+1} \binom{i+1}{j} \tag{3.59}$$

with

$$C_{2i+1} = \frac{1}{\sqrt{\pi}} \frac{\Gamma(i+\frac{3}{2})}{\Gamma(i+2)} = \binom{2(i+1)}{i+1} 2^{-2(i+1)} \tag{3.60}$$

a constant that only depends on i. Finally, Equation (3.49) becomes

$$\begin{aligned}\dot{\phi}_{\bar{\alpha}_d} &= \frac{1}{A^2} \sum_{i=1}^{\infty} \bar{\alpha}_{2i+1} C_{2i+1} \sum_{j=0}^{i+1} \binom{i+1}{j} u^{2(i+1-j)} v^{2j} \\ &= \frac{1}{A^2} \sum_{i=1}^{\infty} \bar{\alpha}_{2i+1} C_{2i+1} \left(u^2+v^2\right)^{i+1} \\ &= \frac{1}{A^2} \sum_{i=1}^{\infty} \bar{\alpha}_{2i+1} C_{2i+1} A^{2(i+1)}.\end{aligned} \tag{3.61}$$

3.2.2.8 Averaged solution in polar coordinates of the oscillator with polynomial stiffness

The system of equations from (3.38) in polar coordinates reads

$$\begin{cases} \dot{A} = -\frac{\varepsilon}{\omega}\left(\bar{\zeta}\omega_0\omega A - \frac{\bar{\gamma}}{2}\sin\phi\right) \\ \dot{\phi} = -\frac{\varepsilon}{\omega A}\left(\sum_{i=1}^{\infty} \bar{\alpha}_{2i+1} C_{2i+1} A^{2i+1} - \frac{\Omega}{2}A - \frac{\bar{\gamma}}{2}\cos\phi\right). \end{cases} \tag{3.62}$$

At steady state, $\dot{A} = \dot{\phi} = 0$. It results that

$$\begin{cases} \bar{\zeta}\omega_0\omega A = \frac{\bar{\gamma}}{2}\sin\phi \\ \sum_{i=1}^{\infty} \bar{\alpha}_{2i+1} C_{2i+1} A^{2i+1} - \frac{\Omega}{2}A = \frac{\bar{\gamma}}{2}\cos\phi. \end{cases} \tag{3.63}$$

3.2.3 Stability analysis

As for the Duffing oscillator, the stability analysis can be performed by studying the eigenvalues of the Jacobian matrix of the equations of motion from (3.63)

$$\det(\mathbf{J}) = \begin{vmatrix} -2\bar{\zeta}\omega_0\omega - \lambda & 2\sum_{i=1}^{\infty} \bar{\alpha}_{2i+1} C_{2i+1} A^{2i+1} - \Omega A \\ -2\sum_{i=1}^{\infty}(2i+1)\bar{\alpha}_{2i+1} C_{2i+1} A^{2i} + \Omega & -2\bar{\zeta}\omega_0\omega A - \lambda. \end{vmatrix} \tag{3.64}$$

Again, the solution is asymptotically stable if all the eigenvalues λ of the system have a strictly negative real part, which is not the case when

$$4\bar{\zeta}^2\omega_0^2\omega^2 A + \left(2\sum_{i=1}^{\infty} \bar{\alpha}_{2i+1} C_{2i+1} A^{2i+1} - \Omega A\right)\left(2\sum_{i=1}^{\infty}(2i+1)\bar{\alpha}_{2i+1} C_{2i+1} A^{2i} - \Omega\right) < 0. \tag{3.65}$$

The loss of stability happens between fold bifurcations, *i.e.*, when $\frac{\partial\omega}{\partial A} = 0$. This is proven by adding together the square of the two relations in Equation (3.63)

$$4\bar{\zeta}^2\omega_0^2\omega^2 A^2 + \left(2\sum_{i=1}^{\infty} \bar{\alpha}_{2i+1} C_{2i+1} A^{2i+1} - \Omega A\right)^2 = \bar{\gamma}^2 \tag{3.66}$$

taking the derivative with respect to A and setting $\frac{\partial\omega}{\partial A} = 0$, which imposes a fold bifurcation. We finally find that these folds occur when

$$4\bar{\zeta}^2\omega_0^2\omega^2 A + \left(2\sum_{i=1}^{\infty} \bar{\alpha}_{2i+1} C_{2i+1} A^{2i+1} - \Omega A\right)\left(2\sum_{i=1}^{\infty}(2i+1)\bar{\alpha}_{2i+1} C_{2i+1} A^{2i} - \Omega\right) = 0. \tag{3.67}$$

3.2.4 Amplitude and phase resonances

Amplitude resonance occurs when both $\frac{\partial A}{\partial\omega}$ and $\frac{\partial A}{\partial\phi}$ are equal to 0. From Equation (3.63), we obtain

$$\begin{cases} \frac{\partial A}{\partial\phi} = \frac{\bar{\gamma}}{2\bar{\zeta}\omega_0\omega}\left(\cos\phi - \frac{\sin\phi}{\omega}\frac{\partial\omega}{\partial\phi}\right) = 0 \\ \frac{\partial A}{\partial\omega} = \frac{\bar{\gamma}}{2\bar{\zeta}\omega_0\omega}\left(\cos\phi\frac{\partial\phi}{\partial\omega} - \frac{\sin\phi}{\omega}\right) = 0. \end{cases} \tag{3.68}$$

Both relations are equivalent. $\frac{\partial\omega}{\partial\phi}$ is obtained by isolating Ω in the second relation of (3.63) and making use of the chain rule $\frac{\partial\omega}{\partial\phi} = \frac{\partial\omega}{\partial\Omega}\frac{\partial\Omega}{\partial\phi}$ with

$$\frac{\partial\Omega}{\partial\phi} = \left(4\sum_{i=1}^{\infty} i\bar{\alpha}_{2i+1} C_{2i+1} A^{2i-1} + \frac{\bar{\gamma}}{A^2}\cos\phi\right)\frac{\partial A}{\partial\phi} + \frac{\bar{\gamma}}{A}\sin\phi \tag{3.69}$$

and $\frac{\partial\omega}{\partial\Omega} = \left[\frac{\partial\Omega}{\partial\omega}\right]^{-1} = \frac{\varepsilon}{2\omega}$. It yields

$$\frac{\partial\omega}{\partial\phi} = \frac{\varepsilon}{2\omega}\left(\left[4\sum_{i=1}^{\infty} i\bar{\alpha}_{2i+1} C_{2i+1} A^{2i-1} + \frac{\bar{\gamma}}{A^2}\cos\phi\right]\frac{\partial A}{\partial\phi} + \frac{\bar{\gamma}}{A}\sin\phi\right). \tag{3.70}$$

Eventually,

$$\frac{\partial A}{\partial \phi} = \frac{\bar{\gamma}\sin\phi\left(\omega - \varepsilon\bar{\zeta}\omega_0\tan\phi\right)}{\bar{\zeta}\omega_0\left(2\omega^2\tan\phi + \varepsilon\left(4\sum_{i=1}^{\infty} i\alpha_{2i+1}C_{2i+1}\left(\frac{\bar{\gamma}}{2\bar{\zeta}\omega_0\omega}\sin\phi\right)^{2i}\tan\phi + 2\bar{\zeta}\omega_0\omega\right)\right)} = 0. \tag{3.71}$$

This relation is verified when

$$\tan\phi_a = \frac{\omega_a}{\varepsilon\bar{\zeta}\omega_0} \tag{3.72}$$

and since we consider small damping ratios $\zeta = \varepsilon\bar{\zeta}$, ϕ_a is close to $\frac{\pi}{2}$.

On the other hand, phase resonance for linear and nonlinear systems occurs when the external forcing counterbalances exactly the damping forces [50]. From the first equation in Equation (3.63), we see that this happens when the phase lag is $\pi/2$. Phase resonance thus occurs in the immediate vicinity of amplitude resonance.

3.2.5 Discussion on the harmonic forcing

In Equation (3.1), the choice was made to have a sine forcing. In the case of a cosine forcing $f\cos\omega t$, the governing equations of motion write

$$\begin{cases} \dot{A} = -\frac{\varepsilon}{\omega}\left(\bar{\zeta}\omega_0\omega A - \frac{\bar{\gamma}}{2}\cos\phi\right) \\ \dot{\phi} = -\frac{\varepsilon}{\omega A}\left(\sum_{i=1}^{\infty}\bar{\alpha}_{2i+1}C_{2i+1}A^{2i+1} - \frac{\Omega}{2}A - \frac{\bar{\gamma}}{2}\sin\phi\right). \end{cases} \tag{3.73}$$

At steady state, $\dot{A} = \dot{\phi} = 0$. It results

$$\begin{cases} \bar{\zeta}\omega_0\omega A = \frac{\bar{\gamma}}{2}\cos\phi \\ \sum_{i=1}^{\infty}\bar{\alpha}_{2i+1}C_{2i+1}A^{2i+1} - \frac{\Omega}{2}A = \frac{\bar{\gamma}}{2}\sin\phi. \end{cases} \tag{3.74}$$

The amplitude resonance condition becomes

$$\tan\phi_a = \frac{\varepsilon\bar{\zeta}\omega_0}{\omega_a} \tag{3.75}$$

and phase resonance resonance occurs when $\phi_p = 0$.

3.3 Applications

3.3.1 The Duffing oscillator

3.3.1.1 Averaged solution of the Duffing oscillator

The equation of motion of the harmonically-forced Duffing oscillator is Equation (2.68). Only α_3 is different from 0 in the polynomial stiffness term and the averaged equations in polar coordinates read

$$\begin{cases} \dot{A} = -\frac{\varepsilon}{\omega}\left(\bar{\zeta}\omega_0\omega A - \frac{\bar{\gamma}}{2}\sin\phi\right) \\ \dot{\phi} = -\frac{\varepsilon}{\omega A}\left(\frac{3}{8}\bar{\alpha}_3A^3 - \frac{\Omega}{2}A - \frac{\bar{\gamma}}{2}\cos\phi\right). \end{cases} \tag{3.76}$$

The steady-state solution around the primary resonance is obtained by setting $\dot{A} = \dot{\phi} = 0$

$$\begin{cases} \bar{\zeta}\omega_0\omega A = \frac{\bar{\gamma}}{2}\sin\phi \\ \frac{\bar{\alpha}_3}{8}\left(3A^2 - \frac{4\Omega}{\bar{\alpha}_3}\right)A = \frac{\bar{\gamma}}{2}\cos\phi. \end{cases} \tag{3.77}$$

3.3.1.2 Amplitude resonance

Imposing $\tan\phi_a = \frac{\omega_a}{\varepsilon\bar{\zeta}\omega_0}$ in Equation (3.77), it is possible to derive A_a, ω_a and ϕ_a as a function of the unscaled system parameters

$$\begin{cases} A_a = \sqrt{\frac{2\omega_0^2}{3\alpha_3}\left((\zeta^2-1) + \sqrt{(1-\zeta^2)^2 + \frac{3\alpha_3\gamma^2}{4\zeta^2\omega_0^6}}\right)} \\ \omega_a = \frac{\omega_0}{\sqrt{2}}\sqrt{1 - 3\zeta^2 + \sqrt{(1-\zeta^2)^2 + \frac{3\alpha_3\gamma^2}{4\zeta^2\omega_0^6}}} \\ \tan\phi_a = \frac{\sqrt{1-3\zeta^2+\sqrt{(1-\zeta^2)^2+\frac{3\alpha_3\gamma^2}{4\zeta^2\omega_0^6}}}}{\sqrt{2}\zeta}. \end{cases} \tag{3.78}$$

To the best of our knowledge, this is the first time that an explicit function for the amplitude, frequency and phase lag at amplitude resonance is derived for the Duffing oscillator.

3.3.1.3 Phase resonance

Imposing $\phi_p = \pi/2$ in Equations (3.77) yields

$$\begin{cases} A_p = \frac{\gamma}{2\zeta\omega_0\omega_p} \\ \omega_p = \omega_0\sqrt{1 + \frac{3\alpha_3}{4\omega_0^2}A_p^2} \end{cases} \tag{3.79}$$

from which the expressions of the amplitude and frequency at phase resonance as a function of the forcing amplitude only can be deduced

$$\begin{cases} A_p = \sqrt{\frac{2\omega_0^2}{3\alpha_3}\left(\sqrt{1 + \frac{3\alpha_3\gamma^2}{4\zeta^2\omega_0^6}} - 1\right)} \\ \omega_p = \frac{\omega_0}{\sqrt{2}}\sqrt{1 + \sqrt{1 + \frac{3\alpha_3\gamma^2}{4\zeta^2\omega_0^6}}}. \end{cases} \tag{3.80}$$

We note that Equations (3.79) correspond to those that would be obtained by applying the energy balance principle to the NNMs of the undamped, unforced system and neglecting higher-order harmonics, as performed in Section 2.3.1.4. Under this latter assumption, this means that phase resonance testing amounts to exciting the underlying NNMs.

3.3.1.4 Difference between amplitude and phase resonances

The difference between amplitude and phase resonances of the Duffing oscillator is negligible if the system is weakly nonlinear, *i.e.*, if $\varepsilon \ll 1$. Indeed, similarly to what was

achieved in Section 2.2.3.3 in the linear case, we compute ΔA, $\Delta\omega$ and $\Delta\phi$

$$\begin{aligned}
\Delta A &= \sqrt{\frac{2\omega_0^2}{3\alpha_3}}\left(\sqrt{(\zeta^2-1)+\sqrt{(1-\zeta^2)^2+\frac{3\alpha_3\gamma^2}{4\zeta^2\omega_0^6}}}-\sqrt{\sqrt{1+\frac{3\alpha_3\gamma^2}{4\zeta^2\omega_0^6}}-1}\right)\\
\Delta\omega &= \frac{\omega_0}{\sqrt{2}}\left(\sqrt{1-3\zeta^2+\sqrt{\left(1-\zeta^2\right)^2+\frac{3\alpha_3\gamma^2}{4\zeta^2\omega_0^6}}}-\sqrt{1+\sqrt{1+\frac{3\alpha_3\gamma^2}{4\zeta^2\omega_0^6}}}\right)\\
\Delta\phi &= \frac{\sqrt{1-3\zeta^2+\sqrt{\left(1-\zeta^2\right)^2+\frac{3\alpha_3\gamma^2}{4\zeta^2\omega_0^6}}}}{\sqrt{2}\zeta}-\frac{\pi}{2}
\end{aligned} \tag{3.81}$$

and perform a Taylor series expansion around $\varepsilon = 0$, we find

$$\begin{aligned}
\Delta A &= \frac{\bar{\zeta}\bar{\gamma}}{4\omega_0^2}\varepsilon^2+\mathcal{O}\left(\varepsilon^3\right)=\mathcal{O}\left(\varepsilon^2\right)\\
\Delta\omega &= -\omega_0^2\bar{\zeta}^2\varepsilon^2+\mathcal{O}\left(\varepsilon^3\right)=\mathcal{O}\left(\varepsilon^2\right)\\
\Delta\phi &= -\bar{\zeta}\varepsilon+\mathcal{O}\left(\varepsilon^2\right)=\mathcal{O}\left(\varepsilon\right)
\end{aligned} \tag{3.82}$$

which is similar to what was obtained in the linear case. The main difference is that, for the Duffing oscillator, we assume small forcing and nonlinear stiffness in addition to small damping. Figure 3.1 displays the NFRC of the Duffing oscillator for $\zeta = 0.5\%$, $\omega_0 = 1$ rad/s and $\alpha_3 = 0.1$ N/(kg.m^3). It confirms that there is no distinguishable difference between the amplitude and phase resonance curves.

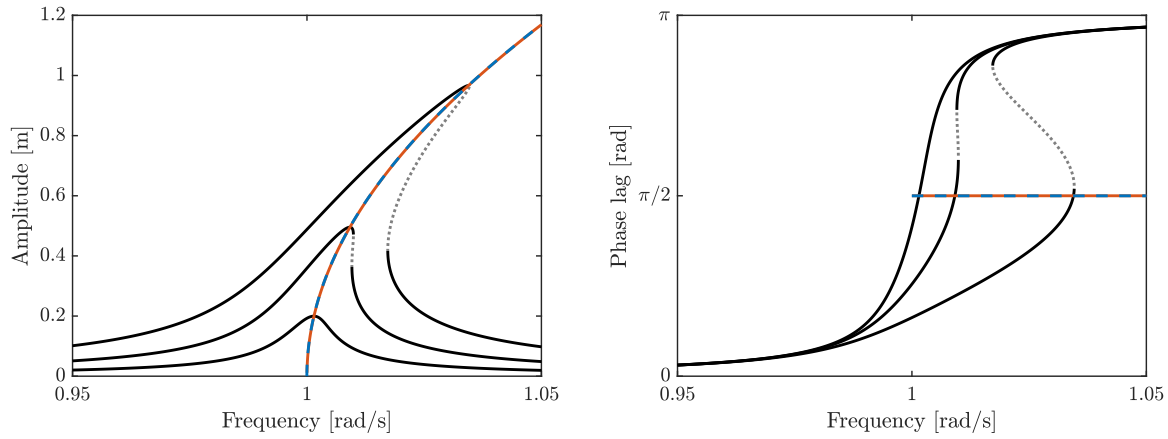

(a) **(b)**

Figure 3.1: NFRCs (black: stable; grey: unstable) around the primary resonance of the Duffing oscillator for forcing amplitudes of 0.002 N/kg, 0.005 N/kg and 0.01 N/kg. Amplitude (blue) and phase (orange) resonance curves: (a) amplitude and (b) phase lag.

3.3.1.5 Comparison between the averaging method and other methods

The equations of motion obtained with the AM in Equation (3.77) can be directly compared to those obtained with the MMS and the HBM with one or more harmonics. The equations of motion using the MMS are directly obtained from [4]

$$\begin{cases} \bar{\zeta}\omega_0^2 A = \frac{\bar{\gamma}}{2}\sin\phi \\ \frac{\bar{\alpha}_3}{8}\left(3A^2 - \frac{8\omega_0\Omega}{\bar{\alpha}_3}\right)A = \frac{\bar{\gamma}}{2}\cos\phi \end{cases} \tag{3.83}$$

with $\omega - \omega_0 = \varepsilon\Omega$ in this case. These results are compared to the HBM with 15 harmonics, considered as the reference solution, in Figures 3.2 and 3.3 for the hardening and softening cases, respectively. First, in both cases, the AM results are in much better agreement with the reference solution than the MMS results. Second, the MMS results in the hardening case overestimate the maximum amplitude whereas it is underestimated in the softening case. This is explained by the fact that both phase and amplitude resonances are reached when $\phi = \pi/2$. Therefore, $A_a = A_p = \frac{\gamma}{2\zeta\omega_0^2}$ with the MMS, which is exactly the amplitude at phase resonance of the linear oscillator. On the other hand, the AM results show that near resonance, *i.e.*, near $\phi = \pi/2$, the solution is $A \approx \frac{\gamma}{2\zeta\omega_0\omega}$, which is inversely proportional to the frequency ω. In the hardening case, $\omega > \omega_0$ and the amplitude at amplitude resonance is thus lower than in the linear case, whereas it is greater in the softening case since $\omega < \omega_0$. This is what is observed in Figures 3.2 and 3.3. The difference between AM and MMS comes from the fact that a linear detuning with respect to the linear resonance frequency is considered in the MMS, *i.e.*, $\omega - \omega_0 = \varepsilon\Omega$, whereas $\omega^2 - \omega_0^2 = \varepsilon\Omega$ is considered in the AM. This is also the reason why an explicit function of the amplitude, frequency and phase lag at amplitude resonance is not encountered in the literature, since the Duffing oscillator studied using the MMS does not differentiate between phase and amplitude resonances. Finally, it should be noted that the HBM limited to only one harmonic gives the same results as the AM.

3.3.2 The Helmholtz oscillator

The Helmholtz oscillator contains a quadratic stiffness. The mass-normalized equation of motion reads

$$\ddot{x}(t) + 2\zeta\omega_0\dot{x}(t) + \omega_0^2 x(t) + \alpha_2 x^2(t) = \gamma\sin\omega t. \tag{3.84}$$

Since the stiffness terms with even powers do not participate in the motion around the primary resonance when applying a first-order AM, it results that it behaves as a linear oscillator

$$\begin{cases} 2\bar{\zeta}\omega_0\omega A = \bar{\gamma}\sin\phi \\ \Omega A = \bar{\gamma}\cos\phi. \end{cases} \tag{3.85}$$

Therefore, the solution at amplitude resonance expressed with the unscaled parameters is

$$\begin{cases} A_a = \frac{\gamma}{2\zeta\omega_0^2\sqrt{1-\zeta^2}} \\ \omega_a = \omega_0\sqrt{1-\zeta^2} \\ \phi_a = \frac{\sqrt{1-\zeta^2}}{\zeta} \end{cases} \tag{3.86}$$

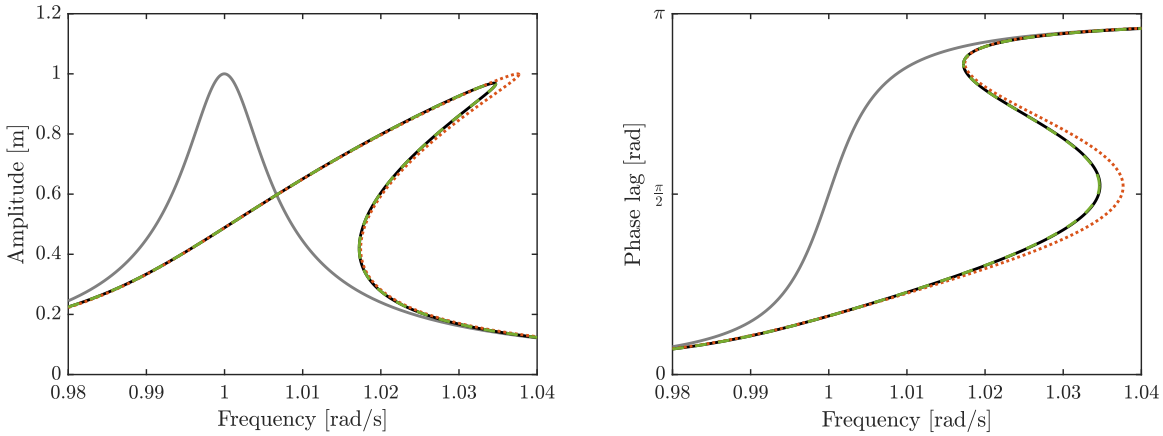

Figure 3.2: NFRCs around the primary resonance of the hardening Duffing oscillator for a forcing amplitude of 0.01 N/kg using the HBM (black), the AM (blue), the MMS (orange) and compared to the linear case (grey): (a) amplitude and (b) phase lag.

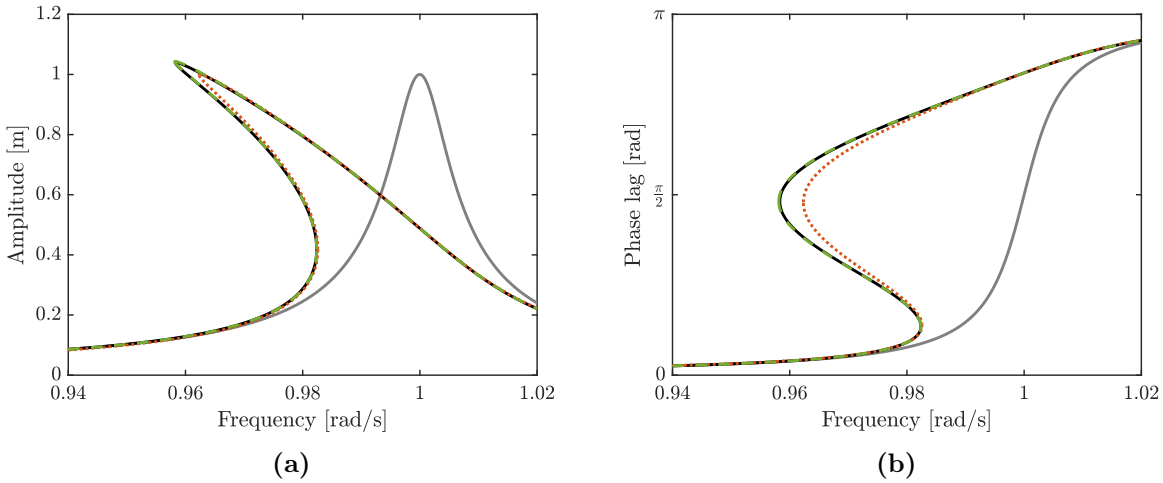

Figure 3.3: NFRCs around the primary resonance of the softening Duffing oscillator for a forcing amplitude of 0.01 N/kg using the HBM (black), the AM (blue), the MMS (orange) and compared to the linear case (grey): (a) amplitude and (b) phase lag.

and is close to phase resonance as discussed in Section 2.2.3.3. Figure 3.4 compares the NFRC of the Helmholtz oscillator obtained with Equation (3.85) and the reference solution obtained with the HBM. We see that the softening effect of the quadratic stiffness is missed by the AM. However, even for the reference solution, there is no distinguishable difference between the amplitude and phase resonance curves. Therefore, the conclusion made in Section 3.2.4 that phase resonance occurs in the vicinity of amplitude resonance still holds even when the quadratic nonlinearity cannot be neglected. Furthermore, we see that the amplitude at amplitude resonance of the reference solution is higher than the one of the AM. This is due to the fact that amplitude resonance occurs for a lower frequency for the reference solution than the averaged solution. Indeed, assuming that amplitude resonance can still be written $A_a \approx A_p = \frac{\bar{\gamma}}{2\bar{\zeta}\omega_0\omega}$, the lower the frequency, the higher the amplitude.

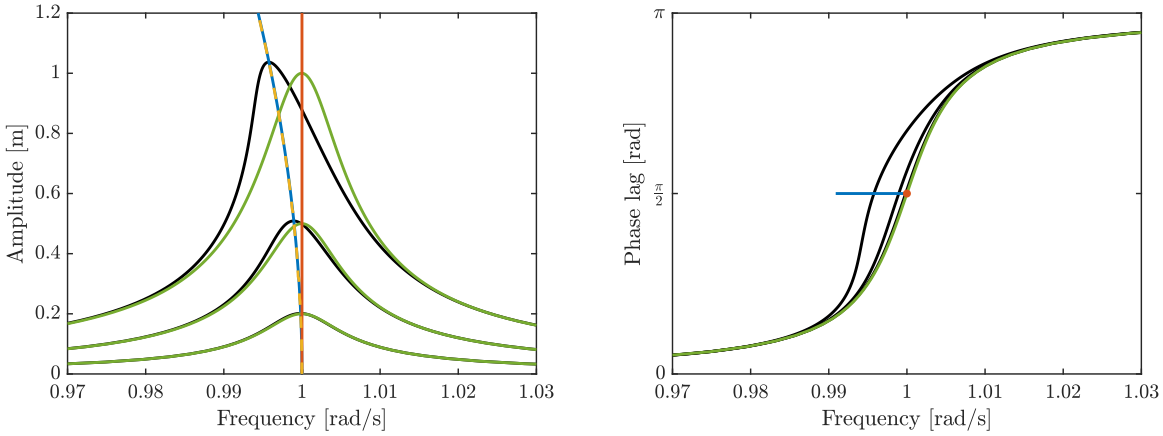

(a) **(b)**

Figure 3.4: NFRCs (HBM: black; AM: green) around the primary resonance of the Helmholtz oscillator for forcing amplitudes of 0.002 N/kg, 0.005 N/kg and 0.01 N/kg, amplitude (HBM: yellow) and phase resonance (HBM: blue; AM: orange) curves: (a) amplitude and (b) phase lag.

3.3.3 The oscillator with quintic and sceptic stiffness

The mass-normalized equation of the oscillator with quintic and sceptic stiffness terms is

$$\ddot{x}(t) + 2\zeta\omega_0\dot{x}(t) + \omega_0^2 x(t) + \alpha_5 x^5(t) + \alpha_7 x^7(t) = \gamma \sin \omega t. \tag{3.87}$$

In polar coordinates, the equations of motion read

$$\begin{cases} \dot{A} = -\frac{\varepsilon}{\omega}\left(\bar{\zeta}\omega_0\omega A - \frac{\bar{\gamma}}{2}\sin\phi\right) \\ \dot{\phi} = -\frac{\varepsilon}{\omega A}\left(\frac{5}{16}\bar{\alpha}_5 A^5 + \frac{35}{128}\bar{\alpha}_7 A^7 - \frac{\Omega}{2}A - \frac{\bar{\gamma}}{2}\cos\phi\right). \end{cases} \tag{3.88}$$

At steady-state

$$\begin{cases} \bar{\zeta}\omega_0\omega A = \frac{\bar{\gamma}}{2}\sin\phi \\ \frac{5}{16}\bar{\alpha}_5 A^5 + \frac{35}{128}\bar{\alpha}_7 A^7 - \frac{\Omega}{2}A = \frac{\bar{\gamma}}{2}\cos\phi. \end{cases} \tag{3.89}$$

The NFRCs computed with the AM and compared with the HBM are depicted in Figure 3.5. The agreement is almost perfect for both the NFRCs and the phase resonance curves. Again, the phase resonance curve predicts accurately the locus of points of maximum amplitude.

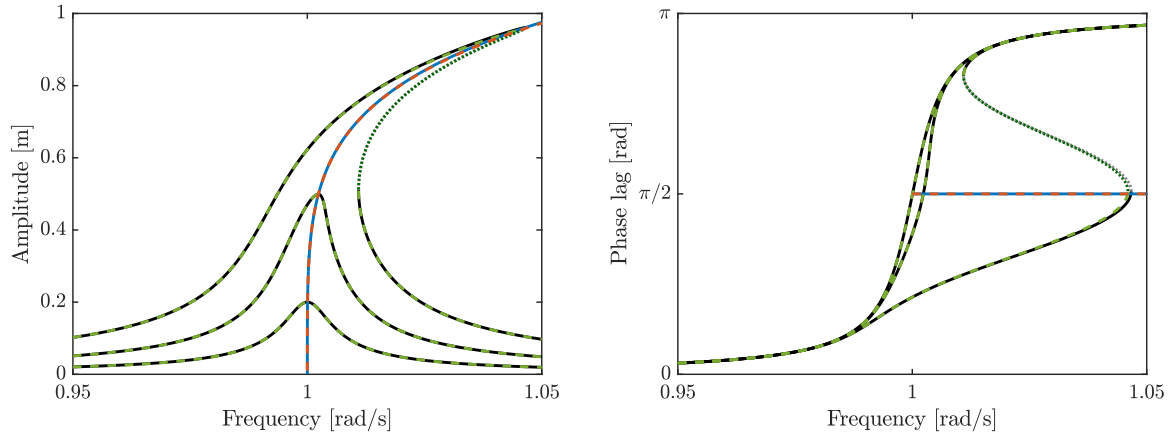

(a) **(b)**

Figure 3.5: NFRCs (HBM: black (stable) and grey (unstable); AM: solid green (stable) and dotted green (unstable)) around the primary resonance of the oscillator with quintic and sceptic stiffness for forcing amplitudes of 0.002 N/kg, 0.005 N/kg and 0.01 N/kg and the phase resonance curve (HBM: blue; AM: orange): (a) amplitude and (b) phase lag.

3.3.4 Oscillator with only one odd stiffness term

The mass-normalized equation of the oscillator with one nonlinear stiffness term of order d, with d odd, is

$$\ddot{x}(t) + 2\zeta\omega_0\dot{x}(t) + \omega_0^2 x(t) + \alpha_d x^d(t) = \gamma \sin \omega t. \tag{3.90}$$

At steady-state

$$\begin{cases} \bar{\zeta}\omega_0\omega A = \frac{\bar{\gamma}}{2}\cos\phi \\ \bar{\alpha}_d C_d A^d - \frac{\Omega}{2}A = \frac{\bar{\gamma}}{2}\sin\phi \end{cases} \tag{3.91}$$

where

$$C_d = \binom{d+1}{\frac{d+1}{2}} 2^{-d-1}. \tag{3.92}$$

At phase resonance, $\phi_p = \frac{\pi}{2}$, it yields

$$\begin{cases} A_p = \frac{\gamma}{2\zeta\omega_0\omega_p} \\ \omega_p = \omega_0\sqrt{1 + \frac{2\alpha_d C_d}{\omega_0^2} A_p^{d-1}}. \end{cases} \tag{3.93}$$

From the second relation of (3.93), we see that the frequency at phase resonance ω_p increases (decreases) when $\alpha_d > 0$ ($\alpha_d < 0$), the oscillator is said to be hardening (softening).

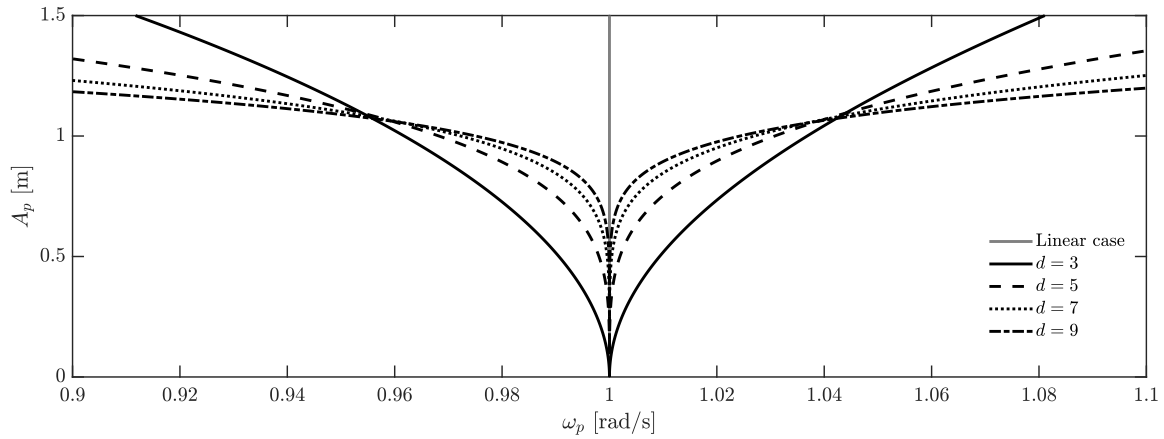

Figure 3.6: Comparison of the phase resonance curves of oscillators with polynomial stiffness term.

The phase resonance curves for oscillators with different values of d is presented in Figure 3.6 with $\alpha_d = \pm 0.1$ N/(kg.m^d). At low amplitudes, the effect of the nonlinearity on the detuning is more important when d is small. The tendency changes at around 4% of detuning in both the hardening and softening cases, where the greater d, the greater the detuning.

3.4 Conclusion

In this chapter, first-order AM was applied to characterize the primary resonance of an oscillator with nonlinear polynomial stiffness. The first important finding is that amplitude resonance always occurs when $\tan \phi_a = \frac{\omega_a}{\varepsilon \zeta \omega_0}$ regardless of the powers included in the polynomial stiffness function[1]. Secondly, we demonstrated that phase resonance, which occurs when the motion is in quadrature with the excitation, happens in the immediate neighbourhood of amplitude resonance for light to moderate damping, i.e., for damping ratios of the order or less than 1%. The resonant phase lag at primary resonance is thus equal to $\pi/2$. The distinction between the amplitude and phase resonances of nonlinear oscillators is rarely discussed in the literature; these results complement what was obtained in [50, 56].

An important difficulty when considering amplitude resonance is that a method for identifying experimentally the amplitude resonance curve has not yet been devised. Conversely, a direct identification of the phase resonance curve is possible thanks to phase-locked loops, see, e.g., [16–20]. Phase resonance has thus the potential to establish a rigorous link between numerical and experimental modal analysis of nonlinear systems.

[1]We, however, note that the stiffness terms with even powers do not participate in the motion at first order.

Chapter 4

Secondary resonances of nonlinear oscillators

4.1 Introduction

Unlike primary resonances, there exists no linear counterpart to secondary resonances; they exist solely due to the nonlinearity present in the system. The $l{:}\nu$ resonance occurs when the frequency of the l-th harmonic is close to the natural frequency of the system, *i.e.*, when $\omega_l = \frac{l\omega}{\nu} \simeq \omega_0$. In 1949 and 1950, Levenson and Stoker classified the resonances of a Duffing oscillator in 4 categories, namely the primary resonance of order 1:1, the superharmonic resonances of order l:1, the subharmonic resonances of order 1:ν and the ultra-subharmonic resonances of order $l{:}\nu$ [39, 66]. Since then, these resonances were extensively studied for the damped Duffing oscillator. For instance, the superharmonic resonances that are in the direct continuation or bifurcate out of the main branch were studied in [22, 71, 72]. More recently, Marchionne et al. showed numerically that the $l{:}\nu$ resonances with $\nu > 1$ are isolated from the main branch [68].

Similarly to the primary resonance, secondary resonances can be studied analytically using perturbation techniques [11, 23, 32]. Using a first-order MMS, the 3:1 and 1:3 resonances of the Duffing oscillator were studied in [4, 12]. First-order averaging was also used to obtain approximations to the 1:1, 3:1 and 1:3 resonances [15, 73], with results comparable to those of the MMS. To obtain analytically more complex resonances, higher-order perturbation techniques must be employed [11, 70, 74]. Using a higher-order AM, Yagasaki was able to find analytical solutions of several $l{:}\nu$ resonances with l and ν nonnecessarily equal to 1 [13–15]. Perturbation techniques were also applied to other nonlinear systems in order to find secondary resonances of SDOF systems [13, 14, 75, 76] and two-DOF systems [13, 77]. However, the main focus of those analytical studies is generally on the amplitude-frequency relations and not on the amplitude-phase lag relations.

The main thrust of this chapter is thus to pay specific attention to the amplitude-phase lag relation of the l-th harmonic of the $l{:}\nu$ resonance with the objective to extend the phase resonance concept to secondary resonances. To this end, the resonant phase lag ϕ_l is defined as the phase lag associated with the amplitude resonance of the l-th

harmonic.

This chapter revisits the work initiated in [13–15, 55] by studying analytically the resonant behavior of a harmonically-forced oscillator with polynomial stiffness of order d. A first-order AM is used to study the d:1 and 1:d resonances and derive the corresponding resonant phase lags. This is illustrated on a Duffing oscillator, a Helmholtz oscillator and an oscillator with quintic nonlinearity. Then, higher-order AM is employed to study the superharmonic (l:1), subharmonic (1:ν) and ultra-subharmonic (l:ν) resonances of the Duffing oscillator.

4.2 First-order averaging

4.2.1 Weakly nonlinear oscillator with hard excitation

The equation of motion of a weakly nonlinear oscillator with hard excitation is

$$\ddot{x}(t) + \omega_0^2 x(t) = \varepsilon \bar{f}_{nl}\left(x(t), \dot{x}(t)\right) + \gamma \sin \omega t \tag{4.1}$$

with $0 < \varepsilon \ll 1$ and $\gamma = \mathcal{O}(1)$ whose effect on the response away from ω_0 is not small. If $\varepsilon = 0$, then Equation (4.1) has a periodic solution $x(t) = \Lambda \sin \omega t$ with $\Lambda = \gamma/(\omega_0^2 - \omega^2)$ away from ω_0. Introducing $z(t) = x(t) - \Lambda \sin \omega t$ in Equation (4.1) yields a weakly nonlinear oscillator

$$\ddot{z}(t) + \omega_0^2 z(t) = \varepsilon \bar{f}_{nl}(z(t), \dot{z}(t), \omega t) \tag{4.2}$$

and, as for the primary resonance in Chapter 3, the response of Equation (4.2) is expressed using a Van der Pol transformation with a frequency ω_l close to a fraction of the natural frequency such that $\omega_l^2 - \omega_0^2 = \varepsilon \Omega_l$

$$z(t) = u_l(t) \cos \omega_l t - v_l(t) \sin \omega_l t \tag{4.3}$$

and the velocity is such that

$$\dot{z}(t) = -u_l(t)\omega_l \sin \omega_l t - v_l(t)\omega_l \cos \omega_l t. \tag{4.4}$$

Equation (4.4) holds only if

$$\dot{u}_l(t) \cos \omega_l t - \dot{v}_l(t) \sin \omega_l t. \tag{4.5}$$

Equation (4.2) now reads

$$u_l(t)\omega_l \sin \omega_l t + v_l(t)\omega_l \cos \omega_l t = -\varepsilon \left(\bar{f}_{nl}(z(t), \dot{z}(t), \omega t) + \Omega_l z(t) \right) \tag{4.6}$$

which can be transformed into a system of first-order equations using Equation (4.5)

$$\begin{cases} \dot{u}_l(t) = -\frac{\varepsilon}{\omega_l} \left(\bar{f}_{nl}(z(t), \dot{z}(t), \omega t) + \Omega_l z(t) \right) \sin \omega_l t \\ \dot{v}_l(t) = -\frac{\varepsilon}{\omega_l} \left(\bar{f}_{nl}(z(t), \dot{z}(t), \omega t) + \Omega_l z(t) \right) \cos \omega_l t. \end{cases} \tag{4.7}$$

In polar coordinates $z(t) = A_l(t)\sin\left(\omega_l t - \phi_l(t)\right)$ with

$$\begin{cases} A_l(t) = \sqrt{u_l^2(t) + v_l^2(t)} \\ \phi_l(t) = \text{atan2}(-u_l(t), -v_l(t)) \end{cases} \tag{4.8}$$

Equation (4.7) reads

$$\begin{cases} \dot{A}_l(t) = \frac{\varepsilon}{\omega_l}\left(\bar{f}_{nl}(z(t), \dot{z}(t), \omega t) + \Omega_l z(t)\right)\cos\left(\omega_l t - \phi_l\right) \\ \dot{\phi}_l(t) = \frac{\varepsilon}{A_l\omega_l}\left(\bar{f}_{nl}(z(t), \dot{z}(t), \omega t) + \Omega_l z(t)\right)\sin\left(\omega_l t - \phi_l\right) \end{cases} \tag{4.9}$$

and is suitable to apply first or higher-order AM [14, 15]. For first-order AM, Equation (4.9) is integrated over one period during which A_l and ϕ_l are considered constant since they are slowly varying with time

$$\begin{cases} \dot{A}_l(t) = \frac{\varepsilon}{\omega_l}\frac{1}{T^*}\int\limits_0^{T^*}\left(\bar{f}_{nl}(z(t), \dot{z}(t), \omega t) + \Omega_l z(t)\right)\cos\left(\omega_l t - \phi_l\right)\mathrm{d}t \\ \dot{\phi}_l(t) = \frac{\varepsilon}{A_l(t)\omega_l}\frac{1}{T^*}\int\limits_0^{T^*}\left(\bar{f}_{nl}(z(t), \dot{z}(t), \omega t) + \Omega_l z(t)\right)\sin\left(\omega_l t - \phi_l\right)\mathrm{d}t \end{cases} \tag{4.10}$$

where T^* is the least common multiple between $T = \frac{2\pi}{\omega}$ and $T_l = \frac{2\pi}{\omega_l}$, *i.e.*, $T^* = \frac{2\nu\pi}{\omega}$. Finally, the displacement $x(t) = A_l\sin\left(\omega_l t - \phi_l\right) + \Lambda\sin\omega t$ can be seen as a Fourier Series with two harmonics, namely the primary harmonic ($l = \nu = 1$) of amplitude Λ and no phase lag and the l-th harmonic of amplitude A_l and phase lag ϕ_l.

4.2.2 Oscillator with polynomial stiffness of order d

The equation of motion is

$$m\ddot{x}(t) + c\dot{x}(t) + kx(t) + k_d x^d(t) = f\sin\omega t \tag{4.11}$$

where k_d represents the nonlinear stiffness coefficient of order d. The natural frequency of the undamped, linearized system is $\omega_0 = \sqrt{\frac{k}{m}}$. Through mass normalization, Equation (4.11) can be recast into

$$\ddot{x}(t) + 2\zeta\omega_0\dot{x}(t) + \omega_0^2 x(t) + \alpha_d x^d(t) = \gamma\sin\omega t \tag{4.12}$$

where $\alpha_d = k_d/m$. Equation (4.12) is scaled such that $\zeta = \varepsilon\bar{\zeta}$ and $\alpha_d = \varepsilon\bar{\alpha}_d$, with $\bar{\zeta}$, $\bar{\alpha}_d = \mathcal{O}(1)$ and $0 < \varepsilon \ll 1$. The resulting system is a weakly nonlinear oscillator with hard excitation

$$\ddot{x}(t) + \omega_0^2 x(t) = \varepsilon\left(-2\bar{\zeta}\omega_0\dot{x}(t) - \bar{\alpha}_d x^d(t)\right) + \gamma\sin\omega t \tag{4.13}$$

and has the same form as Equation (4.1). It is thus suitable for first-order AM. Following the procedure detailed in Section 4.2.1 and dropping the time dependence for A_l and ϕ_l

for conciseness, the following system is obtained

$$\begin{cases} \dot{A}_l = \dfrac{\varepsilon}{\omega_l}\dfrac{1}{T^*}\displaystyle\int_0^{T^*}\left(-2\bar{\zeta}\omega_0\left(\dot{z}(t)+\Lambda\omega\cos\omega t\right)-\bar{\alpha}_d\left(z(t)+\Lambda\sin\omega t\right)^d+\Omega_l z(t)\right) \\ \qquad\qquad \cos\left(\omega_l t-\phi_l\right)\mathrm{d}t \\ \dot{\phi}_l = \dfrac{\varepsilon}{A_l\omega_l}\dfrac{1}{T^*}\displaystyle\int_0^{T^*}\left(-2\bar{\zeta}\omega_0\left(\dot{z}(t)+\Lambda\omega\cos\omega t\right)-\bar{\alpha}_d\left(z(t)+\Lambda\sin\omega t\right)^d+\Omega_l z(t)\right) \\ \qquad\qquad \sin\left(\omega_l t-\phi_l\right)\mathrm{d}t \end{cases} \tag{4.14}$$

For clarity, Equation (4.14) is rewritten as

$$\begin{cases} \dot{A}_l = \frac{\varepsilon}{\omega_l}\left(\dot{A}_{l,\bar{\zeta}}+\dot{A}_{l,\bar{\alpha}}+\dot{A}_{l,\Omega_l}\right) \\ \dot{\phi}_l = \frac{\varepsilon}{A_l\omega_l}\left(\dot{\phi}_{l,\bar{\zeta}}+\dot{\phi}_{l,\bar{\alpha}}+\dot{\phi}_{l,\Omega_l}\right) \end{cases} \tag{4.15}$$

where the pairs $\left(\dot{A}_{l,\bar{\zeta}},\dot{\phi}_{l,\bar{\zeta}}\right)$, $\left(\dot{A}_{l,\bar{\alpha}},\dot{\phi}_{l,\bar{\alpha}}\right)$ and $\left(\dot{A}_{l,\Omega_l},\dot{\phi}_{l,\Omega_l}\right)$ correspond to the $\dot{A}_l$ and $\dot{\phi}_l$ coordinates of the damping, polynomial stiffness and frequency detuning, respectively. Letting $\theta_l=\omega_l t$ in Equation (4.14), the averaged equations for the damping, frequency detuning and polynomial stiffness terms are derived.

4.2.2.1 Averaging of the damping term

For $\dot{A}_{l,\bar{\zeta}}$ and $\dot{\phi}_{l,\bar{\zeta}}$, we have respectively

$$\dot{A}_{l,\bar{\zeta}} = -\frac{1}{2\pi}\int_0^{2l\pi} 2\bar{\zeta}\omega_0\left(A_l\omega_l\cos\left(\theta_l-\phi_l\right)+\Lambda\omega\cos\frac{\nu\theta_l}{l}\right)\cos\left(\theta_l-\phi_l\right)\mathrm{d}\theta_l = -\bar{\zeta}\omega_0\omega_l l A_l \tag{4.16}$$

and

$$\dot{\phi}_{l,\bar{\zeta}} = -\frac{1}{2\pi}\int_0^{2l\pi} 2\bar{\zeta}\omega_0\left(A_l\omega_l\cos\left(\theta_l-\phi_l\right)+\Lambda\omega\cos\frac{\nu\theta_l}{l}\right)\sin\left(\theta_l-\phi_l\right)\mathrm{d}\theta_l = 0. \tag{4.17}$$

4.2.2.2 Averaging of the frequency detuning term

For $\dot{A}_{l,\Omega_l}$ and $\dot{\phi}_{l,\Omega_l}$, we have respectively

$$\dot{A}_{l,\Omega_l} = \frac{1}{2\pi}\int_0^{2l\pi} A_l\Omega_l\sin\left(\theta_l-\phi_l\right)\cos\left(\theta_l-\phi_l\right)\mathrm{d}\theta_l = 0 \tag{4.18}$$

and

$$\dot{\phi}_{l,\Omega_l} = \frac{1}{2\pi}\int_0^{2l\pi} A_l\Omega_l\sin\left(\theta_l-\phi_l\right)\sin\left(\theta_l-\phi_l\right)\mathrm{d}\theta_l = \frac{l\Omega_l}{2}A_l. \tag{4.19}$$

4.2.2.3 Averaging of the polynomial stiffness term

For $\dot{A}_{l,\bar{\alpha}}$ and $\dot{\phi}_{l,\bar{\alpha}}$, we have respectively

$$\dot{A}_{l,\bar{\alpha}} = -\frac{1}{2\pi}\int_0^{2l\pi} \bar{\alpha}_d \left(A_l \sin\left(\theta_l - \phi_l\right) + \Lambda \sin\frac{\nu\theta_l}{l}\right)^d \cos\left(\theta_l - \phi_l\right) \mathrm{d}\theta_l \tag{4.20}$$

and

$$\dot{\phi}_{l,\bar{\alpha}} = -\frac{1}{2\pi}\int_0^{2l\pi} \bar{\alpha}_d \left(A_l \sin\left(\theta_l - \phi_l\right) + \Lambda \sin\frac{\nu\theta_l}{l}\right)^d \sin\left(\theta_l - \phi_l\right) \mathrm{d}\theta_l. \tag{4.21}$$

Solving $\dot{A}_{l,\bar{\alpha}}$ and $\dot{\phi}_{l,\bar{\alpha}}$ is not trivial and requires a symbolic software, such as *Mathematica*. However, for the d:1 ($l = d$ and $\nu = 1$) and the 1:d ($l = 1$ and $\nu = d$) resonances, there exists an elegant analytical solution for both $\dot{A}_{l,\bar{\alpha}}$ and $\dot{\phi}_{l,\bar{\alpha}}$. It can be expressed using the binomial expansion

$$\left(A_l \sin\left(\theta_l - \phi_l\right) + \Lambda \sin\frac{\nu\theta_l}{l}\right)^d = \sum_{p=0}^{d} \binom{d}{p} \left(A_l \sin\left(\theta_l - \phi_l\right)\right)^{d-p} \left(\Lambda \sin\frac{\nu\theta_l}{l}\right)^p \tag{4.22}$$

together with the expansion of odd and even powers of trigonometric functions [73, 78]

$$\begin{cases} \sin^{2i+1}\psi = \frac{1}{2^{2i}} \sum\limits_{p=0}^{i} (-1)^{i-p} \binom{2i+1}{p} \sin\left((2i-2p+1)\psi\right) \\ \sin^{2i}\psi = \frac{1}{2^{2i-1}} \sum\limits_{p=0}^{i-1} (-1)^{i-p} \binom{2i}{p} \cos\left(2(i-p)\psi\right) + \frac{1}{2^{2i}} \binom{2i}{i} \end{cases} \tag{4.23}$$

Therefore, the focus of this section is on the d:1 and 1:d resonances of the oscillator with polynomial stiffness x^d.

Averaging of the polynomial stiffness term for the d:1 superharmonic resonance

In this case, $l = d$ and $\nu = 1$, and a distinction must be made between odd and even values of d. When d is odd, we have

$$\dot{A}_{d,\bar{\alpha}} = -(-1)^{\frac{d-1}{2}} \bar{\alpha}_d \frac{d}{2^d} \Lambda^d \sin\phi_d \tag{4.24}$$

and

$$\begin{aligned} \dot{\phi}_{d,\bar{\alpha}} = -(-1)^{\frac{d-1}{2}} \frac{d}{2^{d+1}} \bar{\alpha}_d \Bigg(& 2\Lambda^d \cos\phi_d + \binom{2p}{p} A_d^d + \\ & \sum_{q=1}^{p-1} \binom{d}{2q} \binom{d-2q+1}{p-q} \binom{2q}{q} A_d^{d-2q} \Lambda^{2q} \Bigg) \end{aligned} \tag{4.25}$$

with $p = \frac{d+1}{2}$. When d is even,

$$\dot{A}_{d,\bar{\alpha}} = -(-1)^{\frac{d}{2}} \bar{\alpha}_d \frac{d}{2^d} \Lambda^d \cos\phi_d \tag{4.26}$$

and

$$\dot{\phi}_{d,\bar{\alpha}} = -(-1)^{\frac{d+2}{2}} \frac{d}{2^d} \bar{\alpha}_d \Lambda^d \sin\phi_d \tag{4.27}$$

Averaging of the polynomial stiffness term for the 1:d subharmonic resonance

In this case, $l = 1$ and $\nu = d$. When d is odd, we have

$$\dot{A}_{1,\bar{\alpha}} = (-1)^{\frac{d-1}{2}} \frac{d}{2^d} \bar{\alpha}_d A_1^{d-1} \Lambda \sin d\phi_1 \tag{4.28}$$

and

$$\begin{aligned} \dot{\phi}_{1,\bar{\alpha}} = \frac{d}{2^{d+1}} \bar{\alpha}_d \Bigg(\binom{2p}{p} A_1^d + \\ \sum_{q=1}^{p-1} \binom{d}{2q} \binom{d-2q+1}{p-q} \binom{2q}{q} A_1^{d-2q} \Lambda^{2q} + (-1)^{\frac{d-1}{2}} 2 A_1^{d-1} \Lambda \cos d\phi_1 \Bigg) \end{aligned} \tag{4.29}$$

with $p = \frac{d+1}{2}$. When d is even,

$$\dot{A}_{1,\bar{\alpha}} = -(-1)^{\frac{d+2}{2}} \frac{d}{2^d} \bar{\alpha}_d A_1^{d-1} \Lambda \cos d\phi_1 \tag{4.30}$$

and

$$\dot{\phi}_{1,\bar{\alpha}} = -(-1)^{\frac{d}{2}} \frac{d}{2^d} \bar{\alpha}_d A_1^{d-1} \Lambda \sin d\phi_1. \tag{4.31}$$

4.2.3 Averaged solution of the oscillator with polynomial stiffness of order d

4.2.3.1 d:1 superharmonic resonance

The averaged equations that govern the d:1 resonance are

$$\begin{cases} \dot{A}_d = \frac{\varepsilon}{\omega_d} \left(-\bar{\zeta} \omega_0 \omega_d d A_d - (-1)^{\frac{d-1}{2}} \bar{\alpha}_d \frac{d}{2^d} \Lambda^d \sin \phi_d \right) \\ \dot{\phi}_d = \frac{\varepsilon}{A_d \omega_d} \Bigg(\frac{d\Omega_d}{2} A_d - (-1)^{\frac{d-1}{2}} \frac{d}{2^{d+1}} \bar{\alpha}_d \Bigg(2\Lambda^d \cos \phi_d + \binom{2p}{p} A_d^d \\ \qquad + \sum_{q=1}^{p-1} \binom{d}{2q} \binom{d-2q+1}{p-q} \binom{2q}{q} A_d^{d-2q} \Lambda^{2q} \Bigg) \Bigg) \end{cases} \tag{4.32}$$

when d is odd and

$$\begin{cases} \dot{A}_d = \frac{\varepsilon}{\omega_d} \left(-\bar{\zeta} \omega_0 \omega_d d A_d - (-1)^{\frac{d}{2}} \bar{\alpha}_d \frac{d}{2^d} \Lambda^d \cos \phi_d \right) \\ \dot{\phi}_d = \frac{\varepsilon}{A_d \omega_d} \left(\frac{d\Omega_d}{2} A_d - (-1)^{\frac{d+2}{2}} \frac{d}{2^d} \bar{\alpha}_d \Lambda^d \sin \phi_d \right) \end{cases} \tag{4.33}$$

when d is even.

At steady-state, *i.e.*, when $\dot{A}_d = \dot{\phi}_d = 0$, we have

$$\begin{cases} \bar{\zeta} \omega_0 \omega_d A_d = (-1)^{\frac{d+1}{2}} \frac{1}{2^d} \bar{\alpha}_d \Lambda^d \sin \phi_d \\ \frac{\Omega_d}{2} A_d = (-1)^{\frac{d-1}{2}} \frac{1}{2^{d+1}} \bar{\alpha}_d \left(2\Lambda^d \cos \phi_d + A_d^d \binom{2p}{p} + \sum_{q=1}^{p-1} \binom{d}{2q} \binom{d-2q+1}{p-q} \binom{2q}{q} A_d^{d-2q} \Lambda^{2q} \right) \end{cases} \tag{4.34}$$

when d is odd and

$$\begin{cases} \bar{\zeta}\omega_0\omega_d A_d = (-1)^{\frac{d+2}{2}} \frac{1}{2^d}\bar{\alpha}_d \Lambda^d \cos\phi_d \\ \frac{\Omega_d}{2} A_d = (-1)^{\frac{d+2}{2}} \frac{1}{2^d}\bar{\alpha}_d \Lambda^d \sin\phi_d \end{cases} \tag{4.35}$$

when d is even.

4.2.3.2 1:d subharmonic resonance

The averaged equations that govern the 1:d resonance are

$$\begin{cases} \dot{A}_1 = \frac{\varepsilon}{\omega_1}\left(-\bar{\zeta}\omega_0\omega_1 A_1 - (-1)^{\frac{d-1}{2}}\frac{d}{2^d}\bar{\alpha}_d A_1^{d-1}\Lambda \sin d\phi_1\right) \\ \dot{\phi}_1 = \dfrac{\varepsilon}{A_1\omega_1}\left(\dfrac{\Omega_1}{2}A_1 + \dfrac{d}{2^{d+1}}\bar{\alpha}_d\left(\binom{2p}{p}A_1^d \right.\right. \\ \qquad\qquad \left.\left. + \displaystyle\sum_{q=1}^{p-1}\binom{d}{2q}\binom{d-2q+1}{p-q}\binom{2q}{q}A_1^{d-2q}\Lambda^{2q} + (-1)^{\frac{d-1}{2}}2A_1^{d-1}\Lambda\cos d\phi_1\right)\right) \end{cases} \tag{4.36}$$

when d is odd and

$$\begin{cases} \dot{A}_1 = \frac{\varepsilon}{\omega_1}\left(-\bar{\zeta}\omega_0\omega_1 A_1 - (-1)^{\frac{d+2}{2}}\frac{d}{2^d}\bar{\alpha}_d A_1^{d-1}\Lambda \cos d\phi_1\right) \\ \dot{\phi}_1 = \frac{\varepsilon}{A_1\omega_1}\left(\frac{\Omega_1}{2}A_1 - (-1)^{\frac{d}{2}}\frac{d}{2^d}\bar{\alpha}_d A_1^{d-1}\Lambda \sin d\phi_1\right) \end{cases} \tag{4.37}$$

when d is even.

At steady-state, *i.e.*, when $\dot{A}_1 = \dot{\phi}_1 = 0$, we have

$$\begin{cases} \bar{\zeta}\omega_0\omega_1 = (-1)^{\frac{d+1}{2}}\frac{d}{2^d}\bar{\alpha}_d A_1^{d-2}\Lambda\sin d\phi_1 \\ \frac{\Omega_1}{2}A_1 = -\frac{d}{2^{d+1}}\bar{\alpha}_d\left(\binom{2p}{p}A_1^d + \sum_{q=1}^{p-1}\binom{d}{2q}\binom{d-2q+1}{p-q}\binom{2q}{q}A_1^{d-2q}\Lambda^{2q} + (-1)^{\frac{d-1}{2}}2A_1^{d-1}\Lambda\cos d\phi_1\right) \end{cases} \tag{4.38}$$

when d is odd and

$$\begin{cases} \bar{\zeta}\omega_0\omega_1 = (-1)^{\frac{d}{2}}\frac{d}{2^d}\bar{\alpha}_d A_1^{d-2}\Lambda\cos d\phi_1 \\ \frac{\Omega_1}{2} = (-1)^{\frac{d}{2}}\frac{d}{2^d}\bar{\alpha}_d A_1^{d-2}\Lambda\sin d\phi_1 \end{cases} \tag{4.39}$$

when d is even. It should be noted that when $d = 2$, then the system becomes

$$\begin{cases} \bar{\zeta}\omega_0\omega_1 = -\frac{1}{2}\bar{\alpha}_2\Lambda\cos 2\phi_1 \\ \frac{\Omega_1}{2} = -\frac{1}{2}\bar{\alpha}_2\Lambda\sin 2\phi_1 \end{cases} \tag{4.40}$$

and no longer involves A_1. The $1:2$ subharmonic resonance cannot be approximated using a first-order AM.

4.2.3.3 Resonant phase lags of the d:1 and 1:d resonances of the oscillator with polynomial stiffness

First-order AM gives relations of the form

$$\begin{cases} f_1(A_l, \omega, \phi_l) = 0 \\ f_2(A_l, \omega, \phi_l) = 0. \end{cases} \tag{4.41}$$

for the d:1 and 1:d resonances. If we assume that the frequency is constant, *i.e.*, $\omega \simeq \frac{\nu\omega_0}{l}$, then Equation (4.41) can be rewritten as

$$\begin{cases} f_1(A_l, \phi_l) = 0 \\ f_2(A_l, \phi_l) = 0 \end{cases} \tag{4.42}$$

A direct relationship between A_l and ϕ_l can thus be derived. The resonant phase lag is the one that solves $\frac{\mathrm{d}A_l}{\mathrm{d}\phi_l}$.

d:1 superharmonic resonance

Assuming a constant frequency $\omega = \frac{\omega_0}{d}$ and d odd, we have

$$A_d = (-1)^{\frac{d+1}{2}} \frac{1}{2^d} \frac{\bar{\alpha}_d}{\zeta\omega_0^2} \Lambda^d \sin\phi_d \tag{4.43}$$

A_d is positive and maximum when $\phi_d = \frac{\pi}{2}$ or $\phi_d = -\frac{\pi}{2}$ if $\frac{d+1}{2}$ is even or odd, respectively.

When d is even,

$$A_d = (-1)^{\frac{d+2}{2}} \frac{1}{2^d} \frac{\bar{\alpha}_d}{\zeta\omega_0^2} \Lambda^d \cos\phi_d \tag{4.44}$$

A_d is positive and maximum when $\phi_d = 0$ or $\phi_d = \pi$ if $\frac{d+2}{2}$ is even or odd, respectively.

1:d subharmonic resonance

Assuming a constant frequency $\omega = d\omega_0$ and d odd,

$$A_1 = \left((-1)^{\frac{d+1}{2}} \frac{d}{2^d} \frac{\bar{\alpha}_d}{\zeta\omega_0^2} \Lambda \sin d\phi_1 \right)^{\frac{1}{2-d}} \tag{4.45}$$

A_1 is positive and maximum when $\phi_1 = \frac{3\pi}{2d} + \frac{2i\pi}{d}$ with $i = 0, \ldots, d$ or $\phi_1 = \frac{\pi}{2d} + \frac{2i\pi}{d}$ with $i = 0, \ldots, d$ if $\frac{d+1}{2}$ is even or odd, respectively. It is interesting to note that in both cases, $\frac{\pi}{2}$ is always a resonant phase lag.

When d is even,

$$A_1 = \left((-1)^{\frac{d}{2}} \frac{d}{2^d} \frac{\bar{\alpha}_d}{\zeta\omega_0^2} \Lambda \sin d\phi_1 \right)^{\frac{1}{2-d}} \tag{4.46}$$

A_1 is positive and maximum when $\phi_1 = \frac{\pi}{d} + \frac{2i\pi}{d}$ with $i = 0, \ldots, d$ or $\phi_1 = \frac{2i\pi}{d}$ with $i = 0, \ldots, d$ if $\frac{d}{2}$ is even or odd, respectively.

4.2.4 The Duffing oscillator

To study the secondary resonances of the Duffing oscillator, Equation (2.68) is scaled such that $\zeta = \bar{\zeta}$ and $\alpha_3 = \varepsilon\bar{\alpha}_3$, with $\bar{\zeta}$, $\bar{\alpha}_3 = \mathcal{O}(1)$:

$$\ddot{x}(t) + \omega_0^2 x(t) = -\varepsilon \left(2\bar{\zeta}\omega_0 \dot{x}(t) + \bar{\alpha}_3 x^3(t) \right) + \gamma \sin\omega t. \tag{4.47}$$

Applying the procedure from Section 4.2.1 yields a weakly nonlinear oscillator

$$\ddot{z}(t) + \omega_0^2 z(t) = -\varepsilon \left(\bar{\alpha}_3 (z(t) + \Lambda \sin \omega t)^3 + 2\bar{\zeta}\omega_0 (\dot{z}(t) + \omega \Lambda \cos \omega t) \right) \tag{4.48}$$

for which first-order AM can be applied for the 3:1 and 1:3 resonances. Unless specified otherwise, the system parameters are $\zeta = 0.005$, $\omega_0 = 1$ and $\alpha_3 = 0.1$ N/m^2.

4.2.4.1 3:1 superharmonic resonance

From Equation (4.32), first-order AM when $l = 3$ and $\nu = 1$ (such that $\varepsilon\Omega_3 = 9\omega^2 - \omega_0^2$) provides

$$\begin{cases} \dot{A}_3 = -\frac{\varepsilon}{\omega} \left(\bar{\zeta}\omega_0 \omega A_3 - \frac{\bar{\alpha}_3 \Lambda^3}{24} \sin \phi_3 \right) \\ \dot{\phi}_3 = -\frac{\varepsilon}{\omega A_3} \left(\frac{\bar{\alpha}_3}{24} \left(3A_3^2 + 6\Lambda^2 - \frac{4\Omega_3}{\bar{\alpha}_3} \right) A_3 - \frac{\bar{\alpha}_3 \Lambda^3}{24} \cos \phi_3 \right). \end{cases} \tag{4.49}$$

At steady-state

$$\begin{cases} \frac{24\bar{\zeta}\omega_0 \omega}{\bar{\alpha}_3} A_3 = \Lambda^3 \sin \phi_3 \\ \left(3A_3^2 + 6\Lambda^2 - \frac{4\Omega_3}{\bar{\alpha}_3} \right) A_3 = \Lambda^3 \cos \phi_3 \end{cases} \tag{4.50}$$

Amplitude resonance

The amplitude resonance for the $3:1$ resonance occurs when $\frac{\partial A_3}{\partial \omega} = \frac{\partial A_3}{\partial \phi_3} = 0$

$$\begin{cases} \frac{\partial A_3}{\partial \phi} = \frac{\bar{\alpha}_3 \Lambda^3}{24\zeta\omega_0\omega} \left(\left[\frac{7\omega^2 - \omega_0^2}{\omega(\omega_0^2 - \omega^2)} \right] \sin \phi_3 \frac{\partial \omega}{\partial \phi_3} + \cos \phi_3 \right) = 0 \\ \frac{\partial A_3}{\partial \omega} = \frac{\bar{\alpha}_3 \Lambda^3}{24\zeta\omega_0\omega} \left(\left[\frac{7\omega^2 - \omega_0^2}{\omega(\omega_0^2 - \omega^2)} \right] \sin \phi_3 + \cos \phi_3 \frac{\partial \phi_3}{\partial \omega} \right) = 0. \end{cases} \tag{4.51}$$

Isolating Ω_3 from (4.50), using the chain rule $\frac{\partial \omega}{\partial \phi_3} = \frac{\partial \omega}{\partial \Omega_3} \frac{\partial \Omega_3}{\partial \phi_3}$ and inserting it in $\frac{\partial A_3}{\partial \phi_3}$ gives

$$\frac{\partial A_3}{\partial \phi_3} = \frac{\bar{\alpha}_3 \Lambda^3 \left(\frac{(7\omega^2 - \omega_0^2)}{\omega(\omega_0^2 - \omega^2)} \frac{\varepsilon\bar{\zeta}\omega_0}{3} \sin \phi_3 + \left(1 - \varepsilon \frac{\bar{\alpha}_3 \Lambda^2}{3(\omega_0^2 - \omega^2)} + \varepsilon \frac{2\bar{\zeta}\omega_0 \omega}{\omega_0^2 - \omega^2} \frac{1}{\tan \phi_3} \right) \cos \phi_3 \right)}{24\zeta\omega_0\omega \left(1 - \varepsilon \left(\frac{\bar{\alpha}_3 \Lambda^2}{3(\omega_0^2 - \omega^2)} + \frac{2\bar{\zeta}\omega_0 \omega}{\omega_0^2 - \omega^2} \frac{1}{\tan \phi_3} - \frac{\bar{\alpha}_3^3 \Lambda^3 \sin {\phi_3}^2}{6912 \bar{\zeta}^2 \omega_0^2 \omega^3} - \frac{\bar{\zeta}\omega_0}{3 \sin \phi_3 \tan \phi_3} \right) \right)}. \tag{4.52}$$

The numerator is 0 when

$$\tan^2 \phi_3 - \frac{3\omega(\omega_0^2 - \omega^2)}{\varepsilon\bar{\zeta}\omega_0(\omega_0^2 - 7\omega^2)} \left(1 - \frac{\varepsilon\bar{\alpha}_3 \Lambda^2}{3(\omega_0^2 - \omega^2)} \right) \tan \phi_3 - \frac{6\omega^2}{(\omega_0^2 - 7\omega^2)} = 0. \tag{4.53}$$

Solving this equation for $\tan \phi_3$ and keeping only the leading term, the phase lag at amplitude resonance writes

$$\tan \phi_{3,a} = \frac{3\omega_a(\omega_0^2 - \omega_a^2)}{\varepsilon\bar{\zeta}\omega_0(\omega_0^2 - 7\omega_a^2)}. \tag{4.54}$$

Since ω is close to $\frac{\omega_0}{3}$ for the 3:1 resonance, it follows that

$$\frac{\omega_0^2 - \omega_a^2}{\omega_0^2 - 7\omega_a^2} \simeq 4 \tag{4.55}$$

which yields

$$\tan\phi_{3,a} = \frac{12\omega_a}{\varepsilon\bar{\zeta}\omega_0}. \tag{4.56}$$

Inserting this relation in Equations (4.50) and assuming that the static response is constant, i.e., $\Lambda \approx \Lambda_* = \frac{9\gamma}{8\omega_0}$, provides an expression of the amplitude of the third harmonic and of the frequency at amplitude resonance

$$\begin{cases} A_{3,a} = \frac{\alpha_3\Lambda_*^3}{2\zeta\omega_0\sqrt{\zeta^2\omega_0^2+144\omega_a^2}} \\ \omega_a = \sqrt{\frac{-c_2+\sqrt{c_2^2-4c_1c_3}}{2c_1}} \end{cases} \tag{4.57}$$

where

$$\begin{cases} c_1 = \frac{1728}{\alpha_3} \\ c_2 = -144\left(2\Lambda_*^2 + \frac{4\omega_0^2}{3\alpha_3} - \frac{3\zeta^2}{4\alpha_3}\right) \\ c_3 = \left(\frac{2\zeta^2\omega_0^2}{3\alpha_3} - 2\Lambda_*^2 - \frac{4\omega_0^2}{3\alpha_3}\right)\zeta^2\omega_0^2 - \frac{\alpha_3^2\Lambda_*^6}{4\zeta^2\omega_0^2}. \end{cases} \tag{4.58}$$

Phase resonance

For weak damping, Equation (4.56) shows that $\tan\phi_{3,a}$ takes very large values at amplitude resonance. Amplitude resonance thus occurs near $\phi_{3,a} = \pi/2$, i.e., when there is phase quadrature between the third harmonic of the displacement and the forcing. The phase resonance for the 3:1 superharmonic resonance can thus be associated with a phase lag of $\phi_{3,p} = \pi/2$, in accordance with what was found in Section (4.2.3.3). The averaged equations of motion (4.50) become:

$$\begin{cases} A_{3,p} = \frac{\alpha_3\Lambda^3}{24\zeta\omega_0\omega_p} \\ A_{3,p} = \sqrt{\frac{4\Omega_3}{3\bar{\alpha}_3} - 2\Lambda^2}. \end{cases} \tag{4.59}$$

If we assume again that $\Lambda \approx \Lambda_*$, it is possible to derive a closed-form expression for $A_{3,p}$ and ω_p

$$\begin{cases} A_{3,p} = \frac{\alpha_3\Lambda_*^3}{24\zeta\omega_0\omega_p} \\ \omega_p = \sqrt{\frac{-c_2+\sqrt{c_2^2-4c_1c_3}}{2c_1}} \end{cases} \tag{4.60}$$

where

$$\begin{cases} c_1 = \frac{1728}{\alpha_3} \\ c_2 = -144\left(2\Lambda_*^2 + \frac{4\omega_0^2}{3\alpha_3}\right) \\ c_3 = -\frac{\alpha_3^2\Lambda_*^6}{4\zeta^2\omega_0^2}. \end{cases} \tag{4.61}$$

Stability analysis

Stability analysis is performed by studying the eigenvalues of the Jacobian matrix of the equations of motion from (4.50)

$$\det(\mathbf{J}) = \begin{vmatrix} -\frac{24\bar{\zeta}\omega_0\omega}{\bar{\alpha}_3} - \lambda & 3A_3^3 + \left(6\Lambda^2 - \frac{4\Omega_3}{\bar{\alpha}_3}\right) A_3 \\ -9A_3^2 - 6\Lambda^2 - \frac{4\Omega_3}{\bar{\alpha}_3} & -\frac{24\bar{\zeta}\omega_0\omega}{\bar{\alpha}_3} A_3 - \lambda. \end{vmatrix} \tag{4.62}$$

As for primary resonances, the solution is asymptotically stable if all the eigenvalues λ of the system have a strictly negative real part (see Appendix A). This is not the case when

$$\left(3A_3^3 + \left(6\Lambda^2 - \frac{4\Omega_3}{\bar{\alpha}_3}\right) A_3\right)\left(9A_3^2 + 6\Lambda^2 - \frac{4\Omega_3}{\bar{\alpha}_3}\right) + \frac{576\bar{\zeta}^2\omega_0^2\omega^2}{\bar{\alpha}_3^2} < 0. \tag{4.63}$$

The loss of stability happens between fold bifurcations, *i.e.*, when $\frac{\partial\omega}{\partial A} = 0$. This is proven by adding together the square of the two relations in Equation 4.50, taking the derivative with respect to A and setting $\frac{\partial\omega}{\partial A} = 0$, which imposes a fold bifurcation. We finally find that these folds occur when

$$\left(3A_3^3 + \left(6\Lambda^2 - \frac{4\Omega_3}{\bar{\alpha}_3}\right) A_3\right)\left(9A_3^2 + 6\Lambda^2 - \frac{4\Omega_3}{\bar{\alpha}_3}\right) + \frac{576\bar{\zeta}^2\omega_0^2\omega^2}{\bar{\alpha}_3^2} = 0. \tag{4.64}$$

Results and discussion

Still assuming $\Lambda \approx \Lambda_*$, we compute ΔA, $\Delta\omega$ and $\Delta\phi$, as in Section 2.2.3.3 and perform a Taylor series expansion around $\varepsilon = 0$. It yields

$$\begin{aligned} \Delta A &= -\frac{(63 + 8\omega_0^2)}{768\sqrt{2}\omega_0}\zeta^2\varepsilon^2 + \mathcal{O}\left(\varepsilon^3\right) = \mathcal{O}\left(\varepsilon^2\right) \\ \Delta\omega &= -\frac{11\left(2\omega_0^2 - 9\right)}{1024\sqrt{2}\omega_0^4}\Lambda_*^3\alpha_3\zeta\varepsilon^2 + \mathcal{O}\left(\varepsilon^3\right) = \mathcal{O}\left(\varepsilon^2\right) \\ \Delta\phi &= -\frac{211}{256\sqrt{2}}\zeta\varepsilon + \mathcal{O}\left(\varepsilon^2\right) = \mathcal{O}\left(\varepsilon\right). \end{aligned} \tag{4.65}$$

In addition to that, Equation (4.60) shows that the amplitude at resonance is proportional to α_3 and γ but inversely proportional to ω_p. We can rewrite the frequency at phase resonance as

$$\omega_p = \sqrt{\frac{48\zeta\omega_0\left(6\alpha_3\Lambda_*^2 + 4\omega_0^2\right) + \sqrt{2304\zeta^2\omega_0^2\left(6\alpha_3\Lambda_* + 4\omega_0^2\right)^2 + 1728\alpha_3^2\Lambda_*^6}}{3456\zeta\omega_0}} \tag{4.66}$$

and we see that it is proportional to $\sqrt{\alpha_3}$ and $\gamma^{3/2}$. Overall, if α_3 or γ increases, both the amplitude and the frequency at resonance increase. This hardening effect due to the increasing of the forcing is confirmed in Figures 4.1a and 4.1b. In these figures, the NFRCs calculated from Equation (4.50) and the phase resonance curves constructed thanks to Equations (4.60) and (4.61) are compared to the numerical solution computed

with the HBM. Furthermore, the newly-defined concept of a phase resonance for the 3:1 superharmonic resonance is in excellent agreement with the maxima of the third harmonic of the response, as suggested by Equation (4.65). In the case of a softening Duffing oscillator ($\alpha_3 < 0$), the phase lag $\phi_{3,p}$ should be adjusted to $\frac{3\pi}{2}$ in order to have a positive amplitude $A_{3,p}$. This phase lag is still consistent with Equation (4.56).

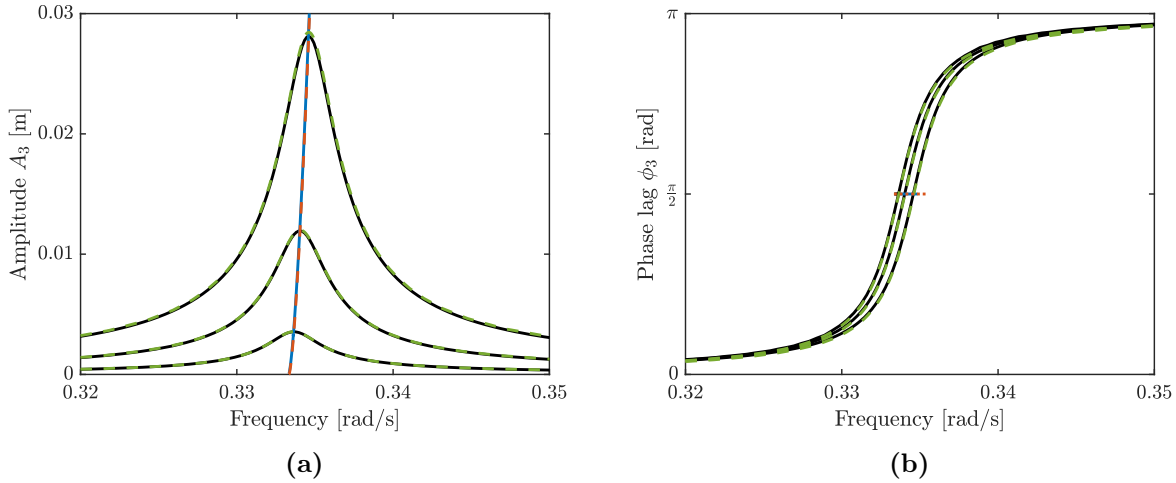

Figure 4.1: NFRCs (HBM: black; AM: green) and phase resonance curves (HBM: blue; AM: orange) around the 3:1 resonance of the Duffing oscillator for forcing amplitudes of 0.1 N/kg, 0.15 N/kg and 0.2 N/kg: (a) amplitude and (b) phase lag.

The effect of an increase in α_3 is compared to the numerical solution in Figure 4.2. The discrepancies between the averaged and numerical solutions are due to a too strong nonlinearity. However, the trend is the same, namely as α_3 increases, both the amplitude and frequency at resonance increases until a fold appears in the NFRC, leading to a loss of stability as discussed in Section 4.2.4.1.

4.2.4.2 1:3 subharmonic resonance

For $l = 1$, $\nu = 3$, Equation (4.36) gives

$$\begin{cases} \dot{A}_1 = -\frac{\varepsilon}{\omega}\left(\bar{\zeta}\omega_0\omega A_1 - \frac{9\bar{\alpha}_3\Lambda}{8}A_1^2\sin 3\phi_1\right) \\ \dot{\phi}_1 = -\frac{\varepsilon}{\omega A_1}\left(\frac{3\bar{\alpha}_3}{8}\left(3A_1^2 + 6\Lambda^2 - \frac{4\Omega_1}{\bar{\alpha}_3}\right)A_1 - \frac{9\bar{\alpha}_3\Lambda}{8}A_1^2\cos 3\phi_1\right). \end{cases} \tag{4.67}$$

For steady-state solutions and assuming $A_1 \neq 0$,

$$\begin{cases} \frac{8\bar{\zeta}\omega_0\omega}{3\bar{\alpha}_3} = 3\Lambda A_1 \sin 3\phi_1 \\ 3A_1^2 + 6\Lambda^2 - \frac{4\Omega_1}{\bar{\alpha}_3} = 3\Lambda A_1 \cos 3\phi_1. \end{cases} \tag{4.68}$$

Adding the square of both relations of (4.68) together gives a quadratic equation in A_1^2

$$9A_1^4 + \left(27\Lambda^2 - \frac{24\Omega_1}{\bar{\alpha}_3}\right)A_1^2 + \left(6\Lambda^2 - \frac{4\Omega_1}{\bar{\alpha}_3}\right)^2 + \frac{64\bar{\zeta}^2\omega_0^2\omega^2}{9\bar{\alpha}_3^2} = 0 \tag{4.69}$$

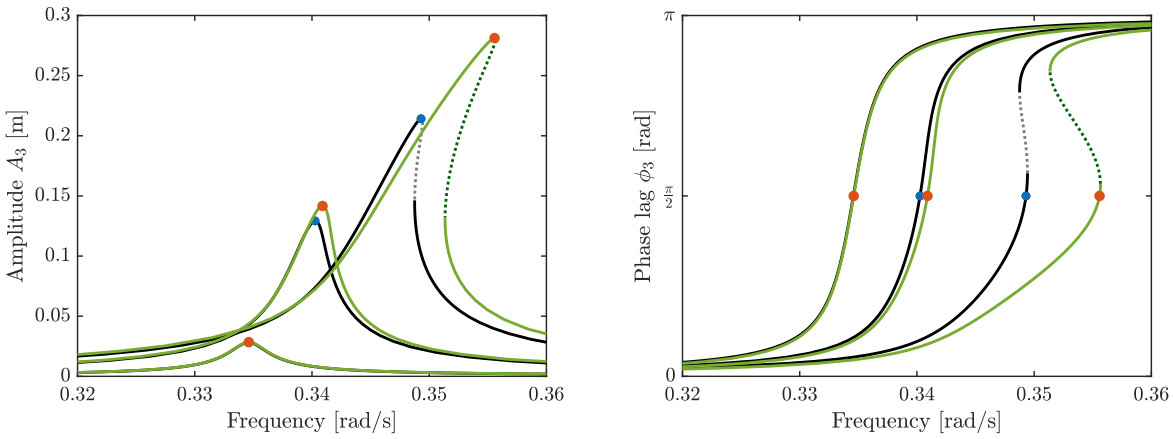

(a) **(b)**

Figure 4.2: NFRCs (HBM: black (stable) and grey (unstable); AM: solid green (stable) and dotted green (unstable)) and phase resonance points (HBM: blue; AM: orange) around the 3:1 resonance of the Duffing oscillator for a forcing amplitude of 0.1 N/kg and $\alpha_3 = 0.1$ N/m^3, 0.5 N/m^3 and 1 N/m^3: (a) amplitude and (b) phase lag.

In order to have A_1 real, we must have that $27\Lambda^2 - \frac{24\Omega_1}{\bar{\alpha}_3} > 0$ and $\left(27\Lambda^2 - \frac{24\Omega_1}{\bar{\alpha}_3}\right)^2 - 36\left(\left(6\Lambda^2 - \frac{4\Omega_1}{\bar{\alpha}_3}\right)^2 + \frac{64\bar{\zeta}^2\omega_0^2\omega^2}{9\bar{\alpha}_3^2}\right) > 0$. The first relation evidences that Ω_1 and $\bar{\alpha}_3$ must have the same sign. The second relation gives the conditions for the existence of the 1:3 subharmonic resonance, illustrated in Figure 4.3 when $\zeta = 0.5\%$ and $\alpha_3 = 0.1$ N/m^3. The boundaries of the existence domain are given by

$$\gamma = \frac{\|\omega_0^2 - \omega_b^2\|}{\sqrt{3\bar{\alpha}_3}}\sqrt{\frac{432}{378}}\sqrt{\Omega_1 \pm \sqrt{\Omega_1^2 - \frac{28}{9}\bar{\zeta}^2\omega_0^2\omega_b^2}} \tag{4.70}$$

where ω_b are the frequencies at the extremities of the isola. We see in Figure 4.3 that (4.70) admits a minimum forcing under which the 1:3 subharmonic resonance does not exist. In this case, a forcing of 0.79 N/kg is required for the existence of the resonance.

Amplitude resonance

Amplitude resonance occurs when $\frac{\partial A_1}{\partial \omega} = \frac{\partial A_1}{\partial \phi} = 0$:

$$\begin{cases} \frac{\partial A_1}{\partial \phi_1} = \frac{8\bar{\zeta}\omega_0}{9\bar{\alpha}_3\Lambda\sin 3\phi_1}\left(\left(1 - \frac{2\omega^2}{\omega_0^2 - \omega^2}\right)\frac{\partial \omega}{\partial \phi_1} - \frac{3\omega}{\tan 3\phi_1}\right) = 0 \\ \frac{\partial A_1}{\partial \omega} = \frac{8\bar{\zeta}\omega_0}{9\bar{\alpha}_3\Lambda\sin 3\phi_1}\left(\left(1 - \frac{2\omega^2}{\omega_0^2 - \omega^2}\right) - \frac{3\omega}{\tan 3\phi_1}\frac{\partial \phi_1}{\partial \omega}\right) = 0 \end{cases} \tag{4.71}$$

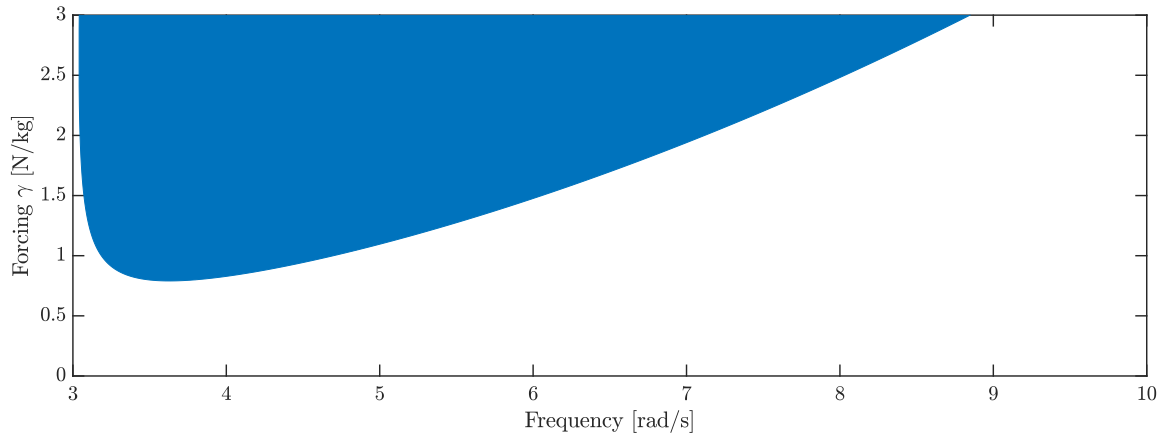

Figure 4.3: Domain of existence (blue area) of the 1:3 subharmonic resonance as a function of the forcing amplitude.

We must have $\sin 3\phi_1 \neq 0$, *i.e.*, $\phi_1 \neq \frac{i\pi}{3}$, where i is an integer. Following the same procedure as for the previous resonances gives:

$$\frac{\partial A_1}{\partial \phi_1} = \frac{8\bar{\zeta}\omega_0}{9\bar{\alpha}_3\Lambda \sin 3\phi_1} \frac{\left(1-\frac{2\omega^2}{\omega_0^2-\omega^2}\right)\varepsilon 9\bar{\zeta}\omega_0 - \frac{3\omega}{\tan 3\phi_1}\left(1-\varepsilon\frac{27\bar{\alpha}_3\Lambda^2}{\omega_0^2-\omega^2}+\varepsilon\frac{6\bar{\zeta}\omega_0}{\omega_0^2-\omega^2}\frac{1}{\tan 3\phi_1}\right)}{1-\varepsilon\frac{27\bar{\alpha}_3\Lambda^2}{\omega_0^2-\omega^2}+\varepsilon\frac{6\bar{\zeta}\omega_0}{\omega_0^2-\omega^2}\frac{1}{\tan 3\phi_1} - \left(1-\frac{2\omega^2}{\omega_0^2-\omega^2}\right)\left(\varepsilon\frac{16\zeta^2\omega_0^2}{3\bar{\alpha}_3\Lambda^2\sin^2 3\phi_1}+\varepsilon\frac{3\bar{\zeta}\omega_0}{\omega\tan 3\phi_1}\right)}. \tag{4.72}$$

The numerator is equal to 0 when:

$$9\varepsilon\bar{\zeta}\omega_0\left(1-\frac{2\omega^2}{\omega_0^2-\omega^2}\right)\tan^2 3\phi_1 - 3\omega\left(1-\varepsilon\frac{27\bar{\alpha}_3\Lambda^2}{\omega_0^2-\omega^2}\right)\tan\phi_1 - \varepsilon\frac{18\bar{\zeta}\omega_0\omega^2}{\omega_0^2-\omega^2} = 0. \tag{4.73}$$

Solving this equation for $\tan 3\phi_1$ and keeping only the leading term, the phase lag at amplitude resonance can be approximated with

$$\tan 3\phi_{1,a} = \frac{\omega_a}{3\bar{\zeta}\omega_0\left(1+\frac{2\omega_a^2}{\omega_a^2-\omega_0^2}\right)}. \tag{4.74}$$

Since ω is close to $3\omega_0$ for the 1:3 resonance, it follows that

$$\frac{2\omega_a^2}{\omega_a^2-\omega_0^2} \simeq \frac{9}{4} \tag{4.75}$$

which yields

$$\tan 3\phi_{1,a} = \frac{4\omega_a}{39\bar{\zeta}\omega_0}. \tag{4.76}$$

Inserting this relation in Equations (4.68) gives:

$$\begin{cases} A_{1,a} = \frac{2\bar{\zeta}\omega_0}{9\bar{\alpha}_3\Lambda}\sqrt{1521\bar{\zeta}^2\omega_0^2+16\omega_a^2} \\ \gamma = \frac{\|\omega_0^2-\omega_a^2\|}{\sqrt{6\bar{\alpha}_3}}\sqrt{(2\Omega_1+13\zeta^2\omega_0^2)^2 \pm \sqrt{(2\Omega_1+13\bar{\zeta}^2\omega_0^2)^2-\frac{8}{9}\bar{\zeta}^2\omega_0^2(1521\bar{\zeta}^2\omega_0^2+16\omega_a^2)}}. \end{cases} \tag{4.77}$$

Unlike the 3 : 1 superharmonic resonance, the static response cannot be assumed to be constant because the frequency varies much faster for the 1:3 subharmonic resonance (see Figure 4.4). An explicit expression for the resonance frequency ω_a as a function of the forcing γ cannot thus be derived. We also note that, due to the $\pm$ sign, there exist two frequencies satisfying (4.77), the greatest (lowest) frequency corresponding to the maximum (minimum) response on the isolated branch. It is thus the greatest frequency which is in relation with the resonance frequency ω_a.

Phase resonance

For weak damping, Equation (4.76) shows that the amplitude resonance occurs near phase lags equal to $\frac{\pi}{6} + \frac{i\pi}{3}$ where i is an integer. For odd (even) values of i, A_1 takes positive (negative) values. Considering positive amplitudes, the phase resonance for the 1:3 subharmonic resonance can be associated with phase lags equal to $\frac{\pi}{2}$, $\frac{7\pi}{6}$ and $\frac{11\pi}{6}$, which is accordance with the results in Section (4.2.3.3). For $\frac{\pi}{2}$, the averaged equations of motion (4.50) can be transformed into

$$\begin{cases} A_{1,p} = \frac{8\bar{\zeta}\omega_0\omega_p}{9\bar{\alpha}_3\Lambda} \\ \gamma = \frac{\|\omega_0^2-\omega_p^2\|}{\sqrt{3\bar{\alpha}_3}}\sqrt{\Omega_1 \pm \sqrt{\Omega_1^2 - \frac{32}{9}\bar{\zeta}^2\omega_0^2\omega_p^2}}. \end{cases} \tag{4.78}$$

The same expressions can be obtained if the two other phase lags are considered instead.

For a softening Duffing oscillator, amplitude resonance still occurs for phase lags ϕ_p near $\frac{\pi}{6} + \frac{i\pi}{3}$ except that positive amplitudes occur now when i is even. Thus, the resonant phase lags are $\frac{\pi}{6}$, $\frac{5\pi}{6}$ and $\frac{3\pi}{2}$.

Stability analysis

Stability analysis is performed by studying the eigenvalues of the Jacobian matrix of the equations of motion from (4.68)

$$\det(\mathbf{J}) = \begin{vmatrix} \frac{8\bar{\zeta}\omega_0\omega}{3A_1^2\bar{\alpha}_3} - \lambda & 9A_1 + \frac{3}{A_1}\left(6\Lambda^2 - \frac{4\Omega_1}{3\bar{\alpha}_3}\right) \\ -3 + \frac{1}{A_1^2}\left(6\Lambda^2 - \frac{4\Omega_1}{3\bar{\alpha}_3}\right) & -\frac{8\bar{\zeta}\omega_0\omega}{A_1\bar{\alpha}_3} - \lambda. \end{vmatrix} \tag{4.79}$$

As for primary resonances, the solution is asymptotically stable if all the eigenvalues λ of the system have a strictly negative real part. This is not the case when

$$\left(9A_1 + \frac{3}{A_1}\left(6\Lambda^2 - \frac{4\Omega_1}{3\bar{\alpha}_3}\right)\right)\left(3 - \frac{1}{A_1^2}\left(6\Lambda^2 - \frac{4\Omega_1}{3\bar{\alpha}_3}\right)\right) - \frac{64\bar{\zeta}^2\omega_0^2\omega^2}{3A_1^3\bar{\alpha}_3^2} < 0. \tag{4.80}$$

The loss of stability happens between fold bifurcations, *i.e.*, when $\frac{\partial\omega}{\partial A} = 0$. This is proven by adding together the square of the two relations in Equation 4.68, taking the derivative with respect to A and setting $\frac{\partial\omega}{\partial A} = 0$, which imposes a fold bifurcation. We finally find that these folds occur when

$$\left(9A_1 + \frac{3}{A_1}\left(6\Lambda^2 - \frac{4\Omega_1}{3\bar{\alpha}_3}\right)\right)\left(3 - \frac{1}{A_1^2}\left(6\Lambda^2 - \frac{4\Omega_1}{3\bar{\alpha}_3}\right)\right) - \frac{64\bar{\zeta}^2\omega_0^2\omega^2}{3A_1^3\bar{\alpha}_3^2} = 0. \tag{4.81}$$

Results and discussion

Figure 4.4 compares the NFRCs and the phase resonance curve corresponding to $\phi_1 = \frac{\pi}{2}$, constructed thanks to Equations (4.68). As anticipated, phase quadrature is found to trace out the locus of the maxima of the different isolated responses. This is also the case for the numerical solution in Figure 4.5.

The fact that phase resonance is located close to the extremities of the isola can be explained by looking at Equation (4.70) and the second relation of Equation (4.78). If we rewrite them using the unscaled system parameters, we have

$$\begin{cases} \gamma = \frac{\|\omega_0^2-\omega_b^2\|}{\sqrt{3\alpha_3}}\sqrt{\frac{432}{378}}\sqrt{(\omega_{l,b}^2-\omega_0^2) \pm \sqrt{(\omega_{l,b}^2-\omega_0^2)^2 - \frac{28}{9}\zeta^2\omega_0^2\omega_b^2}} \\ \gamma = \frac{\|\omega_0^2-\omega_p^2\|}{\sqrt{3\alpha_3}}\sqrt{(\omega_{l,p}^2-\omega_0^2) \pm \sqrt{(\omega_{l,p}^2-\omega_0^2)^2 - \frac{32}{9}\zeta^2\omega_0^2\omega_p^2}}. \end{cases} \tag{4.82}$$

Assuming that $\sqrt{\frac{432}{378}} \simeq 1$ and that in practice $(\omega_l^2 - \omega_0^2) \gg \zeta \ll 1$ (even though this violates the AM hypotheses), we end up with

$$\begin{cases} \gamma \simeq \frac{\|\omega_0^2-\omega_b^2\|}{\sqrt{3\alpha_3}}\sqrt{(\omega_l^2-\omega_0^2) \pm \sqrt{(\omega_l^2-\omega_0^2)^2 - \mathcal{O}\left(\varepsilon^2\right)}} \\ \gamma = \frac{\|\omega_0^2-\omega_p^2\|}{\sqrt{3\alpha_3}}\sqrt{(\omega_l^2-\omega_0^2) \pm \sqrt{(\omega_l^2-\omega_0^2)^2 - \mathcal{O}\left(\varepsilon^2\right)}} \end{cases} \tag{4.83}$$

As a result, $\omega_b \simeq \omega_p$, which is confirmed in Figure 4.6.

4.2.4.3 Other resonances

We can try to apply first-order AM to obtain the governing equations of higher-order resonances such as the 5:1 and 1:5 resonances. This gives

$$\begin{cases} \dot{A}_5 = -\varepsilon\bar{\zeta}\omega_0 A_5 \\ \dot{\phi}_5 = -\frac{\varepsilon}{40\omega}\left(3\bar{\alpha}_3 A_5^2 + 6\bar{\alpha}_3\Lambda^2 - 4\Omega_5\right) \end{cases} \tag{4.84}$$

and

$$\begin{cases} \dot{A}_1 = -\varepsilon\bar{\zeta}\omega_0 A_1 \\ \dot{\phi}_1 = -\frac{5\varepsilon}{8\omega}\left(3\bar{\alpha}_3 A_1^2 + 6\bar{\alpha}_3\Lambda^2 - 4\Omega_1\right) \end{cases} \tag{4.85}$$

respectively. At steady-state, no information is obtained about the evolution of the phase lag. The amplitude of the l-th harmonic can be either 0 or

$$A_{1,5} = \sqrt{\frac{4\Omega_{1,5}}{3\bar{\alpha}_3} - 2\Lambda^2} \tag{4.86}$$

if the first or second relation of Equations (4.84) and (4.85) is considered, respectively. Higher-order AM is thus necessary to gather information about the phase lag.

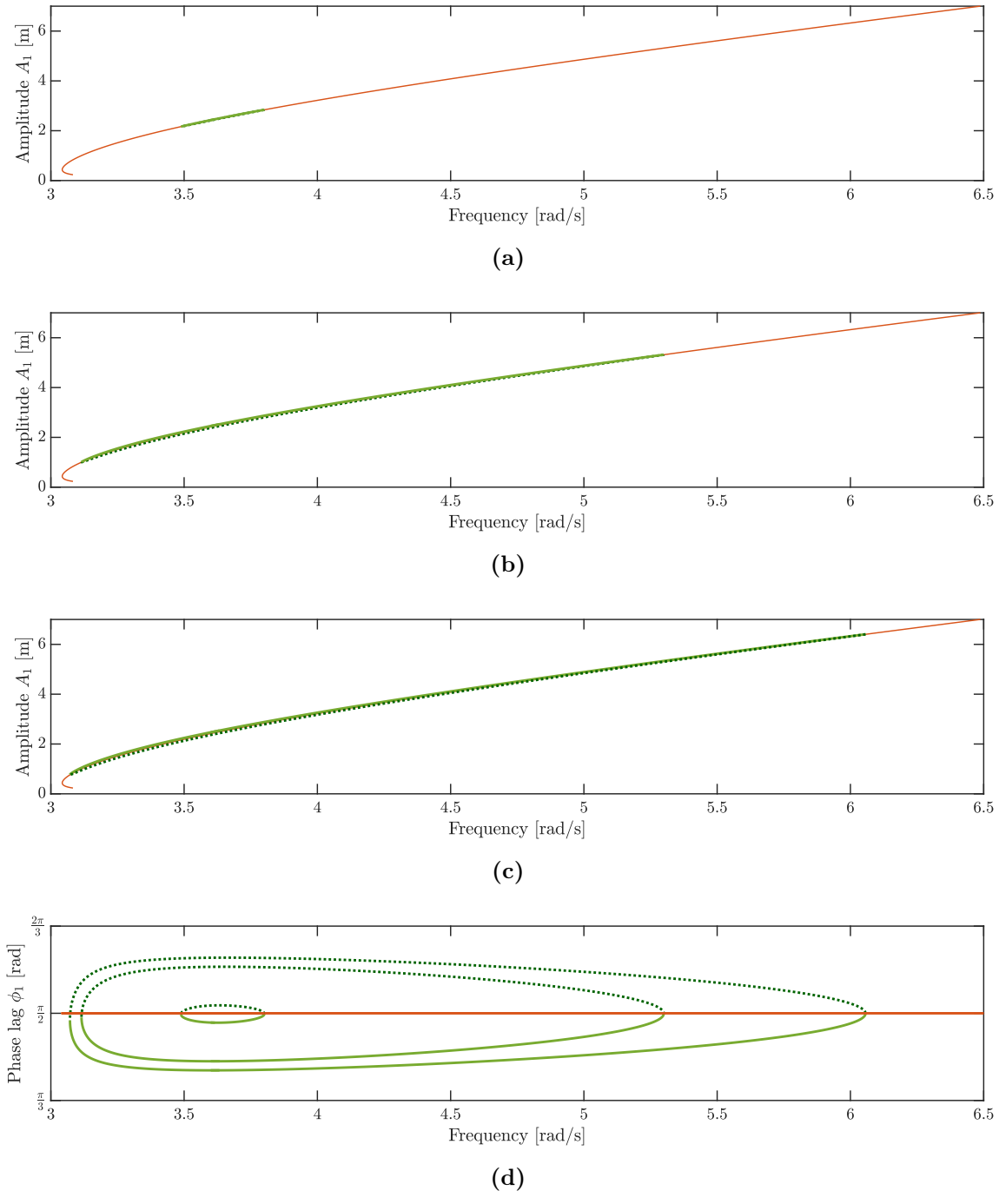

Figure 4.4: NFRCs (solid green: stable; dotted green: unstable) and phase resonance curve (orange) around the 1:3 resonance of the Duffing oscillator with the AM: (a) 0.8 N, (b) 1.2N, (c) 1.5 N and (d) phase lag.

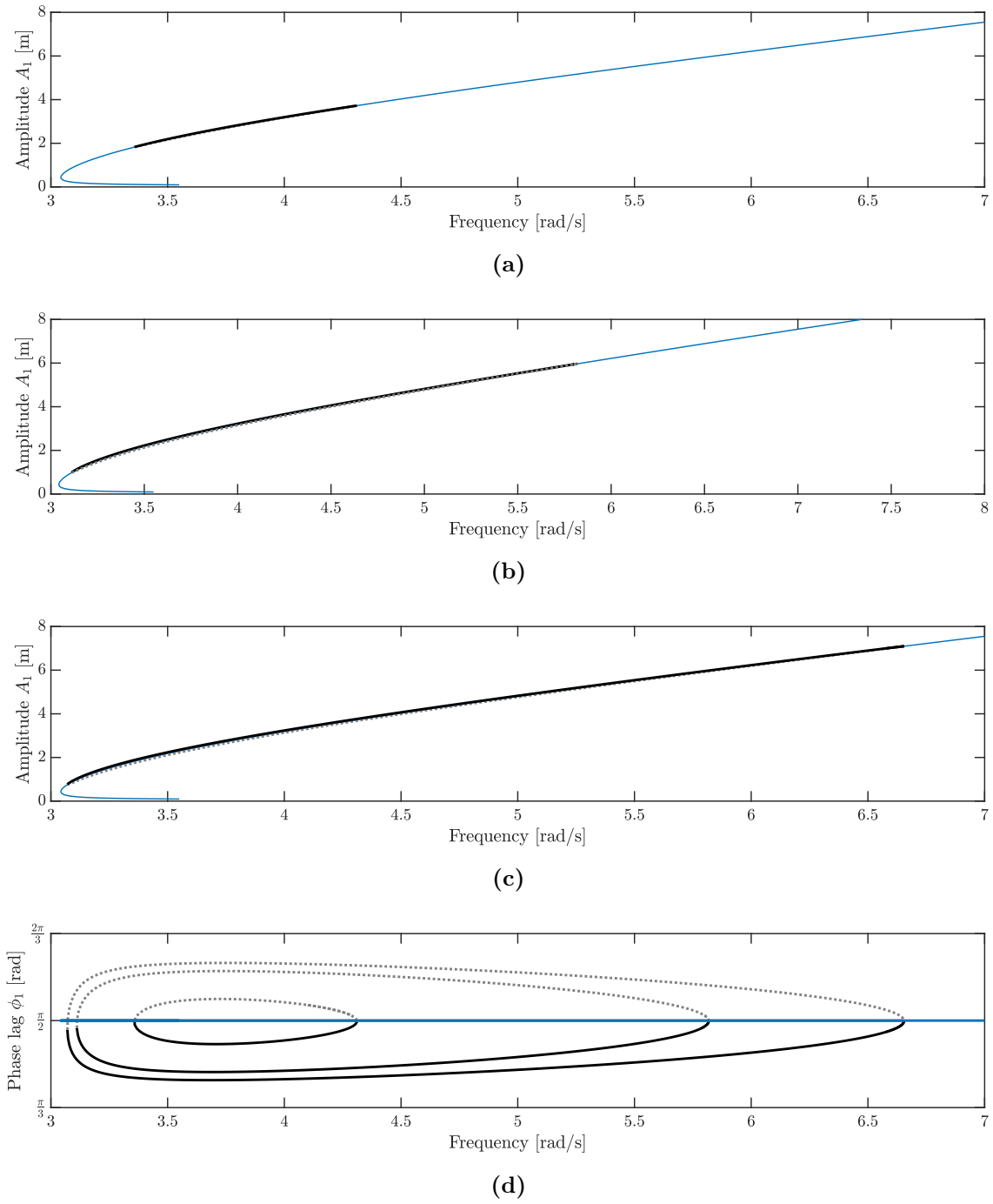

Figure 4.5: NFRCs (black) and phase resonance curve (blue) around the 1:3 resonance of the Duffing oscillator using the HBM: (a) 0.8 N, (b) 1.2N, (c) 1.5 N and (d) phase lag.

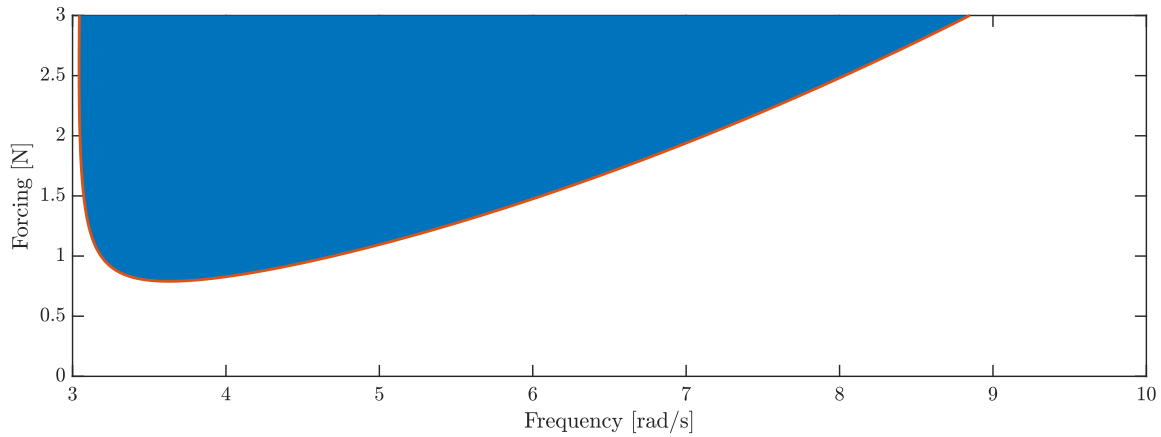

Figure 4.6: Domain of existence (blue area) and phase resonance curve (orange) of the 1:3 subharmonic resonance as a function of the forcing amplitude.

4.2.5 The Helmholtz oscillator

The equation of motion of the weakly nonlinear Helmholtz oscillator is

$$\ddot{x}(t) + \omega_0^2 x(t) = -\varepsilon \left(2\bar{\zeta}\omega_0 \dot{x}(t) + \bar{\alpha}_2 x^2(t)\right) + \gamma \sin \omega t \tag{4.87}$$

The system parameters considered here are $\zeta = 0.005$, $\omega_0 = 1$ and $\alpha_2 = 0.1$ N/m^2.

4.2.5.1 2:1 superharmonic resonance

According to Equation (4.35), the averaged equations of motion around the 2:1 resonance are

$$\begin{cases} \bar{\zeta}\omega_0 \omega A_2 = \frac{1}{8}\bar{\alpha}_2 \Lambda^2 \cos\phi_2 \\ \Omega_2 A_2 = \frac{1}{8}\bar{\alpha}_2 \Lambda^2 \sin\phi_2 \end{cases} \tag{4.88}$$

The system acts as a linear oscillator around the 2:1 resonance since the equations of motion are similar to those obtained for the damped, forced harmonic oscillator in Section 2.2.2. The resonant phase lag is $\phi_2 = 0$, as demonstrated in Section 4.2.3.3. This is confirmed in Figure 4.7 where the amplitude resonance is close to $\phi_2 = 0$. The NFRCs obtained with the AM are also compared to those obtained with the HBM. Though the curves match well, those obtained with the HBM present a slight softening behavior that cannot be obtained with a first-order AM. Still, even with the HBM, $\phi_2 = 0$ is a good indicator of the amplitude resonance.

4.2.5.2 1:2 subharmonic resonance

It was shown in Equation (4.40) that first-order AM does not give accurate equations of motion for a quadratic nonlinearity. This resonance can only be studied numerically. The dynamics of this resonance is quite complex. At forcing starting from 0N, the 1:2 branch crosses the 0 rad/s axis and for forcing amplitudes greater than 0.3 N/kg, the branch is attached to the main branch thanks to bifurcation points but also crosses the 0 rad/s axis.

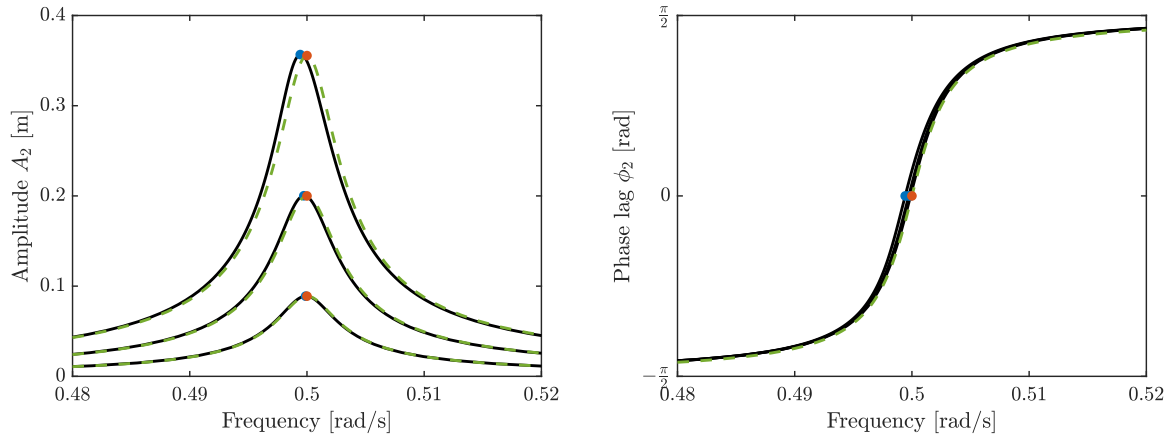

(a) **(b)**

Figure 4.7: NFRCs (HBM: black; AM: green) and phase resonance points (HBM: blue; AM: orange) around the 2:1 resonance of the Helmholtz oscillator for forcing amplitudes of 0.1 N/kg, 0.15 N/kg and 0.2 N/kg: (a) amplitude and (b) phase lag.

Those dynamics are not studied here. Therefore, the 1:2 resonance branch is only studied for an intermediate forcing amplitude. The response is an isolated branch for which the extremities correspond to a minimum and a maximum of amplitude where the phase lag is $\phi_1 = \pi$, in line with the results of Section 4.2.3.3. It is illustrated in Figure 4.8.

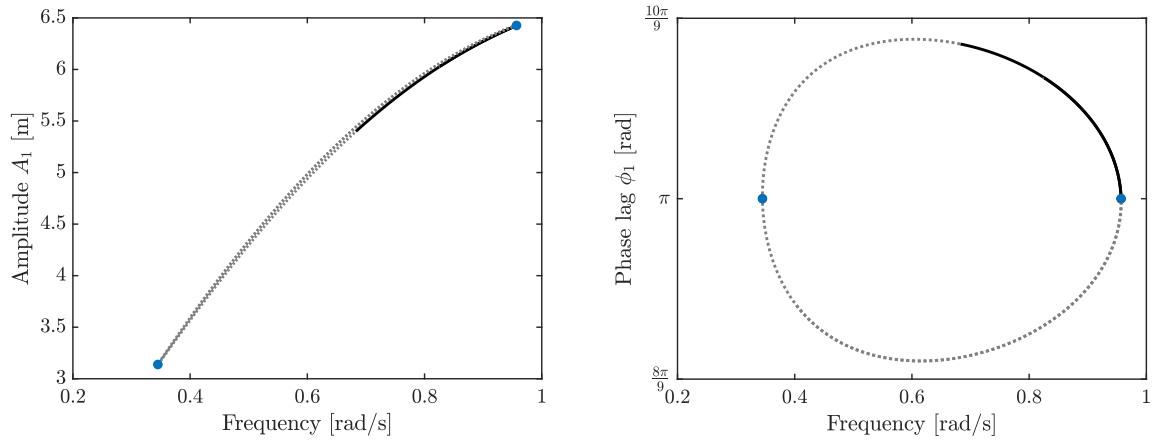

(a) **(b)**

Figure 4.8: NFRC (black) and phase resonance point (blue) using the HBM around the 1:2 resonance of the Helmholtz oscillator for a forcing amplitude of 0.07 N/kg: (a) amplitude and (b) phase lag.

4.2.6 The oscillator with a quintic stiffness

The equation of motion of the oscillator with a weak quintic stiffness is

$$\ddot{x}(t) + \omega_0^2 x(t) = -\varepsilon \left(2\bar{\zeta}\omega_0 \dot{x}(t) + \bar{\alpha}_5 x^5(t)\right) + \gamma \sin \omega t \tag{4.89}$$

The system parameters are $\zeta = 0.005$, $\omega_0 = 1$ and $\alpha_5 = 0.1$ N/m^2.

4.2.6.1 5:1 superharmonic resonance

From Equation (4.34), the averaged equations of motion around the 5:1 resonance are

$$\begin{cases} 160\bar{\zeta}\omega_0\omega A_5 = -\bar{\alpha}_5 \Lambda^5 \sin\phi_5 \\ 16\Omega_5 A_5 - 10\bar{\alpha}_5 \left(1A_5^5 + 6A_5^3\Lambda^2 + 3A_5\Lambda^4\right) = -\bar{\alpha}_5\Lambda^5 \cos\phi_5 \end{cases} \tag{4.90}$$

and the resonant phase lag is $-\frac{\pi}{2}$. This resonance is illustrated in Figure 4.9 where it is compared to the solution obtained with the HBM. Despite a slight amplitude deviation at high forcing amplitudes, both methods give similar results. First, there is a hardening effect, and, second, $\phi_1 = -\frac{\pi}{2}$ describes well the maximum amplitude.

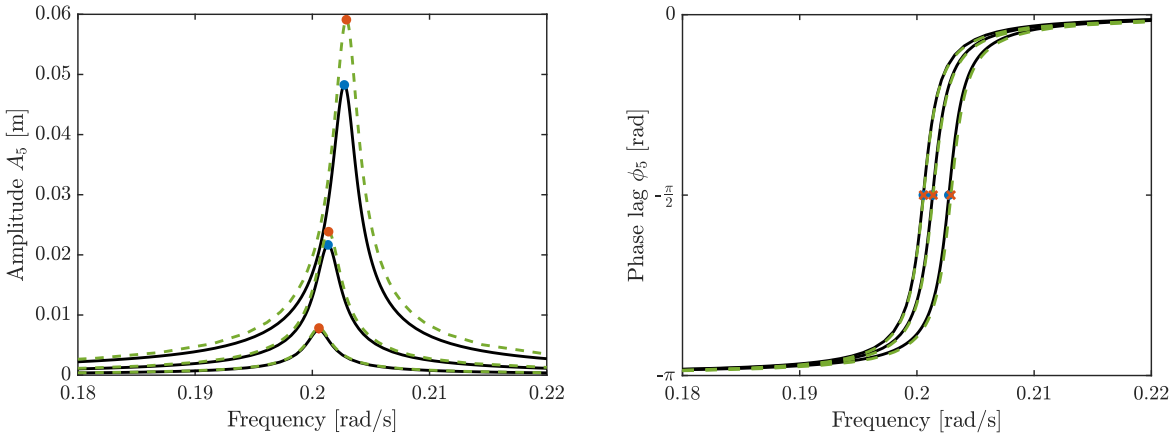

Figure 4.9: NFRCs (HBM: black; AM: green) and phase resonance points (HBM: blue; AM: orange) around the 5:1 resonance of the oscillator with a quintic stiffness for forcing amplitudes of 0.4 N/kg, 0.5 N/kg and 0.6 N/kg: (a) amplitude and (b) phase lag.

4.2.6.2 1:5 subharmonic resonance

From Equation (4.38), the averaged equations of motion around the 1:5 resonance are

$$\begin{cases} 32\bar{\zeta}\omega_0\omega = -25\bar{\alpha}_5\Lambda A_5^3 \sin 5\phi_1 \\ 80\Omega_1 - 50\bar{\alpha}_5 \left(A_4^5 + 6A_5^2\Lambda^2 + 3\Lambda^4\right) = 25\bar{\alpha}_5\Lambda \cos 5\phi_5. \end{cases} \tag{4.91}$$

As for the 1:3 resonance of the Duffing oscillator, the 1:5 resonance starts to appear at a critical forcing and takes the form of an isolated response. This response is not necessarily

close to $5\omega_0$, as assumed in Section 4.2.3.3, but this does not alter the resonant phase lag. Indeed, the response is bounded between two frequencies that correspond to a minimum and a maximum of amplitude characterized by $\phi_1 = \frac{\pi}{2}$, as illustrated in Figure 4.10. This is confirmed by numerical results in Figure 4.11.

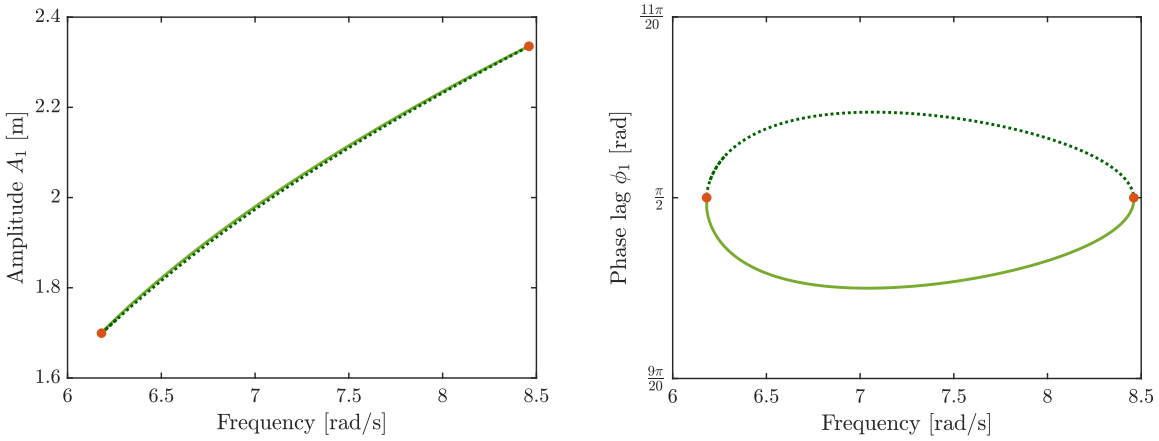

(a) **(b)**

Figure 4.10: NFRC (solid green: stable; dotted green: unstable) and phase resonance points (orange) using the AM around the 1:5 resonance of the oscillator with a quintic stiffness for a forcing amplitude of 3 N/kg: (a) amplitude and (b) phase lag.

4.3 Higher-order averaging

4.3.1 Weakly nonlinear oscillator with hard excitation

For higher-order AM, a weakly nonlinear oscillator with hard excitation is considered, as in Section 4.2.1, but now, the nonlinear term also depends on ε

$$\ddot{x}(t) + \omega_0^2 x(t) = \varepsilon \bar{f}_{nl}\left(x(t), \dot{x}(t), \varepsilon\right) + \gamma \sin \omega t \tag{4.92}$$

Eventually, a weakly nonlinear oscillator is obtained

$$\ddot{z}(t) + \omega_0^2 z(t) = \varepsilon \bar{f}_{nl}(z(t), \dot{z}(t), \omega t, \varepsilon). \tag{4.93}$$

Again, the response of Equation (4.2) is expressed using a Van der Pol transformation with a frequency ω_l close to a fraction of the natural frequency such that $\omega_l^2 - \omega_0^2 = \varepsilon^p \Omega_l$, with p a positive integer

$$z(t) = u_l(t) \cos \omega_l t - v_l(t) \sin \omega_l t \tag{4.94}$$

which can be transformed into a system of first-order equations using Equation (4.5)

$$\begin{cases} \dot{u}_l(t) = -\frac{\varepsilon}{\omega_l}\left(\bar{f}_{nl}(z(t), \dot{z}(t), \omega t) + \varepsilon^{p-1}\Omega_l z(t)\right) \sin \omega_l t \\ \dot{v}_l(t) = -\frac{\varepsilon}{\omega_l}\left(\bar{f}_{nl}(z(t), \dot{z}(t), \omega t) + \varepsilon^{p-1}\Omega_l z(t)\right) \cos \omega_l t. \end{cases} \tag{4.95}$$

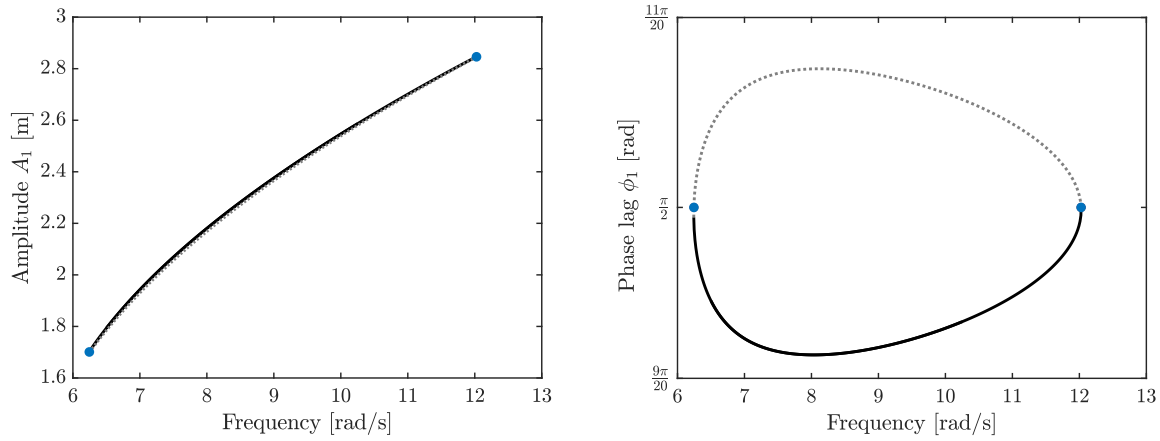

(a) **(b)**

Figure 4.11: NFRC (black) and phase resonance points (blue) using the HBM around the 1:5 resonance of the oscillator with a quintic stiffness for a forcing amplitude of 2 N/kg: (a) amplitude and (b) phase lag.

Higher-order AM can be performed on Equation (4.95) by using the *haverage.m* Mathematica package implemented by Yagasaki [14, 15] and based on the Lie transform algorithm [11].

4.3.2 The Duffing oscillator

To study the secondary resonances of the Duffing oscillator with higher-order AM, Equation (2.68) is scaled such that $\zeta = \varepsilon^q \bar{\zeta}$ and $\alpha_3 = \varepsilon \bar{\alpha}_3$, with $\bar{\zeta}$, $\bar{\alpha}_3 = \mathcal{O}(1)$ and q an integer,

$$\ddot{x}(t) + \omega_0^2 x(t) = -\varepsilon \left(2\varepsilon^{q-1}\bar{\zeta}\omega_0 \dot{x}(t) + \bar{\alpha}_3 x^3(t)\right) + \gamma \sin \omega t. \tag{4.96}$$

Applying the procedure from Section 4.3.1 with $p = 1$, such that $\omega_l^2 - \omega_0^2 = \varepsilon\Omega_l$, yields

$$\ddot{z}(t) + \omega_0^2 z(t) = -\varepsilon \left(\bar{\alpha}_3 (z(t) + \Lambda \sin \omega t)^3 + 2\varepsilon^{q-1}\bar{\zeta}\omega_0 (\dot{z}(t) + \omega\Lambda \cos \omega t)\right) \tag{4.97}$$

The system of first-order equations for $\dot{u}_l$ and $\dot{v}_l$ is

$$\begin{cases} \dot{u}_l = -\frac{\varepsilon}{\omega_l}\left(-2\varepsilon^{q-1}\bar{\zeta}\omega_0 \left(\dot{z}(t) + \omega\Lambda \cos \omega t\right) - \bar{\alpha}_3 \left(z(t) + \Lambda \sin \omega t\right)^3 + \Omega_l z(t)\right) \sin \omega_l t \\ \dot{v}_l = -\frac{\varepsilon}{\omega_l}\left(-2\varepsilon^{q-1}\bar{\zeta}\omega_0 \left(\dot{z}(t) + \omega\Lambda \cos \omega t\right) - \bar{\alpha}_3 \left(z(t) + \Lambda \sin \omega t\right)^3 + \Omega_l z(t)\right) \cos \omega_l t. \end{cases} \tag{4.98}$$

It is solved using the *haverage.m* Mathematica package [14, 15]. The value of q in Equation (4.98) is matched to the order of the AM performed. For each l:ν resonance, the objective is to obtain information about the resonant phase lags around which amplitude resonance occurs. In some cases, the actual solution of the system may differ from the averaged solution. This is because it is not always easy to find the right system parameters such that the exact and averaged solutions match perfectly, as it was the case for the 1:3 resonance in Section 4.2.4.2. However, despite these variations, the global behavior remains consistent, and the conclusions remain valid. For the numerical examples, the system parameters are $\zeta = 0.005$, $\omega_0 = 1$ and $\alpha_3 = 0.1$ N/m^2, unless specified otherwise.

4.3.2.1 Superharmonic resonances

5:1 superharmonic resonance

Second-order AM with $q = 2$ provides the equations governing the 5:1 resonance

$$\begin{cases} \dot{A}_5 = \frac{\varepsilon^2}{2}\left(-2\bar{\zeta}\omega_0 A_5 + \frac{3\bar{\alpha}_3^2\Lambda^5}{1280\omega^3}\sin\phi_5\right) \\ \dot{\phi}_5 = -\frac{\varepsilon}{40\omega}\left(3\bar{\alpha}_3 A_5^2 + 6\bar{\alpha}_3\Lambda^2 - 4\Omega_5\right) + \frac{\varepsilon^2}{2}R_{5:1} \end{cases} \tag{4.99}$$

with

$$\begin{aligned} R_{5:1} =& \frac{-1344\bar{\alpha}_3 A_5\Omega\left(A_5^2+\Lambda^2\right) + \bar{\alpha}_3^2\left(714A^5 + 8991A_5^3\Lambda^2 + 5733A_5\Lambda^4 + 525\Lambda^5\cos\phi_5\right)}{224000A_5\omega^3} \\ &+ \frac{448A_5\left(100\zeta\omega_0^2\omega^2 + \Omega^2\right)}{224000A_5\omega^3}. \end{aligned} \tag{4.100}$$

At steady-state

$$\begin{cases} \bar{\zeta}\omega_0 A_5 = \frac{3\bar{\alpha}_3^2\Lambda^5}{2560\omega^3}\sin\phi_5 \\ 3\bar{\alpha}_3 A_5^2 + 6\bar{\alpha}_3\Lambda^2 - 4\Omega_5 = \mathcal{O}(\varepsilon). \end{cases} \tag{4.101}$$

To find the resonant phase lag from the first relation of Equation (4.101), the frequency is assumed to be constant. Therefore, A_5 is maximum when $\sin\phi_5 = 1$, *i.e.*, when $\phi_5 = \frac{\pi}{2}$. This is represented in Figure 4.12.

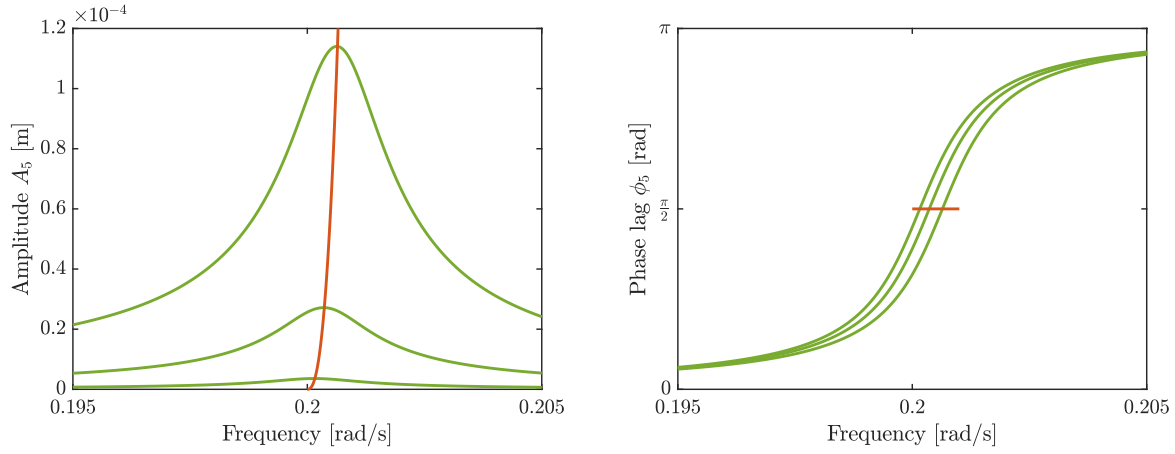

Figure 4.12: NFRCs (green) and phase resonance curve (orange) using the AM around the 5:1 resonance of the Duffing oscillator for forcing amplitudes of 0.1 N/kg, 0.15 N/kg and 0.2 N/kg: (a) amplitude and (b) phase lag.

7:1 superharmonic resonance

Second-order AM with $q = 3$ provides the equations governing the 7:1 resonance

$$\begin{cases} \dot{A}_7 = \frac{\varepsilon^3}{6}\left(-6\bar{\zeta}\omega_0 A_5 + \frac{27\bar{\alpha}_3^3\Lambda^7}{358400\omega^5}\sin\phi_7\right) \\ \dot{\phi}_7 = -\frac{\varepsilon}{56\omega}\left(3\bar{\alpha}_3 A_7^2 + 6\bar{\alpha}_3\Lambda^2 - 4\Omega_7\right) + \mathcal{O}\left(\varepsilon^2\right). \end{cases} \tag{4.102}$$

At steady-state

$$\begin{cases} 6\bar{\zeta}\omega_0 A_7 = \frac{27\bar{\alpha}_3^3\Lambda^7}{358400\omega^5}\sin\phi_7 \\ 3\bar{\alpha}_3 A_7^2 + 6\bar{\alpha}_3\Lambda^2 - 4\Omega_7 = \mathcal{O}\left(\varepsilon\right). \end{cases} \tag{4.103}$$

To find the resonant phase lag from the first relation of Equation (4.124), the frequency is assumed to be constant. Therefore, A_7 is maximum when $\sin\phi_7 = 1$, *i.e.*, when $\phi_7 = \frac{\pi}{2}$. This is depicted in Figure 4.13.

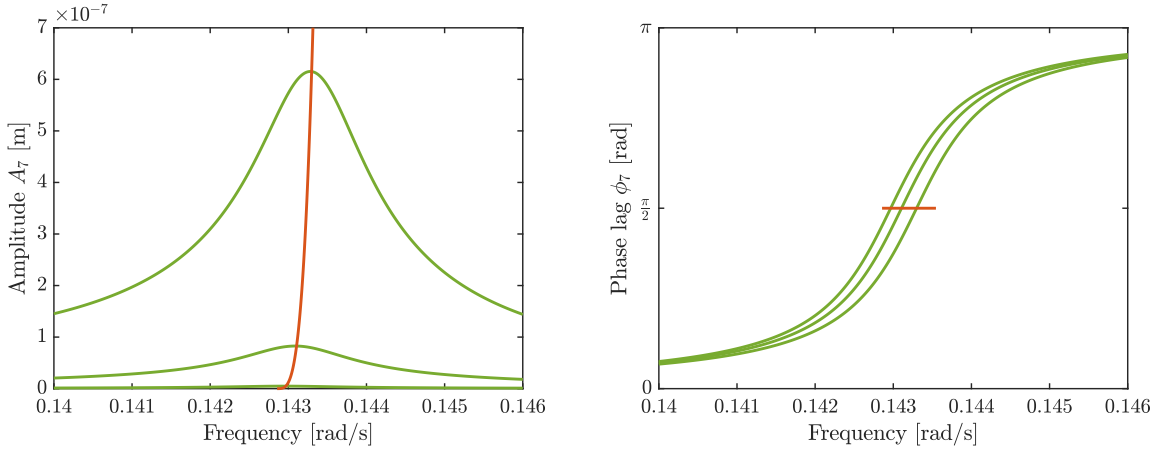

(a) **(b)**

Figure 4.13: NFRCs (green) and phase resonance curves (orange) using the AM around the 7:1 resonance of the Duffing oscillator for forcing amplitudes of 0.1 N/kg, 0.15 N/kg and 0.2 N/kg: (a) amplitude and (b) phase lag.

Even superharmonic resonance

Second-order AM with $q = 2$ provides the equations governing the 2:1 resonance

$$\begin{cases} \dot{A}_2 = \frac{\varepsilon^2}{2}\left(-2\bar{\zeta}\omega_0 A_2 - \frac{21\bar{\alpha}_3^2\Lambda^4 A_2}{640\omega^3}\sin 2\phi_2\right) \\ \dot{\phi}_2 = -\frac{\varepsilon}{16\omega}\left(3\bar{\alpha}_3 A_2^2 + 6\bar{\alpha}_3\Lambda^2 - 4\Omega_2\right) + \mathcal{O}\left(\varepsilon^2\right). \end{cases} \tag{4.104}$$

At steady-state, the first relation of (4.104) gives

$$\bar{\zeta}\omega_0 = -\frac{21\bar{\alpha}_3^2\Lambda^4}{640\omega^3}\sin 2\phi_2 \tag{4.105}$$

There is no longer a direct relation between the amplitude A_2 and phase lag ϕ_2. In fact, solving (4.104) does not give any relevant result. The same problem occurs for higher-order even superharmonic resonances. The only possibility is to study these resonances numerically. Figure 4.14 shows the second harmonic amplitude and phase lag around the 2:1 resonance for different forcing amplitudes. Interestingly, for a same amplitude, there exists two possible phase lags. The two solutions are centered around phase lags of $\frac{3\pi}{4}$ and $-\frac{\pi}{4}$, respectively. These phase lags can be used as the resonant phase lag to construct the phase resonance curve of the 2:1 resonance. Figure 4.15 confirms that the two solutions possess identical maximum values.

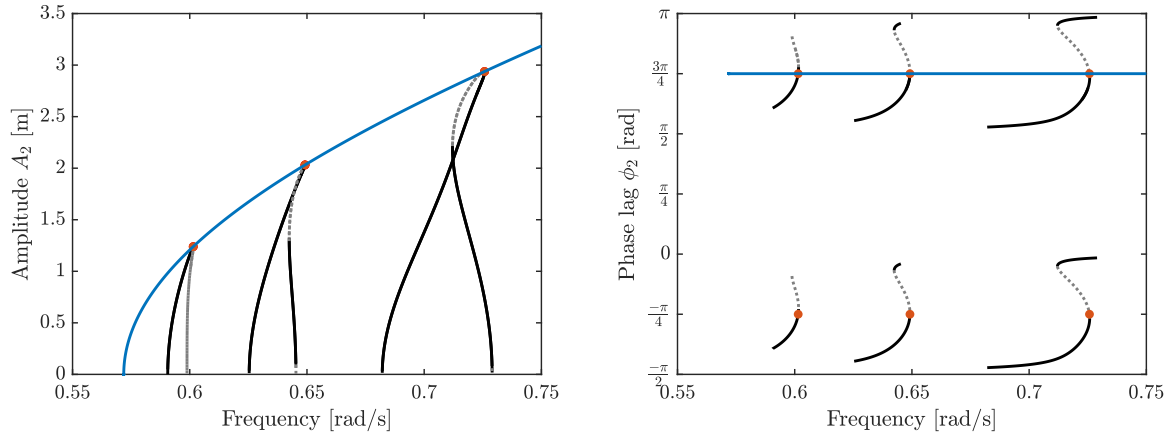

(a) **(b)**

Figure 4.14: NFRCs (black) and phase resonance curves (blue) obtained using the HBM around the 2:1 resonance of the Duffing oscillator for forcing amplitudes of 1.5 N/kg, 2 N/kg and 3 N/kg: (a) amplitude and (b) phase lag.

The same reasoning can be applied for the 4:1 resonance and even higher-order resonances. Figure 4.16 shows that the 4:1 resonance also exhibit two solutions, one centered around a phase lag of $\frac{3\pi}{4}$ and another around a phase lag of $-\frac{\pi}{4}$.

4.3.2.2 Subharmonic resonances

In this section, the focus is on the 1:ν subharmonic resonances. As shown in Section 2.3.2, a minimum forcing is required for their activation. The goal of this section is twofold: (i) find the domain of existence as a function of the forcing amplitude and (ii) compute the resonant phase lags.

First, for q equal to the order of the AM performed, we have at steady state

$$\begin{cases} g(A_1, \omega, \Lambda) = \sin(p\nu\phi_1) \\ 3\bar{\alpha}_3 A_1^2 + 6\bar{\alpha}_3 \Lambda^2 - 4\Omega_1 = \mathcal{O}(\varepsilon) \end{cases} \tag{4.106}$$

where $g(A_1, \omega, \Lambda)$ is a function that is either always positive or always negative. The value of p is either 1 or 2 if ν is odd or even, respectively. Dropping the $\mathcal{O}(\varepsilon)$ term gives an

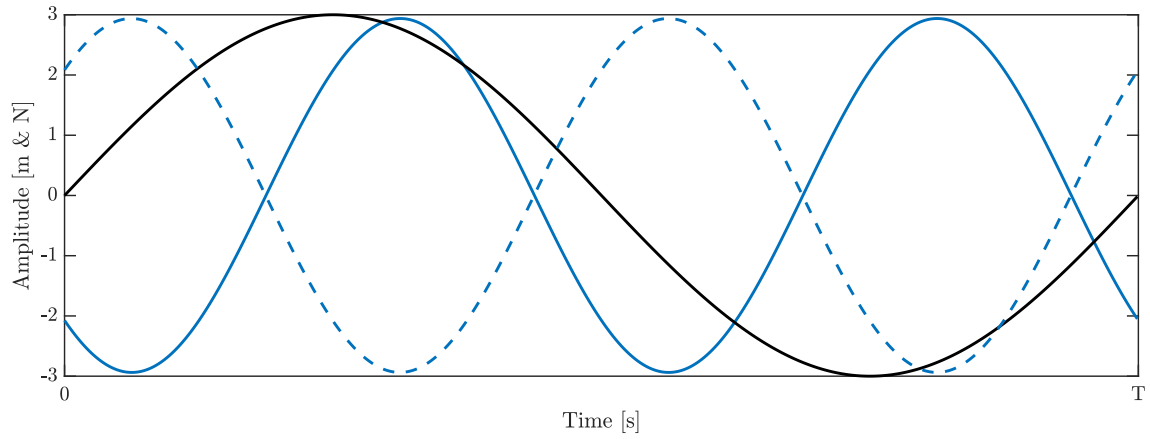

Figure 4.15: Times series of the second harmonic of the 2:1 resonance for a phase lag of $\frac{3\pi}{4}$ rad (solid blue line) and -$\frac{\pi}{4}$ rad (dashed blue line) and compared to the forcing (black).

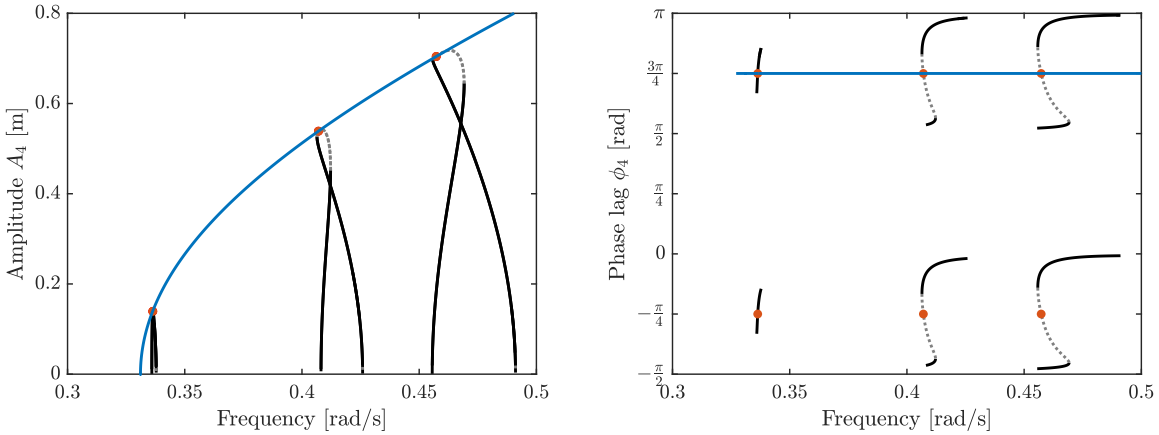

(a) **(b)**

Figure 4.16: NFRCs (black) and phase resonance curves (blue) obtained using the HBM around the 4:1 resonance of the Duffing oscillator for forcing amplitudes of 3 N/kg, 6 N/kg and 9 N/kg: (a) amplitude and (b) phase lag.

approximate solution of the amplitude A_1

$$A_1^2 \simeq \frac{4\Omega_1}{3\bar{\alpha}_3} - 2\Lambda^2. \tag{4.107}$$

This relation can be injected in the first relation of the steady-state motion. Because the sine function is between -1 and 1, the inequality

$$-1 \leq g(\omega, \Lambda) \leq 1. \tag{4.108}$$

is derived. Since $g(\omega, \Lambda)$ no longer depends on A_1 and is either always positive or always negative, one of the inequalities is always verified. The other inequality is used to compute the domain of existence of the resonance. If the forcing exceeds a certain threshold, two frequencies, ω_{inf} and ω_{sup}, define the domain of existence of the 1:ν subharmonic resonance. Conversely, if the forcing is too low, the inequality is not satisfied, and the subharmonic resonance does not exist.

Second,

$$\frac{\partial A_1^2}{\partial \omega} = 8\omega \left(\frac{1}{3\nu^2 \varepsilon \bar{\alpha}_3} - \frac{\gamma^2}{(\omega_0^2 - \omega^2)^3} \right) \tag{4.109}$$

is always positive for hardening Duffing oscillators when $\omega > \omega_0$, i.e., for all subharmonic resonances. This means that all subharmonics have their minimum and maximum of amplitude at the boundaries of their domain of existence, *i.e.*. when $\omega = \omega_{inf}$ and $\omega = \omega_{sup}$, respectively. The resonant phase lag is the one that solves either $\sin(p\nu\phi_1) = 1$ or $\sin(p\nu\phi_1) = -1$, depending on the type of resonance; phase resonance is close to the actual amplitude resonance computed when the $\mathcal{O}(\varepsilon)$ term is not dropped in Equation (4.106). This is shown in the following examples.

1:2 subharmonic resonance

Second-order AM with $q = 2$ provides the equations governing the 1:2 resonance

$$\begin{cases} \dot{A}_1 = -\frac{\varepsilon^2}{2} \left(2\bar{\zeta}\omega_0 A_1 + \frac{33\bar{\alpha}_3^2 \Lambda^2 A_1^3}{4\omega^3} \sin 4\phi_1 \right) \\ \dot{\phi}_1 = -\frac{5\varepsilon}{4\omega} \left(3\bar{\alpha}_3 A_1^2 + 6\bar{\alpha}_3 \Lambda^2 - 4\Omega_1 \right) + \frac{\varepsilon^2}{2} R_{1:2} \end{cases} \tag{4.110}$$

with

$$\begin{aligned} R_{1:2} = &- \frac{660\bar{\alpha}_3^2 A^2 \Lambda^2 \cos(4\phi_1) + 480\bar{\alpha}_3 \Omega_1 \left(A_1^2 + \Lambda^2 \right)}{80\omega^3} \\ &+ \frac{3\bar{\alpha}_3^2 \left(85A_1^4 + 144A^2\Lambda^2 - 60\Lambda^4 \right) + 160\zeta\omega_0^2\omega^2 + 160\Omega_1^2}{80\omega^3}. \end{aligned} \tag{4.111}$$

At steady-state

$$\begin{cases} 2\bar{\zeta}\omega_0 = -\frac{33\bar{\alpha}_3^2 \Lambda^2 A_1^2}{4\omega^3} \sin 4\phi_1 \\ 3\bar{\alpha}_3 A_1^2 + 6\bar{\alpha}_3 \Lambda^2 - 4\Omega_1 = \mathcal{O}(\varepsilon). \end{cases} \tag{4.112}$$

Dropping the $\mathcal{O}(\varepsilon)$ leads to

$$\begin{cases} 2\bar{\zeta}\omega_0 = -\frac{33\bar{\alpha}_3^2 \Lambda^2 A_1^2}{4\omega^3} \sin 4\phi_1 \\ A_1^2 \simeq \frac{4\Omega_1}{3\bar{\alpha}_3} - 2\Lambda^2. \end{cases} \tag{4.113}$$

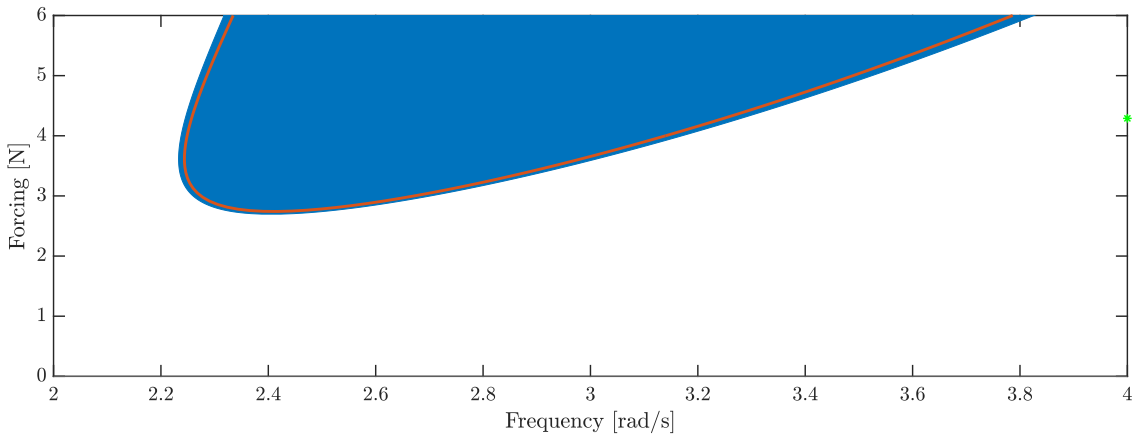

Figure 4.17: Domain of existence (blue area) and phase resonance curve (orange) of the 1:2 subharmonic resonance as a function of the forcing amplitude.

Considering that the sinus function in the first equation of (4.112) is bounded by -1 and 1, an existence condition for A_1 is derived

$$-1 \leq -\frac{8\bar{\zeta}\omega_0\omega^3}{33\bar{\alpha}_3^2\Lambda^2 A_1^2} \leq 1. \tag{4.114}$$

The second inequality is always true. A_1 is thus injected in the first inequality

$$\frac{4\Omega_1}{3\alpha} - 2\Lambda^2 - \frac{8\bar{\zeta}\omega_0\omega^3}{33\bar{\alpha}_3^2\Lambda^2} \geq 0. \tag{4.115}$$

The numerical resolution of Equation (4.115) in Figure 4.17 indicates that, if the forcing exceeds 2.7 N/kg, ω_{inf} and ω_{sup} define the domain of existence of the 1:2 subharmonic resonance. If the forcing is below 2.7 N/kg, the 1:2 subharmonic resonance does not exist. Because Equation (4.109) shows that A_1 is increasing monotonically with respect to frequency since $\bar{\alpha}_3 > 0$, A_1 is thus maximum (minimum) when ω is equal to ω_{sup} (ω_{inf}), and amplitude resonance of Equation (4.113) occurs when $\omega = \omega_{sup}$.

The resonant phase lag occurs when

$$\frac{4\Omega_1}{3\alpha} - 2\Lambda^2 - \frac{8\bar{\zeta}\omega_0\omega^3}{33\bar{\alpha}_3^2\Lambda^2} = 0 \tag{4.116}$$

or, equivalently, when $\sin 4\phi_1 = -1$. This is the case when $\phi_1 = \frac{3\pi}{8} + \frac{i\pi}{2}$, where $i = 0, 1, 2, 3$. These findings are confirmed in Figure 4.18 where Equation (4.112) is solved for a forcing amplitude of 4 N/kg.

1:5 subharmonic resonance

Second-order AM with $q = 2$ provides the equations governing the 1:5 resonance

$$\begin{cases} \dot{A}_1 = -\frac{\varepsilon^2}{2}\left(2\bar{\zeta}\omega_0 A_1 + \frac{1875\bar{\alpha}_3^2\Lambda A_1^4}{128\omega^3}\sin 5\phi_1\right) \\ \dot{\phi}_1 = -\frac{5\varepsilon}{8\omega}\left(3\bar{\alpha}_3 A_1^2 + 6\bar{\alpha}_3\Lambda^2 - 4\Omega_1\right) + \frac{\varepsilon^2}{2}R_{1:5} \end{cases} \tag{4.117}$$

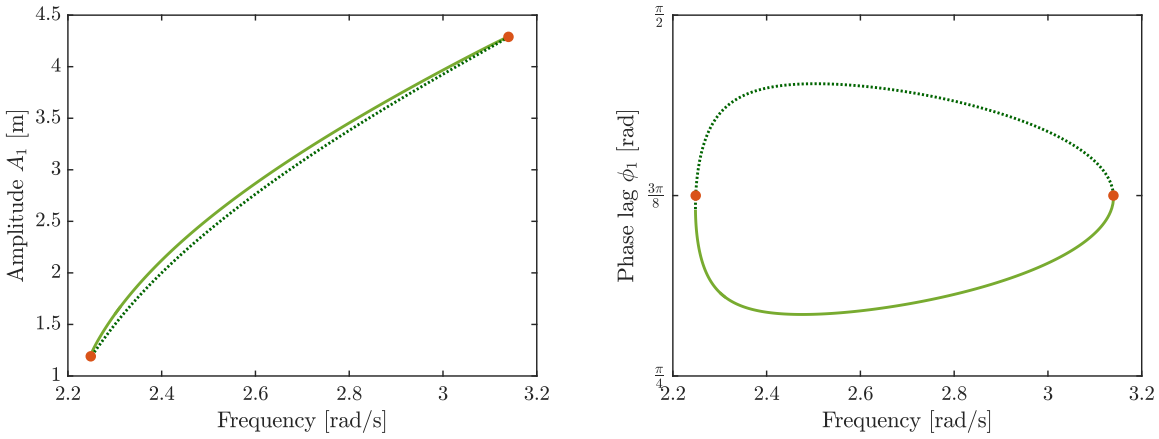

(a) **(b)**

Figure 4.18: NFRC (solid green: stable; dotted green: unstable) and phase resonance points (orange) around the 1:2 resonance of the Duffing oscillator obtained with the AM for a forcing amplitude of 4 N/kg: (a) amplitude and (b) phase lag.

with

$$R_{1:5} = \frac{125\left(-30\bar{\alpha}_3^2 A^3 \Lambda \cos(5\phi_1) - 192\bar{\alpha}_3\Omega_1\left(A_1^2+\Lambda^2\right) + 3\bar{\alpha}_3^2\left(34A_1^4+66A_1^2\Lambda^2+39\Lambda^4\right)+64\Omega_1^2\right)}{256\omega^3} + \frac{5\bar{\zeta}\omega_0^2}{\omega}. \tag{4.118}$$

At steady-state

$$\begin{cases} 2\bar{\zeta}\omega_0 = -\frac{1875\bar{\alpha}_3^2\Lambda A_1^3}{128\omega^3}\sin 5\phi_1 \\ A_1^2 \simeq \frac{4\Omega_1}{3\bar{\alpha}_3} - 2\Lambda^2. \end{cases} \tag{4.119}$$

The existence condition for A_1 is

$$-1 \leq -\frac{256\bar{\zeta}\omega_0\omega^3}{1875\bar{\alpha}_3^2\Lambda A_1^3} \leq 1. \tag{4.120}$$

The first inequality is always true. A_1 is thus injected in the second inequality

$$\frac{256\bar{\zeta}\omega_0\omega^3}{1875\bar{\alpha}_3^2\Lambda} + \left(\frac{4\Omega_1}{3\bar{\alpha}_3} - 2\Lambda^2\right)^{3/2} \geq 0. \tag{4.121}$$

Equation (4.121) is solved numerically to find the domain of existence of the 1:5 resonance. Figure 4.19 evidences that a forcing of 24 N/kg is required to activate the resonance. Equation (4.109) shows that A_1 is increasing monotonically between ω_{inf} and ω_{sup} since $\bar{\alpha}_3 > 0$, A_1 is thus maximum (minimum) when ω is equal to ω_{sup} (ω_{inf}), and amplitude resonance of Equation (4.119) occurs when $\omega = \omega_{sup}$.

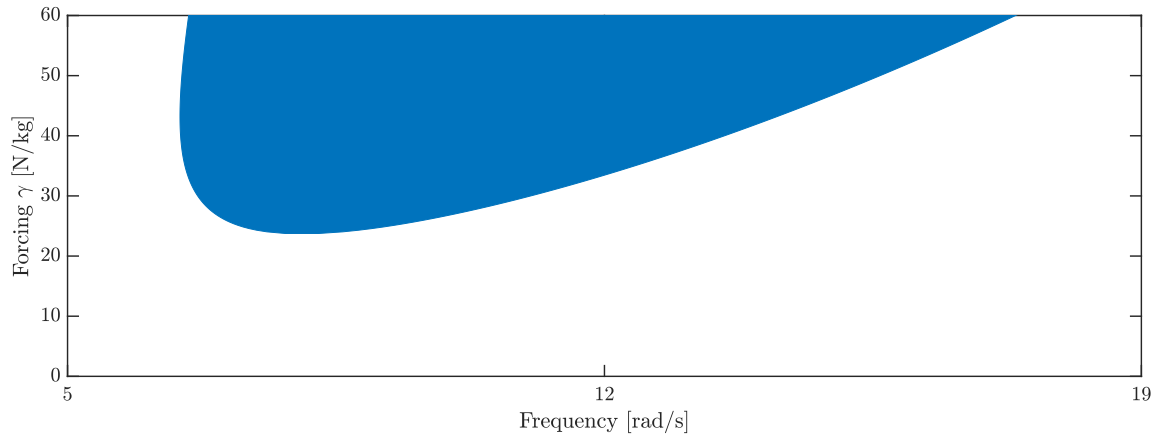

Figure 4.19: Domain of existence (blue area) of the 1:5 subharmonic resonance as a function of the forcing amplitude.

The resonant phase lag occurs when $\omega = \omega_{sup}$

$$\frac{256\bar{\zeta}\omega_0\omega^3}{1875\bar{\alpha}_3^2\Lambda} + \left(\frac{4\Omega_1}{3\bar{\alpha}_3} - 2\Lambda^2\right)^{3/2} = 0 \tag{4.122}$$

or when $\sin 5\phi_1 = 1$. This is the case when $\phi_1 = \frac{\pi}{5} + \frac{2i\pi}{5}$, where $i = 0, 1, 2, 3, 4$ and $\pi/2$ is a resonant phase lag. This is illustrated in Figure 4.20.

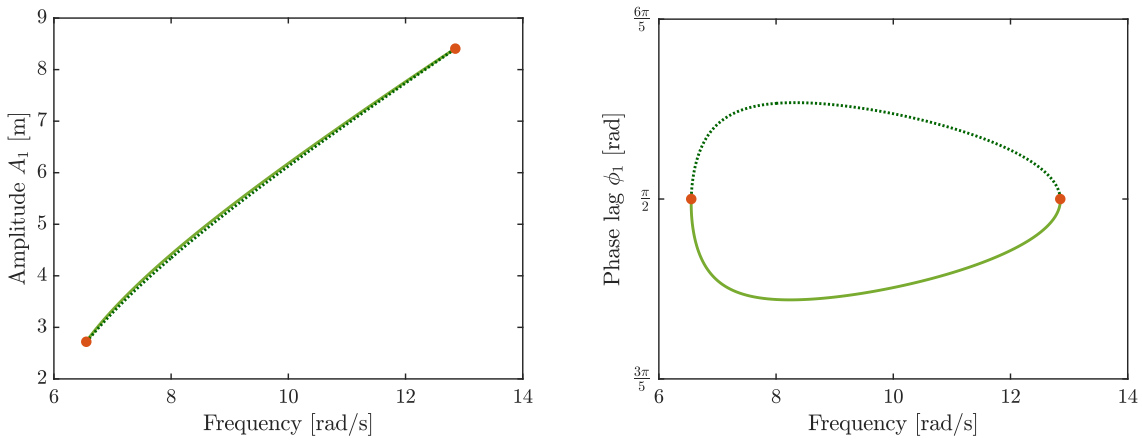

(a) **(b)**

Figure 4.20: NFRC (solid green: stable; dotted green: unstable) and phase resonance points (orange) around the 1:5 resonance of the Duffing oscillator obtained with the AM for a forcing amplitude of 40 N/kg: (a) amplitude and (b) phase lag.

1:7 subharmonic resonance

Third-order AM with $q = 3$ provides the equations governing the 1:7 resonance

$$\begin{cases} \dot{A}_1 = \frac{\varepsilon^3}{6}\left(-6\bar{\zeta}\omega_0 A_1 + \frac{1058841\bar{\alpha}_3^3\Lambda A_1^6}{2048\omega^5}\sin 7\phi_1\right) \\ \dot{\phi}_1 = -\frac{5\varepsilon}{8\omega}\left(3\bar{\alpha}_3 A_1^2 + 6\bar{\alpha}_3\Lambda^2 - 4\Omega_1\right) + \mathcal{O}\left(\varepsilon^2\right). \end{cases} \tag{4.123}$$

At steady-sate

$$\begin{cases} 6\bar{\zeta}\omega_0 = \frac{1058841\bar{\alpha}_3^3\Lambda A_1^5}{2048\omega^5}\sin 7\phi_1 \\ A_1^2 \simeq \frac{4\Omega_1}{3\bar{\alpha}_3} - 2\Lambda^2. \end{cases} \tag{4.124}$$

The existence condition for A_1 is

$$-1 \leq \frac{49152\bar{\zeta}\omega_0\omega^7}{1058841\bar{\alpha}_3^3\Lambda A_1^5} \leq 1. \tag{4.125}$$

The second inequality is always true. A_1 is injected in the first inequality

$$\frac{49152\bar{\zeta}\omega_0\omega^7}{1058841\bar{\alpha}_3^3\Lambda} + \left(\frac{4\Omega_1}{3\bar{\alpha}_3} - 2\Lambda^2\right)^{5/2} \geq 0. \tag{4.126}$$

The resonant phase lag is the one that solves $\sin 7\phi_1 = -1$. This is the case when $\phi_1 = \frac{3\pi}{14} + \frac{i\pi}{2}$, where $i = 0, 1, 2, 3, 4, 5, 6$. We note that $\phi_1 = \frac{\pi}{2}$ is a resonant phase lag. This is illustrated in Figure 4.21, where $\zeta = 0.00005$.

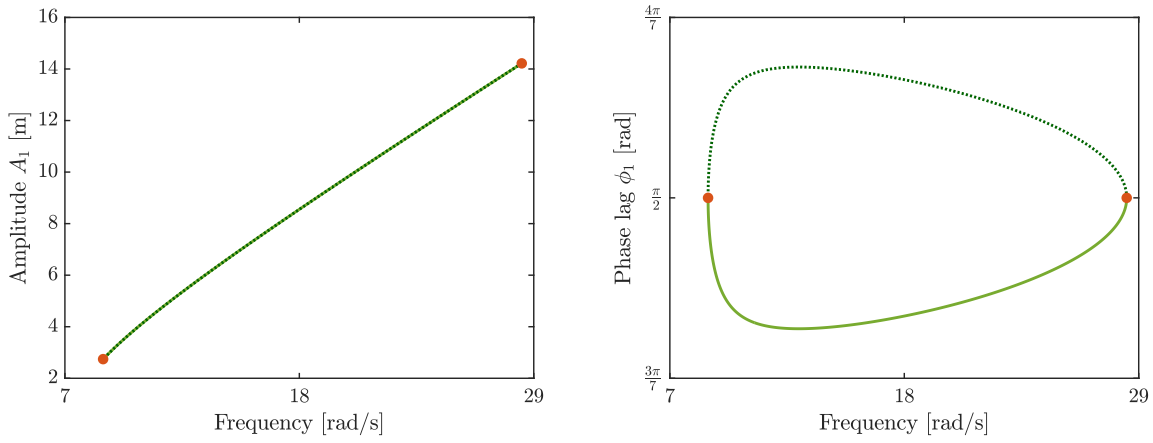

(a) **(b)**

Figure 4.21: NFRC (solid green: stable; dotted green: unstable) and phase resonance points (orange) around the 1:7 resonance of the Duffing oscillator obtained with the AM for a forcing amplitude of 15 N/kg and $\zeta = 0.00005$: (a) amplitude and (b) phase lag.

1:4 subharmonic resonance

Fourth-order AM with $q = 4$ provides the equations governing the 1:4 resonance

$$\begin{cases} \dot{A}_1 = -\frac{\varepsilon^4}{24}\left(24\bar{\zeta}\omega_0 A_1 + \frac{39960\bar{\alpha}_3^4\Lambda^2 A_1^7}{\omega^7}\sin 8\phi_1\right) \\ \dot{\phi}_1 = -\frac{5\varepsilon}{2\omega}\left(3\bar{\alpha}_3 A_1^2 + 6\bar{\alpha}_3\Lambda^2 - 4\Omega_1\right) + \mathcal{O}\left(\varepsilon^2\right). \end{cases} \tag{4.127}$$

At steady-state,

$$\begin{cases} 24\bar{\zeta}\omega_0 = -\frac{39960\bar{\alpha}_3^4\Lambda^2 A_1^6}{\omega^7}\sin 8\phi_1 \\ A_1^2 \simeq \frac{4\Omega_1}{3\bar{\alpha}_3} - 2\Lambda^2. \end{cases} \tag{4.128}$$

The existence condition for A_1 is

$$-1 \leq -\frac{24\bar{\zeta}\omega_0\omega^7}{39960\bar{\alpha}_3^4\Lambda^2 A_1^6} \leq 1. \tag{4.129}$$

The second inequality is always true. A_1 is injected in the first inequality

$$\left(\frac{4\Omega_1}{3\bar{\alpha}_3} - 2\Lambda^2\right)^3 + \frac{24\bar{\zeta}\omega_0\omega^7}{39960\bar{\alpha}_3^4\Lambda^2} \geq 0. \tag{4.130}$$

The resonant phase lag is the one that solves $\sin 8\phi_1 = -1$. This is the case when $\phi_1 = \frac{3\pi}{16} + \frac{i\pi}{4}$, where $i = 0, 1, 2, 3$. This is illustrated for $\phi_1 = \frac{3\pi}{16}$ in Figure 4.22.

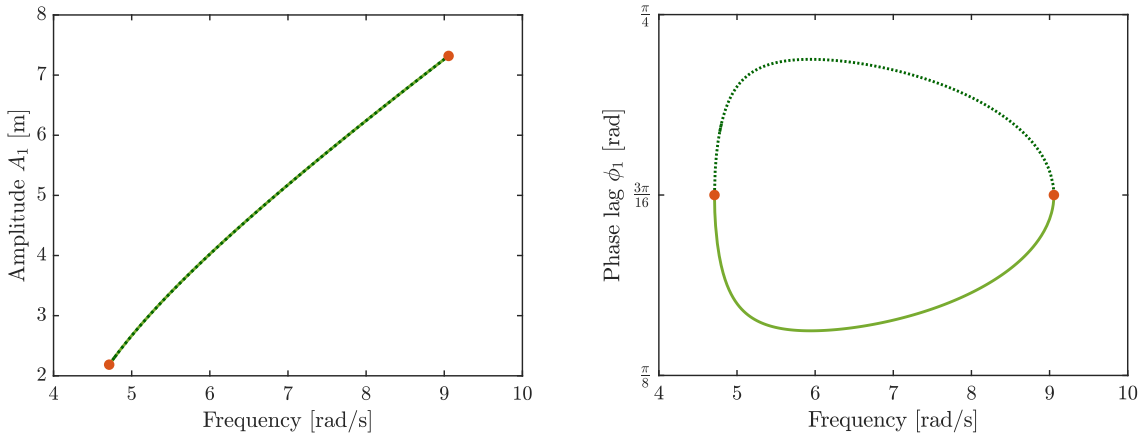

(a) **(b)**

Figure 4.22: NFRC (solid green: stable; dotted green: unstable) and phase resonance points (orange) around the 1:4 resonance of the Duffing oscillator obtained with the AM for a forcing amplitude of 8 N/kg and $\zeta = 0.00005$: (a) amplitude and (b) phase lag.

4.3.2.3 Ultra-subharmonic resonances

The goal of this section is to find the domain of existence of the l:ν resonance and to compute the resonant phase lags.

First, for q equal to the order of the AM performed, we have at steady state

$$\begin{cases} g(A_l, \omega, \Lambda) = \sin(p\nu\phi_l) \\ 3\bar{\alpha}_3 A_l^2 + 6\bar{\alpha}_3\Lambda^2 - 4\Omega_l = \mathcal{O}(\varepsilon) \end{cases} \tag{4.131}$$

where $g(A_l, \omega, \Lambda)$ is a function that is either always positive or always negative. p is either 1 or 2 when both l and ν are odd or not, respectively. Dropping the $\mathcal{O}(\varepsilon)$ term gives an approximate solution of the amplitude A_l

$$A_l^2 \simeq \frac{4\Omega_l}{3\bar{\alpha}_3} - 2\Lambda^2. \tag{4.132}$$

Following the same procedure as previously, the domain of existence of the resonance can be computed from the inequality

$$-1 \leq g(\omega, \Lambda) \leq 1. \tag{4.133}$$

Second,

$$\frac{\partial A_l^2}{\partial \omega} = 8\omega \left(\frac{l^2}{3\nu^2\varepsilon\bar{\alpha}_3} - \frac{\gamma^2}{(\omega_0^2 - \omega^2)^3} \right) \tag{4.134}$$

is always positive for hardening Duffing oscillators when $\omega > \omega_0$, i.e., for ultra-subharmonic resonances with $\nu > l$. As for subharmonics, ultra-subharmonics have their minimum and maximum of amplitude at the boundaries of their domain of existence, *i.e.*. when $\omega = \omega_{inf}$ and $\omega = \omega_{sup}$, respectively. The resonant phase lag is the one that solves either $\sin(p\nu\phi_l) = 1$ or $\sin(p\nu\phi_l) = -1$, depending on the resonance. This phase lag is defined as the phase lag at phase resonance; it is close to the amplitude resonance computed when the $\mathcal{O}(\varepsilon)$ term is not dropped in Equation (4.131).

If $\omega < \omega_0$, i.e., for ultra-subharmonic resonances with $l > \nu$, the derivative can be either positive, negative or positive then negative depending on the value of ω and γ. The phase lag at which the maximum of amplitude occurs can no longer be determined easily. We thus still define the resonant phase lag at the extremities of the isolated branch, *i.e.*. when $\omega = \omega_{inf}$ and $\omega = \omega_{sup}$.

A non-exhaustive list of ultra-subharmonic resonances is studied hereafter and a summary is available in Table 4.1.

5:3 ultra-subharmonic resonance

Third-order AM with $q = 3$ provides the equations governing the 5:3 resonance at steady-state

$$\begin{cases} 6\bar{\zeta}\omega_0 = \frac{85293 A_5 \bar{\alpha}_3^3 \Lambda^5}{1792000\omega^5} \sin 3\phi_5 \\ 3\bar{\alpha}_3 A_5^2 + 6\bar{\alpha}_3\Lambda^2 - 4\Omega_5 = \mathcal{O}(\varepsilon) \end{cases} \tag{4.135}$$

The inequality is

$$\sqrt{\frac{4\Omega_5}{3\bar{\alpha}_3} - 2\Lambda^2} - \frac{10752000\bar{\zeta}\omega_0\omega^5}{85293\bar{\alpha}_3^3\Lambda^5} \geq 0. \tag{4.136}$$

The resonant phase lag is the one that solves $\sin 3\phi_5 = 1$. This holds when $\phi_1 = \frac{\pi}{6} + \frac{2i\pi}{3}$, where $i = 0, 1, 2$. The phase lag $-\frac{\pi}{2}$ is thus a resonant phase lag. Figure 4.23 shows that $-\frac{\pi}{2}$ no longer corresponds to a maximum of amplitude, since $l > \nu$.

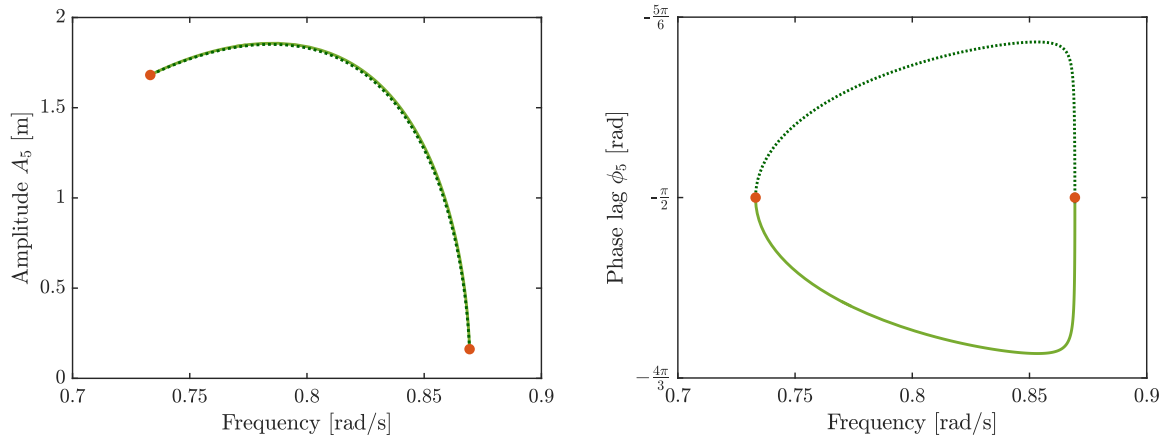

(a) **(b)**

Figure 4.23: NFRC (solid green: stable; dotted green: unstable) and phase resonance points (orange) around the 5:3 resonance of the Duffing oscillator obtained with the AM for a forcing amplitude of 0.7 N/kg and $\zeta = 0.0005$: (a) amplitude and (b) phase lag.

3:2 ultra-subharmonic resonance

Fourth-order AM with $q = 4$ provides the equations governing the 3:2 resonance at steady-state

$$\begin{cases} 24\bar{\zeta}\omega_0 = -\frac{1973735A_3^2\bar{\alpha}_3^4\Lambda^6}{22289904\omega^7}\sin 4\phi_3 \\ 3\bar{\alpha}_3A_3^2 + 6\bar{\alpha}_3\Lambda^2 - 4\Omega_3 = \mathcal{O}(\varepsilon) \end{cases} \tag{4.137}$$

The inequality is

$$\frac{4\Omega_3}{3\bar{\alpha}_3} - 2\Lambda^2 - \frac{534957696\bar{\zeta}\omega_0\omega^7}{1973735\bar{\alpha}_3^4\Lambda^6} \geq 0. \tag{4.138}$$

The resonant phase lag is $\phi_1 = \frac{3\pi}{8} + \frac{i\pi}{2}$, $i = 0, 1$. $\pm\frac{\pi}{2}$ are no longer resonant phase lags.

7:5 ultra-subharmonic resonance

Fifth-order AM with $q = 5$ provides the equations governing the 7:5 resonance at steady-state

$$\begin{cases} 120\bar{\zeta}\omega_0 = \frac{93936279296875A_7^4\bar{\alpha}_3^5\Lambda^7}{545902959788032\omega^9}\sin 5\phi_7 \\ 3\bar{\alpha}_3A_5^2 + 6\bar{\alpha}_3\Lambda^2 - 4\Omega_7 = \mathcal{O}(\varepsilon) \end{cases} \tag{4.139}$$

The inequality is

$$\frac{6550835517456384\bar{\zeta}\omega_0\omega^9}{93936279296875\bar{\alpha}_3^5\Lambda^7} - \left(\frac{4\Omega_7}{3\bar{\alpha}_3} - 2\Lambda^2\right)^2 \leq 0. \tag{4.140}$$

The resonant phase lag is $\phi_1 = \frac{\pi}{10} + \frac{2i\pi}{5}$, $i = 0, 1, 2, 3, 4$. $\frac{\pi}{2}$ is a resonant phase lag (see Figure 4.24).

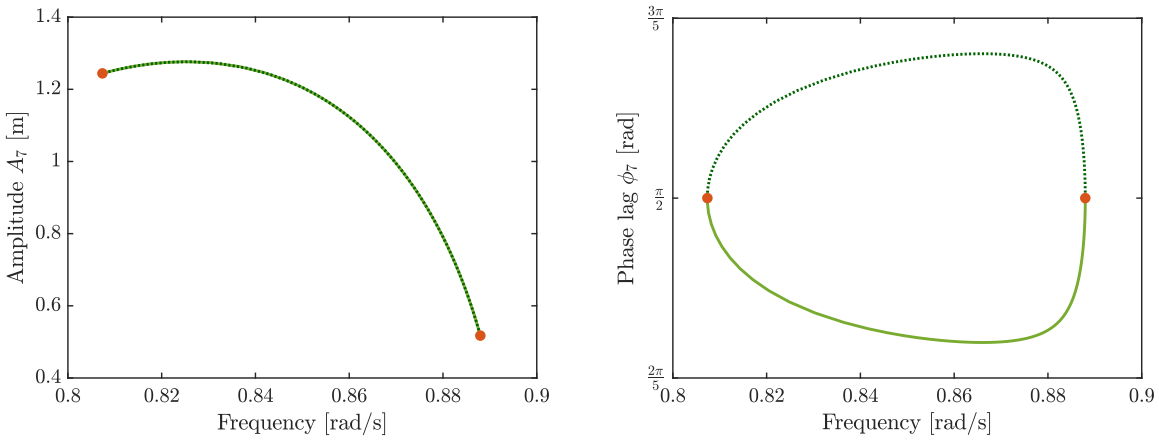

(a) **(b)**

Figure 4.24: NFRC (solid green: stable; dotted green: unstable) and phase resonance points (orange) around the 7:5 resonance of the Duffing oscillator obtained with the AM for a forcing amplitude of 0.4 N/kg and $\zeta = 0.0000005$: (a) amplitude and (b) phase lag.

3:5 ultra-subharmonic resonance

Third-order AM with $q = 3$ provides the equations governing the 3:5 resonance at steady-state

$$\begin{cases} 6\bar{\zeta}\omega_0 = \frac{13296875 A_3^3 \bar{\alpha}_3^3 \Lambda^3}{165888\omega^5} \sin 5\phi_5 \\ 3\bar{\alpha}_3 A_3^2 + 6\bar{\alpha}_3\Lambda^2 - 4\Omega_5 = \mathcal{O}(\varepsilon) \end{cases} \tag{4.141}$$

The inequality is

$$\frac{995328\bar{\zeta}\omega_0\omega^5}{13296875\bar{\alpha}_3^4\Lambda^3} + \left(\frac{4\Omega_5}{3\bar{\alpha}_3} - 2\Lambda^2\right)^{3/2} \geq 0. \tag{4.142}$$

The resonant phase lag is $\phi_1 = \frac{3\pi}{10} + \frac{2i\pi}{5}$, where $i = 0, 1, 2, 3, 4$. $-\frac{\pi}{2}$ is a resonant phase lag (see Figure 4.25).

2:3 ultra-subharmonic resonance

Fourth-order AM with $q = 4$ provides the equations governing the 2:3 resonance at steady-state

$$\begin{cases} 24\bar{\zeta}\omega_0 = -\frac{297257881995 A_3^4 \bar{\alpha}_3^4 \Lambda^4}{282591232\omega^7} \sin 6\phi_3 \\ 3\bar{\alpha}_3 A_2^2 + 6\bar{\alpha}_3\Lambda^2 - 4\Omega_2 = \mathcal{O}(\varepsilon) \end{cases} \tag{4.143}$$

The inequality is

$$\left(\frac{4\Omega_2}{3\bar{\alpha}_3} - 2\Lambda^2\right)^2 - \frac{6782189568\bar{\zeta}\omega_0\omega^7}{297257881995\bar{\alpha}_3^4\Lambda^4} \geq 0. \tag{4.144}$$

The resonant phase lag is $\phi_1 = \frac{\pi}{4} + \frac{i\pi}{3}$, where $i = 0, 1, 2, 3, 4, 5$. As for the 3:2 resonance, neither $\pi/2$ nor $-\pi/2$ is a resonant phase lag (see Figure 4.26).

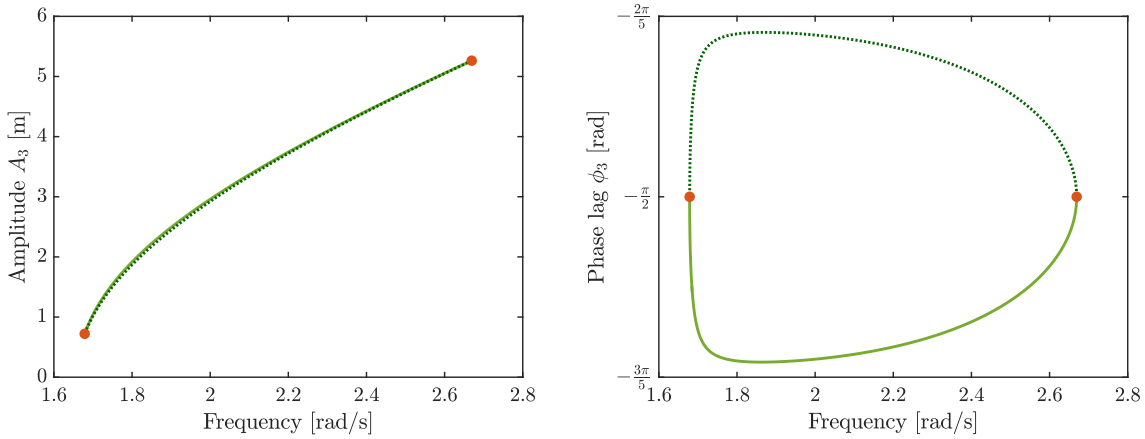

(a) **(b)**

Figure 4.25: NFRC (solid green: stable; dotted green: unstable) and phase resonance points (orange) around the 3:5 resonance of the Duffing oscillator obtained with the AM for a forcing amplitude of 2 N/kg and $\zeta = 0.00005$: (a) amplitude and (b) phase lag.

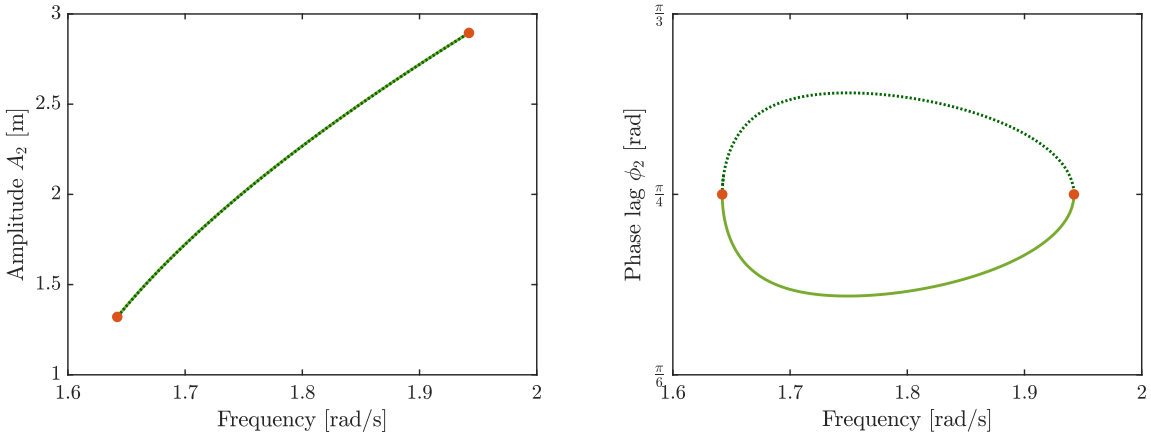

(a) **(b)**

Figure 4.26: NFRC (solid green: stable; dotted green: unstable) and phase resonance points (orange) around the 2:3 resonance of the Duffing oscillator obtained with the AM for a forcing amplitude of 1 N/kg and $\zeta = 0.000005$: (a) amplitude and (b) phase lag.

5:7 ultra-subharmonic resonance

Fifth-order AM with $q = 5$ provides the equations governing the 5:7 resonance at steady-state

$$\begin{cases} 120\bar{\zeta}\omega_0 = \frac{2464600414611158 81 A_5^5 \bar{\alpha}_3^5 \Lambda^5}{13631844000000\omega^9} \sin 7\phi_5 \\ 3\bar{\alpha}_3 A_5^2 + 6\bar{\alpha}_3 \Lambda^2 - 4\Omega_5 = \mathcal{O}(\varepsilon) \end{cases} \tag{4.145}$$

The inequality is

$$\left(\frac{4\Omega_5}{3\bar{\alpha}_3} - 2\Lambda^2\right)^{5/2} + \frac{16358212800000000\bar{\zeta}\omega_0\omega^9}{2464600414611158 8\bar{\alpha}_3^5\Lambda^5} \geq 0. \tag{4.146}$$

The resonant phase lag is $\phi_1 = \frac{3\pi}{14} + \frac{2i\pi}{7}$, where $i = 0, 1, 2, 3, 4, 5, 6$. $\frac{\pi}{2}$ is a resonant phase lag (see Figure 4.27).

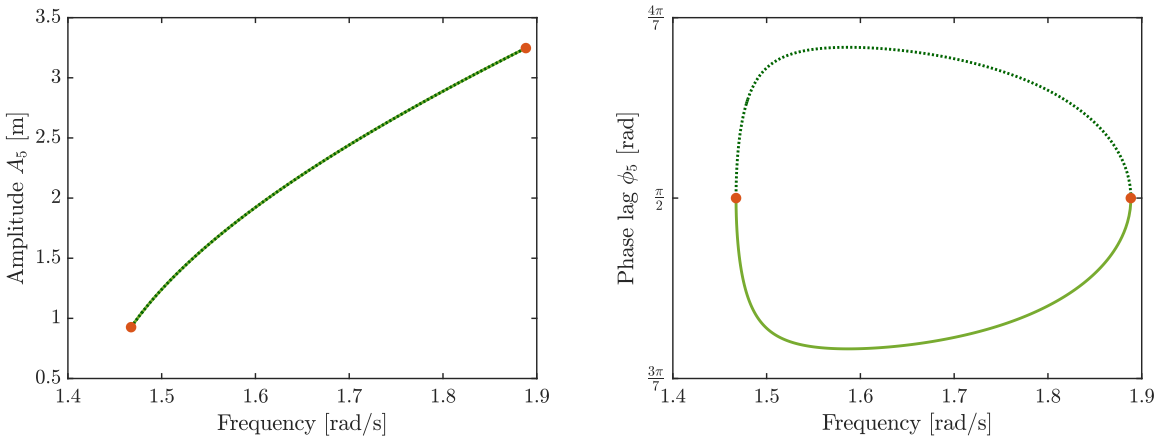

(a) **(b)**

Figure 4.27: NFRC (solid green: stable; dotted green: unstable) and phase resonance points (orange) around the 5:7 resonance of the Duffing oscillator obtained with the AM for a forcing amplitude of 0.5 N/kg and $\zeta = 0.0000005$: (a) amplitude and (b) phase lag.

Resonance	Steady-state equations	Inequality	Resonant phase lag
5:3 $(q=3)$	$\begin{cases} 6\bar{\zeta}\omega_0 = \frac{85293A_5\bar{\alpha}_3^3\Lambda^5}{1792000\omega^5}\sin 3\phi_5 \\ 3\bar{\alpha}_3A_5^2 + 6\bar{\alpha}_3\Lambda^2 - 4\Omega_5 = \mathcal{O}(\varepsilon) \end{cases}$	$\sqrt{\frac{4\Omega_5}{3\bar{\alpha}_3} - 2\Lambda^2} - \frac{10752000\bar{\zeta}\omega_0\omega^5}{85293\bar{\alpha}_3^3\Lambda^5} \geq 0$	$\phi_1 = \frac{\pi}{6} + \frac{2i\pi}{3}$ $i = 0, 1, 2$
3:2 $(q=4)$	$\begin{cases} 24\bar{\zeta}\omega_0 = -\frac{1973735A_3^2\bar{\alpha}_3^4\Lambda^6}{22289904\omega^7}\sin 4\phi_3 \\ 3\bar{\alpha}_3A_3^2 + 6\bar{\alpha}_3\Lambda^2 - 4\Omega_3 = \mathcal{O}(\varepsilon) \end{cases}$	$\frac{4\Omega_3}{3\bar{\alpha}_3} - 2\Lambda^2 - \frac{534957696\bar{\zeta}\omega_0\omega^7}{1973735\bar{\alpha}_3^4\Lambda^6} \geq 0$	$\phi_1 = \frac{3\pi}{8} + \frac{i\pi}{2}$ $i = 0, 1$
7:5 $(q=5)$	$\begin{cases} 120\bar{\zeta}\omega_0 = \frac{93936279296875A_7^4\bar{\alpha}_3^5\Lambda^7}{545902959788032\omega^9}\sin 5\phi_7 \\ 3\bar{\alpha}_3A_5^2 + 6\bar{\alpha}_3\Lambda^2 - 4\Omega_7 = \mathcal{O}(\varepsilon) \end{cases}$	$\frac{6550835517456384\bar{\zeta}\omega_0\omega^9}{93936279296875\bar{\alpha}_3^5\Lambda^7} - \left(\frac{4\Omega_7}{3\bar{\alpha}_3} - 2\Lambda^2\right)^2 \leq 0$	$\phi_1 = \frac{\pi}{10} + \frac{2i\pi}{5}$ $i = 0, 1, 2, 3, 4$
3:5 $(q=3)$	$\begin{cases} 6\bar{\zeta}\omega_0 = \frac{13296875A_3^3\bar{\alpha}_3^3\Lambda^3}{165888\omega^5}\sin 5\phi_5 \\ 3\bar{\alpha}_3A_3^2 + 6\bar{\alpha}_3\Lambda^2 - 4\Omega_5 = \mathcal{O}(\varepsilon) \end{cases}$	$\frac{995328\bar{\zeta}\omega_0\omega^5}{13296875\bar{\alpha}_3^4\Lambda^3} + \left(\frac{4\Omega_5}{3\bar{\alpha}_3} - 2\Lambda^2\right)^{3/2} \geq 0$	$\phi_1 = \frac{3\pi}{10} + \frac{2i\pi}{5}$ $i = 0, 1, 2, 3, 4$
2:3 $(q=4)$	$\begin{cases} 24\bar{\zeta}\omega_0 = -\frac{297257881995A_3^4\bar{\alpha}_3^4\Lambda^4}{282591232\omega^7}\sin 6\phi_3 \\ 3\bar{\alpha}_3A_2^2 + 6\bar{\alpha}_3\Lambda^2 - 4\Omega_2 = \mathcal{O}(\varepsilon) \end{cases}$	$\left(\frac{4\Omega_2}{3\bar{\alpha}_3} - 2\Lambda^2\right)^2 - \frac{6782189568\bar{\zeta}\omega_0\omega^7}{297257881995\bar{\alpha}_3^4\Lambda^4} \geq 0$	$\phi_1 = \frac{\pi}{4} + \frac{i\pi}{3}$ $i = 0, 1, 2, 3, 4, 5$
5:7 $(q=5)$	$\begin{cases} 120\bar{\zeta}\omega_0 = \frac{2464600414611115881A_5^5\bar{\alpha}_3^5\Lambda^5}{13631844000000\omega^9}\sin 7\phi_5 \\ 3\bar{\alpha}_3A_5^2 + 6\bar{\alpha}_3\Lambda^2 - 4\Omega_5 = \mathcal{O}(\varepsilon) \end{cases}$	$\left(\frac{4\Omega_5}{3\bar{\alpha}_3} - 2\Lambda^2\right)^{5/2} + \frac{1635821280000000\bar{\zeta}\omega_0\omega^9}{2464600414611115881\bar{\alpha}_3^5\Lambda^5} \geq 0$	$\phi_1 = \frac{3\pi}{14} + \frac{2i\pi}{7}$ $i = 0, 1, 2, 3, 4, 5, 6$

Table 4.1: Summary of the equations of motions and resonant phase lags of ultra-subharmonic resonances of the Duffing oscillator.

4.3.3 Resonant phase lags of the Duffing oscillator: a summary

4.3.3.1 Superharmonic resonances

For odd l:1 superharmonic resonances, the resonant phase lag solves either $\sin(\phi_l) = -1$ if $l \mod 4 = 1$, *i.e.*, $\phi_l = \frac{\pi}{2}(3 + 4i)$, with i an integer, or $\sin(\phi_l) = 1$ if $l \mod 4 = 3$, *i.e.*, $\phi_l = \frac{\pi}{2}(1 + 4i)$. In both cases, $\phi_l = \frac{\pi}{2}$ is always a resonant phase lag.

For even l:1 superharmonic resonances, it was not possible to conclude anything analytically. However, the numerical study suggests that the resonant phase lag is always $\phi_l = \frac{3\pi}{4} + i\pi$. Interestingly, this value solves $\sin(2\phi_l) = -1$.

4.3.3.2 Subharmonic resonances

For odd 1:ν subharmonic resonances, the mechanism is similar to odd l:1 superharmonic resonances. The resonant phase lag solves $\sin(\nu\phi_1) = -1$ if $l \mod 4 = 1$, *i.e.*, $\phi_1 = \frac{\pi}{2\nu}(3 + 4i)$, with i an integer, or $\sin(\nu\phi_1) = 1$ if $l \mod 4 = 3$, *i.e.*, $\phi_1 = \frac{\pi}{2\nu}(1 + 4i)$. In both cases, $\phi_1 = \frac{\pi}{2}$ is always a resonant phase lag.

For even 1:ν subharmonic resonances, the resonant phase lag solves $\sin(2\nu\phi_l) = -1$, *i.e.*, $\phi_1 = \frac{3\pi}{4\nu} + \frac{i\pi}{\nu}$.

4.3.3.3 Ultra-subharmonic resonances

If both l and ν are odd, then the resonant phase lag solves $\sin(\nu\phi_l) = 1$ or $\sin(\nu\phi_l) = -1$. We can have either $\frac{\pi}{2}$ or $-\frac{\pi}{2}$ as the resonant phase lag.

If either l or ν is even, the resonant phase lag solves $\sin(2\nu\phi_l) = -1$, *i.e.*, $\phi_l = \frac{3\pi}{4\nu} + \frac{i\pi}{\nu}$.

4.4 Conclusion

In this chapter, the secondary resonances of a harmonically-forced oscillator with polynomial stiffness were studied. First, using first-order AM, the governing equations of the d:1 and 1:d resonances of an oscillator of order d were obtained. Amplitude resonance of the resonating harmonic was found to occur around a specific phase lag ϕ_l, nonnecessarily equal to $\frac{\pi}{2}$. This resonant phase lag can be used to track the locus of the resonance peaks.

Second, with higher-order AM, more complex l:ν resonances of the Duffing oscillator were studied. We note that, for some specific ultra-subharmonic resonances, the resonant phase lag did not correspond to the resonance in amplitude, but it was instead close enough from the boundaries of the domain of existence of the isolated branch.

Though only oscillators with polynomial stiffness were studied in this chapter, any type of nonlinear oscillator can be analyzed provided it has a form suitable for first or higher-order averaging.

Chapter 5

Phase resonance nonlinear modes of single-degree-of-freedom systems

This chapter first reviews the existing nonlinear mode definitions, namely the nonlinear normal mode, invariant manifold, extended periodic motion concept and spectral submanifold definitions. Based on the theoretical findings in Chapters 3 and 4, *i.e.*, the l-th harmonic of the l:ν resonance reaches a local maximum when its phase lag is close to the resonant phase lag φ_l, this chapter introduces the concept of a *phase resonance nonlinear mode* (PRNM). The key advantage of PRNMs is that they can be (*i*) applied to both primary and secondary resonances of nonlinear systems, (*ii*) effectively calculated numerically using continuation techniques as detailed in this chapter and (*iii*) robustly identified experimentally using PLLs as discussed in Chapter 6. The stability of PRNMs is also discussed herein.

5.1 Existing nonlinear mode definitions

The main nonlinear mode definitions are briefly reviewed hereafter.

5.1.1 The nonlinear normal mode approach

In linear theory, an undamped normal mode of a damped, forced system is excited when the external forcing compensates exactly the damping force or, equivalently, when the displacement is in phase quadrature with the forcing [1, 21].

The concept of a normal mode was extended to nonlinear systems by Rosenberg [6, 79, 80] who defined a nonlinear normal mode (NNM) as a *vibration in unison* of the underlying conservative system, implying that all degrees of freedom of the system reach their maxima and cross zero simultaneously. This definition was later extended to encompass modal interactions, *i.e.*, when two or more NNMs interact, as *a (nonnecessarily synchronous) periodic motion of the conservative system* [3, 26].

Starting from the equations of motion of a nonlinear system with viscous damping

$$\mathbf{M}\ddot{\mathbf{x}}(t) + \mathbf{C}\dot{\mathbf{x}}(t) + \mathbf{K}\mathbf{x}(t) + \mathbf{f}_{nl}(\mathbf{x}(t)) = \mathbf{f}_{ext}(t) \tag{5.1}$$

where $\mathbf{M}$, $\mathbf{C}$ and $\mathbf{K}$ are the mass, damping and stiffness matrices, respectively, and $\mathbf{f}_{nl}(\mathbf{x}(t))$ and $\mathbf{f}_{ext}(t)$ are the vector of nonlinear and external forces, respectively, a NNM motion is defined as a periodic motion of the undamped, unforced system

$$\mathbf{M}\ddot{\mathbf{x}}(t) + \mathbf{K}\mathbf{x}(t) + \mathbf{f}_{nl}(\mathbf{x}(t)) = \mathbf{0} \tag{5.2}$$

The forcing required to excite a NNM is

$$\mathbf{f}_{ext}(t) = \mathbf{C}\dot{\mathbf{x}}(t) \tag{5.3}$$

which is a multi-point, multi-harmonic forcing for which each harmonic is in phase quadrature with its corresponding harmonic in the response [50].

The concept of a NNM is exemplified on a two-DOF system with a cubic spring attached to the first DOF

$$\begin{cases} \ddot{x}_1 + (2x_1 - x_2) + 0.5x_1^3 = 0 \\ \ddot{x}_2 + (2x_2 - x_1) = 0. \end{cases} \tag{5.4}$$

The natural frequencies of the linearized system are 1 and $\sqrt{3}$ rad/s; they correspond to the in-phase and out-of-phase modes, respectively. Figure 5.1a shows the frequency-energy plot of the in-phase and out-of-phase NNMs. At low amplitudes, or equivalently at low energy levels, the NNM frequencies correspond to those of the linear system. As the energy increases, the system hardens leading to an increase in the NNM frequencies. Specifically, the frequency of the in-phase NNM approaches $\sqrt{2}$ asymptotically whereas the frequency of the out-of-phase NNM goes to infinity when the energy goes to infinity [3].

An interesting feature of NNMs is their modal interactions. They occur when the frequencies of two NNMs are commensurate. In Figure 5.1b, a 3:1 modal interaction happens around 285J where the frequency of the in-phase NNM is one third of the frequency of the out-of-phase NNM. In this neighborhood, the dynamics of the in-phase NNM changes qualitatively. At the bifurcation, the first harmonic disappears and only frequency components proportional to 3ω subsist, as displayed in Figure 5.2. In other words, the in-phase motion transitions to an out-of-phase motion with a frequency three times as large, as shown in Figure 5.3.

5.1.2 The invariant manifold approach

Based on the center manifold technique [81], Shaw and Pierre extended the NNM concept to damped systems. They defined a NNM as a two-dimensional invariant manifold (IM) in phase space [9, 82, 83]. In linear theory, a normal mode is geometrically represented by a hyperplane in phase space. In contrast, NNMs take the form of hypersurfaces tangent to the modal hyperplanes of the linearized system at the equilibrium point. In the absence of internal resonances, the manifold can be parameterized by a single pair of state-space variables.

According to [9, 27], starting from the nonlinear autonomous system with n DOFs

$$\mathbf{M}\ddot{\mathbf{x}}(t) + \mathbf{C}\dot{\mathbf{x}}(t) + \mathbf{K}\mathbf{x}(t) + \mathbf{f}_{nl}(\mathbf{x}(t), \dot{\mathbf{x}}(t)) = \mathbf{0} \tag{5.5}$$

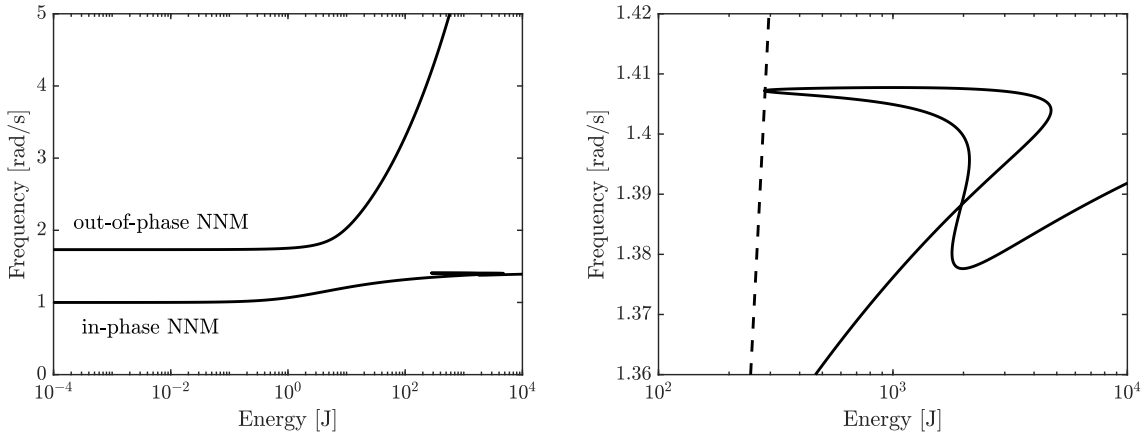

Figure 5.1: Frequency-energy plot of system (5.4): (a) in-phase and out-of-phase NNMs and (b) close-up of the 3:1 modal interaction where the out-of-phase mode (dashed line) is represented at one third of its dominant frequency.

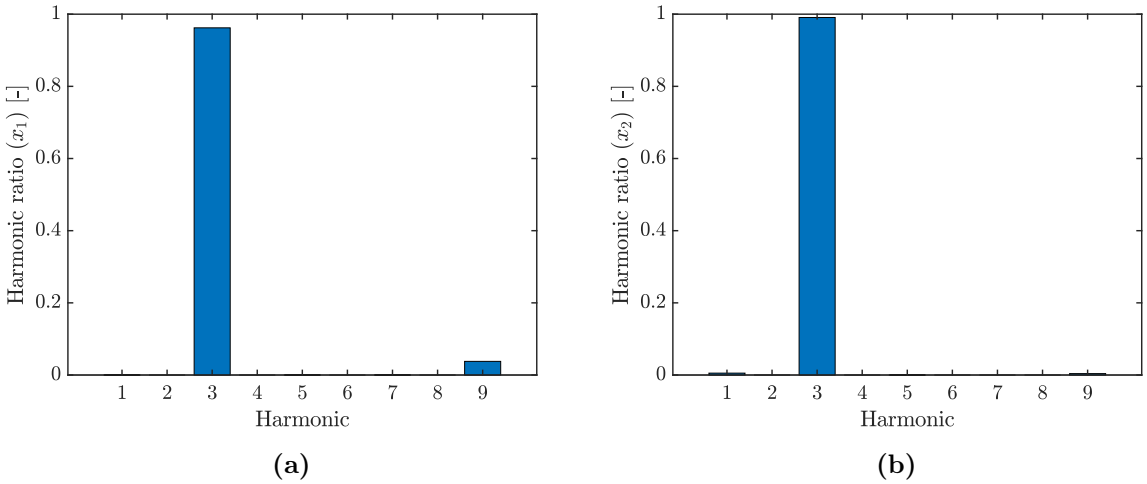

Figure 5.2: Harmonic ratios for the 3:1 modal interaction: (a) x_1 and (b) x_2.

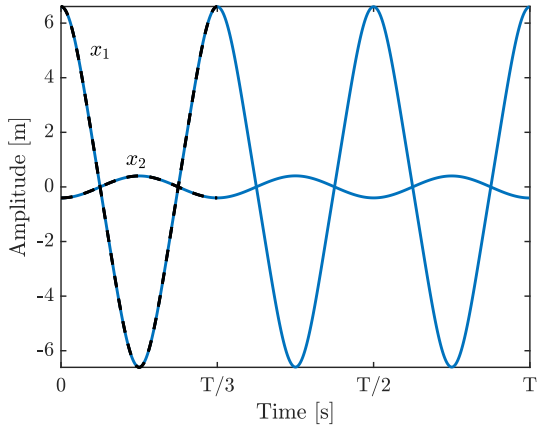

Figure 5.3: Time series of the 3:1 modal interaction over the in-phase NNM period T (blue: in-phase NNM; black: out-of-phase NNM).

the system is recast into a first-order differential system of equations by letting $\mathbf{z} = [\mathbf{x};\ \dot{\mathbf{x}}]^T$ such that

$$\dot{\mathbf{z}} = \begin{pmatrix} \dot{\mathbf{x}} \\ -\mathbf{M}^{-1}\left[\mathbf{C}\dot{\mathbf{x}} + \mathbf{K}\mathbf{x} + \mathbf{f}_{nl}(\mathbf{x}, \dot{\mathbf{x}}\right] \end{pmatrix} = \begin{pmatrix} \dot{\mathbf{x}} \\ \mathbf{h}(\mathbf{z}). \end{pmatrix} \tag{5.6}$$

The pair of state-space variables is a displacement x_s and a velocity $\dot{x}_s$. The remaining variables are related to $(x_s, \dot{x}_s)$, renamed (u_s, v_s), and are submitted to the constraint equations

$$\begin{aligned} u_i &= U_i(u_s, v_s) \\ v_i &= V_i(u_s, v_s) \end{aligned} \tag{5.7}$$

with $i = 1, \ldots, n;\ i \neq s$. The time derivatives of Equation (5.7), when assuming that the motion occurs on the IM to remove time dependence in the equations of motion, write

$$\begin{aligned} \dot{u}_i &= \frac{\partial U_i(u_s, v_s)}{\partial u_s}\dot{u}_s + \frac{\partial U_i(u_s, v_s)}{\partial v_s}\dot{v}_s \\ \dot{v}_i &= \frac{\partial V_i(u_s, v_s)}{\partial u_s}\dot{u}_s + \frac{\partial V_i(u_s, v_s)}{\partial v_s}\dot{v}_s \end{aligned} \tag{5.8}$$

with $\dot{v}_j = h_j$, where $h_j = h_j(u_s, \mathbf{U}(u_s, v_s), v_s, \mathbf{V}(u_s, v_s))$ with $j = 1, \ldots, n$ are the components of $\mathbf{h}(\mathbf{z})$, $\mathbf{U} = \{U_i : i = 1, \ldots, n;\ i \neq s\}$ and $\mathbf{V} = \{V_i : i = 1, \ldots, n;\ i \neq s\}$.

Equation (5.8) rewrites

$$\begin{aligned} V_i(u_s, v_s) &= \frac{\partial U_i(u_s, v_s)}{\partial u_s}v_s + \frac{\partial U_i(u_s, v_s)}{\partial v_s}h_s \\ h_i &= \frac{\partial V_i(u_s, v_s)}{\partial u_s}v_s + \frac{\partial V_i(u_s, v_s)}{\partial v_s}h_s \end{aligned} \tag{5.9}$$

with $i = 1, \ldots, n;\ i \neq s$. Equation (5.9) is a set of $2n$-2 partial differential equations that can be solved by expanding each $U_i(u_s, v_s)$ and $V_i(u_s, v_s)$ into power series and substitute

them into Equation (5.9). By equating the like-power terms, a set of algebraic equations is derived and can be solved recursively. Once this is achieved, the U_i's and V_i's are substituted into the equations of motion corresponding to x_s and $\dot{x}_s$ to obtain the equations of decoupled, SDOF nonlinear oscillators

$$\begin{cases} \dot{u}_s = v_s \\ \dot{v}_s = h_s(u_s, \mathbf{U}(u_s, v_s), v_s, \mathbf{V}(u_s, v_s)) \end{cases} \tag{5.10}$$

where (u_s, v_s) represent the variables on the IM. There exist n such equations at each equilibrium point, one for each mode, and they contain the nonlinear effects up to the order taken in the power series expansion of the U_i's and V_i's.

The IM technique is exemplified for the system in Equation (5.4) in Figure 5.4 where x_1 and $\dot{x}_1$ are taken as the pair of state-space variables.

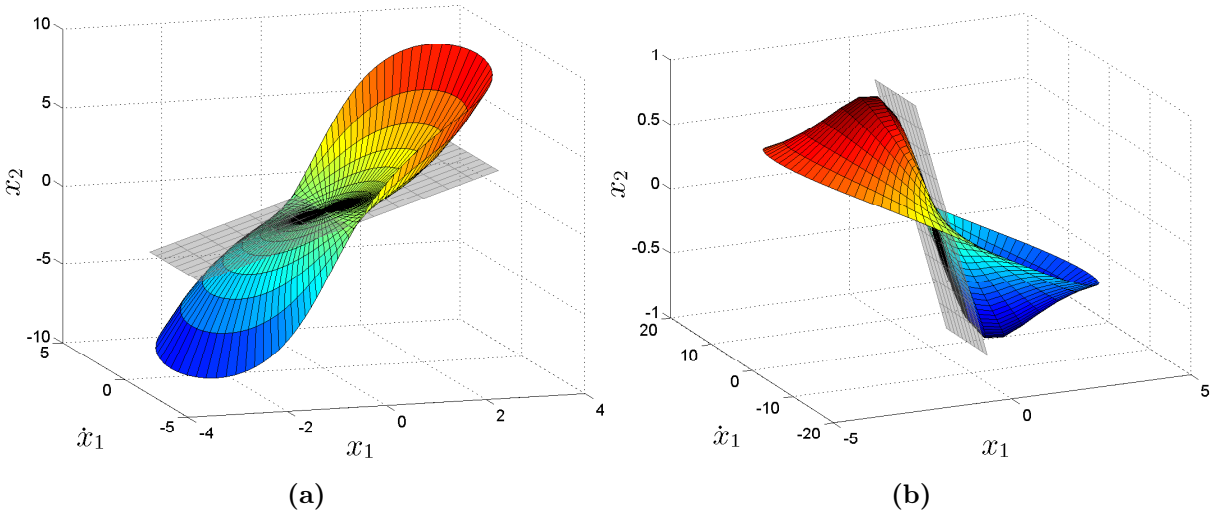

Figure 5.4: Two-dimensional IMs with the corresponding linear normal modes [3]: (a) in-phase mode and (b) out-of-phase mode.

5.1.3 Extended periodic motion concept approach

In 2015, Krack introduced a novel nonlinear mode definition, termed extended periodic motion concept (EPMC), to extend Rosenberg's definition to systems with damping terms of the form of Equation (5.5).

According to the EPMC definition, a nonlinear mode is *as a family of periodic motions of an autonomous nonlinear system. If the system is nonconservative, these periodic motions are enforced by mass-proportional damping/self-excitation* [84]. This definition is consistent with linear modal analysis for symmetric systems with modal damping. In addition to that, the introduced negative damping term can be directly related to the modal damping of the system. However, it can introduce artificial modal coupling and should be avoided around strong modal interactions.

Mathematically, we solve

$$\mathbf{M}\ddot{\mathbf{x}}(t) + \mathbf{C}\dot{\mathbf{x}}(t) + \mathbf{K}\mathbf{x}(t) + \mathbf{f}_{nl}(\mathbf{x}(t), \dot{\mathbf{x}}(t)) - \delta\mathbf{M}\dot{\mathbf{x}}(t) = \mathbf{0} \tag{5.11}$$

where the mass-proportional negative damping term ensures that the system is self-excited. It is related to the modal damping ζ through

$$\zeta = \frac{\delta}{2\omega_0}. \tag{5.12}$$

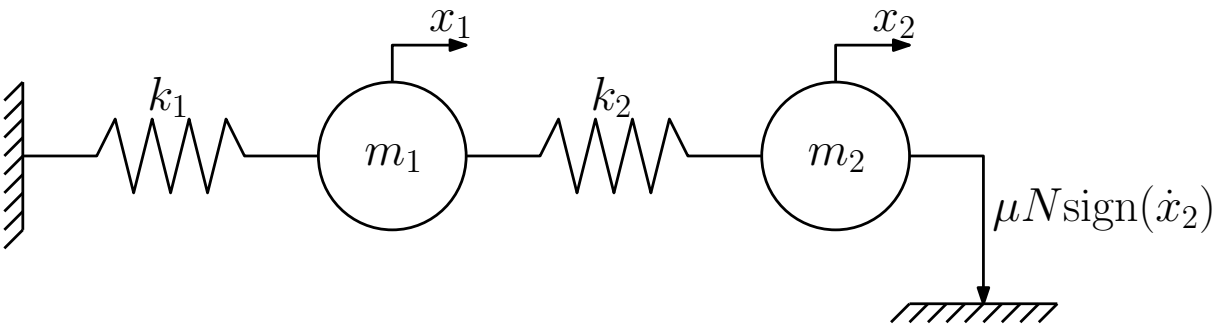

Figure 5.5: Two-DOF system with dry friction

This definition can be applied to system with nonlinear damping terms. This is exemplified on a two-DOF system with Coulomb friction in Figure 5.5 with $m_1 = 1$ kg, $m_2 = 0.02$ kg, $k_1 = 600$ N/m and $k_2 = 40$ N/m. The signum function in the Coulomb friction law, $\mu N \text{sign}(\dot{x}_2)$, is sometimes approximated using the hyperbolic tangent function: $\mu N \tanh(\frac{\dot{x}_2}{\epsilon})$ where ϵ is a small parameter. The lower ϵ, the better the approximation. Here, the friction coefficient is $\mu = 0.2$, the normal force is $N = 10$N and $\epsilon = 0.01$. Damping proportional to the mass and stiffness matrices is introduced in the system, $\mathbf{C} = 0.0315\mathbf{M} + 2.8775 \times 10^{-5}\mathbf{K}$, so that the two vibration modes of the linear system have a damping ratio of 0.1%.

The results are presented in Figure 5.6 where the NFRCs of the system are computed with harmonic forcing on the first DOF. The EPMC curve captures well the resonance behavior of the system and particularly the two limit cases. The first limit case is at low amplitudes for which the second DOF is fully stuck, and the system acts a SDOF system whose natural frequency is

$$\omega_{0,stuck} = \sqrt{\frac{k_1 + k_2}{m_1}} = 25.30 \text{ rad/s}. \tag{5.13}$$

The second limit case is at high amplitude where the second DOF is almost freely slipping. The system thus converges to the underlying linear system, and the natural frequency is

$$\omega_{0,slip} = 24.16 \text{ rad/s}. \tag{5.14}$$

The modal damping ratio computed using Equation (5.12) is shown in Figure 5.6b. At high amplitudes, the damping ratio converges toward 0.1%, *i.e.*, the damping ratio of the underlying linear system. At low amplitudes, the damping ratio is governed by the viscous damper attached to the first DOF and the small contribution of the approximation of the dry friction function. The maximum damping ratio is reached for intermediate amplitudes, where partial slip occurs, in accordance with what is traditionally observed [85–88].

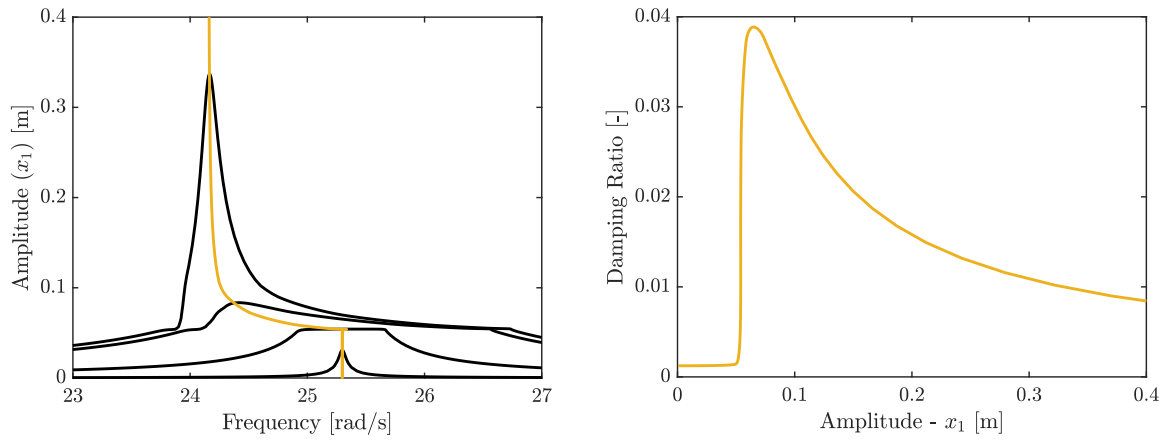

(a) (b)

Figure 5.6: NFRCs (black) and EPMC curve (yellow) of the two-DOF system with dry friction for forcing amplitudes of 0.05 N, 1 N, 3.5 N and 4 N: (a) NFRCs and EPMC curve and (b) modal damping ratio.

5.1.4 The spectral submanifold approach

In the conservative case, the IM approach proposed by Shaw and Pierre [9] is a surface composed with periodic NNM motions. In the non-conservative case, however, such periodic motions are rare or isolated in phase space. IMs are also non-unique, even in linear systems [89–91]. In fact, the computed IM depends on the choice of basis functions, domain boundaries or cost functions used. This non-uniqueness is often ignored in the study of MDOF systems [27].

These issues were addressed by Haller and Ponsioen in [10], where they propose a unified mathematical approach to tackle dissipative systems. Their NNM is defined as a *near-equilibrium quasiperiodic motion in a dissipative, nonlinear system*. The non-uniqueness of the IM is addressed by defining a *spectral submanifold* (SSM) as *the smoothest member of an IM family tangent to a modal subbundle along an NNM*.

Mathematically, considering a nonlinear system of the form

$$\mathbf{M}\ddot{\mathbf{x}}(t) + \mathbf{C}\dot{\mathbf{x}}(t) + \mathbf{K}\mathbf{x}(t) + \mathbf{f}_{nl}(\mathbf{x}(t), \dot{\mathbf{x}}(t)) = \varepsilon \mathbf{f}_{ext}(\mathbf{x}(t), \mathbf{x}(t), \omega_1 \dot{t}, \ldots, \omega_s) \tag{5.15}$$

with $0 \leq \varepsilon \ll 1$, $\mathbf{f}_{nl}(\mathbf{x}(t), \dot{\mathbf{x}}(t)) = \mathcal{O}\left(|\mathbf{x}|^2, |\mathbf{x}||\dot{\mathbf{x}}|, |\dot{\mathbf{x}}|^2\right)$ and $\mathbf{f}_{ext}(\mathbf{x}(t), \mathbf{x}(t), \omega_1 \dot{t}, \ldots, \omega_s)$ the external forcing with the frequency vector $\boldsymbol{\omega} = [\omega_1, \ldots, \omega_s]$, with $s \geq 0$. If $s = 0$, then the system is autonomous, if $s = 1$, the system is harmonically forced and if $s > 1$, the external forcing is quasiperiodic if at least two of the frequencies are rationally incommensurate. By setting $\mathbf{z} = [\mathbf{x}(t); \dot{\mathbf{x}}(t)]^T$, Equation (5.15) can be rewritten in a first-order form

$$\dot{\mathbf{z}} = \begin{pmatrix} \mathbf{0} & \mathbf{I}_n \\ -\mathbf{M}^{-1}\mathbf{K} & -\mathbf{M}^{-1}\mathbf{C} \end{pmatrix} \mathbf{z} + \begin{pmatrix} \mathbf{0} \\ -\mathbf{M}^{-1}\mathbf{f}_{nl}(\mathbf{z}) \end{pmatrix} + \varepsilon \begin{pmatrix} \mathbf{0} \\ \mathbf{M}^{-1}\mathbf{f}_{ext}(\mathbf{z}, \omega_1 t, \ldots, \omega_s) \end{pmatrix} \tag{5.16}$$

where $\mathbf{I}_n$ is the identity matrix of size n. From Equation (5.16) Haller and Ponsioen

defined an NNM as the closure of a multi-frequency solution

$$\mathbf{x}(t) = \sum_{\mathbf{m}=1}^{\infty} \mathbf{x}_{\mathbf{m}} e^{i\langle \mathbf{m}, \boldsymbol{\omega} \rangle t} \tag{5.17}$$

where $\mathbf{m}$ is a multi-index of s nonnegative integers, $\mathbf{x}_{\mathbf{m}}$ are the complex Fourier amplitudes of the real solution $\mathbf{x}(t)$ with respect to the frequencies in the vector $\boldsymbol{\omega} = [\omega_1, \ldots, \omega_s]$. Depending on the value of s, different NNMs can be defined

1. the *trivial NNM* when $s = 0$, namely a fixed point;
2. the *periodic NNM* when either $s = 1$ or $s > 1$ with the elements of $\boldsymbol{\omega}$ rationally commensurate, namely a periodic orbit;
3. the *quasiperiodic NNM* when $s > 1$ with elements of $\boldsymbol{\omega}$ rationally incommensurate, namely a f-dimensional invariant torus.

Finally, a SSM of a NNM $\mathcal{N}$ is defined as an IM $W(\mathcal{N})$ of Equation (5.16) such that

i. $W(\mathcal{N})$ is a subbundle of the normal bundle $N\mathcal{N}$ of $\mathcal{N}$, satisfying $\dim W(\mathcal{N}) = \dim E + \dim \mathcal{N}$ for some spectral subspace E of the operator

$$\begin{pmatrix} \mathbf{0} & \mathbf{I}_n \\ -\mathbf{M}^{-1}\mathbf{K} & -\mathbf{M}^{-1}\mathbf{C} \end{pmatrix} \tag{5.18}$$

ii. The fibers of the bundle $W(\mathcal{N})$ perturb smoothly from the spectral subspace E of the linearized system

$$\dot{\mathbf{z}} = \begin{pmatrix} \mathbf{0} & \mathbf{I}_n \\ -\mathbf{M}^{-1}\mathbf{K} & -\mathbf{M}^{-1}\mathbf{C} \end{pmatrix} \mathbf{z} \tag{5.19}$$

under the addition of the nonlinear and $\mathcal{O}(\varepsilon)$ terms in Equation (5.16);

iii. $W(\mathcal{N})$ has strictly more continuous derivatives along $\mathcal{N}$ than any other IM satisfying (i) and (ii).

Again, depending on the value of s, different SSMs can be defined

1. the *autonomous SSM* when $s = 0$, namely nonlinear continuations of SSMs;
2. the *periodic SSM* when either $s = 1$ or $s > 1$ with the elements of $\boldsymbol{\omega}$ rationally commensurate, namely a three-dimensional IM tangent to a spectral subbundle along a hyperbolic periodic orbit;
3. the *quasiperiodic SSM* when $s > 1$ with elements of $\boldsymbol{\omega}$ rationally incommensurate, namely an IM tangent to a spectral subbundle of a hyperbolic invariant torus.

These NNMs and SSMs are well illustrated in [10].

The spectral submanifold approach has proven efficient for systems with internal resonances [92, 93], reduced-order models with computational efficiency [94] and detection of isolated responses [95].

5.1.5 Other definitions

The aforementioned nonlinear mode definitions are not exhaustive. For instance, Laxalde et al. proposed the *damped motion concept* based on a pseudo-periodic motion [85]. In [96], Grenat et al. proposed an energy resonance nonlinear mode.

5.2 Goal: defining a nonlinear mode that...

5.2.1 ... is a point on the NFRC

The nonlinear modes defined in Section 5.1 all require an unpractical multi-point, multi-harmonic forcing to be identified experimentally. For instance, considering a nonlinear mode $\mathbf{x}_{nnm}(t)$, the forcing $\mathbf{f}_{ext}(t)$ needed to excite it is [50]

$$\mathbf{f}_{ext}(t) = \mathbf{C}\mathbf{x}_{nnm}(t) \tag{5.20}$$

in the case of a nonlinear mode computed using Rosenberg's definition or

$$\mathbf{f}_{ext}(t) = \delta\mathbf{M}\dot{\mathbf{x}}_{nnm}(t) \tag{5.21}$$

in the case of a nonlinear mode computed using the EPMC definition [84]. However, during modal testing, structures are usually excited using a mono-point, mono-harmonic forcing $f\sin\omega t$ applied to the r-th DOF $x_r(t)$.

To reconcile the two situations, the energy balance (EB) criterion [1] was extended to nonlinear systems in [97, 98] to determine the amplitude f of the mono-point, mono-harmonic forcing required to *approximately* excite $\mathbf{x}_{nnm}(t)$. EB states that the energy dissipated by the system in steady-state conditions E_{out} must always be compensated by the input energy E_{in}, i.e., $E_{out} = E_{in}$.

To derive EB, each term in the equations of motion is premultiplied by $\dot{\mathbf{x}}_{nnm}^T(t)$ and integrated over the period T. Because the inertia and stiffness terms are conservative, we have

$$E_{out} = \int_0^T \dot{\mathbf{x}}_{nnm}^T(t)\mathbf{f}_{nc}\left(\dot{\mathbf{x}}_{nnm}(t)\right)\,\mathrm{d}t, \quad E_{in} = \int_0^T \dot{\mathbf{x}}_{nnm}^T(t)\mathbf{f}_{ext}\left(t\right)\,\mathrm{d}t. \tag{5.22}$$

where $\mathbf{f}_{nc}\left(\dot{\mathbf{x}}_{nnm}(t)\right)$ represent the nonconservative forces. The energy injected into the system is

$$E_{in} = \int_0^T \dot{x}_{r,nnm}^T(t) f\sin\omega t\,\mathrm{d}t \tag{5.23}$$

where x_r is the displacement of the forced DOF. Therefore, the forcing amplitude f is

$$f = \frac{\int_0^T \dot{\mathbf{x}}_{nnm}^T(t)\mathbf{f}_{nc}\left(\dot{\mathbf{x}}_{nnm}(t)\right)\,\mathrm{d}t}{\int_0^T \dot{x}_{r,nnm}^T(t)\sin\omega t\,\mathrm{d}t}. \tag{5.24}$$

For illustration, EB is first applied to a Duffing oscillator

$$\ddot{x}(t) + 0.01\dot{x}(t) + x(t) + 0.1x^3(t) = f\sin\omega t \tag{5.25}$$

Figure 5.7 shows that EB provides results in excellent accordance with the NFRCs. This can be explained by the fact that the NNM motions are almost purely mono-harmonic, see Figure 5.7d. Hence, the exact forcing required to excite NNM motions is also almost purely mono-harmonic.

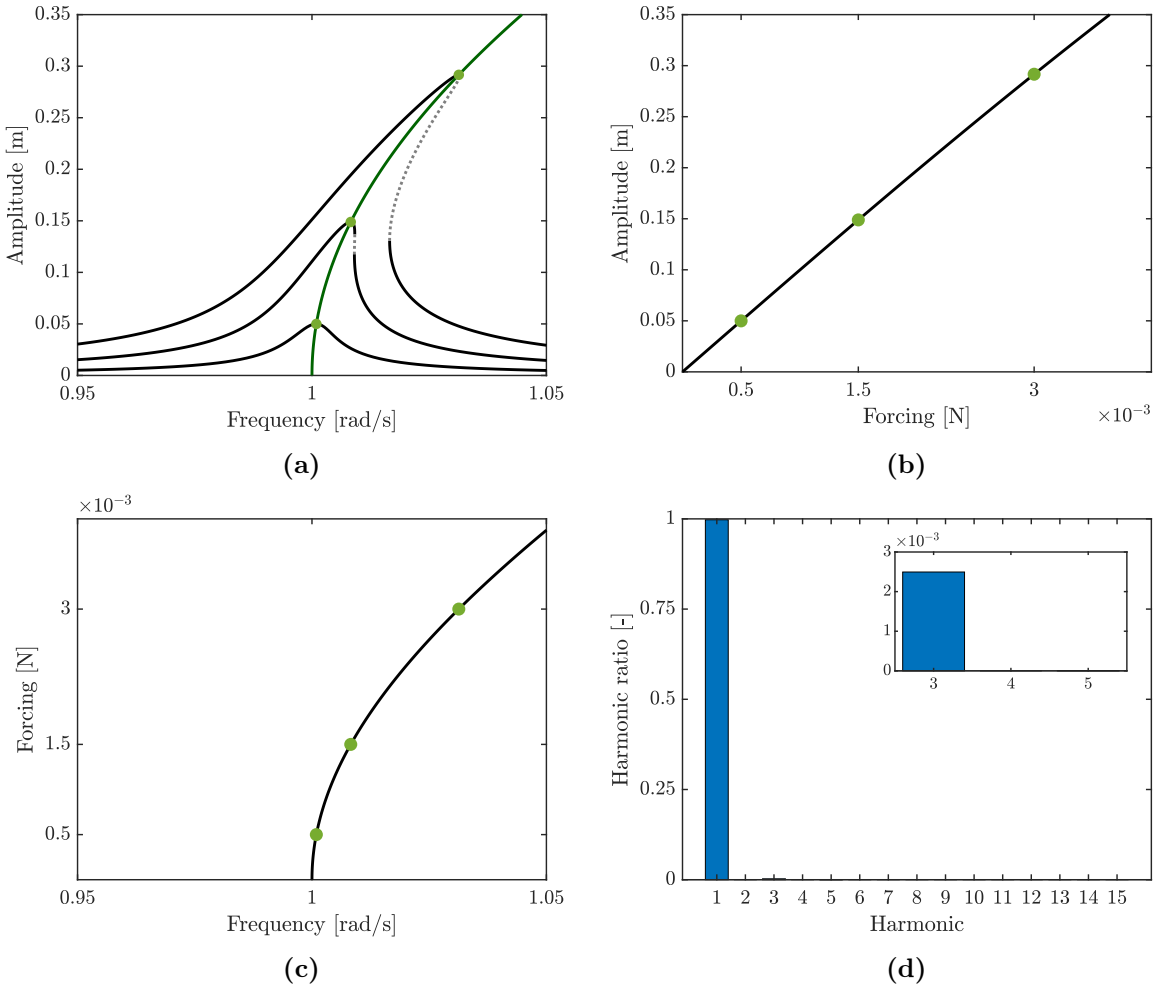

Figure 5.7: EB applied to a Duffing oscillator for f =0.0005 N, 0.0015 N and 0.003 N: (a) NFRCs (black) and NNM backbone (green), (b) amplitude-forcing curve, (c) forcing-frequency curve and (d) harmonic ratios of the NNM for a forcing of 0.003 N. The green dots correspond to the NNM points associated with f =0.0005 N, 0.0015 N and 0.003 N.

A two-DOF system with a cubic spring attached to the first mass is now considered

$$\ddot{x}_1 + 0.02\dot{x}_1 - 0.01\dot{x}_2 + 2x_1 - x_2 + x_1^3 = f\sin\omega t \tag{5.26}$$

$$\ddot{x}_2 + 0.11\dot{x}_2 - 0.01\dot{x}_1 + 2x_2 - x_1 = 0 \tag{5.27}$$

The natural frequencies of the underlying linear system are 1 and $\sqrt{3}$ rad/s. Figure 5.8a depicts the NFRCs in the vicinity of the first mode together with the nonlinear mode solutions obtained with the NNM and EPMC definitions. The loci of amplitude and

phase resonance ($\phi_1 = \frac{\pi}{2}$ for x_1) points are superposed. At relatively low forcing, the agreement between the NNM, EPMC, amplitude and phase resonance curves is excellent. However, for higher forcing, the NNM and EPMC curves deviate away from amplitude and phase resonances. In the presence of modal interactions, the discrepancy can even be more important [99]. Considering now the highest forcing level, $f = 1.5$ N, in Figure 5.8b, EB is exploited to calculate the NNM motion and frequency corresponding to this specific forcing amplitude. The result of EB evidences that the solutions obtained with the NNM and EPMC definitions do not lie on the NFRC, which represents an important limitation of these nonlinear mode definitions.

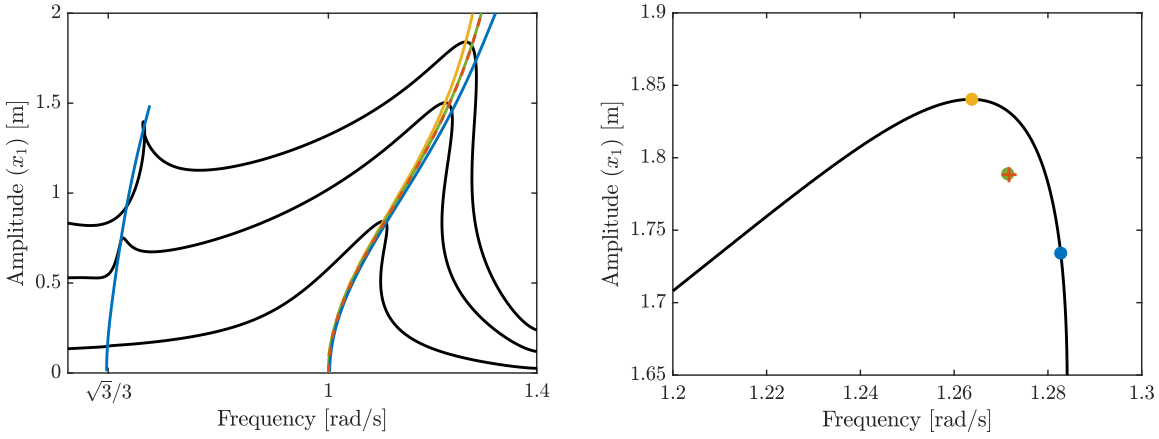

Figure 5.8: NFRCs (black), NNM (green), EPMC (red), amplitude resonance (orange) and phase quadrature points (blue) of the 2DOF system: (a) $f = 0.161, 0.8, 1.5$ N and (b) close-up around the first primary resonance, $f = 1.5$ N.

5.2.2 ... can characterize secondary resonances

Besides the primary resonance of the first mode, Figure 5.8a evidences the existence of a $3:1$ superharmonic resonance of the second mode of the system. This resonance cannot be characterized using the classical nonlinear mode definitions, which represents another limitation of these definitions. We, however, note that the SSMs defined by Haller and co-workers do not suffer from this difficulty, at least for subharmonic resonances.

The concept of a resonant phase lag discussed in Chapters 3 and 4 has the potential to address this limitation. For instance, the phase resonance curve of the 3:1 superharmonic resonance calculated for a phase lag between the third harmonic of the displacement and the forcing equal to $\pi/2$ is displayed in Figure 5.8. It offers an excellent characterization of this secondary resonance.

5.2.3 ... can account for nonlinear nonconservative forces

To be as general as possible, nonlinear modes must be able to account for nonlinear nonconservative forces. This is already the case for the IM, EPMC and SSM approaches

but not for the NNM approach.

5.3 Phase resonance nonlinear modes

Based on the requirements of the previous section and on the developments in Chapters 3 and 4, a resonant phase lag approach seems to be an effective strategy for defining a nonlinear mode, thus termed a *phase resonance nonlinear mode* (PRNM):

- PRNMs are defined for systems forced with a mono-point, mono-harmonic forcing; a PRNM is thus guaranteed to be an actual solution of the NFRC.
- Any secondary resonance can be characterized using PRNMs provided that the corresponding resonant phase lag is known, either analytically or numerically.
- Systems with nonlinear nonconservative forces can be handled without any difficulty.
- A robust experimental identification of PRNMs can be achieved using PLLs.

In the remainder of this section, two constructive methods for computing PRNMs, namely the velocity feedback approach and the resonant phase lag approach, are proposed.

5.3.1 The velocity feedback approach

5.3.1.1 Theoretical framework

We start from the harmonically-forced linear oscillator

$$m\ddot{x}(t) + c\dot{x}(t) + kx(t) = f \sin \omega t. \tag{5.28}$$

To drive this system into resonance requires careful tuning of the excitation frequency ω. A more efficient strategy to operate the system into one of its normal modes is to apply direct velocity feedback [100]

$$m\ddot{x}(t) + c\dot{x}(t) + kx(t) - \mu\dot{x}(t) = 0 \tag{5.29}$$

where the feedback term $\mu\dot{x}(t)$ plays the role of *virtual harmonic forcing*. Because this virtual forcing and the velocity are collinear, phase quadrature with the displacement $x(t)$, and, hence, phase resonance, is naturally enforced when $\mu = c$. This strategy was also used for driving nonlinear systems into primary resonances [84, 101].

We leverage the results in Chapters 3 and 4 to generalize the concept of a velocity feedback for the different families of resonance of a nonlinear system. Taking the Duffing oscillator as an illustrative example, we obtain

- For the primary resonance,

$$m\ddot{x}(t) + c\dot{x}(t) + kx(t) + k_{nl}x^3(t) - \mu\dot{x}_{1,T}(t) = 0 \tag{5.30}$$

  where, unlike [84, 101], the velocity feedback $\dot{x}_{1,T}$ contains only the first harmonic of the velocity. The subscript T indicates that the feedback is a T-periodic signal.

- For $l:\nu$ secondary resonances with phase quadrature points,

$$m\ddot{x}(t) + c\dot{x}(t) + kx(t) + k_{nl}x^3(t) - \mu\dot{x}_{l,T}(t) = 0 \tag{5.31}$$

  where the velocity feedback is the l-th harmonic of the velocity transformed into a T-periodic signal.

- For $l:\nu$ secondary resonances without quadrature points,

$$m\ddot{x}(t) + c\dot{x}(t) + kx(t) + k_{nl}x^3(t) - \mu\dot{x}_{l,T}(t-\alpha) = 0. \tag{5.32}$$

  In this case, the feedback is delayed by $\alpha = \frac{1}{\omega_l}\left(\frac{\pi}{2} - \varphi_l\right)$ where φ_l is the targeted resonant phase lag.

Considering the l-th harmonic of the displacement

$$x_l(t) = A_l \sin(\omega_l t - \phi_l) \tag{5.33}$$

the velocity feedback $\mu\dot{x}_{l,T}(t)$ can be obtained after transforming $\dot{x}_l(t)$ into a T-periodic signal

$$\mu\dot{x}_{l,T}(t) = \mu\omega_l A_l \cos(\omega t - \phi_l). \tag{5.34}$$

Equation (5.34) proves that the velocity feedback and the k-th harmonic of the displacement are in quadrature, as sought.

Considering now the general case, i.e., when the velocity feedback is

$$\mu\dot{x}_{l,T}(t-\alpha) = \mu\omega_l A_l \cos(\omega(t-\alpha) - \phi_l) \tag{5.35}$$

evidences that the periodic solutions of Equations (2.67) and (5.32) are identical since the velocity feedback is equivalent to classical harmonic forcing of frequency ω.

For illustration, the 1:2 subharmonic resonance ($l=1$, $\nu=2$) is taken as an example. Figure 5.9 shows the three steps to calculate the velocity feedback $\dot{x}_{1,T}(t-\alpha)$ in Figure 5.9d from the original velocity $\dot{x}(t)$ in Figure 5.9a. The first step filters out all but the first harmonic of the velocity to obtain $\dot{x}_{1,T_1}(t)$ in Figure 5.9b. This signal has a period $T_1 = 2T$ and is thus transformed during the second step into the T-periodic signal $\dot{x}_{1,T}(t)$ shown in Figure 5.9c. The third step shifts the resulting signal by the delay $\alpha = \pi/8\omega_k = \pi/4\omega$ to obtain the final feedback in Figure 5.9d.

Generalizing this philosophy to systems with n DOFs subjected to harmonic forcing at the r-th DOF

$$\mathbf{M}\ddot{\mathbf{x}}(t) + \mathbf{C}\dot{\mathbf{x}}(t) + \mathbf{K}\mathbf{x}(t) + \mathbf{f}_{nl}(\mathbf{x}(t), \dot{\mathbf{x}}(t)) = \mathbf{f}\sin\omega t \tag{5.36}$$

we define the PRNMs of the $l:\nu$ resonance of the system from Equation (5.36) as

the periodic responses obtained by replacing the harmonic forcing by a T-periodic velocity feedback comprising the l-th harmonic. The feedback is to be delayed by $\alpha = \frac{1}{\omega_l}\left(\frac{\pi}{2} - \varphi_l\right)$ where φ_l is the targeted resonant phase lag

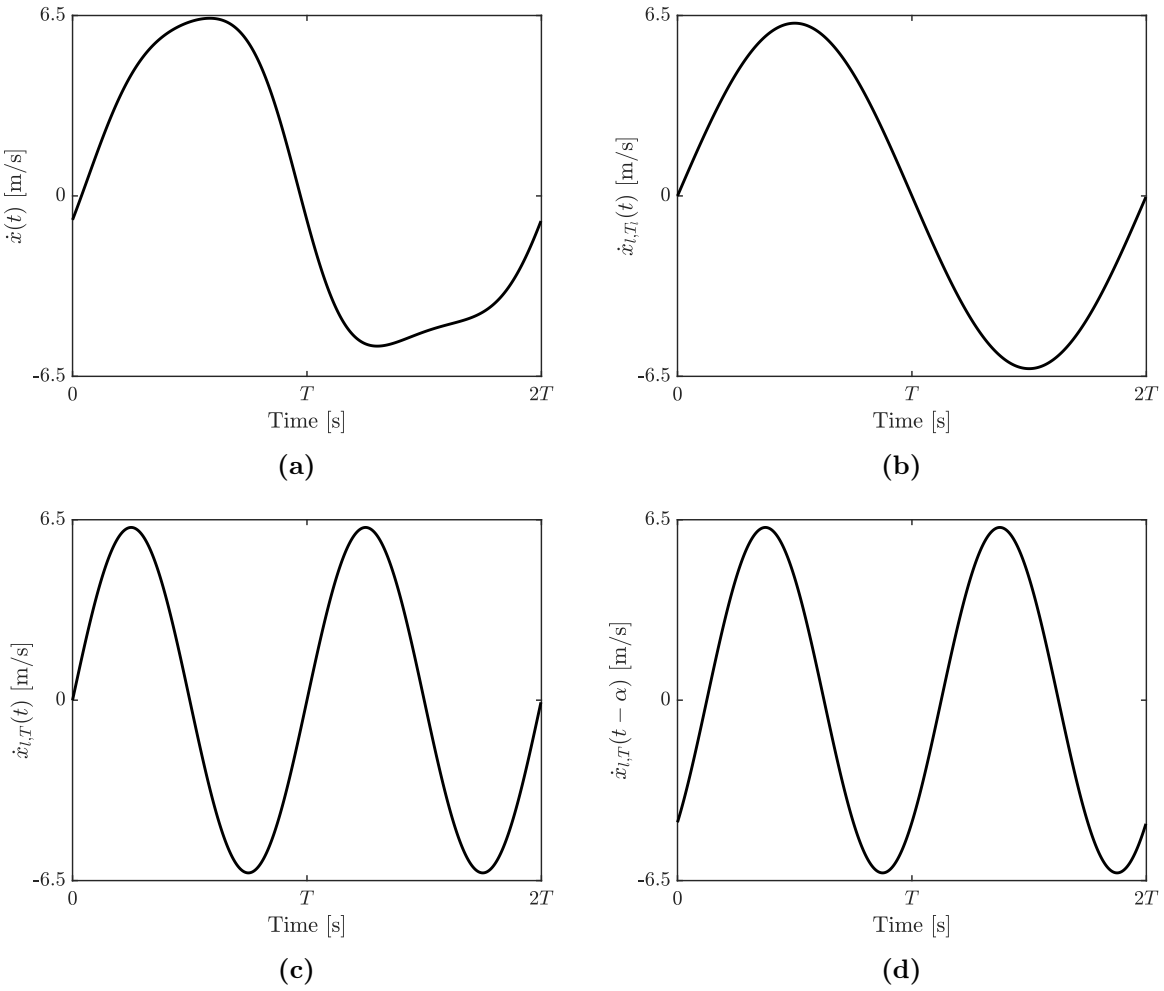

Figure 5.9: Calculation of the velocity feedback: (a) original velocity, (b) after step 1 (filtering), (c) after step 2 (T-periodic) and (d) after step 3 (delay).

5.3.1.2 Computational framework

Mathematically, we solve

$$\mathbf{M}\ddot{\mathbf{x}}(t) + \mathbf{C}\dot{\mathbf{x}}(t) + \mathbf{K}\mathbf{x}(t) + \mathbf{f}_{nl}(\mathbf{x}(t), \dot{\mathbf{x}}(t)) - \mu\dot{\mathbf{x}}_{r,l,T}(t-\alpha) = \mathbf{0}, \tag{5.37}$$

where the feedback vector $\dot{\mathbf{x}}_{r,l,T}(t-\alpha)$ has only one non-zero entry at the r-th DOF, and, without loss of generality, we assume that the feedback gain μ is strictly positive. Because the velocity feedback is a mono-harmonic component of period $T = 2\pi/\omega$, the periodic orbits of (5.37) are actual periodic orbits of (5.36), i.e., those with the assigned phase lag. Equation (5.37) should thus be interpreted as an effective reformulation of (5.36) which targets the calculation of the locus of nonlinear phase resonance of the NFRCs.

We now aim to develop an efficient computational framework to obtain accurate numerical approximations of the PRNMs and their oscillations frequencies. In this context, the HBM is a particularly appropriate method because it naturally separates the responses into different harmonics and requires no interpolation to render the signal T-periodic. The

displacement and nonlinear force vectors are thus approximated by truncated Fourier series:

$$\mathbf{x}(t) = \frac{\mathbf{c}_0^x}{\sqrt{2}} + \sum_{l=1}^{N_h} \left(\mathbf{s}_l^x \sin \omega_l t + \mathbf{c}_l^x \cos \omega_k t\right) \tag{5.38}$$

$$\mathbf{f}_{nl}(t) = \frac{\mathbf{c}_0^f}{\sqrt{2}} + \sum_{l=1}^{N_h} \left(\mathbf{s}_l^f \sin \omega_k t + \mathbf{c}_l^f \cos \omega_k t\right) \tag{5.39}$$

or, in a more compact form,

$$\mathbf{x}(t) = (\mathbf{Q}(t) \otimes \mathbf{I}_n)\mathbf{X} \tag{5.40}$$

$$\mathbf{f}_{nl}(t) = (\mathbf{Q}(t) \otimes \mathbf{I}_n)\mathbf{F}_{nl} \tag{5.41}$$

where $\mathbf{Q}(t) = \left[1/\sqrt{(2)} \;\; \sin \omega_1 t \;\; \cos \omega_1 t \;\; \ldots \;\; \sin \omega_{N_h} t \;\; \cos \omega_{N_h} t\right]$, $\otimes$ stands for the Kronecker tensor product and $\mathbf{X}$ and $\mathbf{F}_{nl}$ are the vectors containing the Fourier coefficients of the displacement and nonlinear forces, respectively. Similarly, the velocity feedback can be written using the Fourier coefficients of the displacement as:

$$\mu \dot{\mathbf{x}}_{r,l,T}(t-\alpha) = \mu(\mathbf{Q}(t) \otimes \mathbf{I}_n)\left(\mathbf{R}_\alpha \mathbf{T}_T \mathbf{T}_f \boldsymbol{\nabla}(\omega) \otimes \mathbb{I}_r\right)\mathbf{X} \tag{5.42}$$

where

- $(\boldsymbol{\nabla}(\omega) \otimes \mathbb{I}_r)\,\mathbf{X}$ contains only the Fourier coefficients of the velocity measured at the r-th DOF. $\mathbb{I}_r$ is a $(n \times n)$ a null matrix except for the r-th diagonal term which is equal to 1. The operator $\boldsymbol{\nabla}(\omega) = \mathrm{diag}(0, \boldsymbol{\nabla}_1, ..., \boldsymbol{\nabla}_l, ..., \boldsymbol{\nabla}_{N_h})$ is a differential operator coming from the time derivative of $\mathbf{Q}(t)$with

$$\boldsymbol{\nabla}_l = \begin{bmatrix} 0 & -\omega_l \\ \omega_l & 0 \end{bmatrix} \tag{5.43}$$

- $\mathbf{T}_f$ is a $(2N_h + 1) \times (2N_h + 1)$ null matrix except for the two diagonal elements corresponding to the l-th harmonic which are equal to 1. $\mathbf{T}_f$ thus filters out all harmonic components different from l, as schematized in the time domain in Figure 5.9b.

- $\mathbf{T}_T$ is a $(2N_h + 1) \times (2N_h + 1)$ null matrix except for the elements whose rows and columns correspond to the Fourier coefficients of ω and ω_l, respectively. Those elements are equal to 1. $\mathbf{T}_T$ transforms the velocity into a T-periodic signal, see Figure 5.9c.

- $\mathbf{R}_\alpha = \mathrm{diag}(0, \mathbf{0}, ..., \mathbf{R}_\nu, ..., \mathbf{0})$ is a rotation matrix which shifts the harmonic component by an angle $\frac{\nu}{l}\alpha\omega_l = \alpha\omega$, as in Figure 5.9d, where

$$\mathbf{R}_\nu = \begin{pmatrix} \cos \alpha\omega & \sin \alpha\omega \\ -\sin \alpha\omega & \cos \alpha\omega \end{pmatrix}. \tag{5.44}$$

  When the targeted phase lag φ_l is $\frac{\pi}{2}$, then $\alpha = 0$, which means that the rotation matrix $\mathbf{R}_\nu$ is the identity matrix. For the other resonances, $\alpha = \frac{1}{\omega_l}\left(\frac{\pi}{2} - \varphi_l\right)$.

By inserting Equations (5.40), (5.41) and (5.42) into Equation (5.37) and removing the time dependency with a Galerkin procedure, the PRNMs can be obtained by solving the system:

$$\mathbf{A}(\omega)\mathbf{X} + \mathbf{F}_{nl}(\mathbf{X}) - \mu \left(\mathbf{R}_\alpha \mathbf{T}_T \mathbf{T}_f \boldsymbol{\nabla}(\omega) \otimes \mathbb{I}_r\right) \mathbf{X} = 0 \tag{5.45}$$

where $\mathbf{A}(\omega) = \boldsymbol{\nabla}^2(\omega) \otimes \mathbf{M} + \boldsymbol{\nabla}(\omega) \otimes \mathbf{C} + \mathbf{I}_{2N_h+1} \otimes \mathbf{K}$ is the dynamic stiffness matrix.

Equation (5.45) provides $2N_h + 1$ equations for $2N_h + 2$ unknowns, namely the vector $\mathbf{X}$ and the gain μ. An additional equation is therefore required to close the system. This equation, termed phase condition, sets the sine coefficient of the k-th harmonic component to 0. Eventually, a resonance can be characterized at different amplitudes by taking the frequency ω as a continuation parameter. The PRNMs and the corresponding resonance frequencies are obtained through vector $\mathbf{X}$ and ω, respectively. To retrieve the phase lag ϕ_l defined in Equation (2.60), the relation $\phi_l = \text{atan2}(-c_l^x, s_l^x) - \omega_l \alpha - \frac{\omega_l}{\omega}\left(\text{atan2}(-c_l^x, s_l^x) - \frac{\pi}{2}\right)$ must be considered.

5.3.1.3 Stability

We suppose that the PRNM with the velocity feedback approach from Equation (5.37), which admits a periodic solution $\mathbf{x}^*(t)$, is perturbed with a periodic solution $\mathbf{s}(t)$ modulated by an exponential decay

$$\mathbf{p}(t) = \mathbf{x}^*(t) + e^{\bar{\sigma}t}\mathbf{s}(t). \tag{5.46}$$

The nonlinear forces are linearized around $\mathbf{x}^*(t)$, it yields

$$\begin{aligned}\mathbf{M}\ddot{\mathbf{x}}^* + \mathbf{C}\dot{\mathbf{x}}^* + \mathbf{K}\mathbf{x}^* + \mathbf{f}_{nl}(\mathbf{x}^*, \dot{\mathbf{x}}^*) - \mu\dot{\mathbf{x}}^*_{r,l,T} + \Big(\bar{\sigma}^2\mathbf{M}\mathbf{s} + \bar{\sigma}\left(2\mathbf{M}\dot{\mathbf{s}} + \mathbf{C}\mathbf{s}\right) + \mathbf{M}\ddot{\mathbf{s}} + \mathbf{C}\dot{\mathbf{s}} + \mathbf{K}\mathbf{s} \\ + \frac{\partial \mathbf{f}_{nl}}{\partial \mathbf{x}}\mathbf{s} + \frac{\partial \mathbf{f}_{nl}}{\partial \dot{\mathbf{x}}}\left(\bar{\sigma}\mathbf{s} + \dot{\mathbf{s}}\right) - \mu\left(\bar{\sigma}\mathbf{s}_{r,l,T} + \dot{\mathbf{s}}_{r,l,T}\right)\Big) e^{\bar{\sigma}t} = \mathbf{0}\end{aligned} \tag{5.47}$$

Since $\mathbf{x}^*(t)$ is a solution of Equation (5.37), it remains

$$\begin{aligned}\bar{\sigma}^2\mathbf{M}\mathbf{s} + \bar{\sigma}\left(2\mathbf{M}\dot{\mathbf{s}} + \mathbf{C}\mathbf{s} + \frac{\partial \mathbf{f}_{nl}}{\partial \dot{\mathbf{x}}}\mathbf{s} - \mu\mathbf{s}_{r,l,T}\right) + \mathbf{M}\ddot{\mathbf{s}} + \mathbf{C}\dot{\mathbf{s}} + \mathbf{K}\mathbf{s} + \frac{\partial \mathbf{f}_{nl}}{\partial \mathbf{x}}\mathbf{s} + \frac{\partial \mathbf{f}_{nl}}{\partial \dot{\mathbf{x}}}\dot{\mathbf{s}}_{r,l,T} - \mu\dot{\mathbf{s}}_{r,l,T} \\ = \mathbf{0}.\end{aligned} \tag{5.48}$$

Using the HBM formalism such that $\mathbf{x}^*(t) = (\mathbf{Q}(t) \otimes \mathbf{I}_n)\mathbf{X}^*$ and $\mathbf{s}(t) = (\mathbf{Q}(t) \otimes \mathbf{I}_n)\mathbf{S}$ where $\mathbf{X}^*$ and $\mathbf{S}$ contain the Fourier coefficients of $\mathbf{x}^*$ and $\mathbf{s}$, respectively, we obtain

$$\left(\Delta_{VF,2}\bar{\sigma}^2 + \Delta_{VF,1}\bar{\sigma} + \Delta_{VF,0}\right) e^{\bar{\sigma}t}\mathbf{S} = \mathbf{0} \tag{5.49}$$

with

$$\begin{aligned}
\Delta_{VF,2} &= \mathbf{I}_{2N_h+1} \otimes \mathbf{M} \\
\Delta_{VF,1} &= 2\nabla(\omega)\mathbf{M} \otimes + \mathbf{I}_{2N_h+1} \otimes \mathbf{C} + (\mathbf{Q}(t) \otimes \mathbf{I}_n)^{\dagger} \frac{\partial \mathbf{f}_{nl}}{\partial \dot{\mathbf{x}}}\Big|_{\dot{\mathbf{x}}=\dot{\mathbf{x}}^*} (\mathbf{Q}(t) \otimes \mathbf{I}_n) - \mu \left(\mathbf{R}_\alpha \mathbf{T}_T \mathbf{T}_f \otimes \mathbb{I}_r\right) \\
\Delta_{VF,0} &= \mathbf{A}(\omega) + \frac{\partial \mathbf{F}_{nl}}{\partial \mathbf{X}}\Big|_{\mathbf{X}=\mathbf{X}^*} - \mu \left(\mathbf{R}_\alpha \mathbf{T}_T \mathbf{T}_f \nabla(\omega) \otimes \mathbb{I}_r\right)
\end{aligned} \tag{5.50}$$

where the exponent † stands for the pseudo-inverse matrix. The $\bar{\boldsymbol{\sigma}}$ Hill's coefficients are thus the ones that solve the quadratic eigenvalue problem

$$\left(\Delta_{VF,2}\bar{\sigma}^2 + \Delta_{VF,1}\bar{\sigma} + \Delta_{VF,0}\right)\mathbf{S} = \mathbf{0}. \tag{5.51}$$

Equation (5.51) can be recast into a classical linear eigenvalue problem [29] and the Hill's coefficients are the eigenvalues of the matrix

$$\mathbf{B}_{VF} = \begin{bmatrix} -\Delta_{VF,2}^{-1}\Delta_{VF,1} & -\Delta_{VF,2}^{-1}\Delta_{VF,0} \\ \mathbf{I}_{n(2N_h+1)} & \mathbf{0}_{n(2N_h+1)} \end{bmatrix}. \tag{5.52}$$

Only the $2n$ with the smallest imaginary part in modulus approximate the $\bar{\boldsymbol{\sigma}}$ Floquet exponents [102]. The mechanical system is unstable if at least one of the Floquet exponents has a positive real part, otherwise, it is asymptotically stable.

5.3.1.4 Illustration on a two-degree-of-freedom system

The velocity feedback approach is now applied to a two-DOF system whose equations of motion are

$$\begin{cases} \ddot{x}_1 + 0.02\dot{x}_1 - 0.01\dot{x}_2 + 6x_1 - 5x_2 + x_1^3 = f\sin\omega t \\ \ddot{x}_2 - 0.01\dot{x}_1 + 0.02\dot{x}_2 - 5x_1 + 6x_2 = 0. \end{cases} \tag{5.53}$$

This is illustrated in Figure 5.10. The PRNM curve of the first mode of vibration accurately models the hardening effect of the cubic nonlinearity and passes well through the resonant points. However, for the second mode of vibration, though it also passes well through the resonant point, the PRNM curve is totally unstable while the NFRC, which is still in the linear regime, is stable. The velocity feedback can thus destabilize the system and give different stability results compared to the NFRC.

This can be explained even in the linear regime of Equation (5.53). For a general unforced linear system of the form

$$\mathbf{M}\ddot{\mathbf{x}}(t) + \mathbf{C}\dot{\mathbf{x}}(t) + \mathbf{K}\mathbf{x}(t) = \mathbf{0} \tag{5.54}$$

the free response is a contribution of the damped modes of the system such that

$$\mathbf{x}(t) = \sum_{i=1}^{2n} w_i \mathbf{z}_i e^{\upsilon_i t} \tag{5.55}$$

where w_i, $\mathbf{z}_i$ and υ_i are the modal amplitude, eigenmode and eigenfrequency of the i-th damped mode of Equation (5.54) [1]. The eigenmodes and eigenfrequencies come in

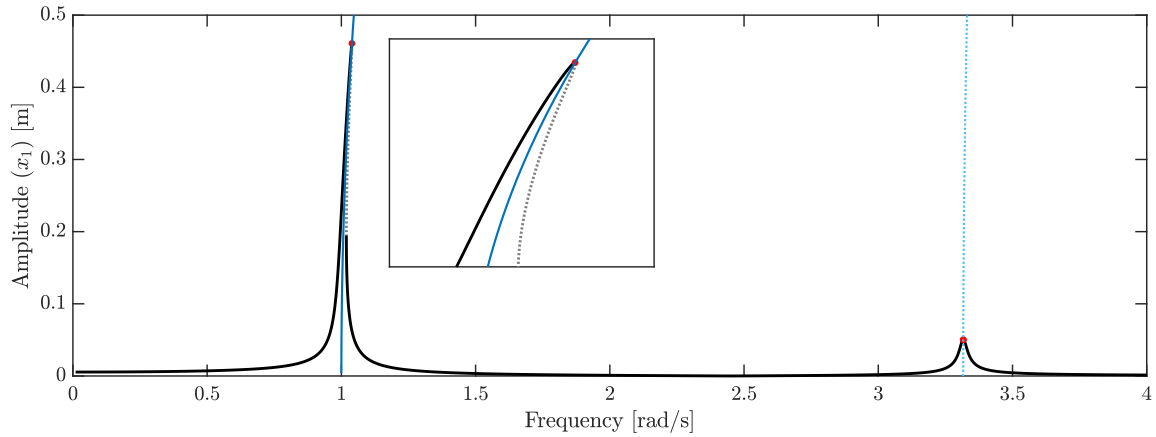

Figure 5.10: NFRC (black) and PRNM curve obtained with the velocity feedback approach (blue) of the system from Equation (5.53) for a forcing amplitude of 0.01 N.

complex conjugate pairs and the modal amplitudes depend on the initial conditions. The pairs of eigenfrequencies υ_i are computed as

$$\upsilon_i = -\beta_i \pm i\omega_i \tag{5.56}$$

where

$$\begin{aligned} \beta_i &= \frac{c_i}{2m_i} \\ \omega_i &= \sqrt{\frac{k_i}{m_i} - \left(\frac{c_i}{2m_i}\right)^2} \end{aligned} \tag{5.57}$$

with m_i, c_i and k_i the modal mass, damping and stiffness terms such that

$$m_i = \mathbf{z}_i^\ddagger \mathbf{M} \mathbf{z}_i \tag{5.58}$$

$$c_i = \mathbf{z}_i^\ddagger \mathbf{C} \mathbf{z}_i \tag{5.59}$$

$$k_i = \mathbf{z}_i^\ddagger \mathbf{K} \mathbf{z}_i \tag{5.60}$$

and $\mathbf{z}_i^\ddagger$ the complex conjugate of $\mathbf{z}_i$. In this case, each β_i is positive such that the real part of each λ_i is negative and the motion is decaying. This is expected since there is no external forcing. In the presence of a velocity feedback, the equations of motion become

$$\mathbf{M}\ddot{\mathbf{x}}(t) + (\mathbf{C} - \mathbb{I}_r \mu)\,\dot{\mathbf{x}}(t) + \mathbf{K}\mathbf{x}(t) = \mathbf{0}, \tag{5.61}$$

and the complex eigenmodes and eigenfrequencies vary with the gain μ. Specifically, the damped modal damping values are now computed as

$$c_i = \mathbf{z}_i^\dagger \,(\mathbf{C} - \mathbb{I}_r \mu)\,\mathbf{z}_i. \tag{5.62}$$

The i-th mode of vibration is excited when $c_i = 0$ and $c_{j,j\neq i} \neq 0$. Furthermore, the stability of the system is affected by $c_{j,j\neq i}$. If all $c_{j,j\neq i} > 0$ then the system is stable since

all the modes, except the i-th mode, are decaying. However if at least one $c_{j,j\neq i} < 0$, then the contribution of this mode grows exponentially with time. This is what happens for the system from Equation (5.53) in the linear regime. When $c_1 = 0$, then $c_2 > 0$ and the system is stable for the first mode. For the second mode, when $c_2 = 0$, then $c_1 < 0$ and the system is unstable. This is illustrated in Figure 5.11.

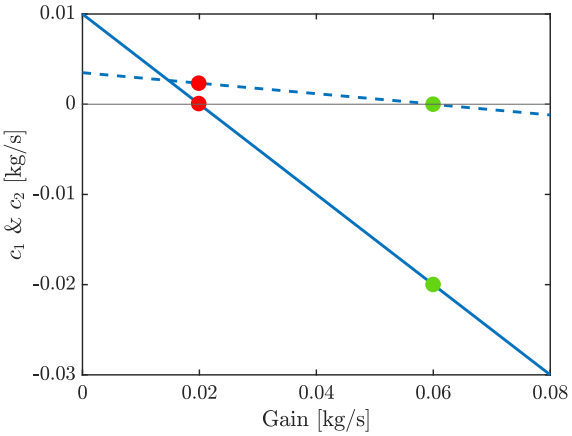

Figure 5.11: Evolution of c_1 (solid blue) and c_2 (dashed blue) as a function of the gain μ. The points where $c_1 = 0$ and $c_2 = 0$ are shown with red and green dots, respectively.

A similar stability analysis can be found in [20]. In the nonlinear regime, the mechanism is similar but we need to rely on the Floquet exponents to compute the stability.

5.3.2 The resonant phase lag approach

5.3.2.1 Theoretical framework

We start from a harmonically-forced nonlinear oscillator

$$m\ddot{x}(t) + c\dot{x}(t) + kx(t) + f_{nl}(x(t), \dot{x}(t)) = f \sin \omega t. \tag{5.63}$$

Since the solution is periodic, $x(t)$ can be decomposed into a Fourier series. Considering the l-th harmonic of the displacement

$$x_l(t) = A_l \sin(\omega_l t - \phi_l) \tag{5.64}$$

phase resonance is achieved through precise tuning ω such that $\phi_l = \text{atan2}(-c_l, s_l) = \varphi_l$. Once this done, the phase lag is locked and a continuation procedure is applied. With this approach, we define the PRNMs of the $l : \nu$ resonance of the system from Equation (5.36) as

the periodic responses obtained when the l-th harmonic of the response at the harmonically forced location is excited at its resonant phase lag φ_l.

5.3.2.2 Computational framework

Mathematically, we solve:

$$\mathbf{M}\ddot{\mathbf{x}}(t) + \mathbf{C}\dot{\mathbf{x}}(t) + \mathbf{K}\mathbf{x}(t) + \mathbf{f}_{nl}(\mathbf{x}(t), \dot{\mathbf{x}}(t)) - \mathbf{f}_r \sin \omega t = \mathbf{0} \tag{5.65}$$

where the vector $\mathbf{f}$ has only one non-zero entry of strictly positive amplitude f at the r-th DOF. Using the HBM formalism as for the velocity feedback approach, Equation (5.65) provides $2N_h + 1$ equations for $2N_h + 2$ unknowns, namely the vector $\mathbf{X}$ and the forcing amplitude f. The phase condition added to close the system sets the phase lag of the l-th harmonic to the desired resonant phase lag φ_l

$$\text{atan2}(-c_l, s_l) = \varphi_l. \tag{5.66}$$

5.3.2.3 Stability

We suppose that the PRNM with the resonant phase lag approach from Equation (5.65), which admits also a periodic solution $\mathbf{x}^*(t)$, is perturbed with a periodic solution $\mathbf{s}(t)$ modulated by an exponential decay

$$\mathbf{p}(t) = \mathbf{x}^*(t) + e^{\bar{\sigma}t}\mathbf{s}(t) \tag{5.67}$$

and we apply the same methodology as in the velocity feedback approach. The $\bar{\boldsymbol{\sigma}}$ Hill's coefficients are thus the ones that solve the quadratic eigenvalue problem

$$\left(\Delta_{PL,2}\bar{\sigma}^2 + \Delta_{PL,1}\bar{\sigma} + \Delta_{PL,0}\right)\mathbf{S} = \mathbf{0} \tag{5.68}$$

with

$$\begin{aligned}
\Delta_{PL,2} &= \mathbf{I}_{2N_h+1} \otimes \mathbf{M} \\
\Delta_{PL,1} &= 2\nabla(\omega)\mathbf{M} \otimes + \mathbf{I}_{2N_h+1} \otimes \mathbf{C} + (\mathbf{Q}(t) \otimes \mathbf{I}_n)^\dagger \frac{\partial \mathbf{f}_{nl}}{\partial \dot{\mathbf{x}}}\Big|_{\dot{\mathbf{x}}=\dot{\mathbf{x}}^*} (\mathbf{Q}(t) \otimes \mathbf{I}_n) \\
\Delta_{PL,0} &= \mathbf{A}(\omega) + \frac{\partial \mathbf{F}_{nl}}{\partial \mathbf{X}}\Big|_{\mathbf{X}=\mathbf{X}^*}.
\end{aligned} \tag{5.69}$$

Again, Equation (5.68) can be recast into a classical linear eigenvalue problem [29] and the Hill's coefficients are the eigenvalues of the matrix

$$\mathbf{B}_{PL} = \begin{bmatrix} -\Delta_{PL,2}^{-1}\Delta_{PL,1} & -\Delta_{PL,2}^{-1}\Delta_{PL,0} \\ \mathbf{I}_{n(2N_h+1)} & \mathbf{0}_{n(2N_h+1)} \end{bmatrix}. \tag{5.70}$$

Since the equations that describe the stability of the PRNM with the resonant phase lag approach are the same as the ones when computing the NFRC with the HBM [29], the stability is the same. Therefore, if the NFRC is stable at the targeted phase resonance, then the PRNM with the resonant phase lag approach is also stable, and conversely.

5.3.2.4 Illustration on a two-degree-of-freedom system

The PRNM with the resonant phase lag approach is also applied to the system from Equation (5.53) in Figure 5.12. The PRNM curves of the first and second modes of vibration accurately model the hardening effect of the cubic nonlinearity and pass well through the resonant points. Contrary to the velocity feedback approach, the stability of the PRNM curves is the same as the NFRC since their stability equations are the same, as described in Section 5.3.2.3. For this reason, the resonant phase lag approach is used throughout the rest of this chapter.

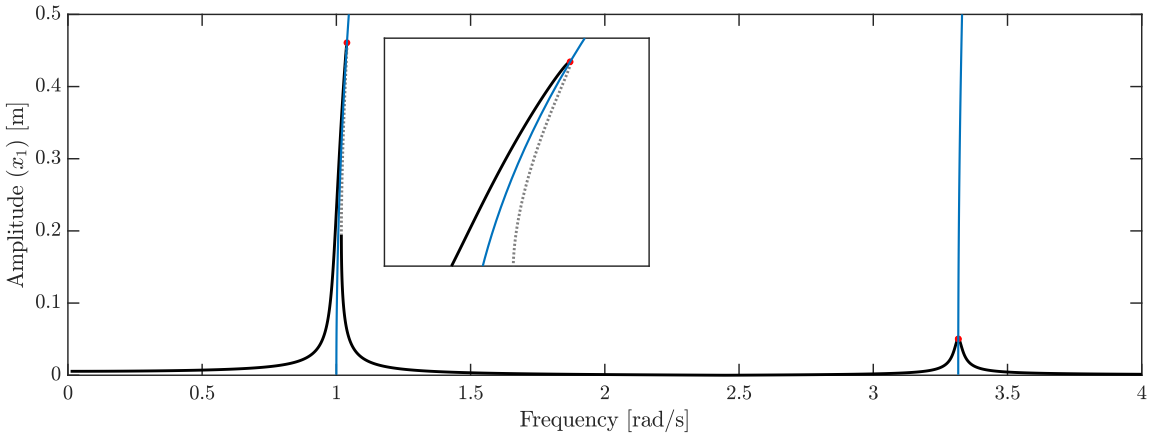

Figure 5.12: NFRC (black: stable; grey: unstable) and PRNM curve obtained with the resonant phase lag approach (blue) of the system from Equation (5.53) for a forcing amplitude of 0.01 N.

5.4 Illustration on different types of nonlinear oscillators

5.4.1 The Duffing oscillator

The first system studied is the Duffing oscillator

$$\ddot{x}(t) + 2\zeta\omega_0\dot{x}(t) + \omega_0^2 x(t) + \alpha_3 x^3(t) = \gamma \sin \omega t. \tag{5.71}$$

The system parameters are $\zeta = 0.5\%$, $\omega_0 = 1$ rad/s and $\alpha_3 = 1$ N/(kg.m^3). The different resonances are calculated using $8 \times \nu$ harmonics where the value of ν depends on the type of resonance studied. The primary resonance as well as the most dominant secondary resonances and their corresponding PRNM curves are shown in Figure 5.14 for a forcing of γ =1 N/kg. These resonances as well as the other ultra-subharmonic resonances are studied in detail hereafter.

5.4.1.1 Primary resonance

Figure 5.15 illustrates the primary resonance and its corresponding PRNM curve calculated for a resonant phase lag equal to $\pi/2$. Since each PRNM is defined for a specific

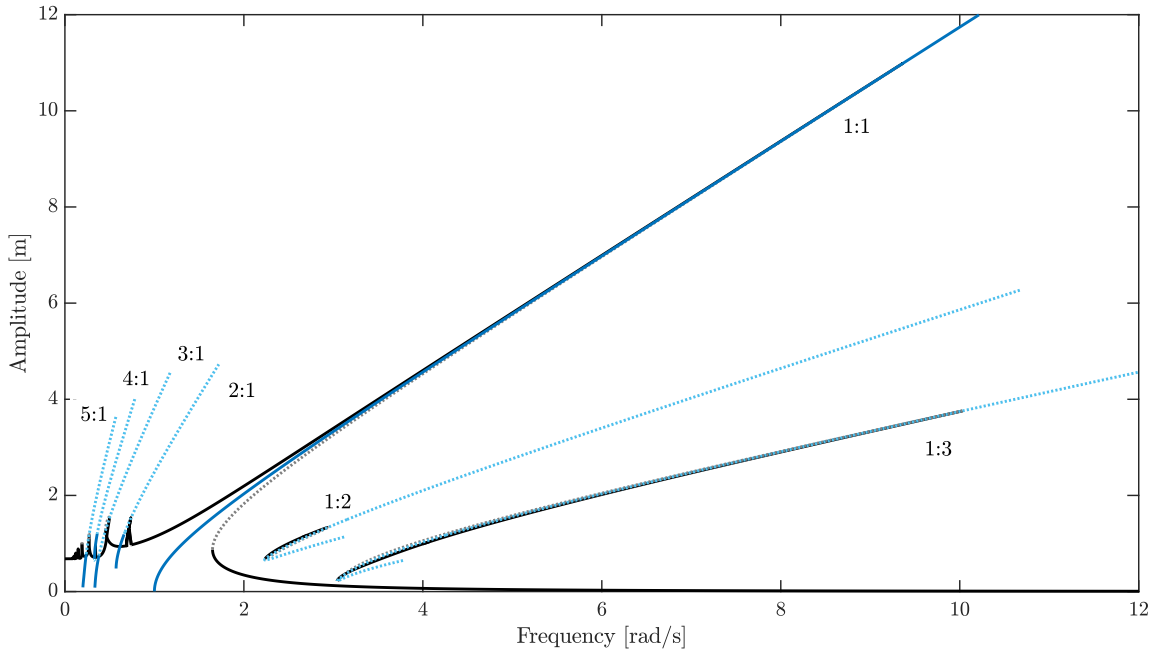

Figure 5.13

Figure 5.14: NFRC (black: stable; grey: unstable) and the PRNM curves (solid blue: stable; dotted blue: unstable) of the Duffing oscillator for γ =1 N/kg.

forcing amplitude, the amplitude and frequency evolution with respect to the forcing amplitude in Figures 5.15c and 5.15d can calculated in a straightforward manner. This is contrast with the NNMs for which EB must be applied to represent (approximately) these relations.

5.4.1.2 Superharmonic resonances

The resonant phase lag for odd superharmonic resonances is $\pi/2$. The NFRCs and PRNM curves for the 3:1, 5:1 and 7:1 resonances are presented in Figure 5.16. If additional harmonics were considered in the response computation, higher-order odd superharmonic resonances could also be calculated.

For the 2:1 and 4:1 resonances, Section 4.3.3.1 evidenced that two solutions that perfectly superimpose in absolute value exist and that their phase lag evolves around $\frac{3\pi}{4}$ and $-\frac{\pi}{4}$, respectively. As depicted in Figure 5.17, these phase lags can also be utilized for obtaining the PRNM curves of higher-order even superharmonic resonances.

5.4.1.3 Subharmonic resonances

Section 4.3.3.2 highlighted that the resonant phase lag is either $\frac{\pi}{2}$ or $\frac{3\pi}{4}$, depending on whether ν is odd or even, respectively. The PRNM curves are plotted in Figures 5.18 and 5.19 for the 1:3 and 1:2 resonances, respectively.

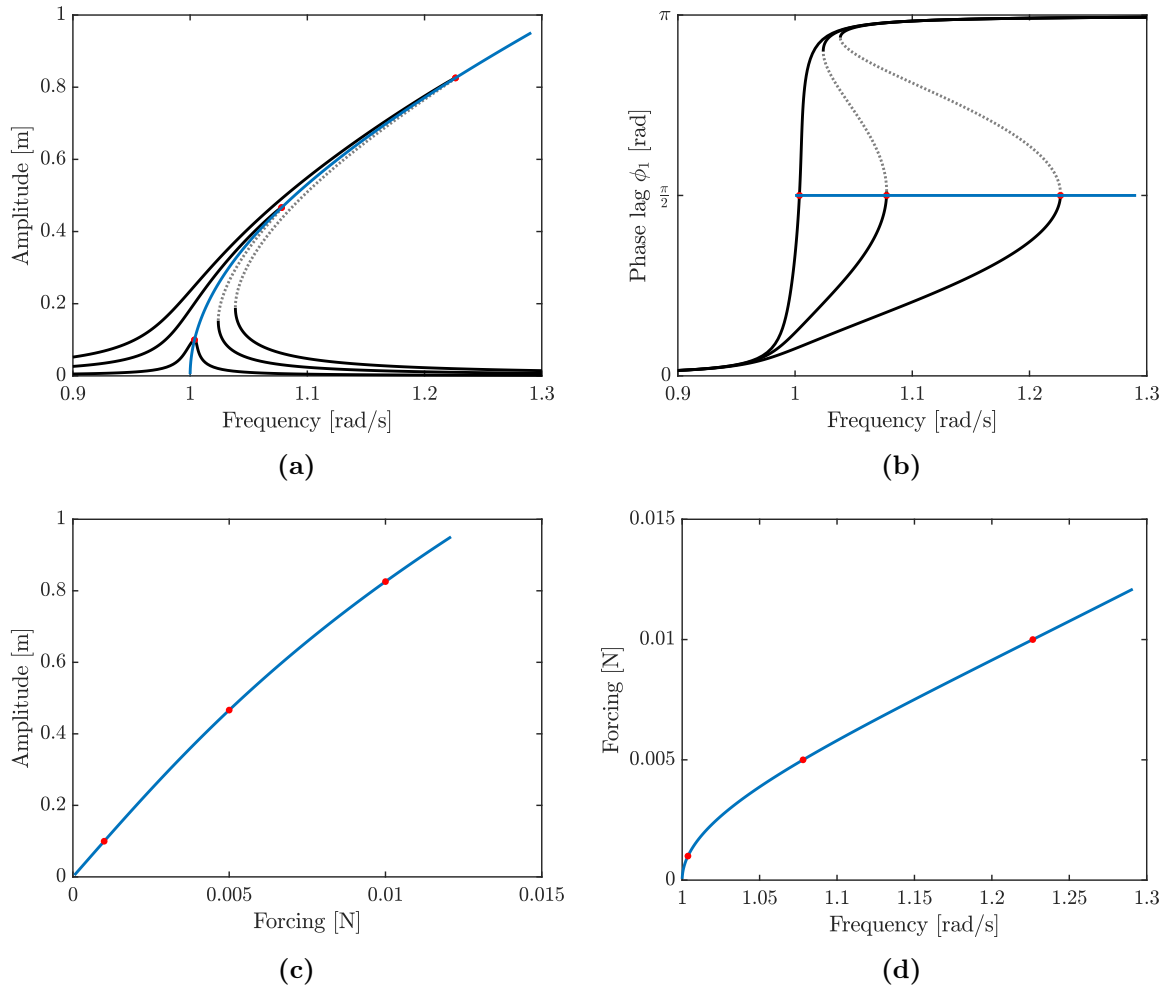

Figure 5.15: NFRCs (black: stable; grey: unstable) and PRNM curve (blue) of the primary resonance of the Duffing oscillator for γ=0.001 N/kg, 0.005 N/kg, 0.01 N/kg: (a) amplitude, (b) phase lag, (c) amplitude-forcing curve and (d) forcing-frequency curve.

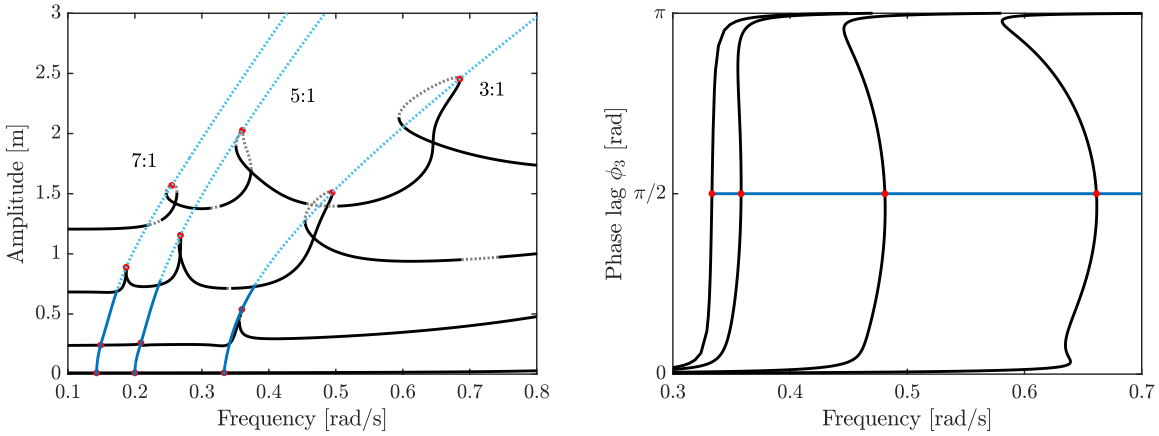

(a) **(b)**

Figure 5.16: NFRCs (black: stable; grey: unstable) and PRNM curves (solid blue: stable; dotted blue: unstable) of the 3:1, 5:1 and 7:1 superharmonic resonances for γ=0.01 N/kg, 0.25 N/kg, 1 N/kg and 3 N/kg: (a) amplitude and (b) phase lag of the 3rd harmonic component of the 3:1 resonance (computed with only 3 harmonics and without the stability for better readability).

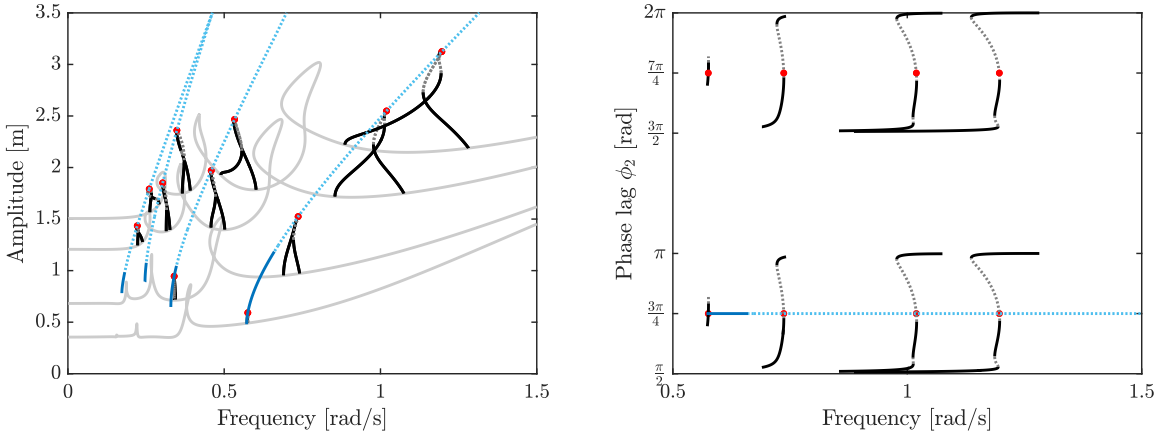

(a) **(b)**

Figure 5.17: NFRCs (black: stable; grey: unstable) and PRNM curves (solid blue: stable; dotted blue: unstable) of the 2:1, 4:1, 6:1 and 8:1 superharmonic resonances for γ=0.04 N/kg, 1 N/kg, 3 N/kg and 5 N/kg: (a) amplitude and (b) phase lag of the 2nd harmonic component of the 2:1 resonance.

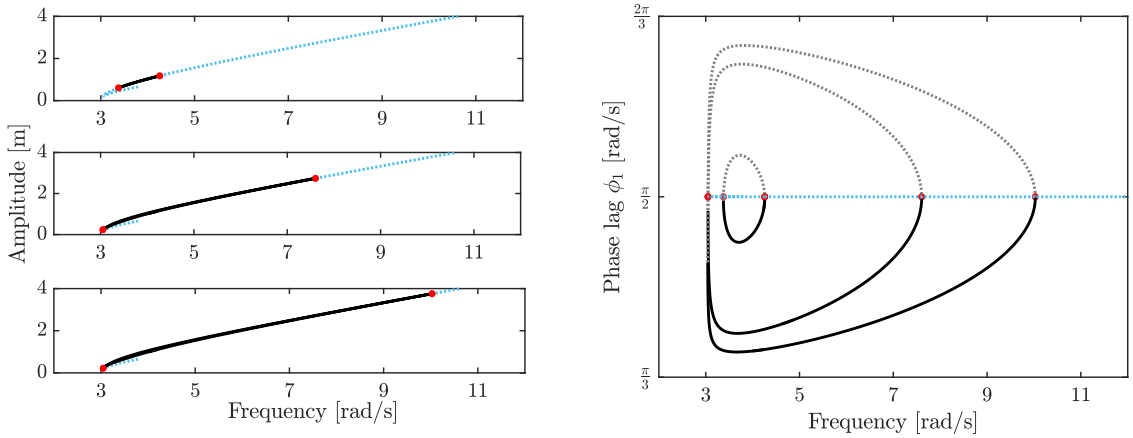

(a) **(b)**

Figure 5.18: NFRCs (black: stable; grey: unstable) and PRNM curve (solid blue: stable; dotted blue: unstable) of the 1:3 subharmonic resonance for γ =0.25 N/kg, 0.6 N/kg and 1 N/kg: (a) amplitude and (b) phase lag of the 1st harmonic component.

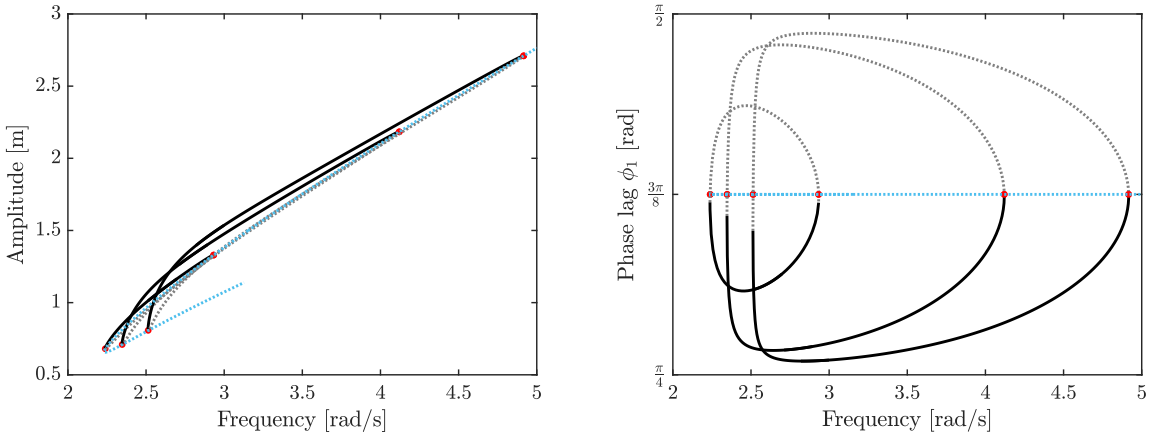

(a) **(b)**

Figure 5.19: NFRCs (black: stable; grey: unstable) and PRNM curve (solid blue: stable; dotted blue: unstable) of the 1:2 subharmonic resonance for γ =1 N/kg, 2 N/kg and 3 N/kg: (a) amplitude and (b) phase lag of the 1st harmonic component.

5.4.1.4 Ultra-subharmonic resonances

Section 4.3.3.3 demonstrated that ultra-subharmonic resonances of order $l{:}\nu$ exhibit similar behavior to superharmonic and subharmonic resonances. If both l and ν are odd, the resonant phase lag is either $\frac{\pi}{2}$ or $-\frac{\pi}{2}$, depending on the cases. If either l or ν is even, the resonant phase lag is always $\frac{3\pi}{4\nu}$. The PRNM curves are represented in Figures 5.20, 5.21, 5.22 and 5.23 for the 3:2, 3:5, 2:3 and 5:3 resonances, respectively.

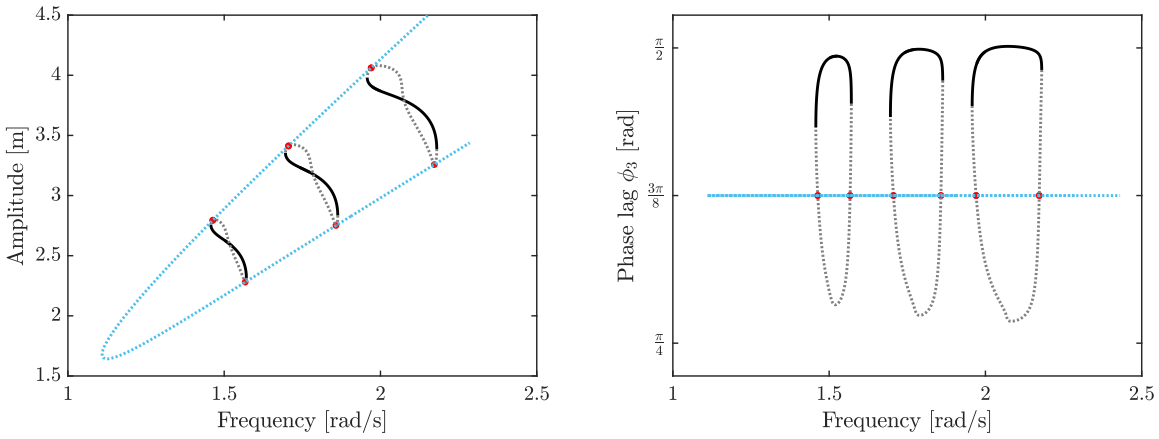

(a) **(b)**

Figure 5.20: NFRCs (black: stable; grey: unstable) and PRNM curve (solid blue: stable; dotted blue: unstable) of the 3:2 subharmonic resonance for γ =3 N/kg, 5 N/kg and 8 N/kg: (a) amplitude and (b) phase lag of the 3rd harmonic component.

5.4.2 The Helmholtz-Duffing oscillator

The second system studied is the Helmhotz-Duffing oscillator

$$\ddot{x}(t) + 2\zeta\omega_0\dot{x}(t) + \omega_0^2 x(t) + \alpha_2 x^2(t) + \alpha_3 x^3(t) = \gamma \sin \omega t. \tag{5.72}$$

with $\zeta = 0.5\%$, $\omega_0 = 1$ rad/s, $\alpha_2 = 1.2$ N/(kg.m^2) and $\alpha_3 = 1$ N/(kg.m^3). Only the most prominent secondary resonances are studied; they are calculated using $8 \times \nu$ harmonics.

Figure 5.24 displays the NFRC of this oscillator as well as the corresponding PRNM curves. The choice of the resonant phase lag is explained hereafter.

5.4.2.1 Primary resonance

Chapter 3 demonstrated that a phase lag of $\frac{\pi}{2}$ can be used to characterize any oscillator with polynomial stiffness, which is the case here. The PRNM curve in Figure 5.24 effectively characterizes the softening effect resulting from the quadratic nonlinearity at low forcing amplitudes as well as the hardening effect arising from the cubic nonlinearity at higher forcing amplitudes.

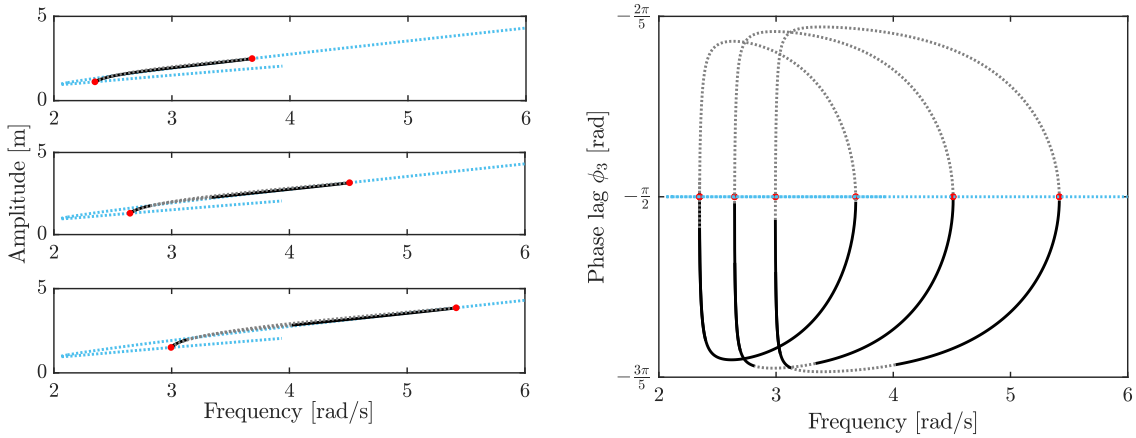

(a) **(b)**

Figure 5.21: NFRCs (black: stable; grey: unstable) and PRNM curve (solid blue: stable; dotted blue: unstable) of the 3:5 subharmonic resonance for γ =3 N/kg, 5 N/kg and 8 N/kg: (a) amplitude and (b) phase lag of the 3rd harmonic component.

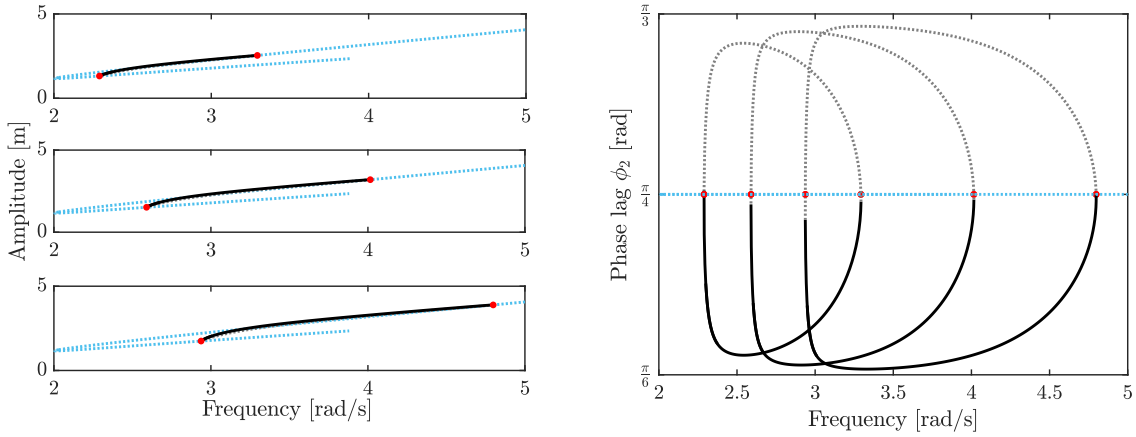

(a) **(b)**

Figure 5.22: NFRCs (black: stable; grey: unstable) and PRNM curve (solid blue: stable; dotted blue: unstable) of the 2:3 subharmonic resonance for γ =3 N/kg, 5 N/kg and 8 N/kg: (a) amplitude and (b) phase lag of the 2nd harmonic component.

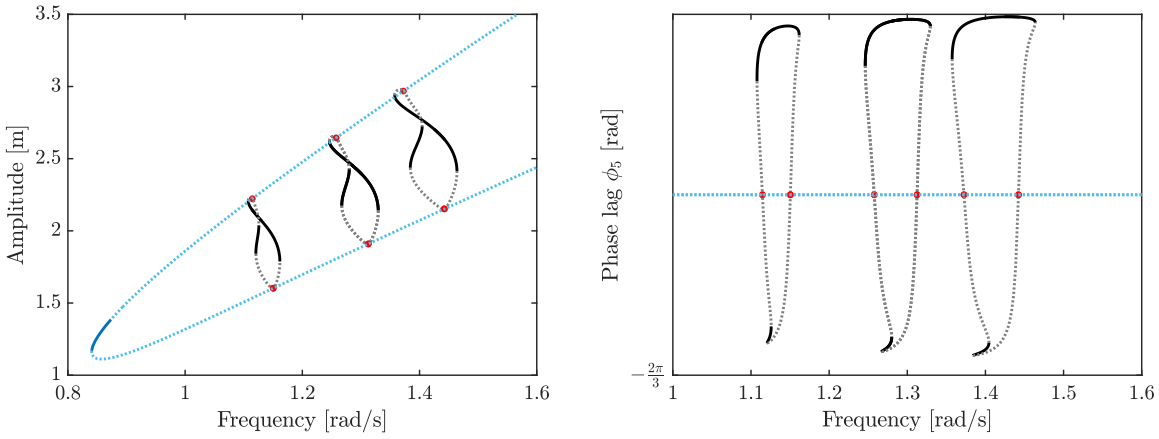

Figure 5.23: NFRCs (black) and PRNM curve (solid blue: stable; dotted blue: unstable) of the 5:3 subharmonic resonance for γ =2 N/kg, 3 N/kg and 4 N/kg: (a) amplitude and (b) phase lag of the 5th harmonic component.

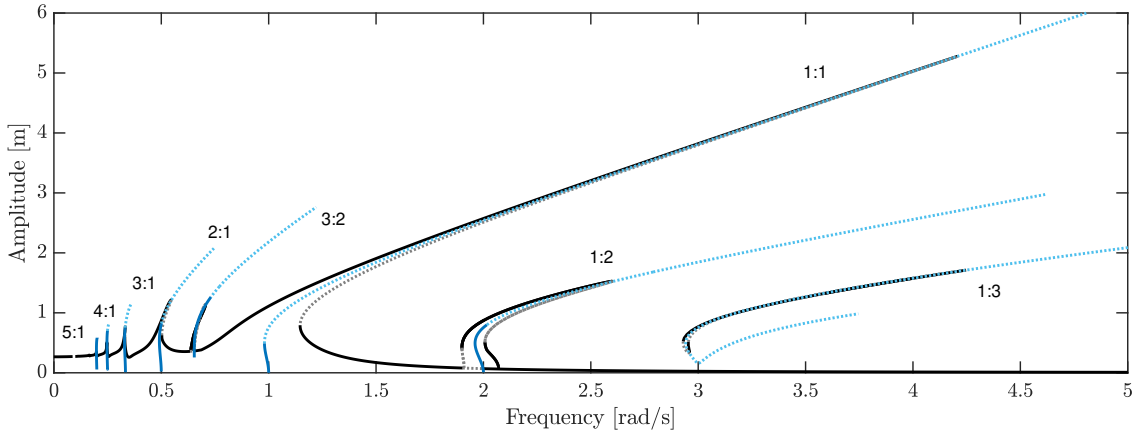

Figure 5.24: NFRC (black: stable; grey: unstable) and the PRNM curves (solid blue: stable; dotted blue: unstable) of the Helmholtz-Duffing oscillator for γ =0.2 N/kg.

5.4.2.2 Secondary resonances

To obtain the resonant phase lag of secondary resonances, the AM procedure in Section 4.3.1 applied to Equation (5.72) gives

$$\begin{aligned}\ddot{z}(t)+\omega_0^2 z(t) = &-\varepsilon\left(\bar{\alpha}_2(z(t)+\kappa\sin\omega t)^2\right.\\ &\left.+\varepsilon\bar{\alpha}_3(z(t)+\kappa\sin\omega t)^3+2\varepsilon^{q-1}\bar{\zeta}\omega_0(\dot{z}(t)+\omega\kappa\cos\omega t)\right)\end{aligned} \tag{5.73}$$

with $\omega_l^2-\omega_0^2=\varepsilon^q\Omega$. In general, the AM leads to a system of equations of the form

$$\begin{cases}\dot{A}_l = f_1(A_l,\phi_l,\omega)\\ \dot{\phi}_l = f_2(A_l,\phi_l,\omega).\end{cases} \tag{5.74}$$

Assuming steady-state conditions and that $\omega\simeq\frac{\nu\omega_0}{l}$ is constant yields

$$\begin{cases}f_1(A_l,\phi_l)=0\\ f_2(A_l,\phi_l)=0.\end{cases} \tag{5.75}$$

Therefore, a direct relationship between A_l and ϕ_l is obtained, and the resonant phase lag can be found using only one of the two equations. The focus is on $f_1(A_l,\phi_l)=0$ herein.

2:1 resonance

First-order AM with $q=1$ gives

$$A_2\zeta\omega_0=\frac{a_2\kappa^2}{8\omega}\cos\phi_2. \tag{5.76}$$

A_2 is maximum when $\phi_2=0$ is considered as the resonant phase lag.

3:1 resonance

Second-order AM with $q=2$ gives

$$2A_3\zeta\omega_0=\frac{\kappa^3(5a_3\omega^2-2a_2^2)}{60\omega^3}\sin\phi_3. \tag{5.77}$$

In this case, two possible phase lags exist, depending on the sign of $5a_3\omega^2-2a_2^2$. If it is positive, the resonant phase lag is $\frac{\pi}{2}$; otherwise, the phase lag is $-\frac{\pi}{2}$. The latter case applies to our example.

4:1 resonance

Third-order AM with $q=3$ gives

$$6A_4\zeta\omega_0=\frac{5a_2\kappa^4(108a_3\omega^2-11a_2^2)}{10752\omega^5}\cos\phi_4. \tag{5.78}$$

Again, there are two possibilities depending on the sign of $108a_3\omega^2-11a_2^2$. The resonant phase lag is 0 (π) if it is positive (negative). The latter case applies to our example.

5:1 resonance

Averaging with $q = 4$ yields

$$24A_5\zeta\omega_0 = \frac{\kappa^5(236a_2^4 - 5724a_2^2a_3\omega^2 + 11907a_3^2\omega^4)}{423360\omega^7}\sin\phi_5. \tag{5.79}$$

If $236a_2^4 - 5724a_2^2a_3\omega^2 + 11907a_3^2\omega^4$ is positive (negative), then the resonant phase lag is $\frac{\pi}{2}$ $(-\frac{\pi}{2})$. The former case applies to our example.

1:3 resonance

Averaging with $q = 2$ yields

$$2A_1\zeta\omega_0 = \frac{9A^2\kappa(6a_2^2 + a_3\omega^2)}{4\omega^3}\sin 3\phi_1. \tag{5.80}$$

In this case, since we consider positive stiffness coefficients, the resonant phase lag can be chosen among $\frac{\pi}{2}$, $\frac{7\pi}{6}$ and $\frac{11\pi}{6}$ as for the Duffing oscillator.

1:2 resonance

As for the Duffing oscillator in Section 4.3.2.1, AM does not provide relevant equations for the 1:2 resonance. A numerical analysis revealed that the phase lags 0 and π accurately approximate the maximum of amplitude of the first harmonic component of the solution. Both solutions have the same maximum amplitude in absolute value, and either of them can be chosen as the resonant phase lag.

3:2 resonance

The same observation as for the 1:2 resonance holds. A numerical study indicates that either 0 and π can be chosen as the resonant phase lags.

Resonance	**Steady-state equation $\mathbf{f_1(A_1, \phi_1) = 0}$**	**Sign discussion**	**Resonant phase lag**
2:1 ($q = 1$)	$A_2\zeta\omega_0 = \frac{a_2\kappa^2}{8\omega}\cos\phi_2$	/	$\phi_2 = 0$
3:1 ($q = 2$)	$2A_3\zeta\omega_0 = \frac{\kappa^3(5a_3\omega^2 - 2a_2^2)}{60\omega^3}\sin\phi_3$	$5a_3\omega^2 - 2a_2^2$	$\phi_3 = \frac{\pi}{2}$ or $\phi_3 = -\frac{\pi}{2}$
4:1 ($q = 3$)	$6A_4\zeta\omega_0 = \frac{5a_2\kappa^4(108a_3\omega^2 - 11a_2^2)}{10752\omega^5}\cos\phi_4$	$108a_3\omega^2 - 11a_2^2$	$\phi_4 = 0$ or $\phi_4 = \pi$
5:1 ($q = 4$)	$24A_5\zeta\omega_0 = \frac{\kappa^5(236a_2^4 - 5724a_2^2a_3\omega^2 + 11907a_3^2\omega^4)}{423360\omega^7}\sin\phi_5$	$236a_2^4 - 5724a_2^2a_3\omega^2 + 11907a_3^2\omega^4$	$\phi_5 = \frac{\pi}{2}$ or $\phi_5 = -\frac{\pi}{2}$
1:3 ($q = 2$)	$2A_1\zeta\omega_0 = \frac{9A^2\kappa(6a_2^2 + a_3\omega^2)}{4\omega^3}\sin 3\phi_1$	$\alpha_2 > 0$ and $\alpha_3 > 0$	$\phi_1 = \frac{\pi}{2} + \frac{2i\pi}{3}$ $i = 0, 1, 2$
1:2	/	/	0 and π
3:2	/	/	0 and π

Table 5.1: Summary of the equations of motions and resonant phase lags of secondary resonances of the Helmholtz oscillator.

5.4.3 An oscillator with piecewise linear stiffness

The governing equation of motion is

$$m\ddot{x}(t) + c\dot{x}(t) + f_s(x(t)) = f\sin\omega t \tag{5.81}$$

with $m = 1$ kg, $c = 0.1$ kg/s. The stiffness function illustrated in Figure 5.25 is

$$f_s(x(t)) = \begin{cases} \text{sign}(x(t))(ka_{p_1} + k_{p_1}(a_{p_2} - a_{p_1}) + k_{p_2}(x(t) - a_{p_2}), & x \geq a_{p_2} + \Delta_a \\ p_{2+}(x(t)), & a_{p_2} - \Delta_a < x < a_{p_2} + \Delta_a \\ \text{sign}(x(t))(ka_{p_1} + k_{p_1}(x(t) - a_{p_1})), & a_{p_1} + \Delta_a \leq x < a_{p_2} - \Delta_a \\ p_{1+}(x(t)), & a_{p_1} - \Delta_a < x < a_{p_1} + \Delta_a \\ kx(t), & -(a_{p_1} - \Delta_a) \leq x \leq a_{p_1} - \Delta_a \\ p_{1-}(x(t)), & -(a_{p_1} + \Delta_a) < x < -(a_{p_1} - \Delta_a) \\ \text{sign}(x(t))(ka_{p_1} + k_{p_1}(x(t) - a_{p_1})), & -(a_{p_2} - \Delta_a) \leq x \leq -(a_{p_1} + \Delta_a) \\ p_{2-}(x(t)), & -(a_{p_2} + \Delta_a) < x < -(a_{p_2} - \Delta_a) \\ \text{sign}(x(t))(ka_{p_1} + k_{p_1}(a_{p_2} - a_{p_1}) + k_{p_2}(x(t) - a_{p_2}), & x \leq -(a_{p_2} + \Delta_a) \end{cases} \tag{5.82}$$

where a_{p_1} and a_{p_2} are the clearances, k_{p_1} and k_{p_2} are stiffness values and $p_{1\pm}$ and $p_{2\pm}$ are regularization functions that ensure the continuity of the first derivative of the stiffness function. $p_{1\pm}$ and $p_{2\pm}$ have a size of $2\Delta_a$ and are Hermite polynomials functions such that

$$\begin{aligned} p_{i\pm}(t_p) =& h_{00}(t_p)p_{i,k} + h_{10}(t_p)(x_{i,k+1} - x_{i,k})k'_{i,k} \\ &+ h_{01}(t_p)p_{i,k+1} + h_{11}(t_p)(x_{i,k+1} - x_{i,k})k'_{i,k+1} \end{aligned} \tag{5.83}$$

where $i = 1$ or 2, $p_{i,k}$ and $p_{i,k+1}$ are the values of the restoring force at points $x_{i,k} = \text{sign}(x)(a_i - \Delta_a)$ and $x_{i,k+1} = \text{sign}(x)(a_i + \Delta_a)$, respectively. Furthermore, $k'_{i,k}$ and $k'_{i,k+1}$ are the values of the restoring force derivative at points $x_{i,k}$ and $x_{i,k+1}$. $t_p(x) = \frac{x - x_k}{x_{k+1} - x_k}$ is the local scaled abscissa and the $h_{ij}(t_p)$ coefficients of the Hermite polynomials are defined as

$$\begin{cases} h_{00}(t_p) &= 2t_p^3 - 3t_p^2 + 1 \\ h_{10}(t_p) &= t_p^3 - 2t_p^2 + t_p \\ h_{01}(t_p) &= -2t_p^3 + 3t_p^2 \\ h_{11}(t_p) &= t_p^3 - t_p^2 \end{cases} \tag{5.84}$$

as described in [103]. The values are: $a_{p_1} = 0.1$m, $a_{p_1} = 0.3$m, $\Delta_a = 0.01$m, $k = 10$N/m, $k_{p_1} = -5$N/m and $k_{p_2} = 15$N/m.

The NFRC of Equation (5.81) and the corresponding PRNM curve are displayed in Figure 5.26a for f =0.035N. In this case, the response amplitude is greater than 0.1m. The restoring force thus starts to decrease, resulting in a decrease of the resonance frequency.

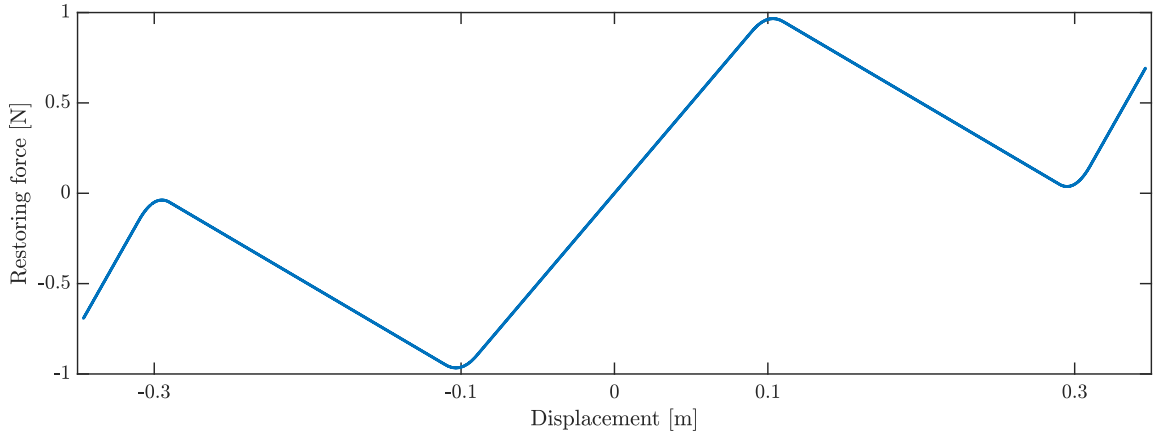

Figure 5.25: Evolution of the restoring force $f_s(x(t))$ as a function of the displacement.

The response amplitude as a function of the forcing amplitude is shown in Figure 5.26b. Interestingly, due to the softening-hardening nature of the restoring force, there is a regime, between 0.0353N and 0.4253N, during which there exist three resonance points. This signals the presence of an isolated branch that would be missed when computing only the NFRC. The birth and merging mechanisms are illustrated in Figure 5.27. For f =0.0356N in Figure 5.27a, the (small) isola is characterized by two resonance points located on the PRNM curve. Then, the isola grows toward the resonance peak of the main branch in Figures 5.27b and 5.27c. Finally, for f =0.0454N in Figure 5.27d, it merges with the main branch close to the resonance points, and a single resonance point remains.

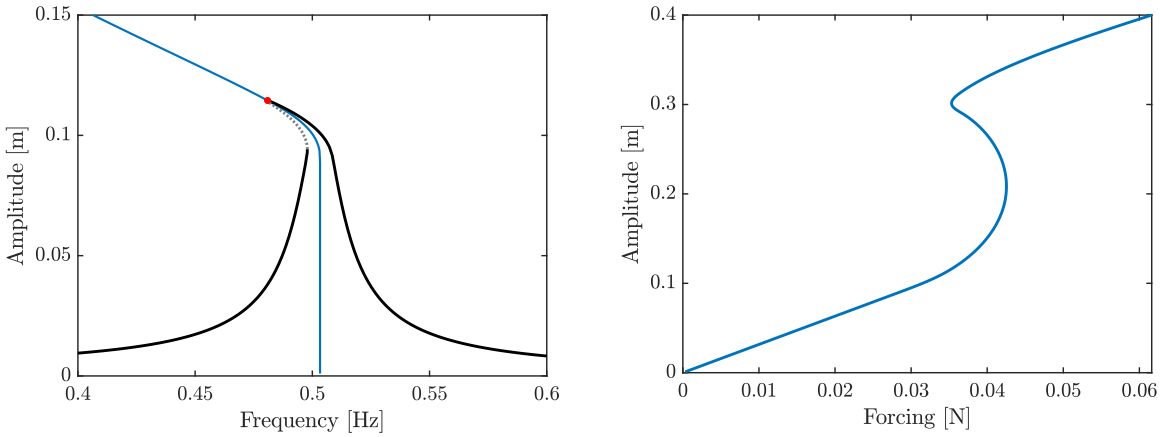

Figure 5.26: Primary resonance of the oscillator with piecewise linear stiffness. (a) NFRC (black: stable; grey: unstable) and PRNM curve (blue) for f =0.035 N; (b) forcing-amplitude plot.

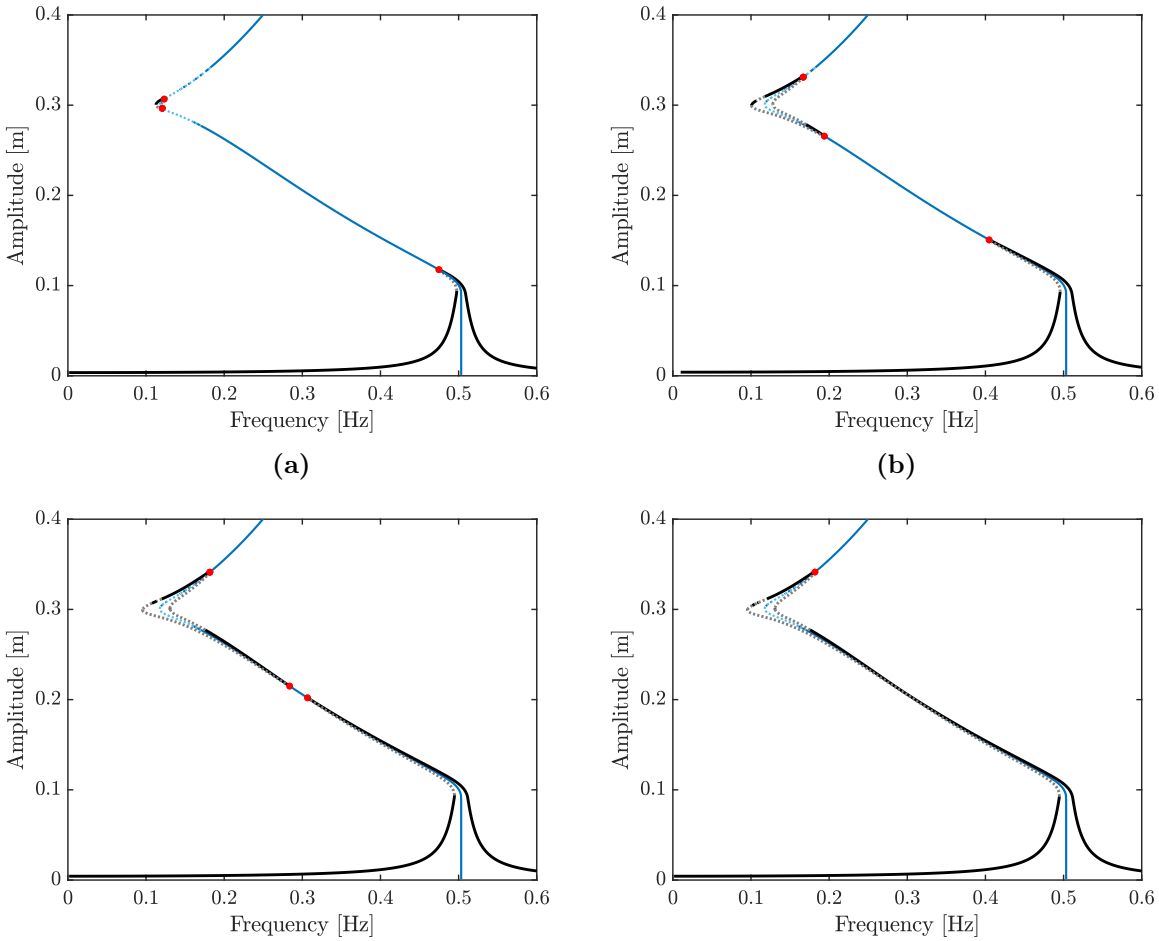

Figure 5.27: NFRCs (black: stable; grey: unstable) and PRNM curve (solid blue: stable; dotted blue: unstable) of the primary resonance of the oscillator with piece-wise linear stiffness for a forcing amplitude of: (b) 0.0356 N, (c) 0.4 N, (c) 0.425 N and (d) 0.4254 N (the red dots correspond to the phase resonance points).

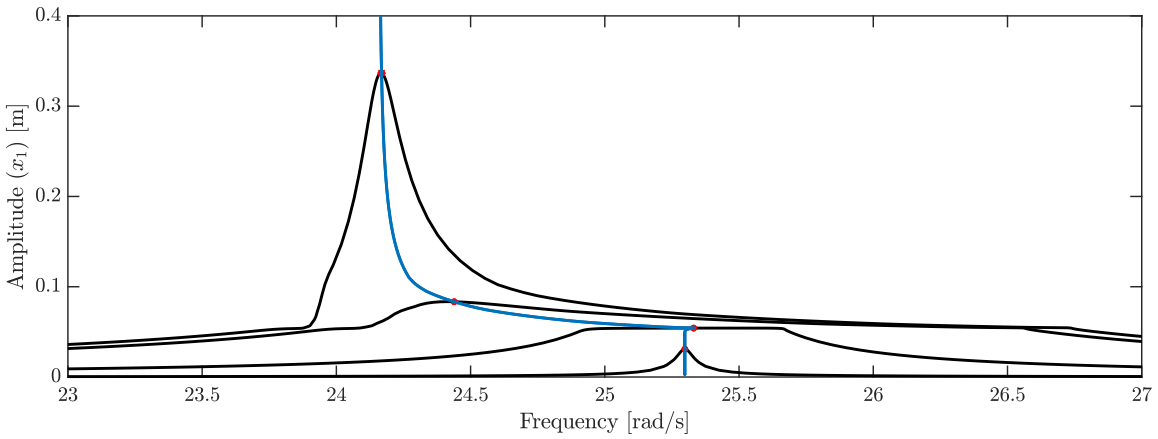

Figure 5.28: NFRC (black) and PRNM curve (blue) of the two-DOF system with Coulomb friction.

5.4.4 An oscillator with Coulomb friction

The PRNM definition can also tackle nonconservative nonlinearities. For illustration, the system described in Section (5.1.3) is analyzed. The PRNM curve in Figure 5.28 accurately predicts the resonance frequency in the stick, stick-slip and slip regions. These results are consistent with those obtained in Section (5.1.3) using EPMC. However, it is important to note that the PRNM points represent actual solutions of the system, contrary to the EPMC curve which represents the solutions of the system forced with a mass-proportional self-excitation.

5.5 Conclusion

In this chapter, the concept of a PRNM was introduced for the first time. The theory behind PRNMs relies on the condition for nonlinear phase resonance through the so-called resonant phase lag φ_l calculated between the l-th harmonic of the $l{:}\nu$ resonance and the forcing. Two computational methods based on a velocity feedback and on the resonant phase lag were developed to compute PRNMs numerically. They result in the same resonance curves but the stability information provided by the velocity feedback approach is different from the actual stability.

Unlike most existing definitions, PRNMs are actual solutions of the NFRC and can be used to characterize secondary resonances. Another distinct advantage of PRNMs is that amplitude-forcing curves are a direct outcome of PRNMs. These curves can be very useful, e.g., for the detection of isolated branches. Finally, PRNMs can be easily identified experimentally using PLLs, as discussed in the next chapter.

Chapter 6

Phase resonance nonlinear modes of multi-degree-of-freedom systems

6.1 Introduction

The primary and secondary resonances of SDOF systems can be characterized by a well-defined phase lag for the harmonic in resonance, as established in Chapters 3 and 4. This resonant phase lag was used in Chapter 5 to compute the PRNM curves of simple nonlinear systems. However, two important aspects of PRNMs remain to be discussed in this chapter.

First, this chapter evidences that the resonant phase lags found analytically for SDOF systems cannot always be extended to the MDOF case. Indeed, the potential interactions between primary and secondary resonances have a direct influence on the evolution of the phase lag of the studied harmonics. As it will be shown, rather than directly applying $\phi_l = \varphi_l$ around the $l{:}\nu$ resonance, a phase lag ϕ_l' that is a combination of carefully selected harmonics should be considered to remove the influence of the other harmonics.

Second, the PRNM definition is applied to two experimental setups, namely a cantilever beam with an artificial cubic stiffness that presents a 5:1 modal interaction and a clamped-clamped beam featuring geometrical nonlinearity.

6.2 A motivating example

To illustrate that the resonant phase lags of SDOF oscillators cannot always be used for MDOF systems, the system

$$\begin{cases} \ddot{x}_1 + 0.02\dot{x}_1 - 0.01\dot{x}_2 + 6x_1 - 5x_2 + x_1^3 = f\sin\omega t \\ \ddot{x}_2 - 0.01\dot{x}_1 + 0.02\dot{x}_2 - 5x_1 + 6x_2 = 0 \end{cases} \tag{6.1}$$

is considered. The natural frequencies of the underlying linear system are 1 are $\sqrt{11}$ rad/s.

The amplitude A_1 and phase lag ϕ_1 of the fundamental harmonic of x_1 are shown in Figure 6.1. In addition to the two primary resonances, an antiresonance is seen for a pul-

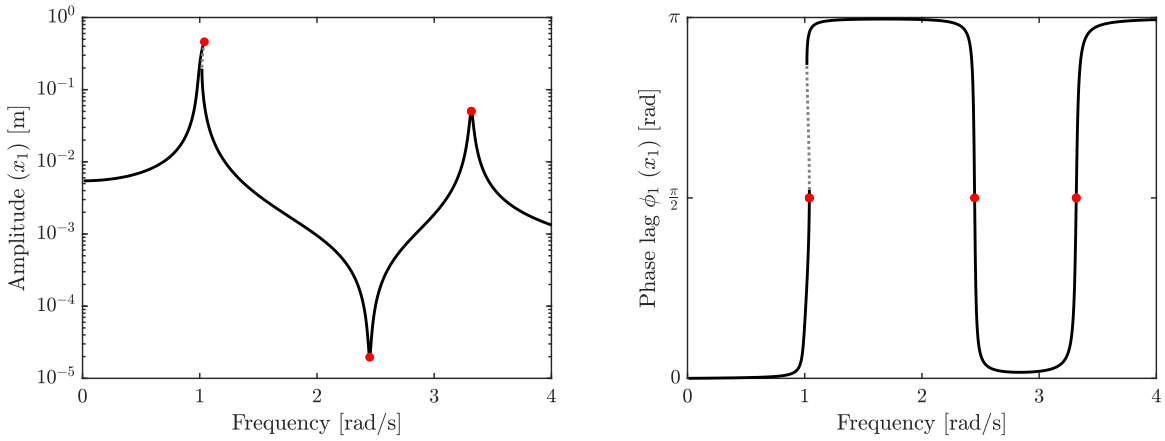

(a) **(b)**

Figure 6.1: NFRC of the fundamental harmonic of x_1 for f =0.01 N. (a) Amplitude A_1 and (b) phase lag ϕ_1. The red dots correspond to the phase quadrature points. Black: stable; grey: unstable.

sation of 2.45 rad/s. Figure 6.2 represents the amplitude A_3 and phase lag ϕ_3 of the third harmonic of x_1. Two 3:1 superharmonic resonances occur around 1/3 and $\sqrt{11}/3$=1.10 rad/s. The 3:1 resonance of the first mode resonates at $\pi/2$, as it was the case for a Duffing oscillator. Around 0.82 rad/s, the phase lag is again $\pi/2$. This corresponds to the antiresonance of the third harmonic since there is a minimum of amplitude in the NFRC at this frequency, located at one third of the antiresonance of the first harmonic. The linear concept of an antiresonance has thus a nonlinear counterpart for non-fundamental harmonics. Then, the amplitude of the third harmonic reaches a maximum at the primary resonance for a phase lag of $3\pi/2$. This value is not further discussed because the phase lag of higher-order harmonics in the vicinity of the primary resonance was never discussed so far in this manuscript. Finally, for the second 3:1 resonance, the resonant phase lag is $3\pi/2$, which departs from the theoretical expectations, i.e., $\pi/2$. This shift of π radians seems to be influenced by the presence of the primary resonance around which the third harmonic also resonates. The question is thus how to get rid of the influence of the primary resonance on higher-order harmonics such that the resonant phase lags found in Chapter 4 can still be used. This is the objective of the next section.

6.3 Phase lag of higher-order harmonics around lower-order harmonics

6.3.1 A phase lag oriented perturbation technique

The phase lag oriented perturbation technique (PLOPT), based on the HBM and developed in [104], focuses on the phase lag evolution of the harmonics of zero, first and second orders. It deliberately omits any resonance frequency corrections; it thus ignores the softening or hardening character of the system. A weakly nonlinear oscillator of the

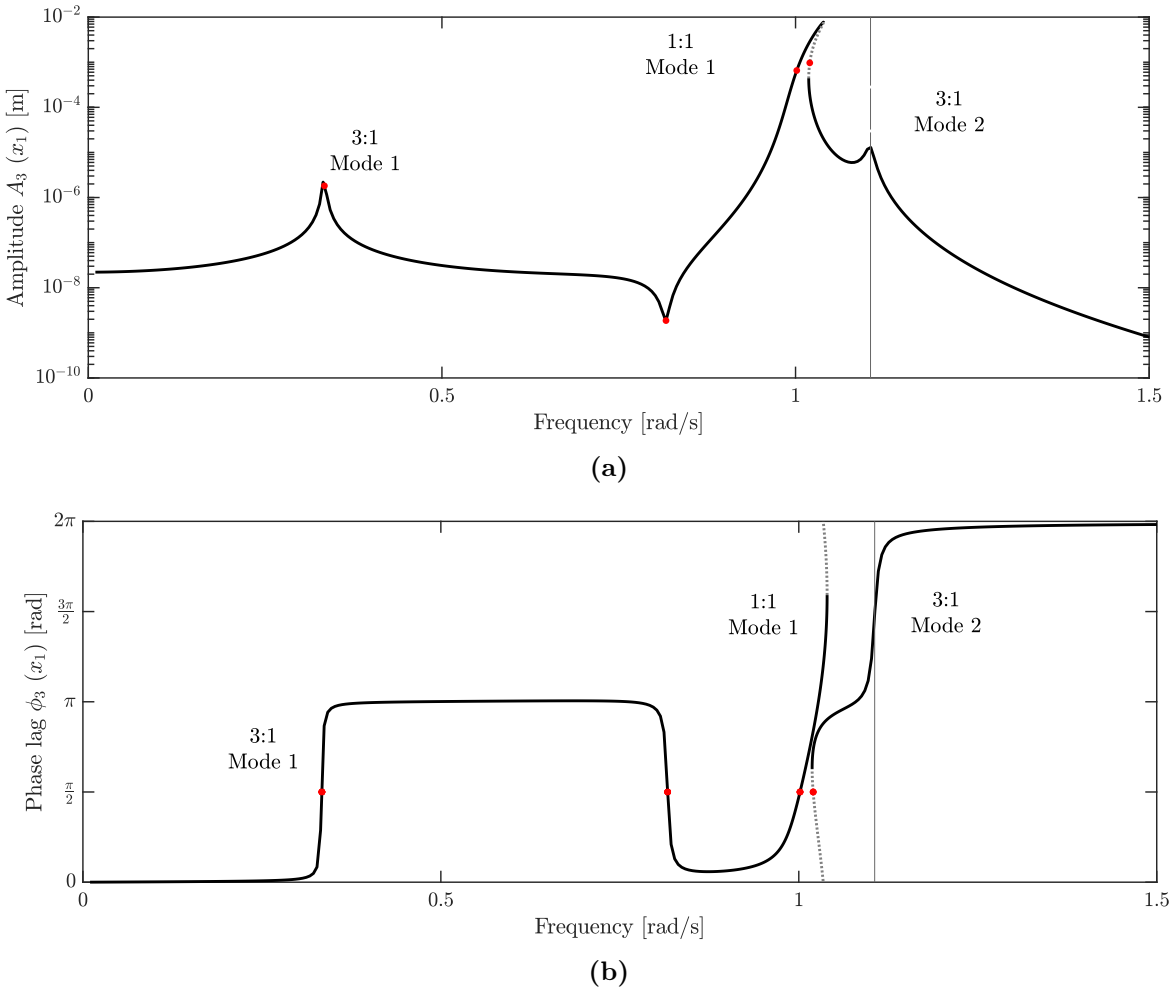

Figure 6.2: NFRC of the third harmonic of x_1 for f =0.01 N. (a) Amplitude A_3 and (b) phase lag ϕ_3. The red dots correspond to the phase quadrature points. Black: stable; grey: unstable.

form is assumed

$$\ddot{x}(t) + 2\zeta\omega_0\dot{x}(t) + \omega_0^2 x(t) + \varepsilon f_{nl}\left(x(t), \dot{x}(t)\right) = \gamma \sin \omega t \tag{6.2}$$

with $0 < \varepsilon \ll 1$. The response of a nonlinear oscillator can be decomposed into a Fourier series

$$x(t) = A_0 + \sum_{i=1}^{N_H} A_i \sin\left(i\omega t - \phi_i\right). \tag{6.3}$$

As for the MMS in Section 2.3.1.3, the solution has an asymptotic expansion such that

$$x(t) = y_0(t) + \varepsilon y_1(t) + \varepsilon^2 y_2(t) + \mathcal{O}\left(\varepsilon^3\right) \tag{6.4}$$

where each y_i can be decomposed into Fourier series. The nonlinear force is also expanded using a Taylor series expansion

$$\begin{aligned} f_{nl}\left(x, \dot{x}\right) &= f_{nl}\left(y_0, \dot{y}_0\right) + \varepsilon\left(\frac{\partial f_{nl}}{\partial x}\left(y_0, \dot{y}_0\right) y_1 + \frac{\partial f_{nl}}{\partial \dot{x}}\left(y_0, \dot{y}_0\right) \dot{y}_1\right) + \mathcal{O}\left(\varepsilon^2\right) \\ &= f_{nl}\left(y_0, \dot{y}_0\right) + \varepsilon f'_{nl}\left(y_0, \dot{y}_0, y_1, \dot{y}_1\right) + \mathcal{O}\left(\varepsilon^2\right) \end{aligned} \tag{6.5}$$

where the time dependence was dropped for conciseness. Inserting Equations (6.4) and (6.5) into (6.2) and equating the like-powers of ε lead to the following system of equations

$$\begin{cases} \ddot{y}_0 + 2\zeta\omega_0\dot{y}_0 + \omega_0^2 y_0 = \gamma \sin \omega t \\ \ddot{y}_1 + 2\zeta\omega_0\dot{y}_1 + \omega_0^2 y_1 = -f_{nl}\left(y_0, \dot{y}_0\right) \\ \ddot{y}_2 + 2\zeta\omega_0\dot{y}_2 + \omega_0^2 y_2 = -f'_{nl}\left(y_0, \dot{y}_0, y_1, \dot{y}_1\right) \end{cases} \tag{6.6}$$

where each equation can be solved based on the lower-order solutions.

6.3.1.1 Zero-th order solution

The first relation in Equation (6.6) is the equation of a simple damped, forced linear oscillator for which the response is $y_0 = A_{0,1} \sin\left(\omega t - \phi_{0,1}\right)$ where $A_{0,1}$ and $\phi_{0,1}$ are governed by

$$\begin{cases} A_{0,1} = \frac{\gamma}{\sqrt{4\zeta^2\omega_0^2\omega^2 + (\omega_0^2 - \omega^2)^2}} \\ \phi_{0,1} = \operatorname{atan2}\left(2\zeta\omega_0\omega, \omega_0^2 - \omega^2\right). \end{cases} \tag{6.7}$$

6.3.1.2 First-order solution

The first-order solution y_1 is the response of a linear oscillator excited by $-f_{nl}\left(y_0, \dot{y}_0\right)$. It is expressed using a Fourier series

$$y_1 = y_{1,0} + \sum_{l=1}^{N_H} y_{1,l} = A_{1,0} + \sum_{l=1}^{N_H} A_{1,l} \sin\left(l\omega t - \phi_{1,l}\right). \tag{6.8}$$

The excitation, which depends on y_0 and $\dot{y}_0$, is also decomposed into a Fourier series

$$\begin{aligned} f_{nl}\left(y_0, \dot{y}_0\right) &= f_{nl}\left(A_{0,1}\sin\omega t - \phi_{0,1}, A_{0,1}\omega\cos\omega t - \phi_{0,1}\right) \\ &= c_0^f\left(A_{0,1}\right) + \sum_{i=l}^{N_H}\left(c_l^f\left(A_{0,1}\right)\cos\left(l\left(\omega t - \phi_{0,1}\right)\right) + s_l^f\left(A_{0,1}\right)\sin\left(l\left(\omega t - \phi_{0,1}\right)\right)\right). \end{aligned} \tag{6.9}$$

It is then projected onto the $(\sin(l\omega t - \phi_{1,l}), \cos(l\omega t - \phi_{1,l}))$ basis such that

$$f_{nl}\left(y_0, \dot{y}_0\right) = C_0^f\left(A_{0,1}\right) + \sum_{l=1}^{N_H}\left(C_l^f\left(A_{0,1}\right)\cos\left(l\omega t - \phi_{0,1}\right) + S_l^f\left(A_{0,1}\right)\sin\left(l\omega t - \phi_{0,1}\right)\right) \tag{6.10}$$

where

$$C_0^f\left(A_{0,1}\right) = \frac{2}{T}\int_0^T f_{nl}\left(y_0, \dot{y}_0\right)\,\mathrm{d}t \tag{6.11}$$

$$C_l^f\left(A_{0,1}\right) = \frac{2}{T}\int_0^T f_{nl}\left(y_0, \dot{y}_0\right)\cos\left(l\omega t - \phi_{1,l}\right)\mathrm{d}t = c_l^f\left(A_{0,1}\right)\cos\phi_l' + s_l^f\left(A_{0,1}\right)\sin\phi_l' \tag{6.12}$$

$$S_l^f\left(A_{0,1}\right) = \frac{2}{T}\int_0^T f_{nl}\left(y_0, \dot{y}_0\right)\sin\left(l\omega t - \phi_{1,l}\right)\mathrm{d}t = s_l^f\left(A_{0,1}\right)\cos\phi_l' - c_l^f\left(A_{0,1}\right)\sin\phi_l' \tag{6.13}$$

with $\phi_l' = \phi_{1,l} - l\phi_{0,1}$. Substituting the Fourier series of y_1 and $f_{nl}\left(y_0, \dot{y}_0\right)$ into the second relation of Equation (6.6) and equating the coefficients of each harmonic $\sin\left(l\omega t - \phi_{1,l}\right)$ and $\cos\left(l\omega t - \phi_{1,l}\right)$ to 0, a system of two equations for each harmonic l is obtained

$$\begin{cases} 2l\zeta\omega_0\omega A_{1,l} + c_l^f\left(A_{0,1}\right)\cos\phi_l' + s_l^f\left(A_{0,1}\right)\sin\phi_l' = 0 \\ \Omega_l A_{1,l} - s_l^f\left(A_{0,1}\right)\cos\phi_l' + c_l^f\left(A_{0,1}\right)\sin\phi_l' = 0 \end{cases} \tag{6.14}$$

with $\Omega_l = \omega_l^2 - \omega_0^2$. The system is easily solved for each $A_{1,l}$ and ϕ_l' with $l > 0$

$$\begin{cases} A_{1,l} = -\frac{1}{2l\zeta\omega_0\omega}\left(s_l^f\left(A_{0,1}\right)\sin\phi_l' + c_l^f\left(A_{0,1}\right)\cos\phi_l'\right) \\ \phi_l' = \operatorname{atan2}\left(-2l\zeta\omega_0\omega s_l^f\left(A_{0,1}\right) - c_l^f\left(A_{0,1}\right)\Omega_l, s_l^f\left(A_{0,1}\right)\Omega_l - 2l\zeta\omega_0\omega c_l^f\left(A_{0,1}\right)\right). \end{cases} \tag{6.15}$$

Usually, $C_0^f\left(A_{0,1}\right) = c_0^f\left(A_{0,1}\right) = 0$.

6.3.1.3 Second-order solution

The second-order solution y_2 from the third relation of (6.6) is the response of a linear oscillator excited by $-f_{nl}'\left(y_0, \dot{y}_0, y_1, \dot{y}_1\right)$. It is expressed using a Fourier series

$$y_2 = y_{2,0} + \sum_{l_2=1}^{N_H} y_{2,l_2} = A_{2,0} + \sum_{l_2=1}^{N_H} A_{2,l_2}\sin\left(l_2\omega t - \phi_{2,l_2}\right) \tag{6.16}$$

and $f'_{nl}\left(y_0, \dot{x}_0, y_1, \dot{y}_1\right)$ can be decomposed into

$$\begin{aligned} f'_{nl}\left(y_0, \dot{y}_0, y_1, \dot{y}_1\right) &= \frac{\partial f_{nl}}{\partial x}\left(y_0, \dot{y}_0\right) y_1 + \frac{\partial f_{nl}}{\partial \dot{x}}\left(y_0, \dot{y}_0\right) \dot{y}_1 \\ &= \sum_{l=1}^{N_H} \left(\frac{\partial f_{nl}}{\partial x}\left(y_0, \dot{y}_0\right) y_{1,l} + \frac{\partial f_{nl}}{\partial \dot{x}}\left(y_0, \dot{y}_0\right) \dot{y}_{1,l} \right) \\ &= \sum_{l=1}^{N_H} f'_{nl,l}\left(y_0, \dot{y}_0, y_{1,l}, \dot{y}_{1,l}\right) \end{aligned} \tag{6.17}$$

where each $f'_{nl,l}\left(y_0, \dot{y}_0, y_{1,l}, \dot{y}_{1,l}\right)$ can be decomposed into a Fourier series such that

$$\begin{aligned} f'_{nl,l}\left(y_0, \dot{y}_0, y_{1,l}, \dot{y}_{1,l}\right) = & c_0^{f'_l}\left(A_{0,1}, A_{1,l}\right) \\ & + \sum_{l_2=1}^{N_H} \Big(c_{l_2}^{f'_l}\left(A_{0,1}, A_{1,l}\right) \cos\left(l_2\omega t - \phi_{1,l} - (l_2 - l)\phi_{0,1}\right) \\ & + s_{l_2}^{f'_l}\left(A_{0,1}, A_{1,l}\right) \sin\left(l_2\omega t - \phi_{1,l} - (l_2 - l)\phi_{0,1}\right) \Big) . \end{aligned} \tag{6.18}$$

Then, each $f'_{nl,l}\left(y_0, \dot{y}_0, y_{1,l}, \dot{y}_{1,l}\right)$ is projected onto the same sine and cosine basis as y_2 in Equation (6.16), *i.e.* the $\left(\sin\left(l_2\omega t - \phi_{2,l_2}\right), \cos\left(l_2\omega t - \phi_{2,l_2}\right)\right)$ basis, such that

$$\begin{aligned} f'_{nl,l}\left(y_0, \dot{y}_0, y_{1,l}, \dot{y}_{1,l}\right) = & C_0^{f'_l}\left(A_{0,1}, A_{1,l}\right) \\ & + \sum_{l_2=1}^{N_H} \Big(C_{l_2}^{f'_l}\left(A_{0,1}, A_{1,l}\right) \cos\left(l_2\omega t - \phi_{2,l_2}\right) \\ & + S_{l_2}^{f'_l}\left(A_{0,1}, A_{1,l}\right) \sin\left(l_2\omega t - \phi_{2,l_2}\right) \Big) \end{aligned} \tag{6.19}$$

where

$$C_0^{f'_l}\left(A_{0,1}, A_{1,l}\right) = \frac{2}{T} \int_0^T f'_{nl,l}\left(y_0, \dot{y}_0, y_{1,l}, \dot{y}_{1,l}\right) \, \mathrm{d}t \tag{6.20}$$

$$\begin{aligned} C_{l_2}^{f'_l}\left(A_{0,1}, A_{1,l}\right) = & \frac{2}{T} \int_0^T f'_{nl,l}\left(y_0, \dot{y}_0, y_{1,l}, \dot{y}_{1,l}\right) \cos\left(l_2\omega t - \phi_{2,l_2}\right) \mathrm{d}t \\ = & c_{l_2}^{f'_l}\left(A_{0,1}, A_{1,l}\right) \cos\phi'_{l,l_2} + s_{l_2}^{f'_l}\left(A_{0,1}, A_{1,l}\right) \sin\phi'_{l,l_2} \end{aligned} \tag{6.21}$$

$$\begin{aligned} S_{l_2}^{f'_l}\left(A_{0,1}, A_{1,l}\right) = & \frac{2}{T} \int_0^T f'_{nl,l}\left(y_0, \dot{y}_0, y_{1,l}, \dot{y}_{1,l}\right) \sin\left(l_2\omega t - \phi_{2,l_2}\right) \mathrm{d}t \\ = & c_{l_2}^{f'_l}\left(A_{0,1}, A_{1,l}\right) \sin\phi'_{l,l_2} + s_{l_2}^{f'_l}\left(A_{0,1}, A_{1,l}\right) \cos\phi'_{l,l_2} \end{aligned} \tag{6.22}$$

with $\phi'_{l,l_2} = \phi_{2,l_2} - \phi_{1,l} - (l_2 - l)\phi_{0,1}$. Substituting the Fourier series of y_2 and $f'_{nl}\left(y_0, \dot{y}_0, y_1, \dot{y}_1\right)$ into the third relation of Equation (6.6) and equating the coefficient of each harmonic to 0 yields

$$\begin{cases} 2l_2\zeta\omega_0\omega A_{2,l_2} + \sum_{l=1}^{N_H} \left(c_{l_2}^{f'_l} \cos\phi'_{l,l_2} + s_{l_2}^{f'} \sin\phi'_{l,l_2} \right) = 0 \\ \Omega_{l_2} A_{2,l_2} - \sum_{l=1}^{N_H} \left(c_{l_2}^{f'_l} \sin\phi'_{l,l_2} + s_{l_2}^{f'_l} \cos\phi'_{l,l_2} \right) = 0 \end{cases} \tag{6.23}$$

with $\Omega_{l_2} = \omega_{l_2}^2 - \omega_0^2$. This system is not trivial since there can be many ϕ_{l,l_2}. However, if the l_2-th harmonic is only generated by only one harmonic l from y_1, then the system is similar to Equation (6.14) and takes the form

$$\begin{cases} 2l_2\zeta\omega_0\omega A_{2,l_2} + c_{l_2}^{f_l'}\cos\phi'_{l,l_2} + s_{l_2}^{f'}\sin\phi'_{l,l_2} = 0 \\ \Omega_{l_2}A_{2,l_2} - c_{l_2}^{f_l'}\sin\phi'_{l,l_2} - s_{l_2}^{f_l'}\cos\phi'_{l,l_2} = 0 \end{cases} \tag{6.24}$$

It can be solved for each A_{2,l_2} and ϕ'_{l,l_2} with $l_2 > 0$

$$\begin{cases} A_{2,l_2} = -\frac{1}{2l_2\zeta\omega_0}\left(s_{l_2}^{f_l'}\sin\phi'_{l,l_2} + c_{l_2}^{f_l'}\cos\phi'_{l,l_2}\right) \\ \phi'_{l,l_2} = \mathrm{atan2}\left(-2l_2\zeta\omega_0\omega s_{l_2}^{f_l'}\left(A_{0,1}\right) - c_{l_2}^{f_l'}\left(A_{0,1}\right)\Omega_{l_2}, s_{l_2}^{f_l'}\Omega_{l_2} + 2l_2\zeta\omega_0\omega c_{l_2}^{f_l'}\right). \end{cases} \tag{6.25}$$

Usually, $C_0^{f_l'} = c_0^{f_l'} = 0$. The more general case where the l_2-th harmonic is generated by multiple harmonics l from y_1 is more complex and beyond the scope of this study.

6.3.2 Application to a weakly nonlinear Duffing oscillator

We consider the weakly nonlinear oscillator

$$\ddot{x} + 2\zeta\omega_0\dot{x} + \omega_0^2 x + \varepsilon x^3 = \gamma\sin\omega t \tag{6.26}$$

with $\zeta = 0.01$, $\omega_0 = 1$ rad/s, $\gamma = 0.003$ N/kg and $\varepsilon = 0.1$.

6.3.2.1 Zero-th order response

The response at the zero-th order is $y_0 = A_{0,1}\sin\left(\omega t - \phi_{0,1}\right)$ where $A_{0,1}$ and $\phi_{0,1}$ are governed by Equation (6.7). Since the higher-order contributions of frequency ω are at least one order lower than y_0, we assume that $A_1 \simeq A_{0,1}$ and $\phi_1 \simeq \phi_{0,1}$ such that the first harmonic component of the response from Equation (6.3) is $\simeq A_1\sin\left(\omega t - \phi_1\right)$. Amplitude resonance of A_1 occurs close to ω_0 as developed in Section 2.2.3 and shown in Figure 6.3.

6.3.2.2 First-order response

The nonlinear term is

$$\begin{aligned} f_{nl}(y_0, \dot{y}_0) =& \frac{3}{4}A_{0,1}^3\sin\left(\omega t - \phi_{0,1}\right) - \frac{1}{4}A_{0,1}^3\sin\left(3\left(\omega t - \phi_{0,1}\right)\right) \\ =& s_1^f\sin\left(\omega t - \phi_{0,1}\right) + s_3^f\sin\left(3\left(\omega t - \phi_{0,1}\right)\right) \end{aligned} \tag{6.27}$$

where $s_1^f = \frac{3}{4}A_{0,1}^3$ and $s_3^f = -\frac{1}{4}A_{0,1}^3$. Using Equations (6.10) and (6.13), $f_{nl}(y_0, \dot{y}_0)$ can be rewritten as

$$\begin{aligned} f_{nl}(y_0, \dot{y}_0) =& s_1^f\left(\sin\phi'_{1,1}\cos\left(\omega t - \phi_{1,1}\right) + \cos\phi'_{1,1}\sin\left(\omega t - \phi_{1,1}\right)\right) \\ &+ s_3^f\left(\sin\phi'_{1,3}\cos\left(3\omega t - \phi_{1,3}\right) + \cos\phi'_{1,3}\sin\left(3\omega t - \phi_{1,3}\right)\right) \end{aligned} \tag{6.28}$$

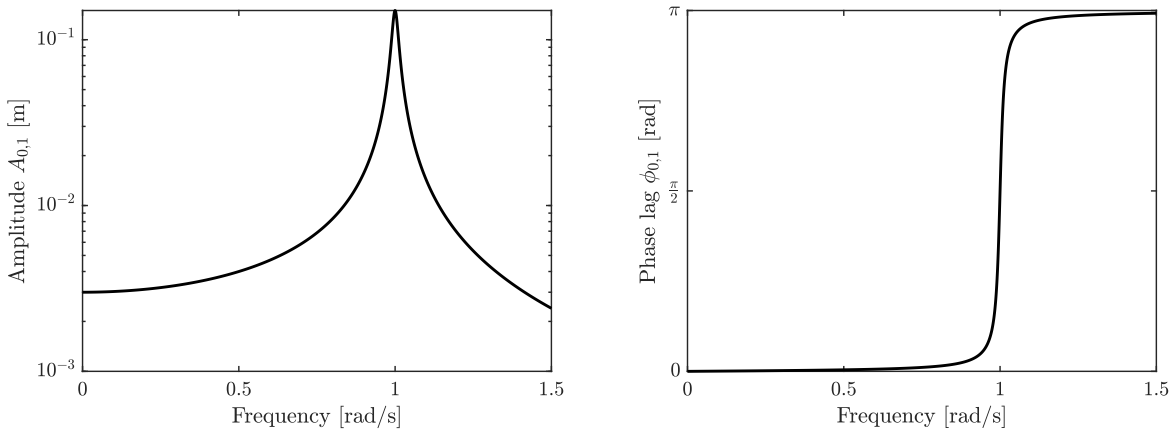

(a) **(b)**

Figure 6.3: NFRC of the first harmonic of the Duffing oscillator using PLOPT. (a) Amplitude $A_{0,1}$ and (b) phase lag $\phi_{0,1}$.

where $\phi'_{1,1} = \phi_{1,1} - \phi_{0,1}$ and $\phi'_{1,3} = \phi_{1,3} - 3\phi_{0,1}$. This signal generates two harmonic responses, *i.e.* $y_{1,1} = A_{1,1}\sin(\omega t - \phi_{1,1})$ and $y_{1,3} = A_{1,3}\sin(3\omega t - \phi_{1,3})$ where $(A_{1,1}, \phi_{1,1})$ and $(A_{1,3}, \phi_{1,3})$ can be solved using Equation (6.14). Here, $y_{1,1}$ only adds a small correction to the first harmonic from Equation (6.3) and is not of interest here. However, $y_{1,3}$ is a newly generated third harmonic component. According to the first relation of Equation (6.14), since $c_3^f = 0$, $A_{1,3}$ can undergo a maximum of amplitude if either s_3^f reaches a maximum, which is the case when $A_{0,1}$ reaches a maximum, or when $\phi'_{1,3} = \frac{\pi}{2}$, when $\Omega_3 = 0$, *i.e.*, at the 3:1 resonance when $\omega = \frac{\omega_0}{3}$.

This is illustrated in Figure 6.4 where ϕ'_3 increases by π at the 3:1 resonance. $\phi_{1,3}$ increases by π at the 3:1 resonance and by 3π at the primary resonance. This latter increase is easily explained since $\phi_{1,3} = \phi'_3 + 3\phi_{0,1}$, and, after the 1:1 resonance, both ϕ'_3 and $\phi_{0,1}$ are equal to π.

Finally, as for the first harmonic, other contributions to the third harmonic will be produced by higher-order responses and will be neglected. We can assume that $A_3 \simeq \varepsilon A_{1,3}$ and $\phi_3 \simeq \phi_{1,3}$ such that the third harmonic component of the response in (6.3) is $A_3\sin(3\omega t - \phi_3)$.

6.3.2.3 Second-order response

Since the first-order response produces two harmonic responses, namely $y_{1,1}$ and $y_{1,3}$, it follows that

$$f'_{nl}(y_0, \dot{y}_0, y_1, \dot{y}_1) = f'_{nl,1}(y_0, \dot{y}_0, y_{1,1}, \dot{y}_{1,1}) + f'_{nl,3}(y_0, \dot{y}_0, y_{1,3}, \dot{y}_{1,3}) \tag{6.29}$$

where

$$f'_{nl,1} = \frac{3}{4}A_{0,1}^2 A_{1,1}\left(2\sin(\omega t - \phi_{1,1}) + \sin(\omega t + \phi_{1,1} - 2\phi_{0,1}) - \sin(3\omega t - 2\phi_{0,1} - \phi_{1,1})\right) \tag{6.30}$$

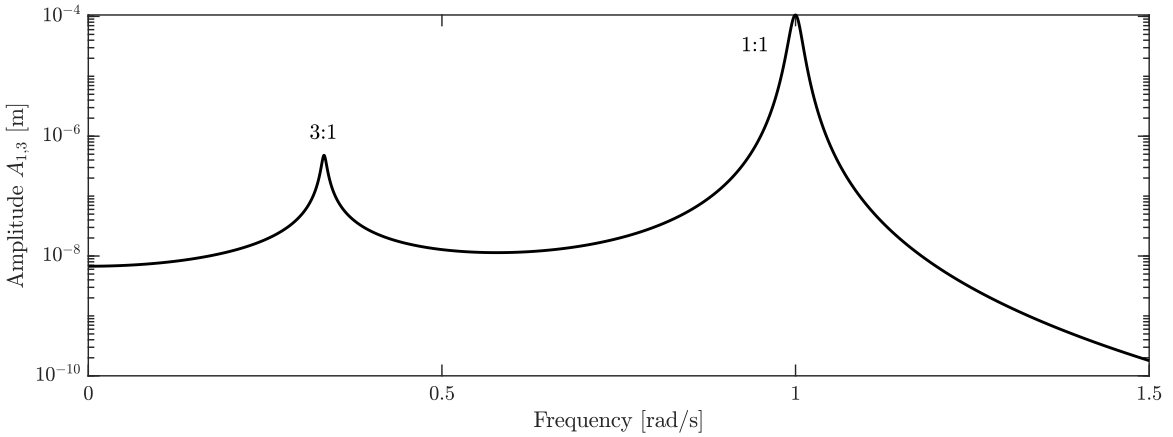

(a)

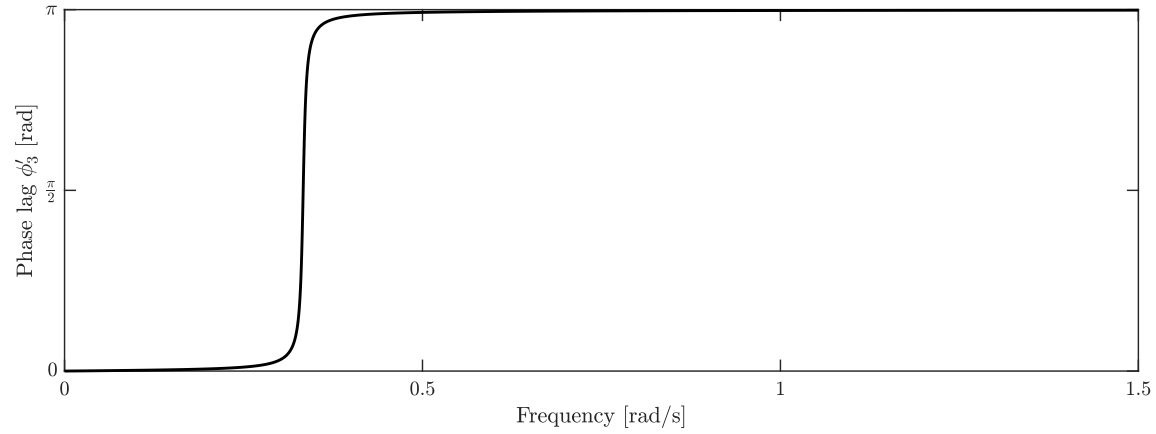

(b)

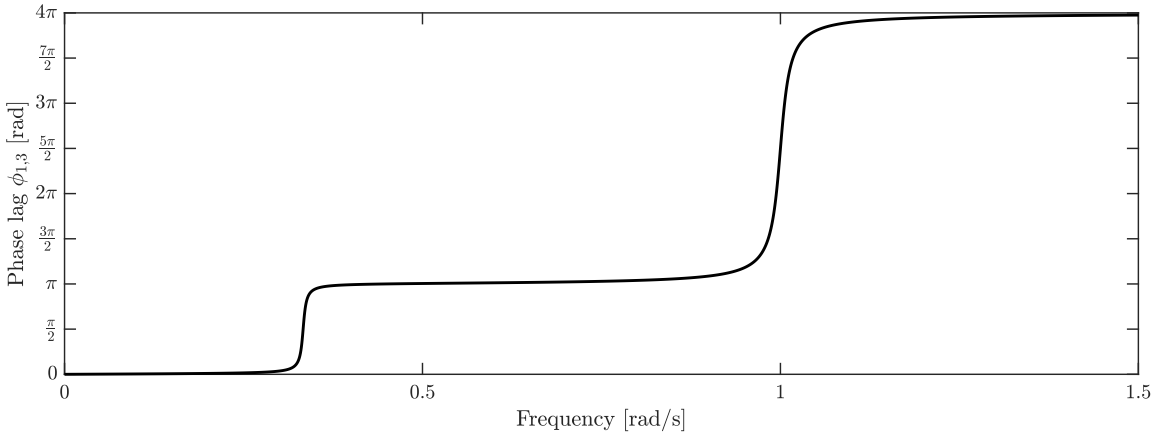

(c)

Figure 6.4: NFRC of the third harmonic of the Duffing oscillator using PLOPT. (a) Amplitude $A_{1,3}$, (b) phase lag ϕ_3' and (c) phase lag $\phi_{1,3}$.

and

$$f'_{nl,3} = \frac{3}{4} A_{0,1}^2 A_{1,3} \left(\sin\left(\omega t - \phi_{1,3} + 2\phi_{0,1}\right) + 2\sin\left(3\omega t - \phi_{1,3}\right) - \sin\left(5\omega t - \phi_{1,3} - 2\phi_{0,1}\right) \right). \tag{6.31}$$

According to Equations (6.19), (6.22) and (6.25), $f'_{nl,1}$ produces only first and third harmonic components for y_2 whereas $f'_{nl,3}$ produces first, third and fifth harmonic components. The second-order contributions for the first and third harmonics are neglected here. However, the fifth harmonic component is a newly-generated harmonic. We can rewrite $f'_{nl,3}$ as

$$\begin{aligned} f'_{nl,3} = {} & s_1^{f'_3} \left(\sin\phi'_{3,1} \cos\left(\omega t - \phi_{2,1}\right) + \cos\phi'_{3,1} \sin\left(\omega t - \phi_{2,1}\right) \right) \\ & + s_3^{f'_3} \left(\sin\phi'_{3,3} \cos\left(3\omega t - \phi_{2,3}\right) + \cos\phi'_{3,3} \sin\left(3\omega t - \phi_{2,3}\right) \right) \\ & + s_5^{f'_3} \left(\sin\phi'_{3,5} \cos\left(5\omega t - \phi_{2,5}\right) + \cos\phi'_{3,5} \sin\left(5\omega t - \phi_{2,5}\right) \right) \end{aligned} \tag{6.32}$$

where $s_1^{f'_3} = \frac{3}{4} A_{0,1}^2 A_{1,3}$, $s_3^{f'_3} = \frac{3}{2} A_{0,1}^2 A_{1,3}$, $s_5^{f'_3} = -\frac{3}{4} A_{0,1}^2 A_{1,3}$, $\phi'_{3,1} =$ and $\phi'_{3,l_2} = \phi_{2,l_2} - \phi_{1,3} - (l_2 - 3)\phi_{0,1}$. The fifth harmonic solution is

$$y_{2,5} = A_{2,5} \sin\left(5\omega t - \phi_{2,5}\right) \tag{6.33}$$

where $A_{2,5}$ and $\phi_{2,5}$ are found using Equation (6.25). Since $c_5^{f'} = 0$, there are 3 possible amplitude resonances for $A_{2,5}$, namely when either $A_{0,1}$ or $A_{1,3}$ reaches a maximum, *i.e.*, at the 1:1 and 3:1 resonances, or when $\phi'_{3,5} = \frac{\pi}{2}$. The latter resonance occurs when $\Omega_5 = 0$, *i.e.*, when $\omega = \frac{\omega_0}{5}$ at the 5:1 resonance.

This is illustrated in Figure 6.5 where $\phi'_{3,5}$ increases by π at the 5:1 resonance. $\phi_{2,5}$ increases by π at the 5:1 resonance, by π at the 3:1 resonance and by 5π at the primary resonance. These two latter increases can be explained considering that $\phi_{2,5} = \phi'_{3,5} + \phi_{1,3} + 2\phi_{0,1}$. Indeed, after the $3:1$ resonance, $\phi_{0,1} = 0$ and $\phi'_{3,5} = \phi_{1,3} = \pi$ so that $\phi_{2,5} = 2\pi$. After the primary resonance, $\phi'_{3,5} = \phi_{0,1} = \pi$ and $\phi_{1,3} = 4\pi$, therefore $\phi_{2,5} = 7\pi$.

Finally, we can assume that $A_5 \simeq \varepsilon^2 A_{2,5}$ and $\phi_5 \simeq \phi_{2,5}$ such that the fifth harmonic component of the response (6.3) is $A_5 \sin\left(5\omega t - \phi_5\right)$.

6.3.2.4 Summary

The results in this section demonstrate that, unlike the phase lag ϕ_3 for the second 3:1 superharmonic resonance in our motivating example, the newly-defined phase lags $\phi'_3 = \phi_3 - 3\phi_1$ and $\phi'_{3,5} = \phi_5 - \phi_3 - 2\phi_1$ do not seem to suffer from the influence of the primary resonance. From now on, $\phi'_{3,5}$ is denoted ϕ'_5. This means that $\phi'_3 = \frac{\pi}{2}$ or $\phi'_5 = \frac{\pi}{2}$ can be used as the resonant phase lags for the 3:1 and 5:1 superharmonic resonances for Duffing-like MDOF systems.

6.3.3 Numerical study of a Duffing oscillator with strong nonlinearity

To validate the previous theoretical findings, we choose the Duffing oscillator

$$\ddot{x} + 2\zeta\omega_0\dot{x} + \omega_0^2 x + x^3 = \gamma \sin\omega t \tag{6.34}$$

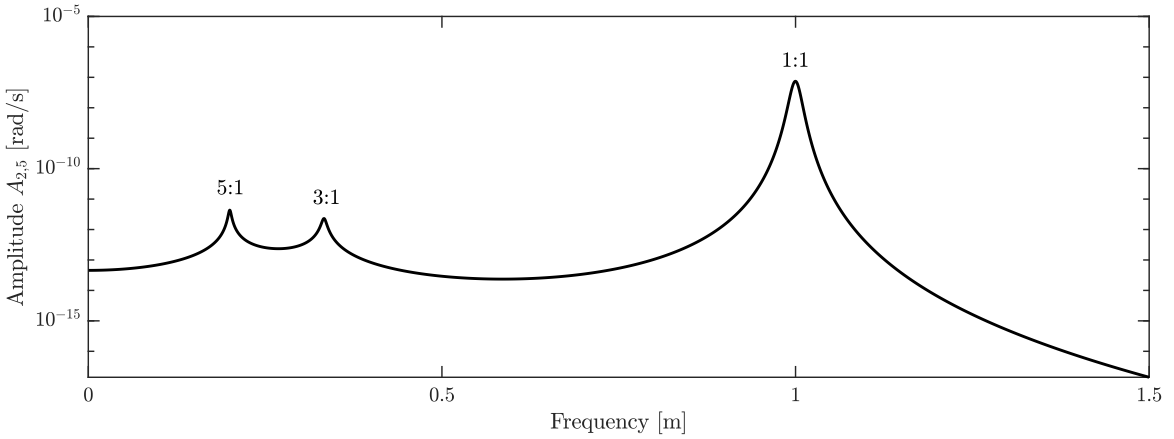

(a)

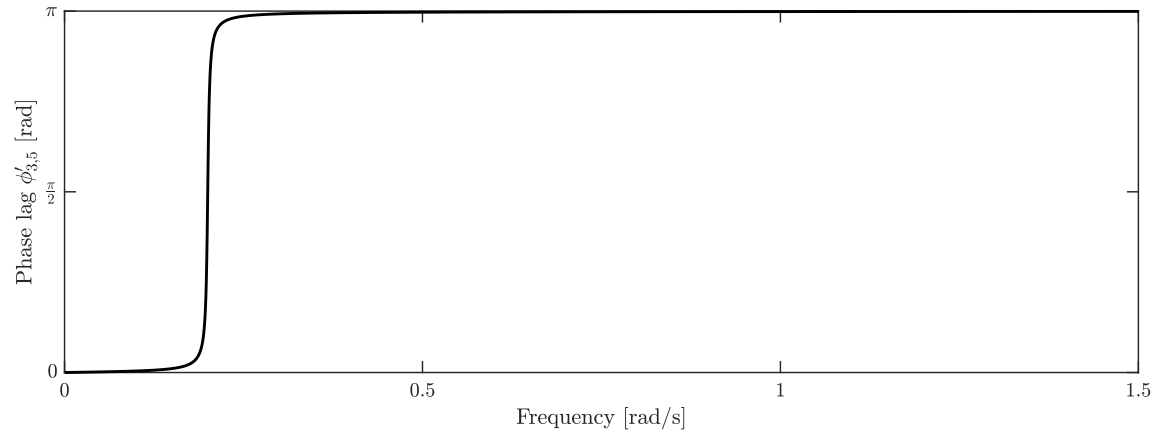

(b)

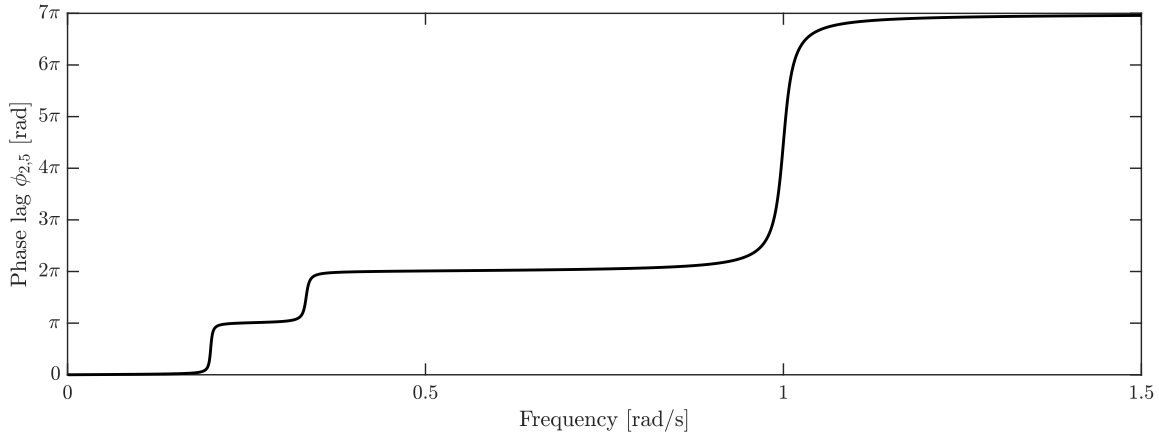

(c)

Figure 6.5: NFRC of the fifth harmonic of the Duffing oscillator using PLOPT. (a) Amplitude $A_{2,5}$, (b) phase lag $\phi'_{3,5}$ and (c) phase lag $\phi_{2,5}$.

with $\zeta = 0.005$, $\omega_0 = 1$ rad/s and $\gamma = 0.01$ N/kg.

6.3.3.1 Zero-th order response: the primary resonance

As expected, the NFRC of the first harmonic in Figure 6.6 only resonates around the primary resonance. The hardening behavior is clearly visible.

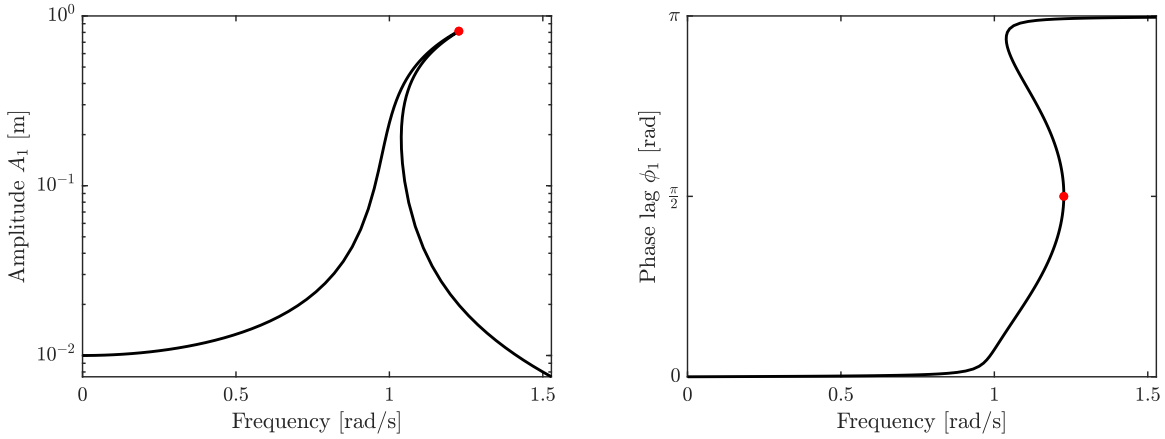

Figure 6.6: NFRC of the first harmonic of the Duffing oscillator. (a) Amplitude A_1 and (b) phase lag ϕ_1. The red dots correspond to the phase quadrature points.

6.3.3.2 First-order response: the 3:1 superharmonic resonance

The NFRC of the third harmonic is shown in Figure 6.7. Around the 3:1 resonance, both ϕ_3 and ϕ_3' increases by π and resonates at $\frac{\pi}{2}$. Around the primary resonance, despite the hardening behavior, ϕ_3' remains around π. Differently, ϕ_3 increases by 3π with the exact same shape as ϕ_1, but with a phase envelope three times greater.

6.3.3.3 Second-order response: the 5:1 superharmonic resonance

The NFRC of the fifth harmonic is presented in Figure 6.8. There are now three amplitude resonances for the fifth harmonic, namely at the 5:1, 3:1 and 1:1 resonances. Around the 5:1 resonance, both ϕ_5 and ϕ_5' increases from 0 to π with $\frac{\pi}{2}$ as the resonant phase lag. Then, ϕ_5' remains at π. On the contrary, ϕ_5 increases by π around the 3:1 resonance and by 5π around the primary resonance.

6.4 PRNMs of two-degree-of-freedom Duffing oscillators with a modal interaction

The case of modal interactions is discussed herein. A modal interaction is an energy transfer between two modes of vibration. It occurs when the frequency of a nonlinear

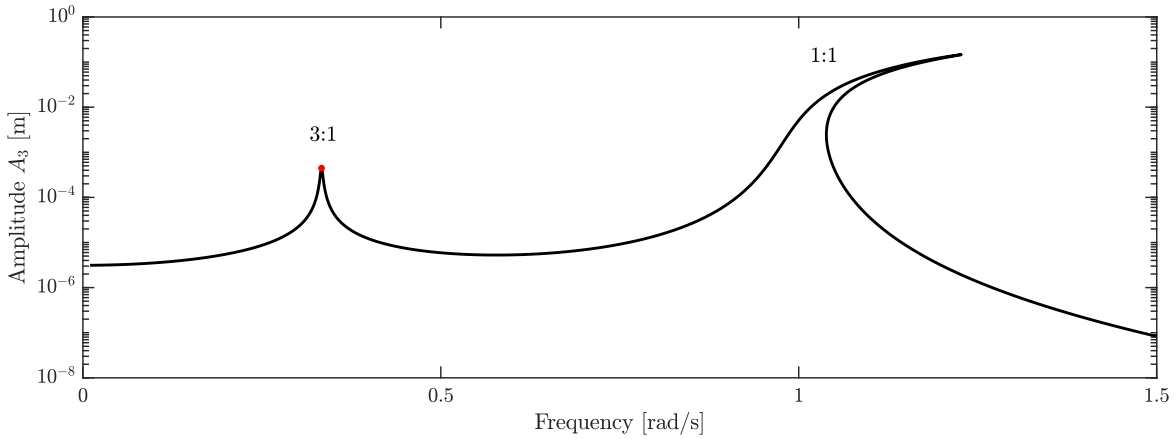

(a)

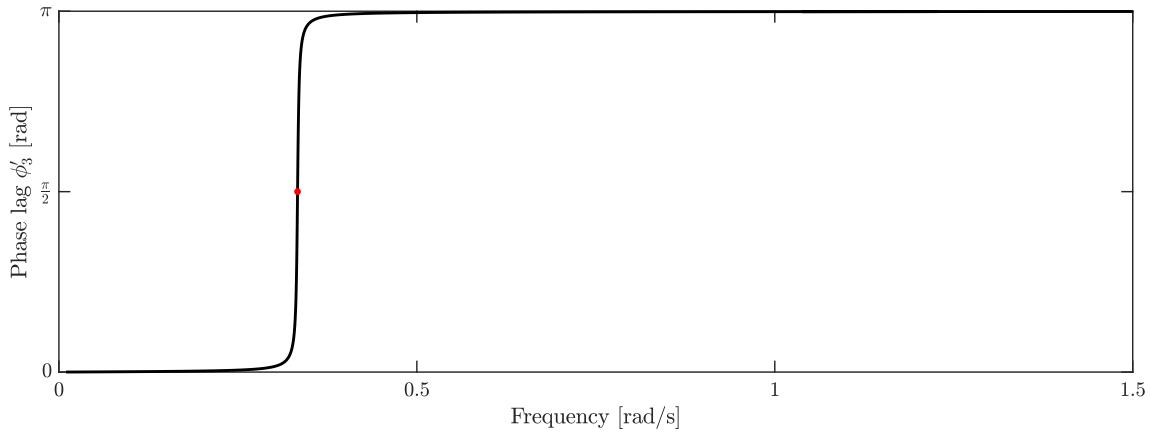

(b)

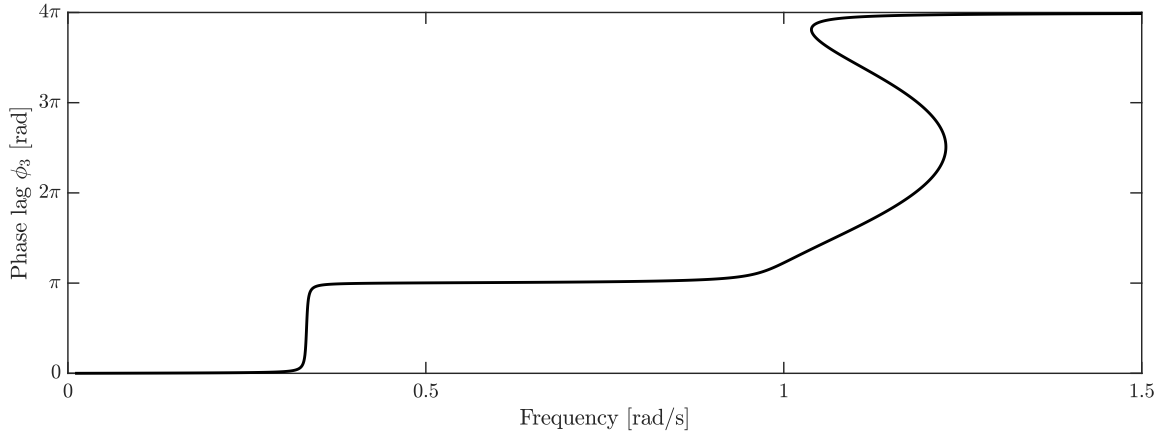

(c)

Figure 6.7: NFRC of the third harmonic of the Duffing oscillator. (a) Amplitude A_3, (b) phase lag ϕ_3' and (c) phase lag ϕ_3. The red dots correspond to the phase quadrature points.

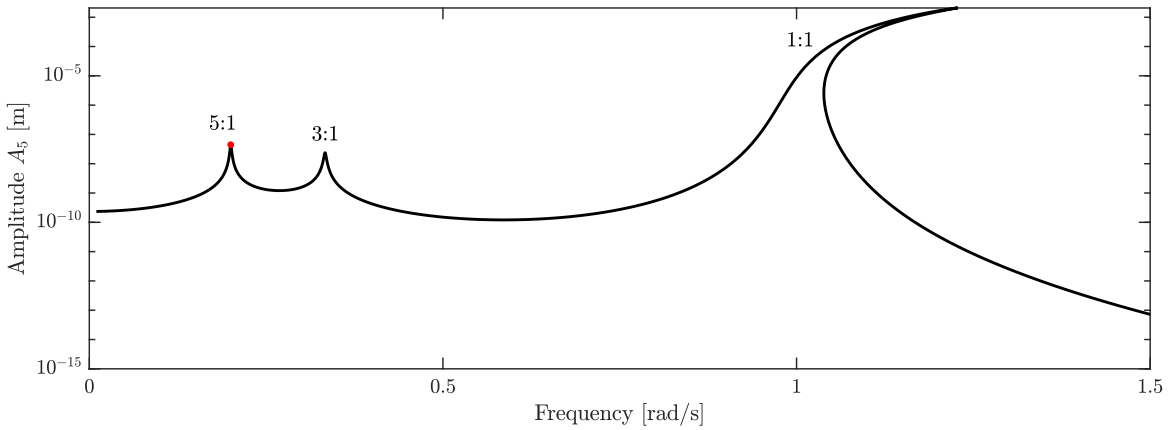

(a)

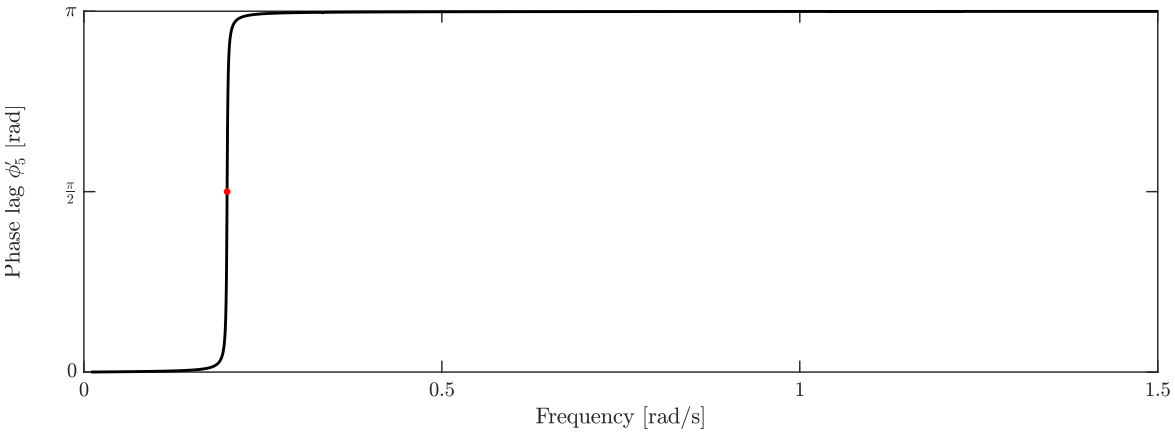

(b)

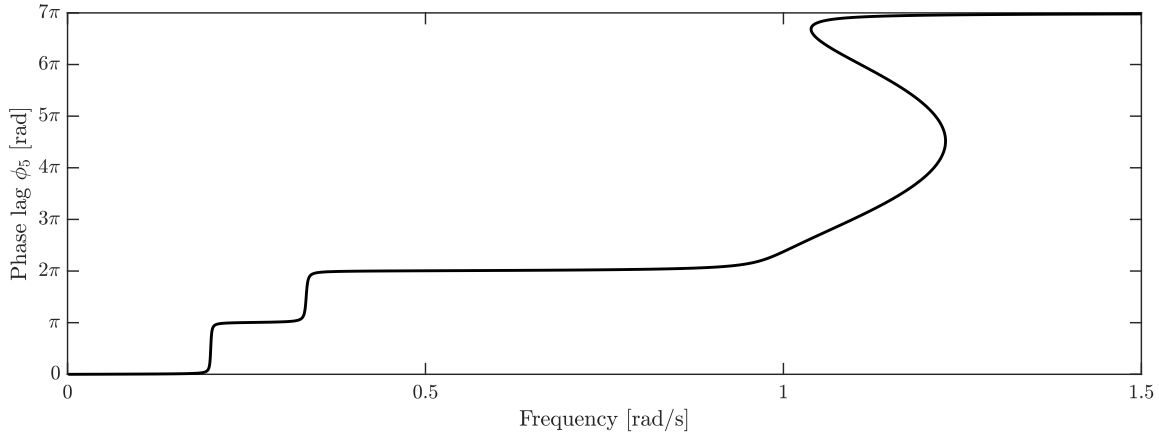

(c)

Figure 6.8: NFRC of the fifth harmonic of the Duffing oscillator. (a) Amplitude A_5, (b) phase lag ϕ_5' and (c) phase lag ϕ_5. The red dots correspond to the phase quadrature points.

primary resonance becomes a fraction of the resonance frequency of a higher-order mode, *i.e.*, when it lies in the superharmonic region of a higher-order mode [3].

6.4.1 System with a 3:1 modal interaction

The system (6.1) is reconsidered in this section. Figure 6.9 displays the NFRC of the third harmonic of x_1 for 0.01N and is to be compared with Figure 6.2. We observe that ϕ_3' is in quadrature three times, namely at the 3:1 superharmonic resonances of the first and second modes and at the antiresonance of the third harmonic. Thus, the influence of the primary resonance on the phase lag of the third harmonic has been completely removed.

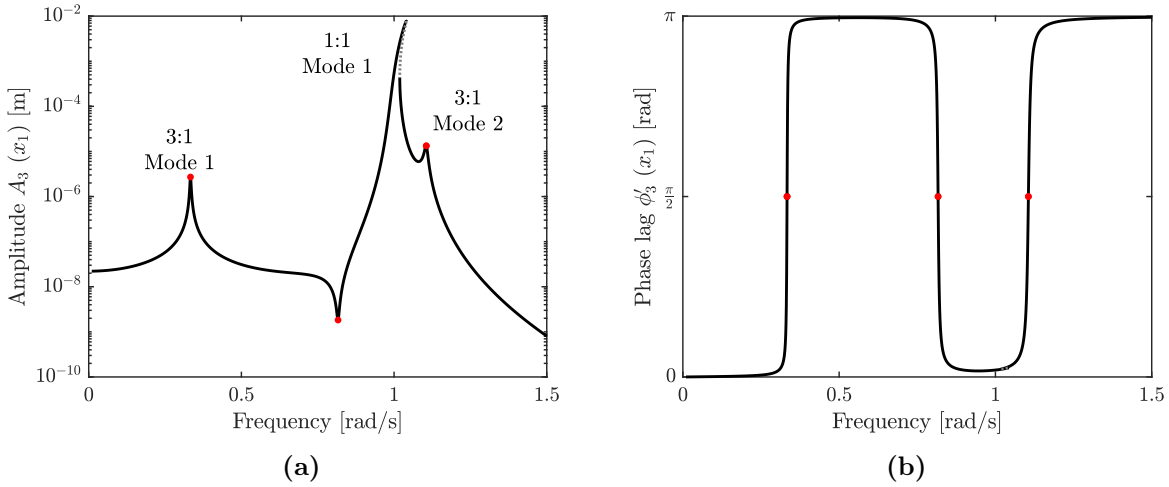

Figure 6.9: NFRC of the third harmonic of x_1 of system (6.1) for f =0.01 N. (a) Amplitude A_3 and (b) phase lag ϕ_3'. The red dots correspond to $\phi_3' = \frac{\pi}{2}$. Black: stable; grey: unstable.

The NFRC of x_1 is represented in Figure 6.10 for two different forcing amplitudes. At 0.05N, an isolated branch created by a 3:1 interaction between the two modes can be observed. At 0.14N, the isola has merged with the peak corresponding to the primary resonance of the first mode. The 1:1 PRNM curve of the first mode (corresponding to $\phi_1 = \pi/2$) represented as a function of the forcing frequency and forcing amplitude in Figures 6.10 and 6.11a, respectively, can provide more insight into these dynamics. Specifically, because two points of the 1:1 PRNM curve belong to the isola, its birth can be predicted accurately. Figure 6.11a indeed indicates that 2 new quadrature points exist when f = 0.0373N; the isola is thus created at this forcing amplitude. On the contrary, the merging of the isola with the main branch does not happen at a phase quadrature point. This is why the elimination of the two phase quadrature points around f =0.17N in Figure 6.11a is only an approximation of the forcing amplitude at which merging occurs. Tracking the fold bifurcations of the NFRC as in [29] represents a more accurate strategy for this purpose.

Looking now at the 3:1 PRNM curve of the second mode (corresponding to $\phi_3' = \pi/2$) in Figure 6.10, the modal interaction is seen to occur in the vicinity of the intersection of the 1:1 PRNM curve of the first mode with the 3:1 PRNM curve of the second mode, as

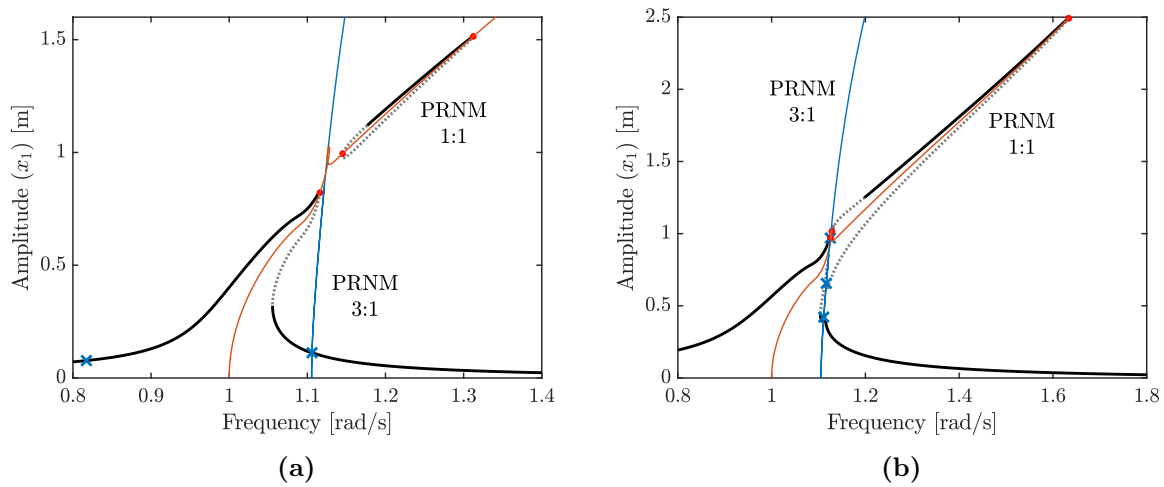

Figure 6.10: NFRC of x_1. (a) f =0.05 N and (b) f =0.14 N. The 1:1 and 3:1 PRNM curves are represented in orange and blue, respectively. The red dots and blue crosses correspond to quadrature points of ϕ_1 and ϕ_3', respectively. Black: stable; grey: unstable.

expected. Besides, in Figure 6.11b, two new points are created on the 3:1 PRNM curve when $f = 0.121$N. The point with the greatest amplitude is located on the left branch of the resonance peak whereas the two other points, located very close from each other, are on the right branch (see Figure 6.12a). As the forcing amplitude increases, the two latter points finally merge around $f = 0.146$N to create an inner isolated branch in Figure 6.12b. To the best of our knowledge, it is the first time that an inner isola due to a superharmonic resonance can be revealed through the calculation of nonlinear modes.

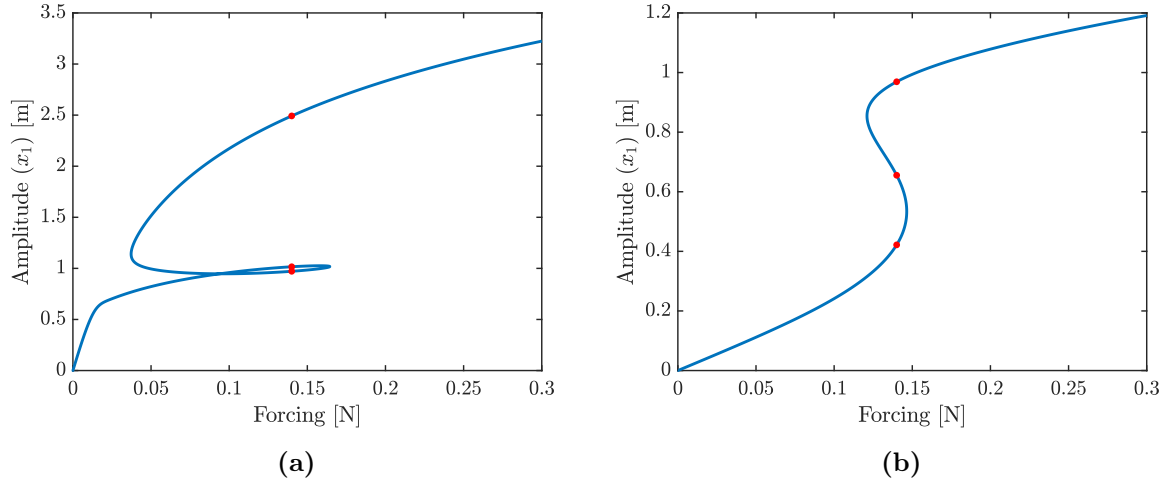

Figure 6.11: Evolution of the PRNM amplitude of x_1 as a function of the forcing amplitude. (a) 1:1 PRNM curve and (b) 3:1 PRNM curve. The red dots correspond to a forcing amplitude of 0.14 N.

Figure 6.13a compares the 1:1 PRNM curve in Figure 6.11a to the curve obtained

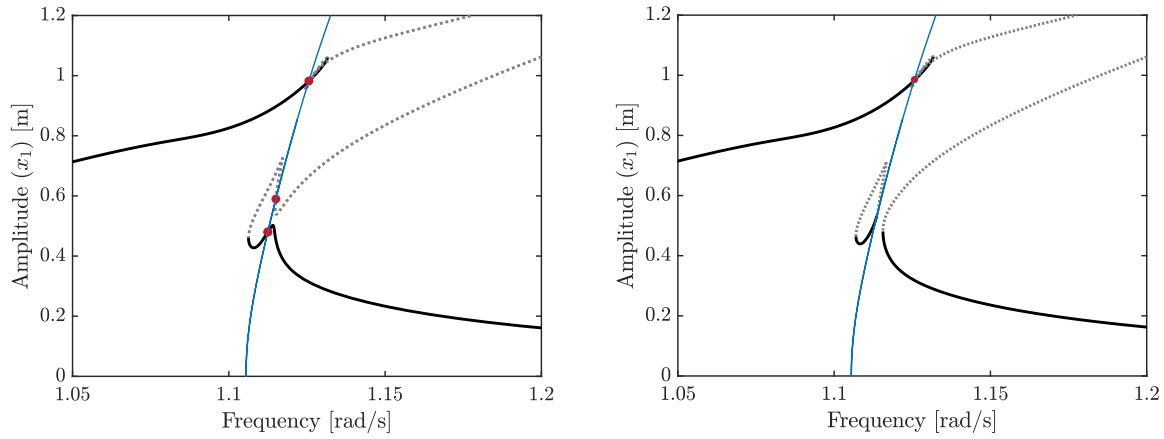

Figure 6.12: NFRC of x_1 and 3:1 PRNM curve (blue) for (a) f =0.145 N and (b) f =0.1465 N. The red dots correspond to quadrature points. Black: stable; grey: unstable.

when combining the NNM and EB principles, which is the usual strategy for computing amplitude-forcing curves [97, 105, 106]. Both methods give very similar results away from the modal interaction. However, the forcing obtained with the NNM and EB tends to infinity close to the modal interaction. As seen in Figure 6.13b, the harmonic content in this neighborhood is mostly a single harmonic of frequency 3ω, in contrast with the frequency content of the forcing which is a single harmonic of frequency ω. According to EB, a forcing with infinite amplitude is thus required to excite the corresponding nonlinear mode, as discussed in Section 5.1.1. This illustrates one important deficiency of EB. We note that energy balancing across multiple harmonics was proposed in [107].

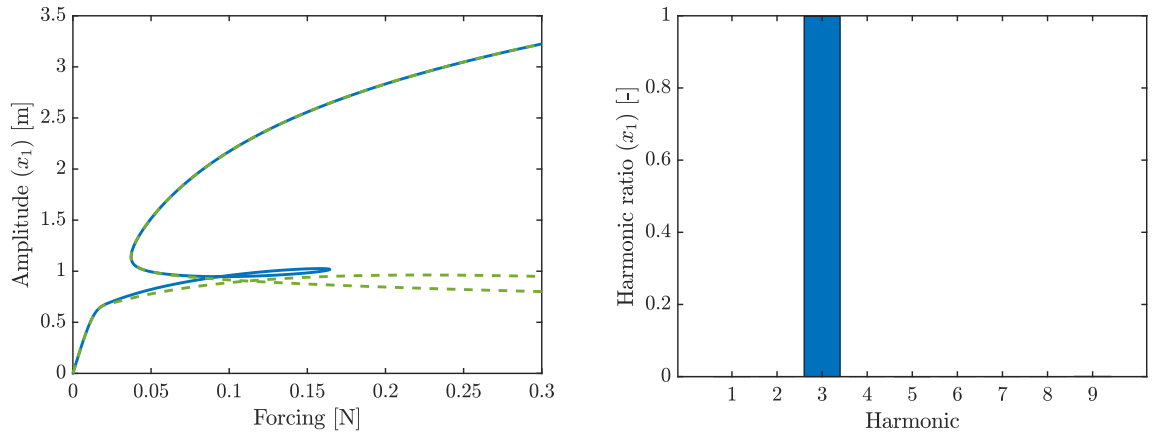

Figure 6.13: (a) 1:1 PRNM curve (blue) and the NNM/EB curve (green) and (b) harmonic ratio at the modal interaction point of the NNM.

6.4.2 System with a 5:1 modal interaction

The system considered in this section is

$$\begin{cases} 5\ddot{x}_1 + 0.1\dot{x}_1 - 0.05\dot{x}_2 + 160x_1 - 150x_2 + x_1^3 = f\sin\omega t \\ 5\ddot{x}_2 - 0.05\dot{x}_1 + 0.4\dot{x}_2 - 150x_1 + 160x_2 = 0. \end{cases} \tag{6.35}$$

The natural frequencies of the underlying linear system are $\sqrt{2}$ are $\sqrt{62}$ rad/s. The antiresonance frequency is 5.657 rad/s. The NFRC of the total response as well as the phase lag of the first harmonic at low forcing, $f = 0.4N$, are depicted in Figure 6.14.

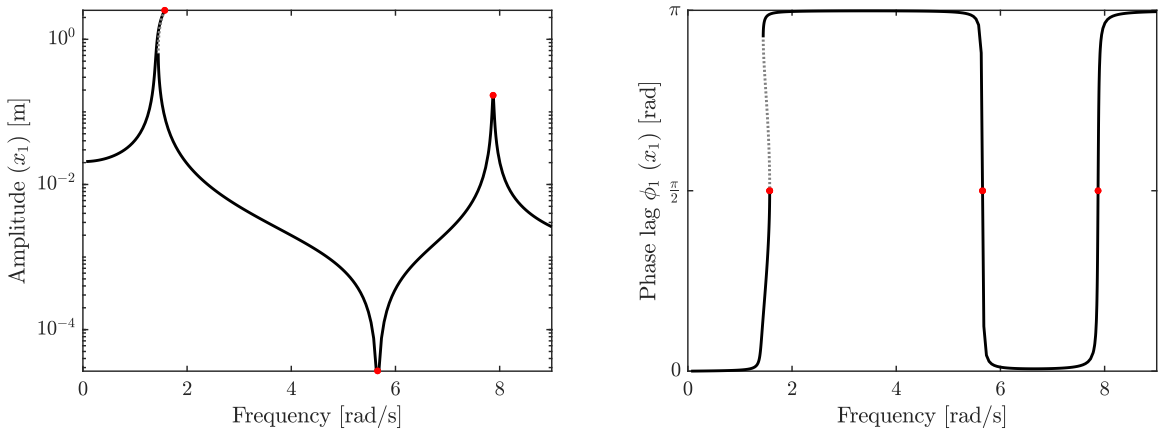

(a) **(b)**

Figure 6.14: NFRC of the system (6.35) for f =0.4 N. (a) Amplitude of x_1 and (b) phase lag ϕ_1 of x_1. The red dots correspond to the phase quadrature points. Black: stable; grey: unstable.

The third harmonic is studied using the newly-defined phase lag ϕ_3'. As shown in Figure 6.15, the 3:1 superharmonic resonances occur at $\sqrt{2}/3$ rad/s and $\sqrt{62}/3$ rad/s. The antiresonance frequency of the third harmonic is 1.885 rad/s. An interesting result in Figure 6.16 is that, for f = 1N, the primary resonance peak passes through the antiresonance of the third harmonic due to the hardening nonlinearity, resulting in a drop in amplitude for this harmonic. However, this loss of amplitude does not impact the overall amplitude of x_1 since the contribution of the third harmonic is negligible.

The fifth harmonic is first investigated using the phase lag ϕ_5, and not ϕ_5', for $f = 0.4$N in Figure 6.17. Its behavior is more complex than the third harmonic since the fifth harmonic resonates at the 5:1, 3:1 and 1:1 resonances. For this forcing, all resonances are well-separated, and their effect on ϕ_5 can be easily interpreted:

- Point 1 is the 5:1 superharmonic resonance of the first mode. The phase lag increases from 0 to π, and the resonant phase lag is $\frac{\pi}{2}$;
- Point 2 is the 3:1 superharmonic resonance of the first mode. The fifth harmonic resonates there, as explained in Section 6.3. The phase lag increases from π to 2π, and the resonant phase lag is $\frac{3\pi}{2}$;

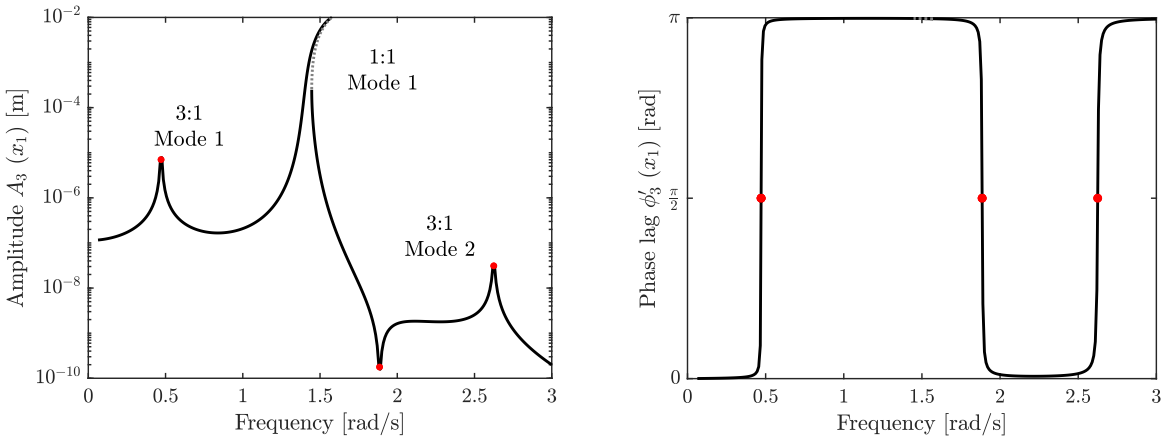

Figure 6.15: NFRC of the third harmonic of x_1 for f =0.4 N. (a) Amplitude A_3 and (b) phase lag ϕ_3'. The red dots correspond to the phase quadrature points. Black: stable; grey: unstable.

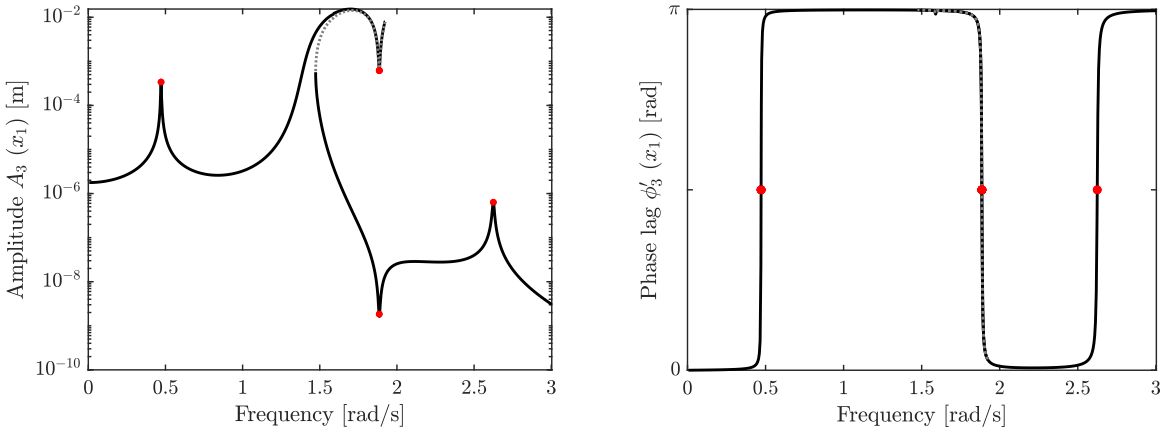

Figure 6.16: NFRC of the third harmonic of x_1 for f =1 N. (a) Amplitude A_3 and (b) phase lag ϕ_3'. The red dots correspond to the phase quadrature points. Black: stable; grey: unstable.

- Point 3 is the antiresonance of the fifth harmonic. It is located at a frequency of $5.6573/5 \simeq 1.131$ rad/s. The phase lag drops from 2π to π;
- Point 4 is the primary resonance. As explained in Section 6.3, ϕ_5 has a phase envelope five times greater than ϕ_1. The phase lag thus increases from π to 6π with a resonant phase lag at $\frac{7\pi}{2}$;
- Point 5 is the 5:1 resonance of the second mode. The phase lag increases from 6π to 7π, and the resonant phase lag is $\frac{13\pi}{2}$;
- Point 6 is the antiresonance of the third harmonic where the fifth harmonic also shows an antiresonance. It is located at a frequency of $5.6573/3 \simeq 1.885$ rad/s. The phase lag drops from 7π to 6π;
- Point 7 is the 3:1 resonance of the second mode. The fifth harmonic also resonates there. The phase lag increases from 6π to 7π, and the resonant phase lag is $\frac{13\pi}{2}$.

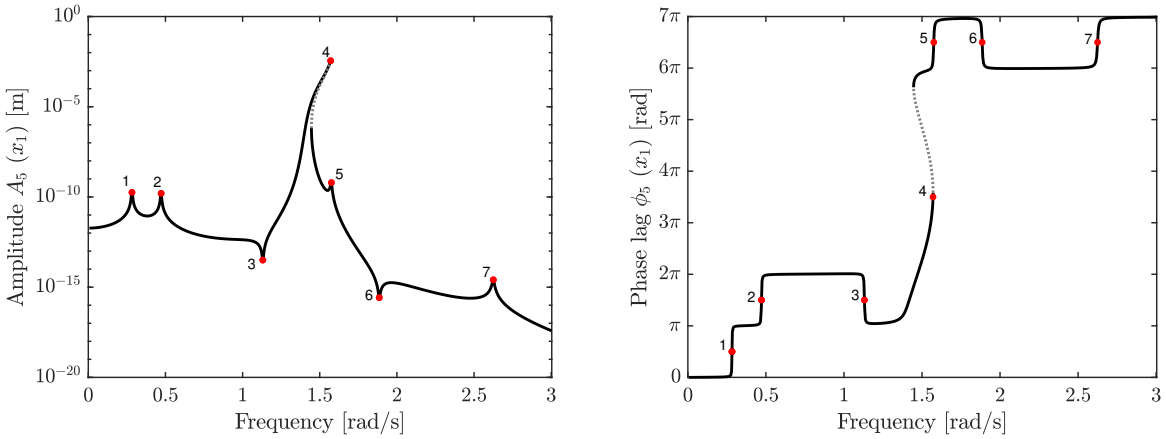

Figure 6.17: NFRC of the fifth harmonic of x_1 for f =0.4 N. (a) Amplitude A_5 and (b) phase lag ϕ_5. The red dots correspond to the phase quadrature points. Black: stable; grey: unstable.

For $f = 0.8$N in Figure 6.18, due to the hardening nonlinearity, the primary resonance crosses the 5:1 resonance of the second mode. Two new resonance points labeled points 8 and 9 appear. These points are characterized by an increase of π rad on the phase lag curve. However, the value of the resonant phase lags for these points is not fixed and depends where they appear on the primary resonance branch. These resonance points also shift the phase lag of point 4 by π.

As discussed in Section 6.2, it is necessary to remove the influence of the lower-order harmonic resonances by using $\phi_5' = \phi_5 - \phi_3 - 2\phi_1$. Figure 6.19 shows that only the two 5:1 superharmonic resonances and the antiresonance of the fifth harmonic resonate in this case.

Finally, Figure 6.20 plots the NFRC and different PRNM curves for $f = 0.8$N. We see that the PRNM curve of the 5:1 resonance of the second mode crosses the 1:1 PRNM

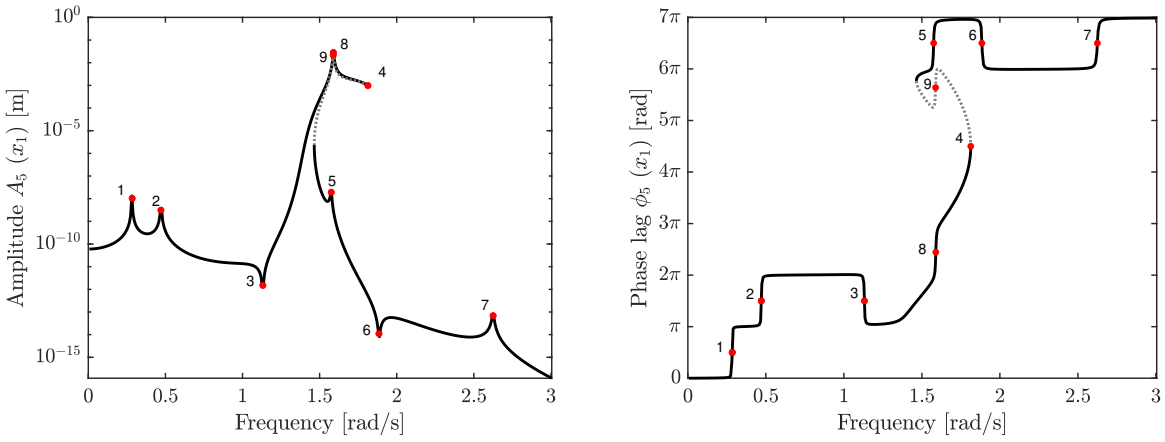

(a) **(b)**

Figure 6.18: NFRC of the fifth harmonic of x_1 for f=0.8 N. (a) Amplitude A_5 of x_1 and (b) phase lag ϕ_5 of x_1. The red dots correspond to the phase quadrature points. Black: stable; grey: unstable.

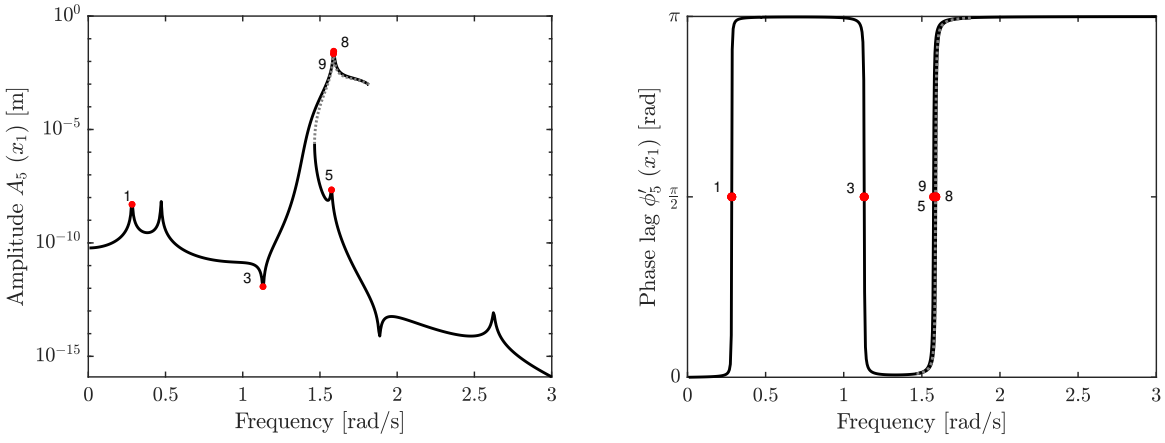

(a) **(b)**

Figure 6.19: NFRC for f =0.8 N. (a) Amplitude A_5 of x_1 and (b) phase lag ϕ_5' of x_1. The red dots correspond to the phase quadrature points. Black: stable; grey: unstable.

curve of the first mode, revealing the presence of a modal interaction. However, contrary to system (6.1), the interaction is not sufficiently strong here to create an isolated branch. Only a small bump can be seen on the primary resonance peak.

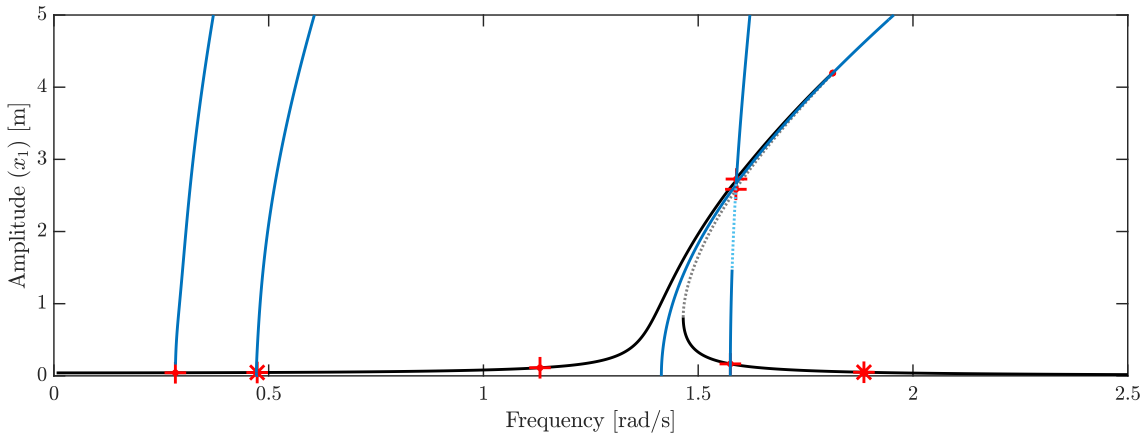

Figure 6.20: NFRC (black) for f =0.8N with the PRNM curves (blue) of the 1:1, 3:1 and 5:1 resonances of the first mode, and the 5:1 resonance of the second mode.

6.5 Experimental demonstration using a nonlinear cantilever beam

The concept of a PRNM is exploited for the dynamical characterization of two real structures, namely a cantilever beam with an artificial cubic nonlinearity in this section and a clamped-clamped beam featuring a geometrical nonlinearity in the next section. The experiments for these systems were conducted by G. Abeloos [104] and T. Zhou [108, 109], respectively.

6.5.1 Phase-locked loop testing

PLL is a key-enabling technology for the PRNM framework. Indeed, the goal of the PLL, schematized in Figure 6.21, is to enforce a specific phase lag, in our case the resonant phase lag φ_l. This method was successfully used for the identifying the backbone curves of primary resonances in [16–19, 61, 110].

The methodology is as follows. An electrodynamic shaker converts a voltage signal into a forcing $f_{ext}(t)$ that is applied to the nonlinear structure. To this end, the user defines a voltage amplitude f_{vol} which is converted into a forcing amplitude f. The time-varying forcing $f_{ext}(t)$ applied to the structure is

$$f_{ext}(t) = f \sin\left(\int_0^t \omega_{ins}(\tau)\,\mathrm{d}\tau\right) \tag{6.36}$$

where $\omega_{ins}(t)$ is the time-varying instantaneous frequency and is governed by a PID (proportional, integral and differential) control law such that

$$\omega_{ins}(t) = \frac{\nu\omega_0}{l} + g_p(\varphi_l - \phi_l(t)) + g_i \int_0^t (\varphi_l - \phi_l(\tau))\,\mathrm{d}\tau - g_d \frac{\mathrm{d}\phi_l}{\mathrm{d}t}(t) \tag{6.37}$$

where g_p, g_p and g_i are user-defined gains. In this thesis, the phase lag of the l-th harmonic is compared to the resonant phase lag φ_l. To compute the phase lag, a phase detector is required. Usually, synchronous demodulation based on low-pass filters is used [16, 18, 19, 111, 112]. However, the adaptive filtering method introduced in [113] and successfully applied in [114] is considered instead. The idea behind adaptive filtering is to reconstruct the output signal $x(t)$ at each time step by performing a linear combination of a basis $\mathbf{q}(t)$ such that

$$\mathbf{w}^T(t)\mathbf{q}(t) \simeq x(t). \tag{6.38}$$

Here, the basis $\mathbf{q}(t)$ is composed of harmonic signals

$$\mathbf{q}(t) = \begin{bmatrix} \frac{1}{\sqrt{2}} \\ \sin\omega_{inst}t \\ \cos\omega_{inst}t \\ \sin 2\omega_{inst}t \\ \cos 2\omega_{inst}t \\ \vdots \\ \sin N_H\omega_{inst}t \\ \cos N_H\omega_{inst}t \end{bmatrix} \tag{6.39}$$

where $\mathbf{w}$ is a vector composed of unknown weights that have to be determined. A simple algorithm to compute $\mathbf{w}$ is the least mean squares algorithm [115]. At each time step i, a mean square error is calculated

$$e(t_i) = x(t_i) - \mathbf{w}^T(t_i)\mathbf{q}(t_i). \tag{6.40}$$

The weights are then updated using

$$\mathbf{w}(t_{i+1}) = \mathbf{w}(t_i) + r_{ss}\mathbf{q}(t_i)e(t_i) \tag{6.41}$$

where r_{ss} is a step size to be defined by the user. Once the error is close to 0, the weights $\mathbf{w}$ correspond to the Fourier coefficients from which the phase lag can be computed.

6.5.2 Experimental setup

The experimental setup displayed in Figure 6.22 is composed of a 100cm × 0.6cm × 2cm cantilever beam made of steel. To ensure that the beam's dynamics remains as linear as possible, both the beam and its clamping were manufactured from a single block. The base was securely fastened to the vibration table using four bolts.

The beam was excited by an electromagnetic shaker (TIRA TV 51075), 30cm away from the base, with a stinger and an impedance head (DYTRAN 5860B) glued to the

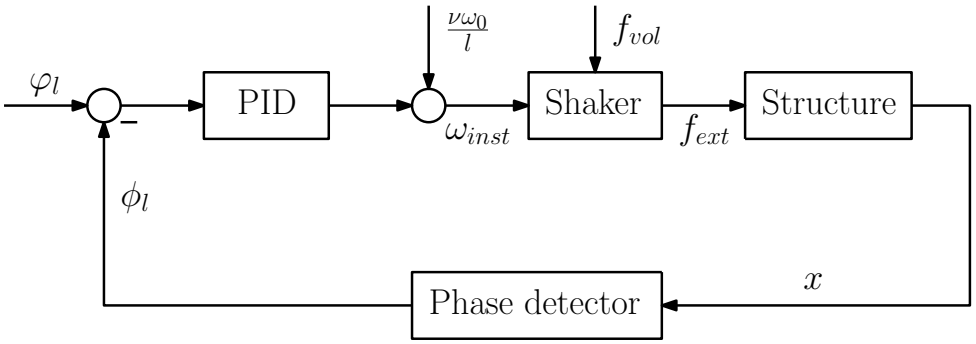

Figure 6.21: Scheme of the Phase-Locked Loop experiment.

Mode	Resonance frequency [Hz]	Antiresonance frequency [Hz]
1	6.2	8.7
2	31.8	55.5
3	78.3	147.4
4	170.9	198.1
5	254.6	297
6	303.5	

Table 6.1: Resonance and antiresonance frequencies of the linear cantilever beam.

surface. The displacement was measured by a laser vibrometer where the forcing was applied. A cubic nonlinearity $f_{nl}(x(t), \dot{x}(t)) = 3 \times 10^{11} x^3(t)$ was introduced artificially in the system using the real-time controller dSPACE MicroLabBox and was applied through the shaker. The force applied by the shaker was thus $f_{shaker}(t) = f(t) - f_{nl}(x(t), \dot{x}(t))$.

To compare the beam's dynamics numerically and experimentally, a linear reduced-order model of the beam with 6 DOFs was developed. The positions of the external forcing and the nonlinearity are on the second DOF, which also corresponds to the position of the laser vibrometer. The experimental and numerical linear FRFs at 0.3N are shown in Figure 6.23 and are found to agree well. The resonance and antiresonance frequencies are listed in Table 6.23.

6.5.3 Numerical results

Primary resonances

The NFRC of the first harmonic for a forcing of 0.08N is shown in Figure 6.24. As expected, each point in phase quadrature corresponds to either a resonance or an antiresonance. The effect of the nonlinearity is mainly seen on the two first resonances where the hardening behavior leads to unstable solutions between the fold bifurcations. The resonance and antiresonance frequencies for this configuration are given in Table 6.2.

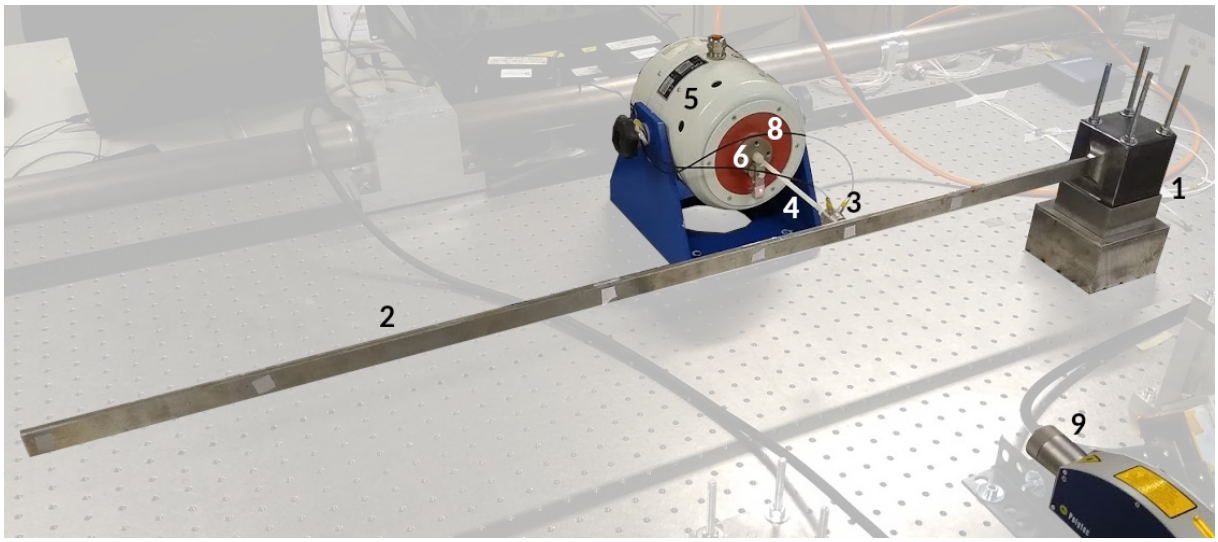

(a)

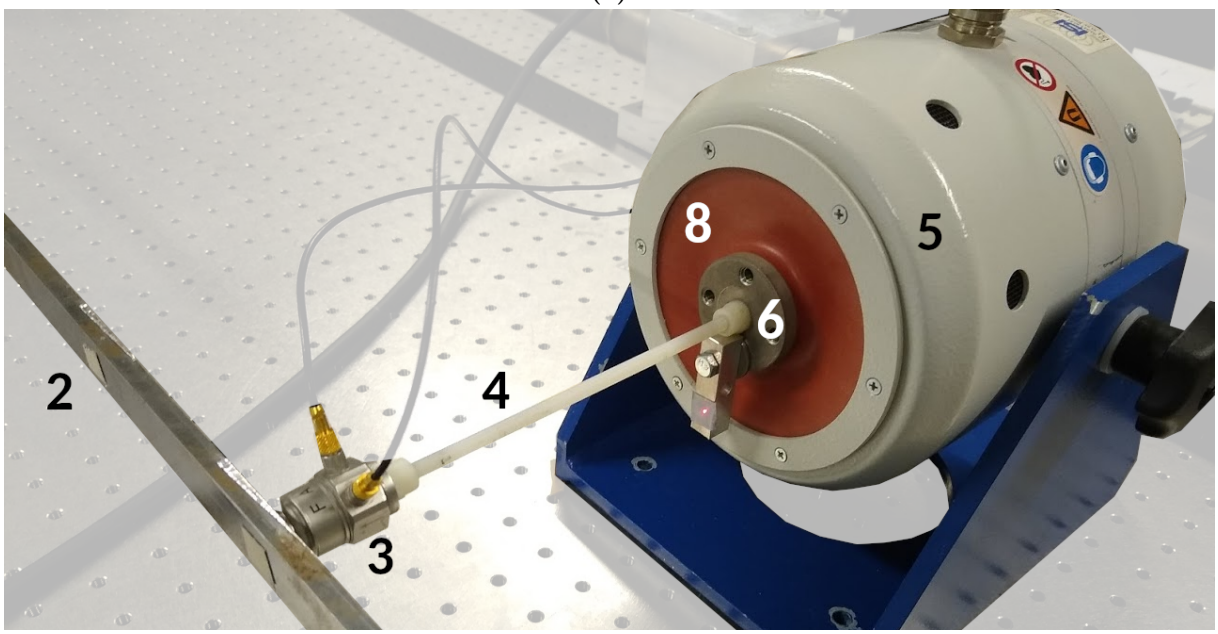

(b)

Figure 6.22: Cantilever beam setup: (1) Fixed base, (2) cantilever beam, (3) impedance head, (4) stinger, (5) shaker's casing, (6) shaker's magnetic core, (7) shaker's electrical coils, (8) shaker's membrane, (9) laser vibrometer.

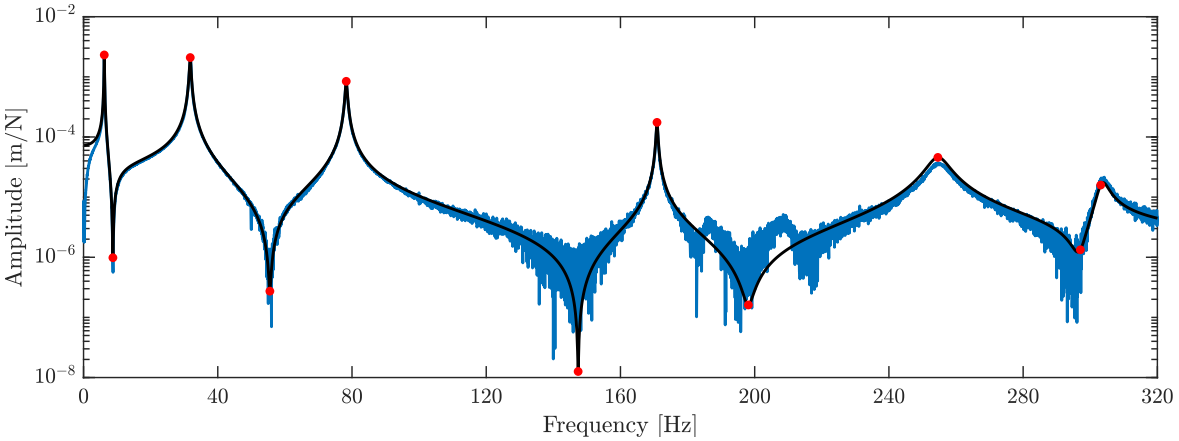

Figure 6.23: NFRC (black: experimental; blue: numerical) of the cantilever beam for a forcing of 0.3 N.

Mode	Resonance frequency [Hz]	Antiresonance frequency [Hz]
1	6.6	8.7
2	33.8	55.5
3	78.5	147.2
4	170.9	198.1
5	254.6	297
6	303	

Table 6.2: Resonances and antiresonances of the first harmonic of the cantilever beam (0.08N).

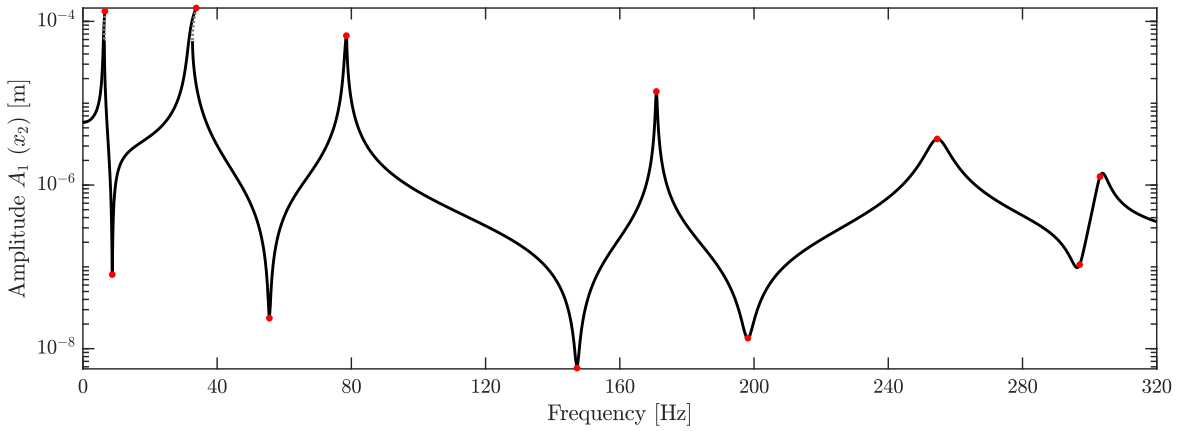

(a)

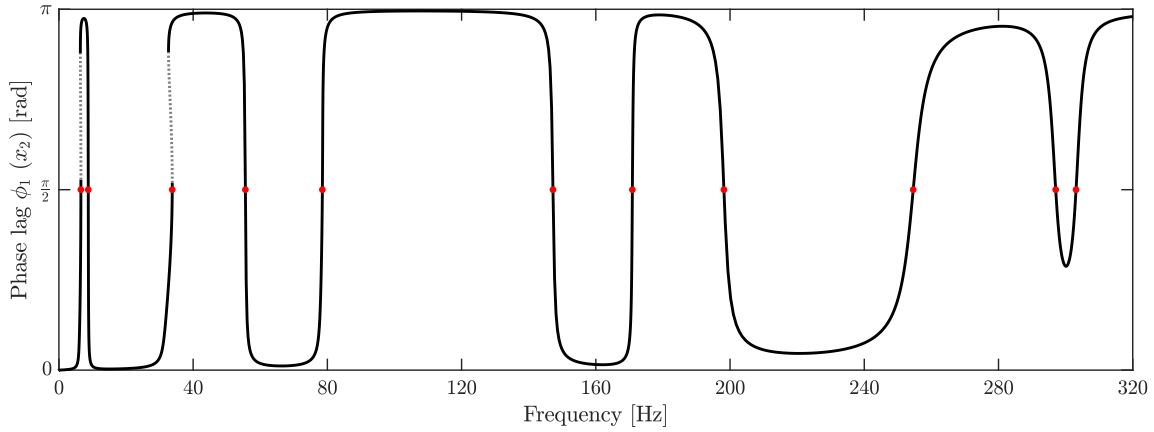

(b)

Figure 6.24: NFRC of the first harmonic of the second DOF of the cantilever beam (0.08N).(a) Amplitude A_1 and (b) phase lag ϕ_1. The red dots correspond to the phase quadrature points. Black: stable; grey: unstable.

Mode	Resonance frequency [Hz]	Antiresonance frequency [Hz]
1	2.1	2.9
2	10.6	18.5
3	26.1	49.1
4	57	66
5	84.9	99
6	101	

Table 6.3: Resonances and antiresonances of the third harmonic of the cantilever beam (0.08N).

3:1 superharmonic resonances

The NFRC of the third harmonic is presented in Figure 6.25. The frequency goes up to 105 Hz to encompass the 3:1 superharmonic resonance of the last primary resonance around 100 Hz. The NFRC comprises many local maxima et minima that correspond to either 3:1 or 1:1 resonances and antiresonances. Figure 6.25c showing the evolution of ϕ_3 can be used to distinguish between them. When the phase lag increases or drops by π, then it is a 3:1 resonance or antiresonance, respectively. When the phase lag increases or drops by 3π, then it is a 1:1 resonance or antiresonance, respectively. At this forcing level, all the 1:1 and 3:1 resonances are well-separated. For higher forcing amplitudes, however, modal interactions can appear, which complicates the interpretation, as discussed in Section 6.4.

If ϕ_3' instead of ϕ_3 is considered, then only the 3:1 resonances and antiresonances are revealed, as shown in Figure 6.25b. The frequencies at which these resonances and antiresonances occur is approximately one third of the frequencies of the nonlinear system from Table 6.1. Therefore, it is expected that the evolution of ϕ_3' resembles that of ϕ_1 in Figure 6.24b but with frequencies divided by three. The corresponding frequencies are reported in Table 6.3.

5:1 superharmonic resonances

A similar analysis for the fifth harmonic can be made from Figure 6.26. In this case, the evolution of ϕ_5 in Figure 6.26c becomes hardly interpretable. Therefore, ϕ_5' is used to detect the 5:1 resonances and antiresonances. As for ϕ_3', its evolution resembles that of ϕ_1 in Figure 6.24b but with frequencies divided by five. The corresponding resonance and antiresonance frequencies are reported in Table 6.4.

At higher forcing amplitudes, a modal interaction is about to happen between the 5:1 superharmonic resonance of the fourth mode and the second mode around 34 Hz. This is evidenced in Figure 6.27a where the PRNM curves of the 1:1 and 5:1 resonances are superposed to the NFRC at 0.3N. The two PRNM curves cross each other around an amplitude of 1.7×10^{-4}m giving rise to a small bump on the main resonance branch. The mechanism is similar to what was described in Section 6.4.2. In addition, the PRNM curves for the 3:1 superharmonic resonance of the third vibration mode obtained using

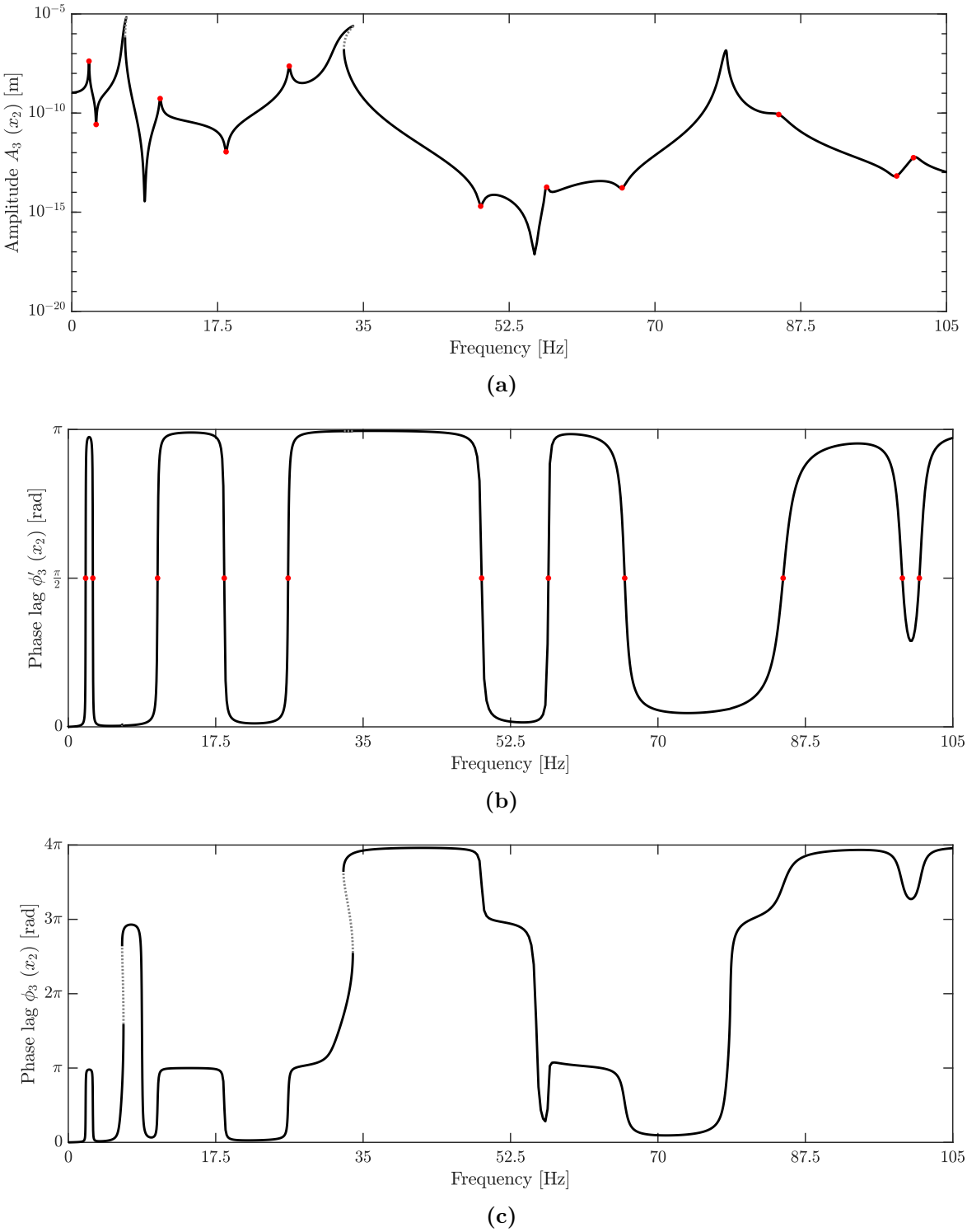

Figure 6.25: NFRC of the third harmonic of the second DOF of the cantilever beam (0.08N). (a) Amplitude A_3, (b) phase lag ϕ_3' and (c) phase lag ϕ_3. The red dots correspond to the phase resonance points. Black: stable; grey: unstable.

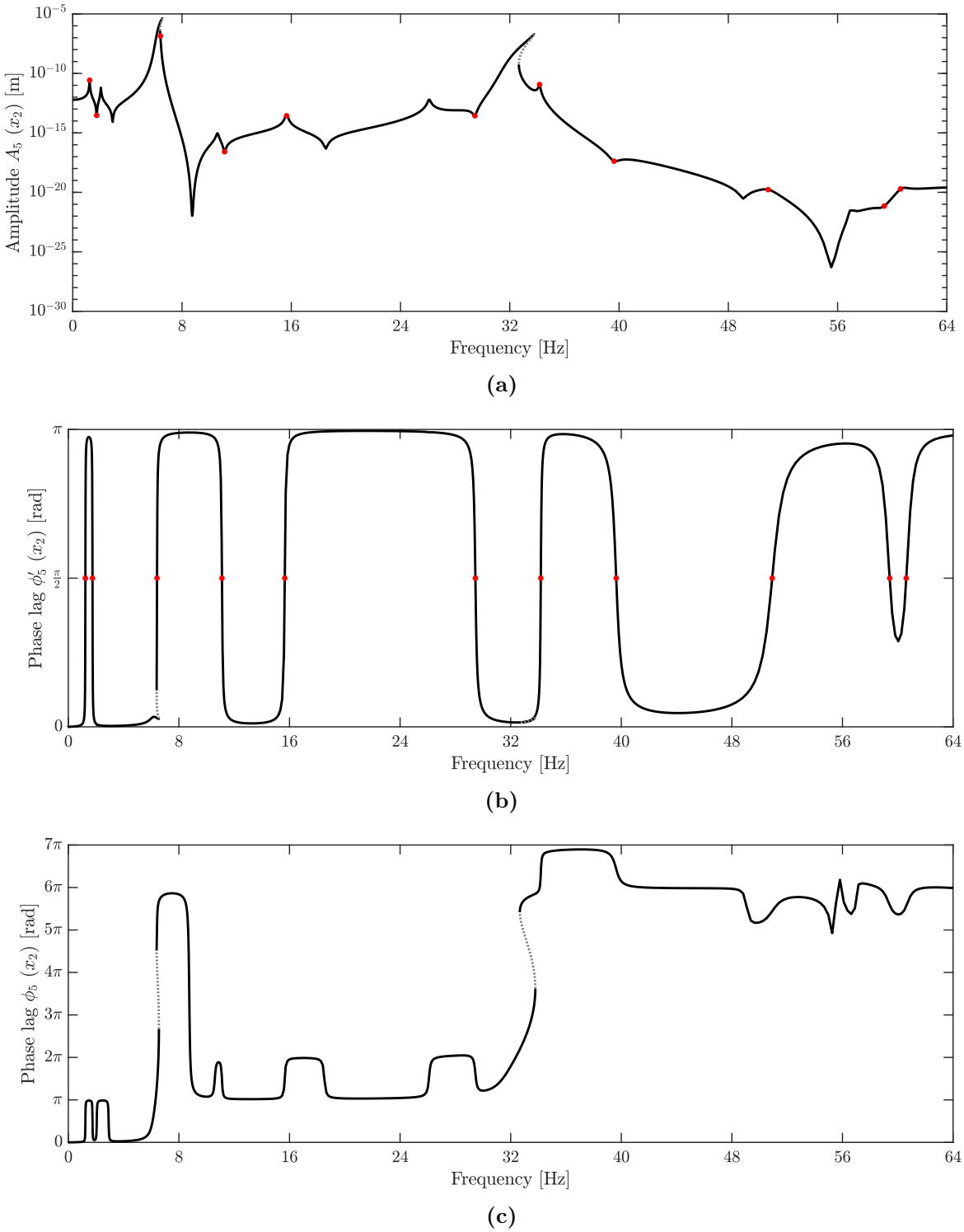

Figure 6.26: NFRC of the fifth harmonic of the second DOF of the cantilever beam (0.08N). (a) Amplitude A_5, (b) phase lag ϕ_5' and (c) phase lag ϕ_5. The red dots correspond to the phase resonance points. Black: stable; grey: unstable.

Mode	Resonance frequency [Hz]	Antiresonance frequency [Hz]
1	1.2	1.8
2	6.4	11.1
3	10.6	29.5
4	34.2	39.6
5	51	59.4
6	60.1	

Table 6.4: Resonances and antiresonances of the fifth harmonic of the cantilever beam (0.08N).

either $\phi_3 = \frac{\pi}{2}$ or $\phi'_3 = \frac{\pi}{2}$ are compared. The two curves are almost identical owing to the fact that this resonance is sufficiently far away from other primary resonances. Close-ups of the phase lag of each harmonic are also shown in Figures 6.27b-d confirming that each harmonic passes through $\frac{\pi}{2}$ at resonance, and even three times for the fifth harmonic due to the modal interaction.

6.5.4 Experimental results

Figure 6.28 presents the experimental results around the second mode at 1N. This forcing level was chosen, because it gives similar response amplitudes as in the numerical case at 0.3N. This discrepancy is to be attributed to higher damping in the experimental beam.

Overall, we obtained an excellent agreement between Figures 6.27 and 6.28. As in the numerical case, when the 5:1 PRNM curve constructed using ϕ'_5 crosses the NFRC in Figure 6.28a, a small bump is present, revealing a 5:1 superharmonic resonance on the main resonance peak. In addition, the 3:1 PRNM curves built using $\phi_3 = \frac{\pi}{2}$ and $\phi'_3 = \frac{\pi}{2}$ resemble each other, as in Figure 6.27a. The experimental phase lags in Figures 6.28b-d also agree well with the numerical phase lags. Specifically, the experimental ϕ'_3 and ϕ'_5 undergo a shift of π, indicating the presence of 3:1 and 5:1 superharmonic resonances, respectively. We just underline that ϕ'_5 is shifted approximately by $-\frac{\pi}{4}$ with respect to the numerical phase lag, which might indicate that the cubic nonlinearity is not the only nonlinearity in the system.

Close-ups of the 3:1 and 5:1 superharmonic resonances are displayed in Figure 6.29. If the topology of the NFRC around the 5:1 resonance remains fairly simple, a loop appears for the 3:1 resonance. Such a dynamical behavior is consistent with what was observed for the Duffing oscillator in Figure 5.16a. We see that the PRNM curves built using $\phi_3 = \phi'_3 = \frac{\pi}{2}$ tend to move away from each other when the forcing amplitude is increased. This can be explained by the hardening nonlinearity which brings the 3:1 resonance closer to zone of influence of the 1:1 resonance.

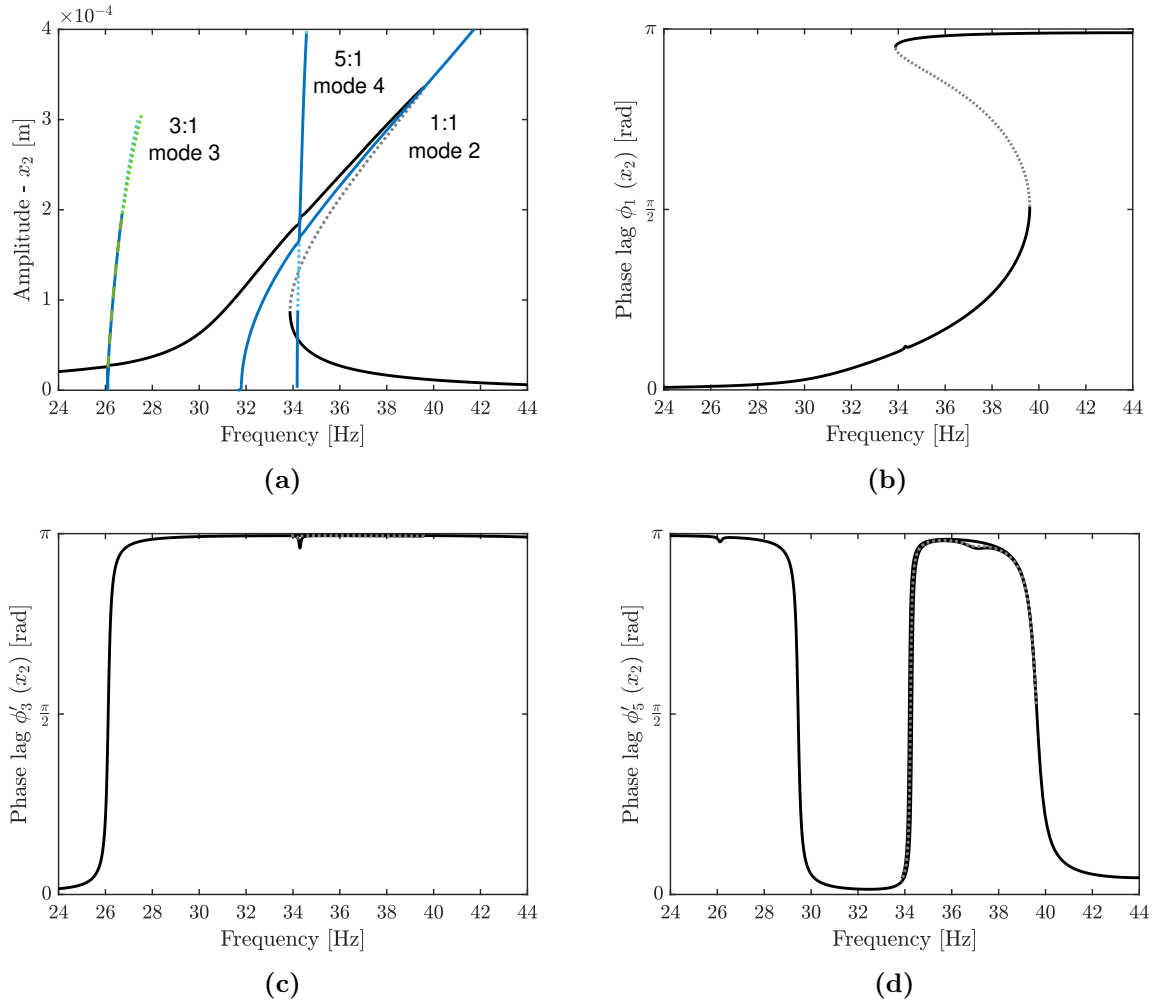

Figure 6.27: (a) NFRC (black) and PRNM curves of the 1:1, 3:1 and 5:1 resonances (blue: $\phi_1 = \phi_3' = \phi_5' = \frac{\pi}{2}$; green: $\phi_3 = \frac{\pi}{2}$) of the numerical beam model around the second mode (0.3N), (b) ϕ_1, (c) ϕ_3' and (d) ϕ_5'.

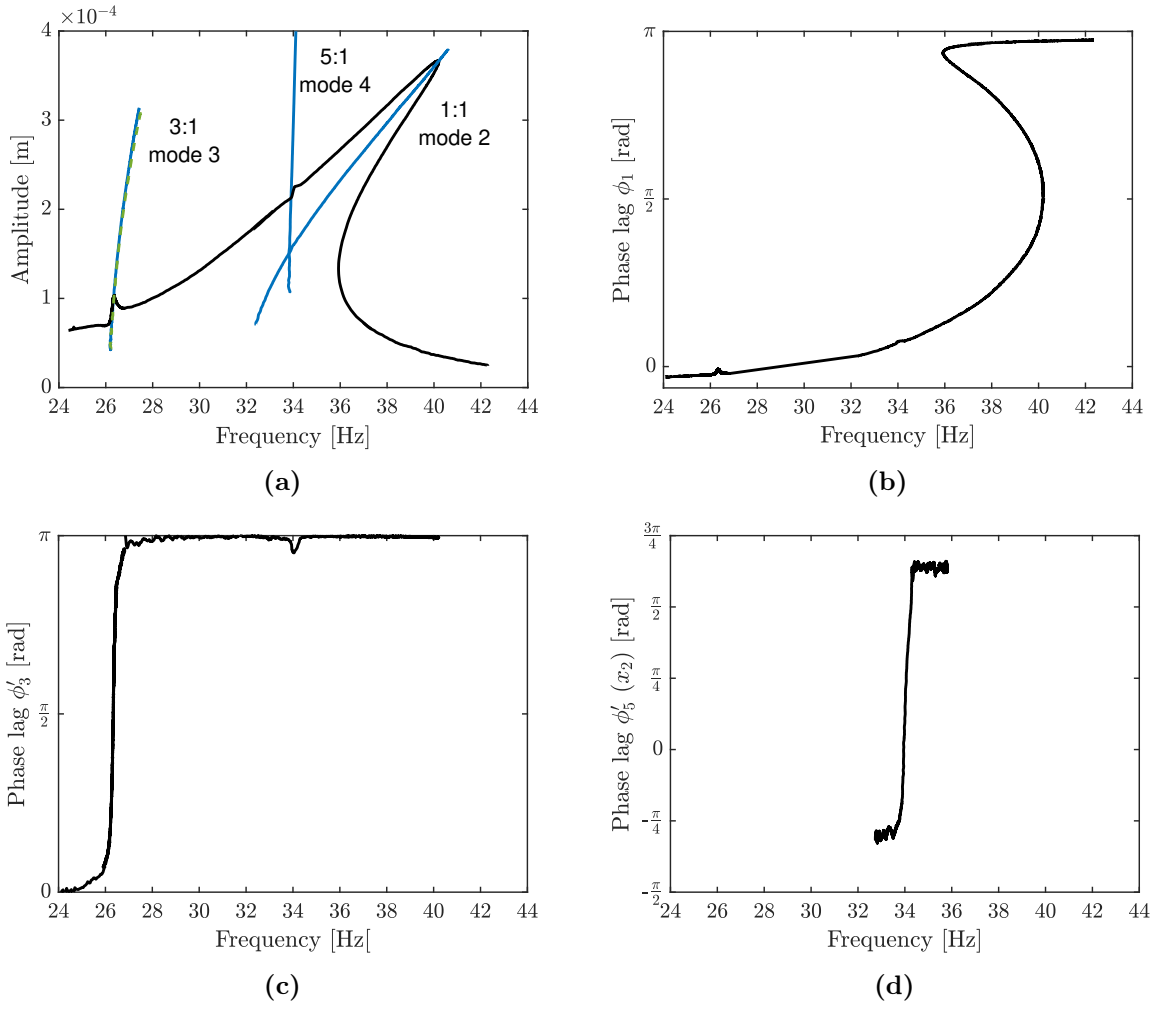

Figure 6.28: (a) NFRC (black) and PRNM curves of the 1:1, 3:1 and 5:1 resonances (blue: $\phi_1 = \phi_3' = \phi_5' = \frac{\pi}{2}$; green: $\phi_3 = \frac{\pi}{2}$) of the experimental beam around the second mode (1N), (b) ϕ_1, (c) ϕ_3' and (d) ϕ_5'.

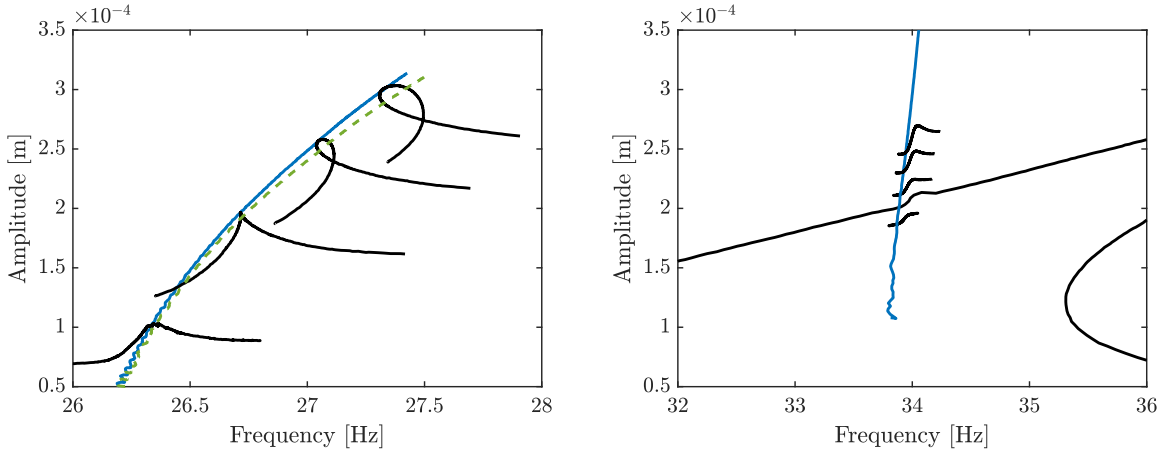

Figure 6.29: NFRC (black) and PRNM curves (blue: $\phi'_3 = \phi'_5 = \frac{\pi}{2}$; green: $\phi_3 = \frac{\pi}{2}$) of the experimental beam. (a) 3:1 resonance between 1 and 4N and (b) 5:1 resonance between 0.5 and 2N.

6.6 Experimental demonstration using a clamped-clamped beam

6.6.1 Experimental setup

The test sample, photographed in Figure 6.30, is a 100cm × 2cm × 0.2cm aluminium beam clamped at both ends to aluminium mounting blocks bolted to a support frame fixed on the vibration table. The beam motion was prescribed by a sliding groove of cross section 20mm × 0.2mm made in the block. During the installation, it was ensured that the initial tension or compression forces along the beam are weak so that there is no important prestress.

The forcing was applied by the same electromagnetic shaker as for the cantilever beam. The shaker was fed by a power amplifier (TIRA BAA 120) working in current mode. It was connected to the beam through a flexible stinger and an impedance head (DYTRAN 5860B). To minimize shaker-structure interaction, the shaker was placed at 3cm from one clamped boundary. The beam response was measured using an accelerometer (DYTRAN 3035G) placed at 12cm from one clamped boundary to ensure good signal-to-noise ratio. The signal was then amplified using a signal conditioner (PCB PIEZOTRONICS 482C).

To measure the NFRC and PRNM curves, a PLL control loop with adaptive filtering was applied thanks to the real-time controller dSpace MicroLabBox. The relations between the signals and the hardware were established using the Real Time Interface whereas the overall control scheme was implemented within Matlab/Simulink.

The 1:1, 2:1, 3:1 and 1:2 resonances of the first beam mode are studied in this section. The configuration of the setup for the 1:1 and 1:2 resonances is such that the distance between the two mounting blocks is 67.8cm while it is 75.4cm for the 2:1 and 3:1 resonances because their amplitude was too low on the former configuration.

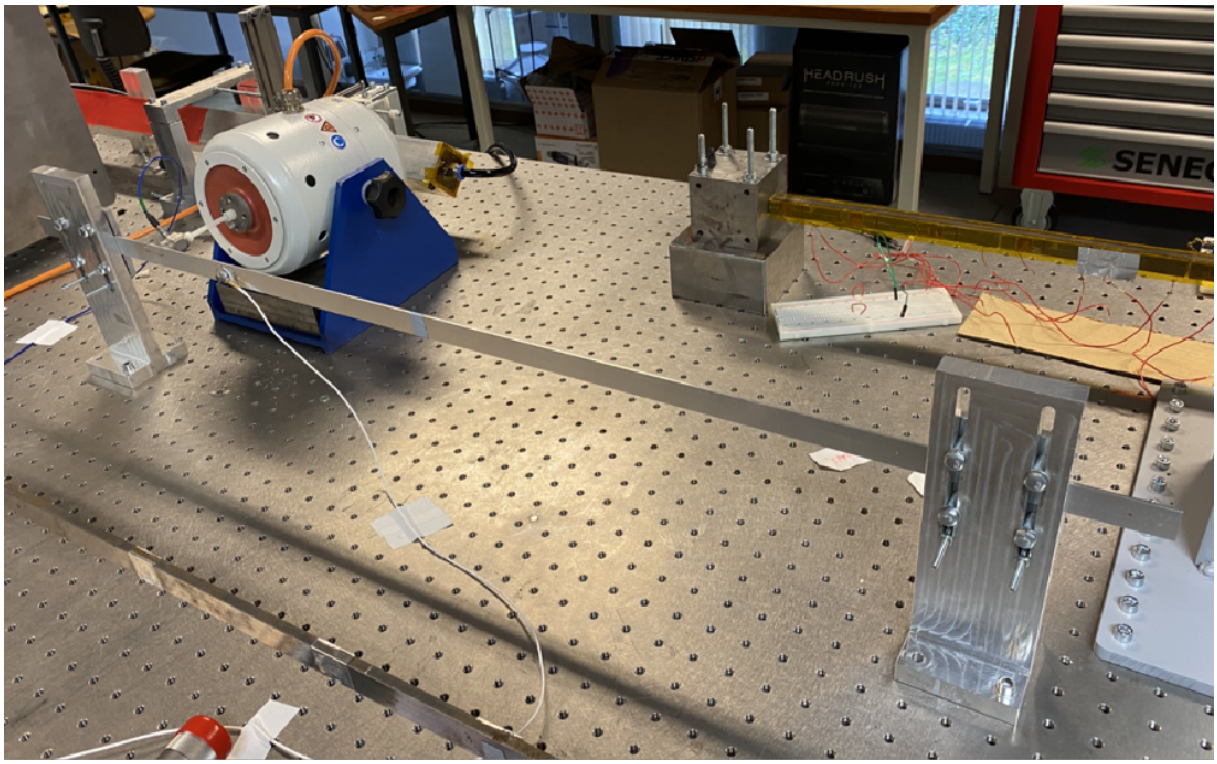

Figure 6.30: Clamped-clamped beam setup.

6.6.2 Experimental results

Primary resonance

The primary resonance of the first beam mode is displayed in Figure 6.31. The NFRC was obtained by sweeping the phase from 0 to π using the PLL controller. The PRNM curve identified by locking the phase at a value of $\pi/2$ is found to trace out accurately the locus of the resonance points. A hardening effect due to the geometrical nonlinearity of the clamped-clamped beam is clearly visible; a slight softening effect can also be noticed.

2:1 superharmonic resonance

During the experiments, the NFRC in Figure 6.32a was found to be in the direct continuation of the main branch. It did not bifurcate from the main branch as in Figure 5.17 for the Duffing oscillator. This behavior indicates a Duffing-Helmholtz-like behavior for which the resonant phase lag of the 2:1 resonance is $\phi_2 = 0$ (see Section 4.2.3.3). This phase lag was adopted in the PLL controller, and the outcome is shown in Figure 6.32b. The resulting PRNMs are located in the close vicinity of the resonance peak (but not exactly on it).

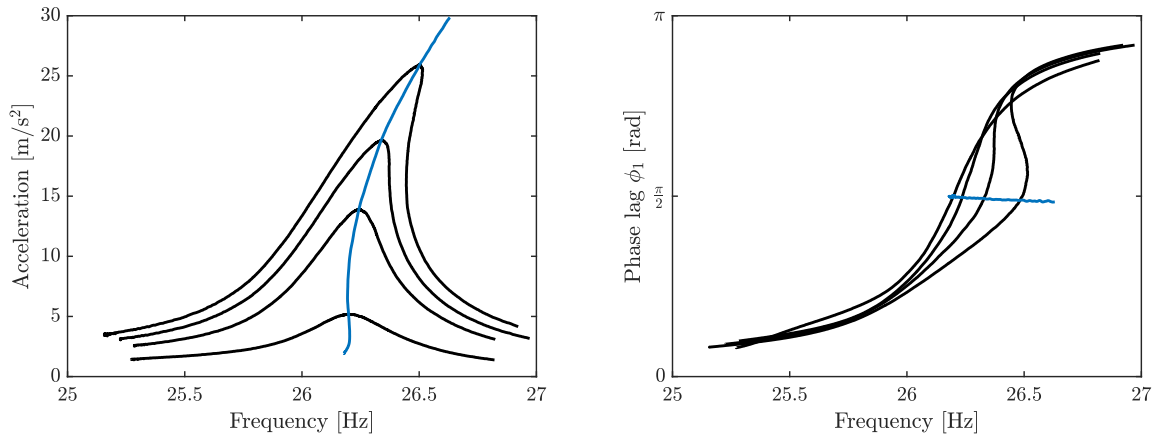

Figure 6.31: NFRC (black) and PRNM curve (blue) of the primary resonance of the first mode of the clamped-clamped beam for 0.2N, 0.4N, 0.5N and 0.6N. (a) Response amplitude vs. forcing frequency and (b) phase lag vs. forcing frequency.

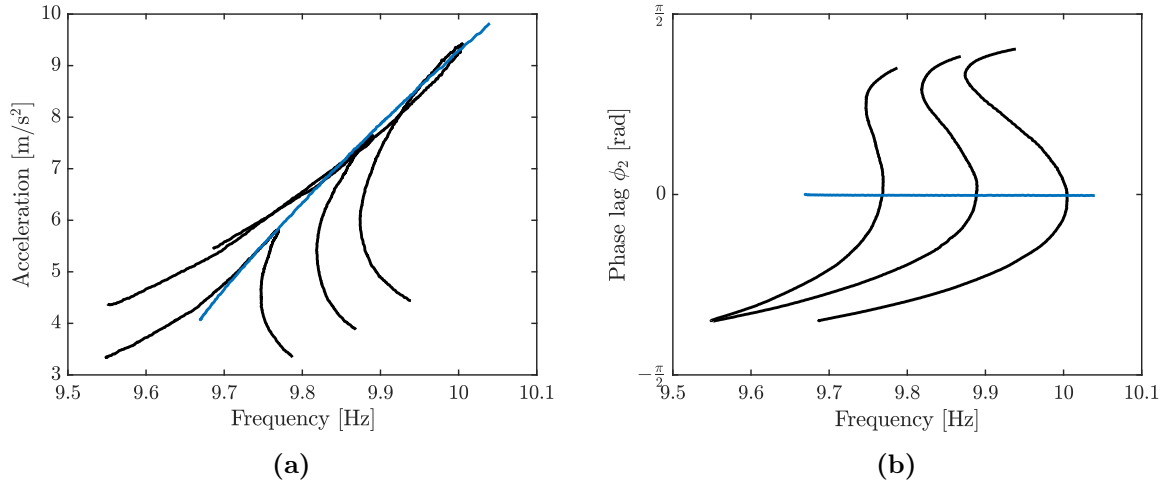

Figure 6.32: NFRC (black) and PRNM curve (blue) of the 2:1 resonance for 4N, 4.5N and 5N. (a) Response amplitude vs. forcing frequency and (b) phase lag vs. forcing frequency.

1:2 subharmonic resonance

The next resonance is the 1:2 resonance displayed in Figure 6.33. Starting from the main branch, an impact hammer was used to jump to these resonances that appear as isolated branches. The phase lag seems to oscillate around 0, as for the 2:1 resonance. The PRNM curves were therefore identified using $\phi_1 = 0$. The experiments also evidenced that the same solution but with a resonant phase lag equal to π can be measured. The PLL strategy did not allow to compute the whole branches and we cannot assure whether the branches eventually connect to the main branch or not, as it is the case for a Helmholtz-Duffing oscillator, as discussed in Section 5.4.2. The resonant phase lag, though, is in agreement with this type of oscillator.

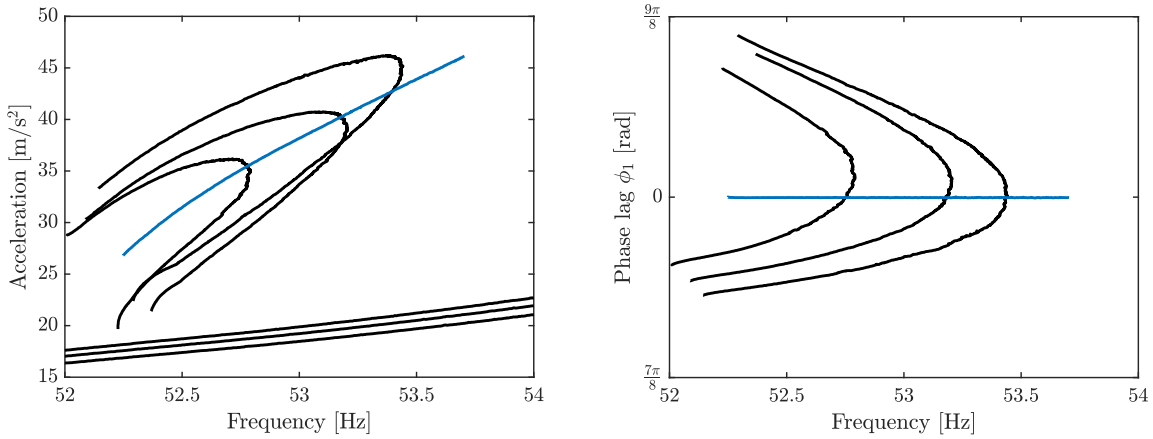

Figure 6.33: NFRC (black) and PRNM curve (blue) of the 1:2 resonance for 2.5N, 2.6N and 2.7N. (a) Response amplitude vs. forcing frequency and (b) phase lag vs. forcing frequency.

3:1 superharmonic resonance

Finally, the 3:1 superharmonic resonance is plotted in Figure 6.34. It appears in the direct continuation of the main branch and features a hardening behavior. The PRNMs were identified using the resonant phase lag $\phi_3 = \frac{\pi}{2}$. These results are in agreement with those in Section 5.4.2.

6.7 Conclusion

Two main challenges were tackled in this chapter, namely *(i)* to apply the proposed PRNM framework to MDOF systems and *(ii)* to validate the PRNM definition experimentally.

In the case of MDOF systems, the primary and secondary resonances of different modes can interact. This influences directly the phase lag of each harmonic and particularly the value of the resonant phase lag. To address this issue, the perturbation technique presented in [104] allowed us to define new phase lags that are linear combination of

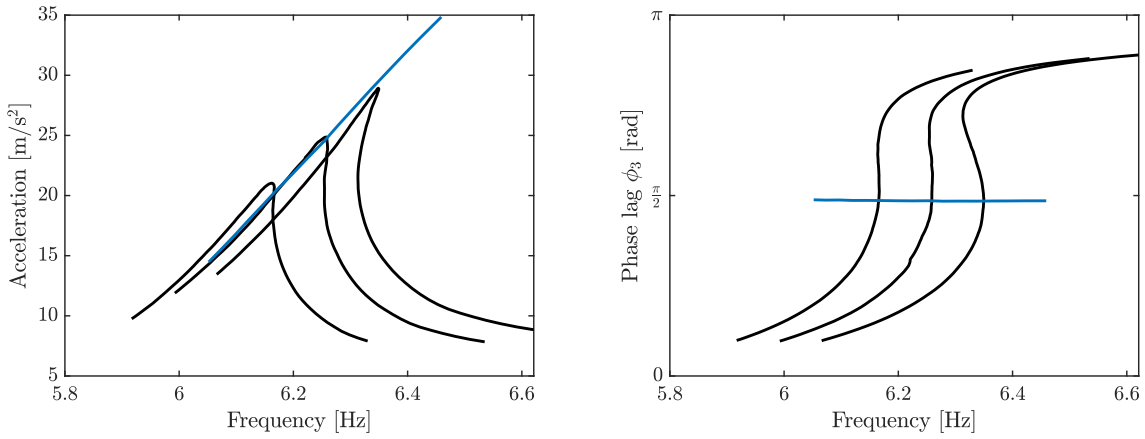

(a) **(b)**

Figure 6.34: NFRC (black) and PRNM curve (blue) of the 3:1 resonance for 3.5N, 4N and 4.5N. (a) Response amplitude vs. forcing frequency and (b) phase lag vs. forcing frequency.

carefully selected harmonics. These phase lags do no longer suffer from the influence of other resonances such that they can be used to construct the PRNM curves of MDOF systems. This was illustrated using two-DOF systems featuring 3:1 and 5:1 superharmonic resonances. Interestingly, based on the analysis of PRNM curves, we were also able to detect outer and inner isolated branches generated by 3:1 resonance phenomena.

Second, two experimental setups were considered to demonstrate the effectiveness of the PRNM framework in practice. The first setup was a cantilever beam with an artificial cubic nonlinearity. The beam featured an interesting 5:1 modal interaction which was successfully identified experimentally thanks to the PRNMs with the newly-defined phase lags and accurately reproduced numerically using a nonlinear reduced-order model. The second setup was a clamped-clamped beam exhibiting geometrically nonlinear behavior. Several secondary resonances of the first beam mode were characterized with the PRNMs curves with well-selected resonant phase lags. This study revealed that the clamped-clamped beam behaves as a Helmholtz-Duffing oscillator.

Chapter 7

Conclusions

7.1 Outcomes of the thesis

Linear and nonlinear systems possess fundamentally different dynamical features. Frequency-amplitude-dependent properties, multi-harmonic responses leading to, e.g., secondary resonances and modal interactions, and isolated responses are among the challenges that were tackled in this thesis. The very rich and complex dynamics of the harmonically-forced Duffing oscillator was evidenced in Chapter 2 where this seemingly simple nonlinear system was found to possess a countable infinity of superharmonic and subharmonic resonances l:ν. Focusing our attention on monopoint and mono-harmonic forcing, the two research questions addressed in this thesis were :

(i) How to define the l:ν resonance of a nonlinear system where l and ν are arbitrary integers?

(ii) How to characterize primary and secondary resonances analytically, numerically and experimentally?

Regarding the first question, Chapter 2 evidenced that, for each $l : \nu$ resonance, the predominance of the l-th harmonic increases when the amplitude of harmonic forcing increases. Therefore, one of the main thrusts of the thesis was to study analytically how this specific harmonic behaves.

To this end, first-order averaging was exploited in Chapter 3 to derive the dynamics of the fundamental harmonic of the response around the primary resonance for oscillators with polynomial stiffness. When studying the amplitude-phase lag relationship, it was found that phase resonance as defined in linear systems, *i.e.*, when the forcing counterbalances exactly the damping term, can be extended to nonlinear oscillators. Specifically, nonlinear phase resonance for a primary resonance occurs when the phase lag of the fundamental harmonic, i.e., the resonant phase lag, is $\frac{\pi}{2}$. Phase resonance thus happens in the immediate vicinity of amplitude resonance for weak to moderate damping.

In Chapter 4, the resonant phase lags of the d:1 and 1:d resonances of an oscillator with polynomial stiffness of order d were derived using first-order averaging,. It was shown that amplitude resonance of the d-th (1st) harmonic for superharmonic (subharmonic)

resonances occurs for phase lags which are not necessarily equal to $\frac{\pi}{2}$. Using higher-order averaging, the resonant phase lags of the l:ν resonances of the Duffing oscillator were also found to differ from $\frac{\pi}{2}$ when either l or ν is even. For some specific subharmonic resonances, the resonant phase lag did not characterize amplitude resonance but rather the boundaries of the existence domain of the isolated response. In summary, in this thesis, a l:ν resonance is defined as the point of the nonlinear frequency response curve (NFRC) where the phase lag of the l-th harmonic equals the corresponding resonant phase lag.

An answer to the second question was provided in Chapter 5 based on the outcomes of Chapters 3 and 4. The concept of a phase resonance nonlinear mode (PRNM) which (*i*) is an actual solution of the NFRC paving the way for a rigorous link between numerical and experimental modal analysis results, (*ii*) can characterize superharmonic, subharmonic and ultra-subharmonic resonances and (*iii*) can include nonlinear nonconservative forces was proposed. The PRNMs rely on the resonant phase lags calculated in previous chapters. Another distinct advantage of a PRNM is that it is directly associated with a specific forcing amplitude. Thus, the response amplitude-forcing amplitude curve can be calculated in a straightforward manner and, in turn, be used to detect outer (or even inner !) isolated responses. Finally, two computational methods based on a velocity feedback and on the resonant phase lag were developed for the numerical calculation of the PRNMs in this chapter.

The last endeavor of the thesis was to identify PRNM curves experimentally. A key enabling technology that was used for this purpose is phase-locked loops. However, in practice, primary and secondary resonances of different modes can interact, influencing the values of the resonant phase lags. To resolve this issue, a specific perturbation technique evidenced that, for l:1 superharmonic resonances, a new phase lag can be defined based on the studied harmonic and the lower-order harmonics. Based on these developments, the PRNM curves of two different experimental beams were successfully identified.

7.2 Perspectives

There remain several unanswered questions that need to be addressed in the future to assess the viability of the present work.

First, the nonlinear oscillator that served as a motivating example throughout the thesis is the Duffing oscillator. Though it covers many aspects of nonlinear oscillations, it is necessary to consider other systems with more complex nonlinearities. This was partially addressed in Chapters 3 and 4 by studying analytically oscillators with polynomial stiffness, and in Chapter 5 by studying numerically oscillators with piece-wise linear/polynomial stiffness and Coulomb friction. However, other important nonlinearities such as damping nonlinearities described by Bouc-Wen or Iwan models deserve our full consideration.

Besides more complex nonlinearities, more complex structures, e.g., with a higher dimensionality, should be considered in the future. A first step in this direction was recently achieved by T. Zhou, postdoctoral researcher at the University of Liège. The NFRCs of the third vibration mode (torsional mode of the wing) of a F-16 aircraft obtained

using classical sine sweeps are displayed in Figure 7.1. Also superposed in this figure is the PRNM curve identified using PLLs which is found to trace out nicely the locus of maximum amplitudes of this resonance. We note that the resonant phase lag is 1 rad/s and not $\frac{\pi}{2}$ rad/s. This discrepancy is attributed to the presence of an antiresonance in the immediate vicinity of the third mode. A 3:1 superharmonic resonance was also identified at one third of the frequency of the third vibration mode in Figure 7.2. Despite the low amplitude of the response and the noise present during the measurements, the phase lag of the third harmonic evidences a shift of approximately π radians around the resonance and is in quadrature with the forcing when the amplitude of the 3:1 superharmonic resonance is maximum.

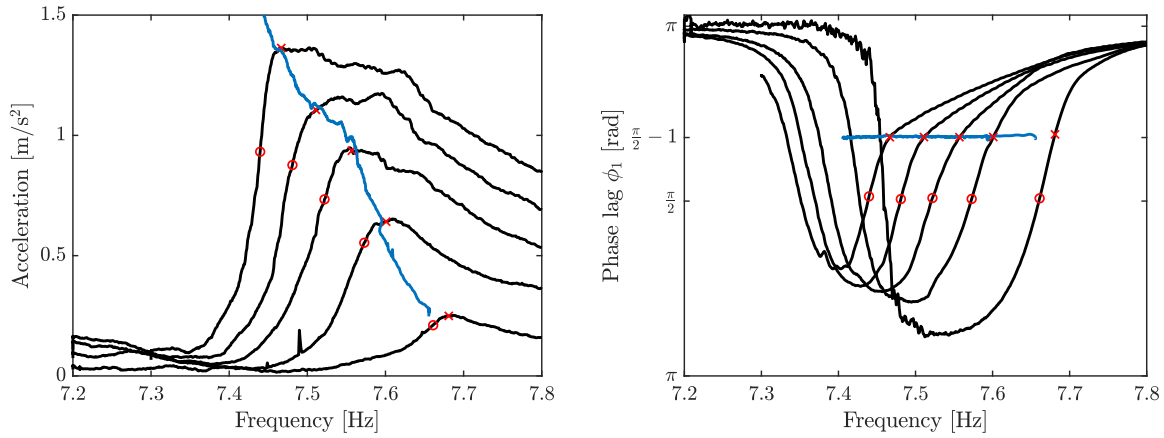

Figure 7.1: NFRCs (black) and PRNM curve (blue) of the primary resonance of the third mode of a F-16 aircraft for increasing forcing amplitudes: (a) amplitude and (b) phase lag ϕ_1. The red crosses and circles correspond to a phase lag of 1 and $\frac{\pi}{2}$, respectively.

Two important assumptions considered in this manuscript are well-separated primary resonances and light damping (with damping ratios of the order of 1% or less). Further investigations should therefore be made to determine whether the concept of a PRNM is still relevant when either one or the other assumption is no longer valid.

Other topics of interest are the extension of the single-nonlinear-mode modal synthesis procedure proposed in [112, 116] to secondary resonances and the generaliza tion of the PLOPT perturbation technique to even superharmonic resonances and subharmonic resonances.

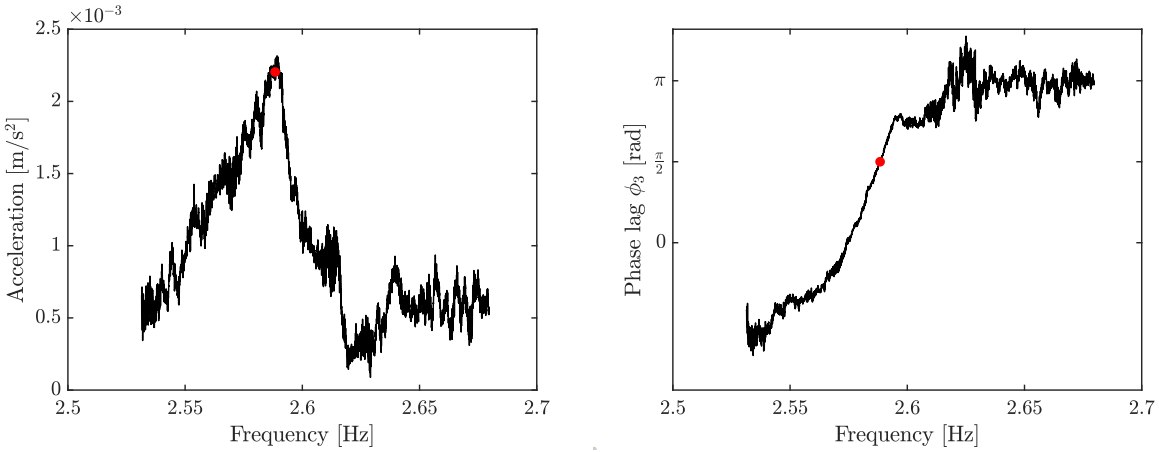

Figure 7.2: NFRC of the 3:1 resonance of the third mode of a F-16 aircraft: (a) amplitude and (b) phase lag ϕ_3. The red cross corresponds to a phase lag of $\frac{\pi}{2}$.

Appendix A

Stability analysis

A.1 Floquet theory

The stability of the solutions is studied using Floquet theory [25, 117]. We consider a set of n first-order differential equations

$$\dot{\mathbf{x}}(t) = \mathbf{g}(\mathbf{x}(t)) \tag{A.1}$$

which admits a T-periodic solution $\mathbf{x}_0(t)$. It can be linearized into time-dependent differential equations

$$\dot{\mathbf{x}}(t) \simeq \mathbf{g}(\mathbf{x}_0(t)) + \mathbf{J}(t)(\mathbf{x}(t) - \mathbf{x}_0(t)) \tag{A.2}$$

where $\mathbf{J}(t) = \frac{\partial \mathbf{f}}{\partial \mathbf{x}}\big|_{\mathbf{x}=\mathbf{x}_0(t)}$ has the same period as $\mathbf{x}_0(t)$, such that $\mathbf{J}(t+T) = \mathbf{J}(t)$. A small perturbation $\mathbf{s}(t)$ is added so that we have $\mathbf{x} = \mathbf{x}_0(t) + \mathbf{s}(t)$. The equation governing the evolution of the perturbation can be rewritten as

$$\dot{\mathbf{s}}(t) = \mathbf{J}(t)\mathbf{s}(t). \tag{A.3}$$

If $\mathbf{s}(t)$ tends to $\mathbf{0}$ as time goes to infinity, then the solution is said to be stable; otherwise, it is unstable. To verify this, we consider the fundamental matrix $\Psi(t)$

$$\Psi(t) = [\psi_1(t), \ldots, \psi_i(t), \ldots, \psi_n(t)] \tag{A.4}$$

such that it verifies

$$\dot{\Psi}(t) = \mathbf{J}(t)\Psi(t) \tag{A.5}$$

where $\psi_i(t)$ is a column-vector solution of Equation (A.3) and where all the $\psi_i(t)$ are linearly independent solutions. If $\Psi(t+T)$ is plugged into Equation (A.3),

$$\dot{\Psi}(t+T) = \mathbf{J}(t+T)\Psi(t+T) = \mathbf{J}(t)\Psi(t+T) \tag{A.6}$$

$\Psi(t+T)$ is also a solution that verifies (A.5). Since there exists only n linearly independent solutions, it must be that $\Phi(t+T)$ is a linear combination of $\Psi(t)$ such that

$$\Psi(t+T) = \Psi(t)\mathcal{M} \longleftrightarrow \mathcal{M} = \Psi^{-1}(t)\Psi(t+T) \tag{A.7}$$

where $\mathcal{M}$ is the *monodromy* matrix. Setting $t = 0$, we have $\mathcal{M} = \Psi^{-1}(0)\Psi(T)$. In particular, if $\Psi(0)$ is the identity matrix $\mathbb{I}$, then

$$\mathcal{M} = \Psi(T) \tag{A.8}$$

can be obtained by integrating Equation (A.5) with the identity matrix as initial conditions. Noting that $\mathcal{M}$ is a constant matrix, we can define its constant matrices of eigenvectors $\mathcal{L}$ and eigenvalues $\boldsymbol{\lambda} = \text{diag}\,[\lambda_1, \ldots, \lambda_n]$, where λ_i is called a Floquet multiplier. Furthermore, through a change of variables, matrix $\mathcal{V}(t)$ is defined as

$$\mathcal{V}(t) = \Psi(t)\mathcal{L} \tag{A.9}$$

where $\mathcal{L}(t)$ is thus a solution of Equation (A.3). We can write

$$\begin{aligned} \Psi(t+T) = \Psi(t)\mathcal{M} &\Leftrightarrow \mathcal{V}(t+T)\mathcal{L}^{-1} = \mathcal{V}(t)\mathcal{L}^{-1}\mathcal{M} \\ &\Leftrightarrow \mathcal{V}(t+T) = \mathcal{V}(t)\mathcal{L}^{-1}\mathcal{M}\mathcal{L} \\ &\Leftrightarrow \mathcal{V}(t+T) = \mathcal{V}(t)\boldsymbol{\lambda}. \end{aligned} \tag{A.10}$$

After a period T, the evolution of $\mathcal{V}(t)$ is driven by the Floquet multipliers. In particular,

$$\begin{aligned} \mathcal{V}(t+T) &= \mathcal{V}(t)\boldsymbol{\lambda} \\ \mathcal{V}(t+2T) &= \mathcal{V}(t+T)\boldsymbol{\lambda} = \mathcal{V}(t)\boldsymbol{\lambda}^2 \\ &\vdots \\ \mathcal{V}(t+NT) &= \mathcal{V}(t)\boldsymbol{\lambda}^N. \end{aligned} \tag{A.11}$$

Since $\boldsymbol{\lambda}$ is a diagonal matrix, we have $\boldsymbol{\lambda}^N = \text{diag}\left[\lambda_1^N, \ldots, \lambda_n^N\right]$. If at least one of the Floquet multipliers tends to infinity when N tends to infinity, then the solution is unstable; otherwise, it is stable. Mathematically,

$$\begin{cases} \text{if } \forall i \in [1, n] \ |\lambda_i| \leq 1 \text{ then the solution is stable} \\ \text{if for any } i \quad |\lambda_i| > 1 \text{ then the solution is unstable} \end{cases} \tag{A.12}$$

Another way of computing the stability of a solution is to look at the Floquet exponents. To do so, $\Psi(t)$ is written in the *Floquet normal form*

$$\Psi(t) = \mathcal{P}(t)e^{t\mathcal{B}} \tag{A.13}$$

where $\mathcal{P}(t)$ is a T-periodic matrix and $\mathcal{B}$ is complex matrix. Therefore,

$$\begin{aligned} \Psi(t+T) &= \mathcal{P}(t+T)e^{(t+T)\mathcal{B}} \\ &= \mathcal{P}(t)e^{t\mathcal{B}}e^{T\mathcal{B}} \\ &= \Psi(t)e^{T\mathcal{B}} \end{aligned} \tag{A.14}$$

and

$$e^{T\mathcal{B}} = \Psi^{-1}(t)\Psi(t+T) = \mathcal{M}. \tag{A.15}$$

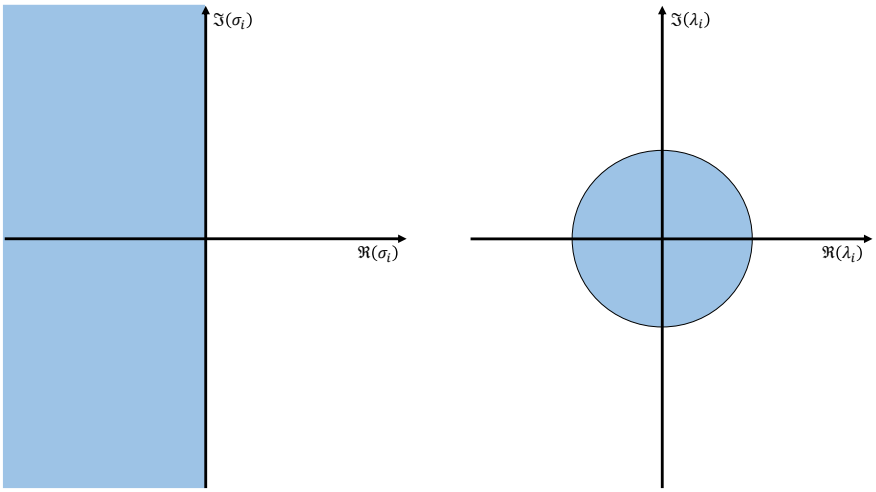

Figure A.1: Graphical representation of the stability regions (blue) using the Floquet exponents (left) and multipliers (right).

Stability can be studied by looking at the eigenvalues of $e^{T\mathcal{B}}$. If $\boldsymbol{\sigma} = \text{diag}\,[\sigma_1, \ldots, \sigma_n]$ contains the n eigenvalues σ_i of $\mathcal{B}$, called the Floquet exponents, then diag $\left[e^{T\sigma_1}, \ldots, e^{\sigma_n}\right]$ contains the eigenvalues of $e^{T\mathcal{B}}$. Since $e^{T\mathcal{B}} = \Psi^{-1}(t)\Psi(t+T) = \mathcal{M}$, then the eigenvalues of $\mathcal{M}$ are the eigenvalues of $e^{T\mathcal{B}}$. The relation between the Floquet multipliers and exponents is

$$\lambda_i = e^{T\sigma_i}. \tag{A.16}$$

Therefore, for stability, the real part of the eigenvalues of $\mathcal{B}$ must be negative. Figure A.1 presents the graphical difference between the Floquet multipliers and exponents.

A.2 Stability of fixed points

A case of practical interest is when $\mathbf{g}(\mathbf{x}_0) = \mathbf{0}$. In this case, the linearization becomes

$$\dot{\mathbf{x}}(t) \simeq \mathbf{J}(\mathbf{x}(t) - \mathbf{x}_0) \tag{A.17}$$

where $\mathbf{J} = \frac{\partial \mathbf{f}}{\partial \mathbf{x}}\Big|_{\mathbf{x}=\mathbf{x}_0}$. Considering a small perturbation such that $\mathbf{x}(t) = \mathbf{x}_0 + \mathbf{s}(t)$, Equation (A.17) can be written as a time-invariant differential equation

$$\dot{\mathbf{s}}(t) \simeq \mathbf{J}\mathbf{s}(t). \tag{A.18}$$

The fundamental matrix can be directly found in the *Floquet normal form*:

$$\Psi(t) = \mathcal{P}e^{\mathbf{J}t} \tag{A.19}$$

where $\mathcal{P}$ is a constant matrix. The stability of the fixed point can be studied by checking the norm of the eigenvalues of $e^{\mathbf{J}T}$ or, similarly, the real part of the eigenvalues of $\mathbf{J}$.

Appendix B

Trigonometric and binomial identities

B.1 Trigonometric integral

The goal of this section is to prove that

$$\int_0^{2\pi} \cos^a\theta \sin^b\theta \,\mathrm{d}\theta = \frac{1}{2}\left[(-1)^a+1\right]\left[(-1)^b+1\right]\frac{\Gamma\left(\frac{a}{2}+\frac{1}{2}\right)\Gamma\left(\frac{b}{2}+\frac{1}{2}\right)}{\Gamma\left(\frac{a}{2}+\frac{b}{2}+1\right)}. \tag{B.1}$$

To do so, the change of variable $\theta \to \theta+\pi$ is operated on the left hand side of (B.1), leaving

$$(-1)^{a+b}\int_{-\pi}^{\pi} \cos^a\theta \sin^b\theta \,\mathrm{d}\theta. \tag{B.2}$$

Since

$$\int_{-\theta_1}^{\theta_1} g(\theta)\,\mathrm{d}\theta = \begin{cases} 0 & \text{if } g(\theta) \text{ is an odd function} \\ 2\int_0^{\theta_1} g(\theta)\,\mathrm{d}\theta & \text{if } g(\theta) \text{ is an even function} \end{cases} \tag{B.3}$$

Equation (B.1) becomes

$$(-1)^{a+b}\left[(-1)^b+1\right]\int_0^{\pi} \cos^a\theta \sin^b\theta \,\mathrm{d}\theta. \tag{B.4}$$

The change of variable $\theta \to \theta+\frac{\pi}{2}$ is applied, yielding

$$(-1)^{a+b}\left[(-1)^b+1\right](-1)^a\int_{-\frac{\pi}{2}}^{\frac{\pi}{2}} \sin^a\theta \cos^b\theta \,\mathrm{d}\theta. \tag{B.5}$$

Thanks to (B.3), (B.5) becomes

$$(-1)^{a+b}\left[(-1)^b+1\right](-1)^a\left[(-1)^a+1\right]\int_0^{\frac{\pi}{2}} \sin^a\theta \cos^b\theta \,\mathrm{d}\theta \tag{B.6}$$

or, simply

$$\left[(-1)^b+1\right]\left[(-1)^a+1\right]\int_0^{\frac{\pi}{2}} \sin^a\theta \cos^b\theta \,\mathrm{d}\theta. \tag{B.7}$$

A last change of variable is operated: $\sin^2\theta \to t$ and Equation (B.7) is rewritten as

$$\frac{1}{2}\left[(-1)^b+1\right]\left[(-1)^a+1\right]\int_0^1 t^{\frac{a+1}{2}-1}(1-t)^{\frac{b+1}{2}-1}\,\mathrm{d}t \tag{B.8}$$

where the integral is the Euler integral of first kind [30]

$$\mathrm{B}(z_1,z_2)=\int_0^1 t^{z_1}(1-t)^{z_2-1}\,\mathrm{d}t=\frac{\Gamma(z_1)\,\Gamma(z_2)}{\Gamma(z_1+z_2)}. \tag{B.9}$$

If $z_1=\frac{a+1}{2}$ and $z_2=\frac{b+1}{2}$, then Equation (B.8) is rewritten as the right hand side of (B.1).

B.2 Binomial identity

The goal of this section is to prove that

$$\binom{2a}{2b}=\binom{a}{b}\frac{\Gamma\left(a+\frac{1}{2}\right)}{\Gamma\left(b+\frac{1}{2}\right)\Gamma\left(a-b+\frac{1}{2}\right)}\sqrt{\pi}. \tag{B.10}$$

First, a binomial coefficient is linked to the Gamma function [30]

$$\binom{a}{b}=\frac{\Gamma(a+1)}{\Gamma(b+1)\Gamma(a-b+1)}. \tag{B.11}$$

Using the change of variable

$$\begin{aligned} z_1 &= a+\frac{1}{2}\\ z_2 &= b+\frac{1}{2}\\ z_3 &= a-b+\frac{1}{2} \end{aligned} \tag{B.12}$$

and the duplication formula [30]

$$\Gamma(2z)=\frac{\Gamma(z)\Gamma\left(z+\frac{1}{2}\right)}{2^{1-2z}\sqrt{\pi}} \tag{B.13}$$

(B.11) is rewritten as

$$
\begin{aligned}
\binom{2a}{2b} &= \frac{\Gamma(2a+1)}{\Gamma(2b+1)\Gamma(2a-2b+1)} \\
&= \frac{\Gamma(2z_1)}{\Gamma(2z_2)\Gamma(2z_3)} \\
&= \frac{\Gamma(z_1)\Gamma\left(z_1+\frac{1}{2}\right)}{2^{1-2z_1}\sqrt{\pi}} \frac{2^{1-2z_2}\sqrt{\pi}}{\Gamma(z_2)\Gamma\left(z_2+\frac{1}{2}\right)} \frac{2^{1-2z_3}\sqrt{\pi}}{\Gamma(z_3)\Gamma\left(z_3+\frac{1}{2}\right)} \\
&= \frac{\Gamma\left(z_1+\frac{1}{2}\right)}{\Gamma\left(z_2+\frac{1}{2}\right)\Gamma\left(z_3+\frac{1}{2}\right)} \frac{\Gamma(z_1)}{\Gamma(z_2)\Gamma(z_3)} \frac{2^{1-2z_2}2^{1-2z_3}}{2^{1-2z_1}}\sqrt{\pi} \\
&= \frac{\Gamma(a+1)}{\Gamma(b+1)\Gamma(a-b+1)} \frac{\Gamma\left(a+\frac{1}{2}\right)}{\Gamma\left(b+\frac{1}{2}\right)\Gamma\left(a-b+\frac{1}{2}\right)}\sqrt{\pi} \\
&= \binom{a}{b} \frac{\Gamma\left(a+\frac{1}{2}\right)}{\Gamma\left(b+\frac{1}{2}\right)\Gamma\left(a-b+\frac{1}{2}\right)}\sqrt{\pi}
\end{aligned}
\tag{B.14}
$$

List of Figures

Bibliography

[1] M. Géradin and D. Rixen. *Mechanical vibrations: Theory and Application to Structural Dynamics*. 3rd. John Wiley & Sons, New York, 2015.

[2] D. J. Ewins. *Modal testing : theory, practice, and application*. 2nd. John Wiley & Sons Inc., 2000.

[3] G. Kerschen, M. Peeters, J. Golinval, and A. Vakakis. "Nonlinear normal modes, Part I: A useful framework for the structural dynamicist". *Mechanical Systems and Signal Processing* Vol. 23, no. 1 (2009), pp. 170–194. DOI: https://doi.org/10.1016/j.ymssp.2008.04.002.

[4] A. H. Nayfeh and D. T. Mook. *Nonlinear oscillations*. John Wiley & Sons, New York, 1995. DOI: 10.1007/0-387-35794-7.

[5] S. Lefschetz. "Linear and nonlinear oscillations". *Modern Mathematics for the Engineer: First Series*. Ed. by E. F. Beckenbach. 1956.

[6] R. M. Rosenberg. "The Normal Modes of Nonlinear n-Degree-of-Freedom Systems". *Journal of Applied Mechanics* Vol. 29, no. 1 (1962), pp. 7–14. DOI: 10.1115/1.3636501. eprint: https://asmedigitalcollection.asme.org/appliedmechanics/article-pdf/29/1/7/5444678/7_1.pdf.

[7] A. Vakakis, L. Manevitch, Y. Mikhlin, V. Pilipchuk, and A. Zevin. *Normal Modes and Localization in Nonlinear Systems*. John Wiley & Sons, New York, 1996. DOI: 10.1007/978-94-017-2452-4.

[8] A. Vakakis. "Non-linear normal modes and their applications in vibration theory: an overview". *Mechanical Systems and Signal Processing* Vol. 11, no. 1 (1997), pp. 3–22. DOI: https://doi.org/10.1006/mssp.1996.9999.

[9] S. Shaw and C. Pierre. "Non-linear normal modes and invariant manifolds". *Journal of Sound and Vibration* Vol. 150, no. 1 (1991), pp. 170–173.

[10] G. Haller and S. Ponsioen. "Nonlinear normal modes and spectral submanifolds: Existence, uniqueness and use in model reduction". *Nonlinear Dynamics* Vol. 86, no. 3 (2016), pp. 1493–1534. DOI: 10.1007/s11071-016-2974-z.

[11] A. H. Nayfeh. *Perturbation methods*. John Wiley & Sons, New York, 1973. DOI: 10.1002/9783527617609.

[12] I. Kovacic and M. J. Brennan, eds. *The Duffing Equation: Nonlinear Oscillators and Their Behaviour*. John Wiley & Sons, Hoboken, 2011. DOI: 10.1002/9780470977859.

[13] K. Yagasaki and T. Ichikawa. "Higher-Order Averaging for periodically forced weakly nonlinear systems". *International Journal of Bifurcation and Chaos* Vol. 09, no. 03 (1999), pp. 519–531. DOI: 10.1142/S0218127499000353.

[14] K. Yagasaki. "Higher-order averaging and ultra-subharmonics in forced oscillators". *Journal of Sound and Vibration* Vol. 210, no. 4 (1998), pp. 529–553. DOI: 10.1006/jsvi.1997.1326.

[15] K. Yagasaki. "Detection of bifurcation structures by higher-order averaging for Duffing's equation". *Nonlinear Dynamics* Vol. 18, no. 2 (1999), pp. 129–158. DOI: 10.1023/A:1008371723533.

[16] S. Peter and R. I. Leine. "Excitation power quantities in phase resonance testing of nonlinear systems with phase-locked-loop excitation". *Mechanical Systems and Signal Processing* Vol. 96 (2017), pp. 139–158. DOI: 10.1016/j.ymssp.2017.04.011.

[17] S. Peter, R. Riethmüller, and R. I. Leine. "Tracking of Backbone Curves of Nonlinear Systems Using Phase-Locked-Loops". *Nonlinear Dynamics, Volume 1*. Ed. by G. Kerschen. Cham: Springer International Publishing, 2016, pp. 107–120. ISBN: 978-3-319-29739-2.

[18] G. Abeloos, F. Müller, F. Erhan, S. Maren, C. Collette, G. Kerschen, M. Brake, P. Tiso, L. Renson, and M. Krack. "A Consistency Analysis of Phase-Locked-Loop Testing and Control-Based Continuation for a Geometrically Nonlinear Frictional System". *Mechanical Systems and Signal Processing* (2022). DOI: 10.1016/j.ymssp.2022.108820.

[19] V. Denis, M. Jossic, C. Giraud-Audine, B. Chomette, A. Renault, and O. Thomas. "Identification of nonlinear modes using phase-locked-loop experimental continuation and normal form". *Mechanical Systems and Signal Processing* Vol. 106 (2018), pp. 430–452. DOI: 10.1016/j.ymssp.2018.01.014.

[20] M. Scheel, S. Peter, R. Leine, and M. Krack. "A phase resonance approach for modal testing of structures with nonlinear dissipation". *Journal of Sound and Vibration* Vol. 435 (2018), pp. 56–73. DOI: https://doi.org/10.1016/j.jsv.2018.07.010.

[21] D. Inman. *Engineering Vibrations*. Pearson, 2014.

[22] U. Parlitz and W. Lauterborn. "Superstructure in the bifurcation set of the Duffing equation $\ddot{x}+d\dot{x}+x+x^3 = f\cos\omega t$". *Physics Letters* Vol. 107A (1985), pp. 351–355. DOI: 10.1016/0375-9601(85)90687-5.

[23] A. H. Nayfeh. *Introduction to perturbation techniques*. John Wiley & Sons, New York, 1981.

[24] H. Keller. *Numerical Methods in Bifurcation Problems*. Springer, Berlin, 1987.

[25] R. Seydel. *Practical bifurcation and stability analysis*. Springer New York, NY, 2010. DOI: 10.1007/978-1-4419-1740-9.

[26] M. Peeters, R. Viguié, G. Sérandour, G. Kerschen, and J.-C. Golinval. "Nonlinear normal modes, Part II: Toward a practical computation using numerical continuation techniques". *Mechanical Systems and Signal Processing* Vol. 23, no. 1 (2009), pp. 195–216. DOI: 10.1016/j.ymssp.2008.04.003.

[27] L. Renson, G. Kerschen, and B. Cochelin. "Numerical computation of nonlinear normal modes in mechanical engineering". *Journal of Sound and Vibration* Vol. 364 (2016), pp. 177–206. DOI: 10.1016/j.jsv.2015.09.033.

[28] M. Krack and J. Gross. *Harmonic Balance for Nonlinear Vibration Problems*. Springer Cham, 2019. DOI: 10.1007/978-3-030-14023-6.

[29] T. Detroux, L. Renson, L. Masset, and G. Kerschen. "The harmonic balance method for bifurcation analysis of large-scale nonlinear mechanical systems". *Computer Methods in Applied Mechanics and Engineering* Vol. 296 (2015), pp. 18–38. DOI: 10.1016/j.cma.2015.07.017.

[30] M. Abramowitz and I. A. Stegun. *Handbook of Mathematical Functions*. Applied Mathematics Series, 1965.

[31] I. Kovacic, L. Cveticanin, M. Zukovic, and Z. Rakaric. "Jacobi elliptic functions: A review of nonlinear oscillatory application problems". *Journal of Sound and Vibration* Vol. 380 (2016), pp. 1–36. DOI: 10.1016/j.jsv.2016.05.051.

[32] J. Guckenheimer and P. J. Holmes. *Averaging Methods in Nonlinear Dynamical Systems*. Springer, 1983. DOI: 10.1007/978-1-4612-1140-2.

[33] N. Krylov and N. Bogolyubov. *Introduction to non-linear mechanics*. Princeton University Press, 1947.

[34] E. P. Petrov and D. J. Ewins. "Analytical Formulation of Friction Interface Elements for Analysis of Nonlinear Multi-Harmonic Vibrations of Bladed Disks ". *Journal of Turbomachinery* Vol. 125, no. 2 (2003), pp. 364–371. DOI: 10.1115/1.1539868.

[35] A. Cardona, T. Coune, A. Lerusse, and M. Geradin. "A multiharmonic method for non-linear vibration analysis". *International Journal for Numerical Methods in Engineering* Vol. 37, no. 9 (1994), pp. 1593–1608. DOI: 10.1002/nme.1620370911.

[36] G. Von Groll and D. Ewins. "The harmonic balance method with arc-length continuation in rotor/stator problems". *Journal of Sound and Vibration* Vol. 241, no. 2 (2001), pp. 223–233. DOI: 10.1006/jsvi.2000.3298.

[37] V. Jaumouillé, J.-J. Sinou, and B. Petitjean. "An adaptive harmonic balance method for predicting the nonlinear dynamic responses of mechanical systems—Application to bolted structures". *Journal of Sound and Vibration* Vol. 329, no. 19 (2010), pp. 4048–4067. DOI: 10.1016/j.jsv.2010.04.008.

[38] L. Salles, L. Blanc, F. Thouverez, and A. Gouskov. "Dynamic analysis of fretting-wear in friction contact interfaces". *International Journal of Solids and Structures* Vol. 48, no. 10 (2011), pp. 1513–1524. DOI: 10.1016/j.ijsolstr.2011.01.035.

[39] J. Stoker. *Nonlinear vibrations in mechanical and electrical systems*. Interscience Publishers, New York, 1995.

[40] G. W. Hill. "On the part of the motion of the lunar perigee which is a function of the mean motions of the sun and moon". *Acta Mathematica* Vol. 8, no. none (1900), pp. 1–36. DOI: 10.1007/BF02417081.

[41] C. Padmanabhan and R. Singh. "Analysis of periodically excited non-linear systems by a parametric continuation technique". *Journal of Sound and Vibration* Vol. 184, no. 1 (1995), pp. 35–58. DOI: 10.1006/jsvi.1995.0303.

[42] S. Stoykov and S. Margenov. "Numerical computation of periodic responses of non-linear large-scale systems by shooting method". *Computers & Mathematics with Applications* Vol. 67, no. 12 (2014), pp. 2257–2267. DOI: 10.1016/j.camwa.2014.01.023.

[43] E. Doedel, A. Champneys, T. Fairgrieve, Y. Kuznetsov, B. Sandstede, and X. Wang. *AUTO 97: Continuation And Bifurcation Software For Ordinary Differential Equations (with HomCont)*. 1999.

[44] A. Dhooge, W. Govaerts, and Y. Kuznetsov. "MATCONT: a Matlab package for numerical bifurcation analysis of ODEs". *ACM Trans. Math. Softw.* Vol. 29 (2003), pp. 141–164. DOI: 10.1145/980175.980184.

[45] B. Fraeijs de Veubeke. *Influence of internal damping on aircraft resonance*. Agard Manual of aeroelasticity. AGARD/OTAN, 1959. URL: https://orbi.uliege.be/handle/2268/206053.

[46] P. Atkins, J. Wright, and K. Worden. "An extension of a force appropriation to the identification of non-linear multi-degree of freedom systems". *Journal of Sound and Vibration* Vol. 237, no. 1 (2000), pp. 23–43. DOI: 10.1006/jsvi.2000.3033.

[47] G. Raze, M. Volvert, and G. Kerschen. "Tracking amplitude extrema of nonlinear frequency responses using the harmonic balance method". *International Journal for Numerical Methods in Engineering* Vol. n/a, no. n/a (), e7376. DOI: 10.1002/nme.7376. eprint: https://onlinelibrary.wiley.com/doi/pdf/10.1002/nme.7376.

[48] E. P. Petrov. "Direct Parametric Analysis of Resonance Regimes for Nonlinear Vibrations of Bladed Disks". *Journal of Turbomachinery* Vol. 129, no. 3 (2006), pp. 495–502. DOI: 10.1115/1.2720487.

[49] A. Renault, O. Thomas, and H. Mahé. "Numerical antiresonance continuation of structural systems". *Mechanical Systems and Signal Processing* Vol. 116 (2019), pp. 963–984. DOI: 10.1016/j.ymssp.2018.07.005.

[50] M. Peeters, G. Kerschen, and J. Golinval. "Dynamic testing of nonlinear vibrating structures using nonlinear normal modes". *Journal of Sound and Vibration* Vol. 330 (2011), pp. 486–509. DOI: 10.1016/j.jsv.2010.08.028.

[51] A. Vizzaccaro, A. Opreni, L. Salles, A. Frangi, and C. Touzé. "High order direct parametrisation of invariant manifolds for model order reduction of finite element structures: application to large amplitude vibrations and uncovering of a folding point". *Nonlinear Dynamics* Vol. 110 (2022), pp. 525–571. DOI: https://doi.org/10.1007/s11071-022-07651-9.

[52] S. Jain and G. Haller. "How to compute invariant manifolds and their reduced dynamics in high-dimensional finite element models". *Nonlinear Dynamics* Vol. 107 (2022), pp. 1417–1450. DOI: https://doi.org/10.1007/s11071-021-06957-4.

[53] D. Ehrhardt, R. Harris, and M. Allen. "Numerical and experimental determination of nonlinear normal modes of a circular perforated plate". *Fracture and Fatigue - Proceedings of the 2013 Annual Conference on Experimental and Applied Mechanics*. Conference Proceedings of the Society for Experimental Mechanics Series. Germany: Springer, 2014, pp. 239–251. ISBN: 9783319007649. DOI: 10.1007/978-3-319-04753-9_25.

[54] J. Zapico-Valle, M. García-Diéguez, and R. Alonso-Camblor. "Nonlinear modal identification of a steel frame". *Engineering Structures* Vol. 56 (2013), pp. 246–259. DOI: 10.1016/j.engstruct.2013.04.026.

[55] A. Leung and T. Fung. "Phase increment analysis of damped Duffing oscillators". *International Journal for Numerical Methods in Engineering* Vol. 28 (1989), pp. 193–209. DOI: 10.1002/nme.1620280114.

[56] M. Cedenese and G. Haller. "How do conservative backbone curves perturb into forced responses? A Melnikov function analysis". *Proceedings of the Royal Society A* Vol. 476 (2020), p. 20190494. DOI: 10.1098/rspa.2019.0494.

[57] K. Yagasaki. "Second-order averaging and melnikov analyses for forced non-linear oscillators". *Journal of Sound and Vibration* Vol. 190, no. 4 (1996), pp. 587–609. DOI: 10.1006/jsvi.1996.0080.

[58] A. H. Nayfeh. *Method of Normal Forms*. Wiley, New York, 1993. DOI: 10.1002/9783527635801.

[59] C.-H. Lamarque, C. Touzé, and O. Thomas. "An upper bound for validity limits of asymptotic analytical approaches based on normal form theory". *Nonlinear Dynamics* Vol. 70, no. 3 (2012), pp. 1931–1949. DOI: 10.1007/s11071-012-0584-y.

[60] C. Touzé, O. Thomas, and A. Chaigne. "Hardening/softening behaviour in nonlinear oscillations of structural systems using non-linear normal modes". *Journal of Sound and Vibration* Vol. 273, no. 1 (2004), pp. 77–101. DOI: https://doi.org/10.1016/j.jsv.2003.04.005.

[61] A. Givois, J.-J. Tan, C. Touzé, and O. Thomas. "Backbone curves of coupled cubic oscillators in one-to-one internal resonance: bifurcation scenario, measurements and parameter identification". *Meccanica* Vol. 55, no. 3 (2020), pp. 481–503. DOI: 10.1007/s11012-020-01132-2.

[62] C. Touzé. "Normal form theory and nonlinear normal modes: Theoretical settings and applications". *Modal Analysis of nonlinear Mechanical Systems*. Ed. by G. Kerschen. Vol. 555. Springer Series CISM courses and lectures. Springer, 2014. DOI: 10.1007/978-3-7091-1791-0_3.

[63] A. L. Elgueta, M. Fiebig-Wittmaack, and M. T. Villacran. "An averaging method applied to a duffing equation". *Applicable Analysis* Vol. 60, no. 3-4 (1996), pp. 359–367. DOI: 10.1080/00036819608840438.

[64] A. F. Vakakis and A. Blanchard. "Exact steady states of the periodically forced and damped Duffing oscillator". *Journal of Sound and Vibration* Vol. 413 (2018), pp. 57–65. DOI: 10.1016/j.jsv.2017.10.030.

[65] Z. Rahman and T. Burton. "Large amplitude primary and superharmonic resonances in the Duffing oscillator". *Journal of Sound and Vibration* Vol. 110, no. 3 (1986), pp. 363–380. DOI: 10.1016/S0022-460X(86)80141-9.

[66] M. E. Levenson. "Harmonic and Subharmonic Response for the Duffing Equation $\ddot{x}+\alpha x+\beta x^3 = F\cos\omega t$ $(\alpha > 0)$". *Journal of Applied Physics* Vol. 20, no. 11 (1949), pp. 1045–1051. DOI: 10.1063/1.1698272.

[67] T. Kalmár-Nagy and B. Balachandran. "Forced Harmonic Vibration of a Duffing Oscillator with Linear Viscous Damping". Ed. by I. Kovacic and M. J. Brennan. John Wiley & Sons, Hoboken, 2011. Chap. 5, pp. 139–174. DOI: 10.1002/9780470977859.

[68] A. Marchionne, P. Ditlevsen, and S. Wieczorek. "Synchronisation vs.resonance: Isolated resonances in damped nonlinear oscillators". *Physica D* Vol. 380-381 (2018), pp. 8–16. DOI: 10.1016/j.physd.2018.05.004.

[69] I. Kovacic and G. Gatti. "Helmholtz, Duffing and Helmholtz-Duffing Oscillators: Exact Steady-State Solutions". *IUTAM Symposium on Exploiting Nonlinear Dynamics for Engineering Systems*. Ed. by I. Kovacic and S. Lenci. Cham: Springer International Publishing, 2020, pp. 167–177. ISBN: 978-3-030-23692-2. DOI: 10.1007/978-3-030-23692-2_15.

[70] J. A. Sanders, F. Verhulst, and J. Murdock. *Averaging Methods in Nonlinear Dynamical Systems*. Springer New York, 1983. DOI: 10.1007/978-0-387-48918-6.

[71] C. L. Olson and M. G. Olsson. "Dynamical symmetry breaking and chaos in Duffing's equation". *American Journal of Physics* Vol. 59, no. 10 (1991), pp. 907–911. DOI: 10.1119/1.16669.

[72] L. Guillot, A. Lazarus, O. Thomas, C. Vergez, and B. Cochelin. "A purely frequency based Floquet-Hill formulation for the efficient stability computation of periodic solutions of ordinary differential systems". *Journal of Computational Physics* Vol. 416 (2020), p. 109477. DOI: https://doi.org/10.1016/j.jcp.2020.109477.

[73] Y. Shen, Y. Zhao, S. Yang, and H. Xing. "A revised averaging method and general forms of approximate solution for nonlinear oscillator with only polynomial-type displacement nonlinearity". *Journal of Vibroengineering* Vol. 16, no. 4 (2014), pp. 1864–1876.

[74] A. Leung and Q. Zhang. "Higher order normal form and period averaging". *Journal of Sound and Vibration* Vol. 217, no. 5 (1998), pp. 795–806. DOI: 10.1006/jsvi.1998.1752.

[75] Y. Wang, X. Jing, H. Dai, and F.-M. Li. "Subharmonics and ultra-subharmonics of a bio-inspired nonlinear isolation system". *International Journal of Mechanical Sciences* Vol. 152 (2019), pp. 167–184. DOI: 10.1016/j.ijmecsci.2018.12.054.

[76] R. Alcorta, S. Baguet, B. Prabel, P. Piteau, and G. Jacquet-Richardet. "Period doubling bifurcation analysis and isolated sub-harmonic resonances in an oscillator with asymmetric clearances". *Nonlinear Dynamics* Vol. 98, no. 4 (2019), pp. 2939–2960. DOI: 10.1007/s11071-019-05245-6.

[77] A. F. Vakakis. "Fundamental and subharmonic resonances in a system with a '1-1' internal resonance". *Nonlinear Dynamics* Vol. 3, no. 2 (1992), pp. 123–143. DOI: 10.1007/BF00118989.

[78] A. Polyanin and A. Manzhirov. *Handbook of Mathematics for Engineers and Scientists*. Chapman & Hall/CRC Press, 2006. ISBN: 978-1584885023. DOI: 10.1201/9781420010510.

[79] R. Rosenberg. "On Nonlinear Vibrations of Systems with Many Degrees of Freedom". Advances in Applied Mechanics Vol. 9 (1966). Ed. by G. Chernyi, H. Dryden, P. Germain, L. Howarth, W. Olszak, W. Prager, R. Probstein, and H. Ziegler, pp. 155–242. DOI: 10.1016/S0065-2156(08)70008-5.

[80] R. M. Rosenberg. "Normal Modes of Nonlinear Dual-Mode Systems". *Journal of Applied Mechanics* Vol. 27, no. 2 (1960), pp. 263–268. DOI: 10.1115/1.3643948.

[81] J. Carr. *Applications of Centre Manifold Theory*. Springer New York, 1981. DOI: 10.1007/978-1-4612-5929-9.

[82] S. Shaw and C. Pierre. "Normal Modes for Non-Linear Vibratory Systems". *Journal of Sound and Vibration* Vol. 164, no. 1 (1993), pp. 85–124. DOI: 10.1006/jsvi.1993.1198.

[83] S. Shaw and C. Pierre. "Normal Modes of Vibration for Non-Linear Continuous Systems". *Journal of Sound and Vibration* Vol. 169, no. 3 (1994), pp. 319–347. DOI: 10.1006/jsvi.1994.1021.

[84] M. Krack. "Nonlinear modal analysis of nonconservative systems: Extension of the periodic motion concept". *Computers & Structures* Vol. 154 (2015), pp. 59–71. DOI: 10.1016/j.compstruc.2015.03.008.

[85] D. Laxalde and F. Thouverez. "Complex non-linear modal analysis for mechanical systems: Application to turbomachinery bladings with friction interfaces". *Journal of Sound and Vibration* Vol. 322, no. 4 (2009), pp. 1009–1025. DOI: 10.1016/j.jsv.2008.11.044.

[86] L. Pesek, L. Pust, P. Snabl, V. Bula, M. Hajzman, and M. Byrtus. "Dry-Friction Damping in Vibrating Systems, Theory and Application to the Bladed Disc Assembly". *Nonlinear Structural Dynamics and Damping*. Cham: Springer International Publishing, 2019, pp. 169–259. ISBN: 978-3-030-13317-7. DOI: 10.1007/978-3-030-13317-7_6.

[87] A. Sinha and J. H. Griffin. "Friction damping of flutter in gas turbine engine airfoils". *Journal of Aircraft* Vol. 20, no. 4 (1983), pp. 372–376. DOI: 10.2514/3.44878.

[88] K. Popp, L. Panning, and W. Sextro. "Vibration Damping by Friction Forces: Theory and Applications". *Journal of Vibration and Control* Vol. 9, no. 3-4 (2003), pp. 419–448. DOI: 10.1177/107754603030780.

[89] A. J. Hillis, S. A. Neild, B. W. Drinkwater, and P. D. Wilcox. "Global crack detection using bispectral analysis". *Proceedings of the Royal Society A: Mathematical, Physical and Engineering Sciences* Vol. 462, no. 2069 (2006), pp. 1515–1530. DOI: 10.1098/rspa.2005.1620. eprint: https://royalsocietypublishing.org/doi/pdf/10.1098/rspa.2005.1620.

[90] G. I. Cirillo, A. Mauroy, L. Renson, G. Kerschen, and R. Sepulchre. "Global Parametrization of the Invariant Manifold Defining Nonlinear Normal Modes Using the Koopman Operator". 2015, V006T10A049. DOI: 10.1115/DETC2015-46366.

[91] G. Cirillo, A. Mauroy, L. Renson, G. Kerschen, and R. Sepulchre. "A spectral characterization of nonlinear normal modes". *Journal of Sound and Vibration* Vol. 377 (2016), pp. 284–301. DOI: 10.1016/j.jsv.2016.05.016.

[92] M. Li, S. Jain, and G. Haller. "Nonlinear analysis of forced mechanical systemswith internal resonance using spectral submanifolds, Part I: Periodic response and forced response curve". *Nonlinear Dynamics* Vol. 110, no. 2 (2022), pp. 1005–1043. DOI: 10.1007/s11071-022-07714-x.

[93] M. Li and G. Haller. "Nonlinear analysis of forced mechanical systems with internal resonance using spectral submanifolds, Part II: Bifurcation and quasi-periodic response". *Nonlinear Dynamics* Vol. 110, no. 2 (2022), pp. 1045–1080. DOI: 10.1007/s11071-022-07476-6.

[94] S. Ponsioen, S. Jain, and G. Haller. "Model reduction to spectral submanifolds and forced-response calculation in high-dimensional mechanical systems". *Journal of Sound and Vibration* Vol. 488 (2020), p. 115640. DOI: 10.1016/j.jsv.2020.115640.

[95] S. Ponsioen, T. Pedergnana, and G. Haller. "Analytic prediction of isolated forced response curves from spectral submanifolds". *Nonlinear Dynamics* Vol. 98, no. 4 (2019), pp. 2755–2773. DOI: 10.1007/s11071-019-05023-4.

[96] C. Grenat, S. Baguet, R. Dufour, and C.-H. Lamarque. "Generalization of conservative nonlinear normal modes to the non-conservative equation of motion". 2018.

[97] T. Hill, S. Neild, and A. Cammarano. "An analytical approach for detecting isolated periodic solution branches in weakly nonlinear structures". *Journal of Sound and Vibration* Vol. 379 (2016), pp. 150–165. DOI: https://doi.org/10.1016/j.jsv.2016.05.030.

[98] Y. Sun, A. Vizzaccaro, J. Yuan, and L. Salles. "An extended energy balance method for resonance prediction in forced response of systems with non-conservative nonlinearities using damped nonlinear normal mode". *Nonlinear Dynamics* Vol. 103, no. 4 (2021), pp. 3315–3333. DOI: 10.1007/s11071-020-05793-2.

[99] L. Renson, T. Hill, D. Ehrhardt, D. Barton, and S. Neild. "Force appropriation of nonlinear structures". *Proceedings of the Royal Society A: Mathematical, Physical, and Engineering Sciences* Vol. 474 (2018), p. 20170880. DOI: 10.1098/rspa.2017.0880.

[100] I. Sokolov and V. Babitsky. "Autoresonant mechatronic systems". *Mechatronics* Vol. 5 (1995), pp. 483–495.

[101] I. Sokolov and V. Babitsky. "Phase control of self-sustained vibration". *Journal of Sound and Vibration* Vol. 248 (2001), pp. 725–744. DOI: https://doi.org/10.1006/jsvi.2001.3810.

[102] G. Moore. "Floquet Theory as a Computational Tool". *SIAM Journal on Numerical Analysis* Vol. 42, no. 6 (2005), pp. 2522–2568.

[103] L. Renson, J. P. Noël, and G. Kerschen. "Complex dynamics of a nonlinear aerospace structure: numerical continuation and normal modes". *Nonlinear Dynamics* Vol. 79, no. 2 (2015), pp. 1293–1309. DOI: 10.1007/s11071-014-1743-0.

[104] G. Abeloos. "Control-based methods for the identification of nonlinear structures". PhD thesis. ULiège - Université de Liège [Sciences Appliquées], Liège, Belgium, 2022.

[105] R. Kuether, L. Renson, T. Detroux, C. Grappasonni, G. Kerschen, and M. Allen. "Nonlinear normal modes, modal interactions and isolated resonance curves". *Journal of Sound and Vibration* Vol. 351 (2015). DOI: 10.1016/j.jsv.2015.04.035.

[106] T. Detroux. "Performance and Robustness of Nonlinear Systems Using Bifurcation Analysis". PhD thesis. ULiège - Université de Liège, 2016.

[107] D. Hong, T. L. Hill, and S. A. Neild. "Efficient energy balancing across multiple harmonics of nonlinear normal modes". *Nonlinear Dynamics* Vol. 108, no. 4 (2022), pp. 2935–2959. DOI: 10.1007/s11071-022-07428-0.

[108] T. Zhou and G. Kerschen. "Identification of Secondary Resonances using a Control-based Method". *Third International Nonlinear Dynamics Conference (NODYCON 2023)*. 2023.

[109] T. Zhou and G. Kerschen. *Identification of Secondary Resonances of Nonlinear Systems using Phase-Locked Loop Testing*. 2024. arXiv: 2401.01151 [eess.SY].

[110] A. Givois, C. Giraud-Audine, J.-F. Deü, and O. Thomas. "Experimental analysis of nonlinear resonances in piezoelectric plates with geometric nonlinearities". *Nonlinear Dynamics* Vol. 102, no. 3 (2020), pp. 1451–1462. DOI: 10.1007/s11071-020-05997-6.

[111] M. Scheel, T. Weigele, and M. Krack. "Challenging an experimental nonlinear modal analysis method with a new strongly friction-damped structure". *Journal of Sound and Vibration* Vol. 485 (2020), p. 115580. DOI: 10.1016/j.jsv.2020.115580.

[112] S. Peter, M. Scheel, M. Krack, and R. I. Leine. "Synthesis of nonlinear frequency responses with experimentally extracted nonlinear modes". *Mechanical Systems and Signal Processing* Vol. 101 (2018), pp. 498–515. DOI: https://doi.org/10.1016/j.ymssp.2017.09.014.

[113] B. Widrow, J. Glover, J. McCool, J. Kaunitz, C. Williams, R. Hearn, J. Zeidler, J. Eugene Dong, and R. Goodlin. "Adaptive noise cancelling: Principles and applications". *Proceedings of the IEEE* Vol. 63, no. 12 (1975), pp. 1692–1716. DOI: 10.1109/PROC.1975.10036.

[114] G. Abeloos, L. Renson, C. Collette, and G. Kerschen. "Stepped and swept control-based continuation using adaptive filtering". *Nonlinear Dynamics* Vol. 104, no. 4 (2021), pp. 793–3808. DOI: 10.1007/s11071-021-06506-z.

[115] S. Haykin. *Adaptive filter theory*. 4th. Prentice Hall, 2002.

[116] W. Szemplińska-Stupnicka. "The modified single mode method in the investigations of the resonant vibrations of non-linear systems". *Journal of Sound and Vibration* Vol. 63, no. 4 (1979), pp. 475–489. DOI: https://doi.org/10.1016/0022-460X(79)90823-X.

[117] C. Chicone. *Ordinary Differential Equations with Applications*. Springer New York, NY, 1991.

Publications

The complete list of the author's publications is available in the institutional repository ORBI (https://orbi.uliege.be/profile?uid=p169527)

Publications associated with the thesis

Journal articles

M. Volvert and G. Kerschen. "Phase resonance nonlinear modes of mechanical systems". *Journal of Sound and Vibration* Vol. 511 (2021), p. 116355. DOI: 10.1016/j.jsv.2021.116355

M. Volvert and G. Kerschen. "Resonant phase lags of a Duffing oscillator". *International Journal of Non-Linear Mechanics* Vol. 146 (2022), p. 104150. DOI: 10.1016/j.ijnonlinmec.2022.104150

Conference proceedings and presentations

M. Volvert and G. Kerschen. "Analytical study of the amplitude and phase resonances of a Duffing oscillator". *Proceedings of ISMA2022 including USD2022 International Conference on Noise and Vibration Engineering*. Leuven, Belgium, 2022. URL: https://hdl.handle.net/2268/297633

M. Volvert and G. Kerschen. "Phase Quadrature Backbone Curve for Nonlinear Modal Analysis of Nonconservative Systems". *Topics in Modal Analysis & Testing, Volume 8*. Ed. by B. Dilworth and M. Mains. Cham: Springer International Publishing, 2021, pp. 207–209. ISBN: 978-3-030-47717-2. DOI: 10.1007/978-3-030-47717-2_20

M. Volvert and G. Kerschen. "Characterizing Fundamental, Superharmonic, and Subharmonic Resonances Using Phase Resonance Nonlinear Modes". *Advances in Nonlinear Dynamics*. Ed. by W. Lacarbonara et al. Cham: Springer International Publishing, 2022, pp. 661–671. ISBN: 978-3-030-81162-4. DOI: 10.1007/978-3-030-81162-4_57

M. Volvert and G. Kerschen. "Numerical and Analytical Study of the Phase Resonances of a Duffing Oscillator". *Topics in Modal Analysis & Parameter Identification, Volume 8*. Ed. by B. J. Dilworth, T. Marinone, and M. Mains. Cham: Springer International

Publishing, 2023, pp. 11–13. ISBN: 978-3-031-05445-7. DOI: 10.1007/978-3-031-05445-7_2

M. Volvert and G. Kerschen. "Phase resonance of an oscillator with polynomial stiffness". Lyon, France, 2022. URL: https://hdl.handle.net/2268/297633

M. Volvert and G. Kerschen. "Resonant phase lags of an oscillator with polynomial stiffness". Anglais. Rome, Italy, 2023. URL: https://hdl.handle.net/2268/307785

Publication in collaborations

Journal articles

A. Fantetti et al. "The impact of fretting wear on structural dynamics: Experiment and Simulation". *Tribology International* Vol. 138 (2019), pp. 111–124. DOI: 10.1016/j.triboint.2019.05.023

G. Raze, M. Volvert, and G. Kerschen. "Tracking amplitude extrema of nonlinear frequency responses using the harmonic balance method". *International Journal for Numerical Methods in Engineering* Vol. n/a, no. n/a (), e7376. DOI: 10.1002/nme.7376. eprint: https://onlinelibrary.wiley.com/doi/pdf/10.1002/nme.7376. URL: https://onlinelibrary.wiley.com/doi/abs/10.1002/nme.7376

Conference proceedings and presentations

G. Abeloos, M. Volvert, and G. Kerschen. "Experimental Characterization of Superharmonic Resonances Using Phase-Lock Loop and Control-Based Continuation". *Nonlinear Structures & Systems, Volume 1.* Ed. by M. R. Brake et al. Cham: Springer International Publishing, 2023, pp. 131–133. DOI: 10.1007/978-3-031-04086-3_19